Studies on Vascular Changes and Immune Cell Role in the Ischemic Brain By *In Vivo* Two-Photon Microscopy

Thesis

UNRESTRICTED

STUDIES ON VASCULAR CHANGES AND IMMUNE CELL ROLE IN THE ISCHEMIC BRAIN BY *IN VIVO* TWO-PHOTON MICROSCOPY

Stefano Fumagalli

(Personal Identifier: A4155818)

Laboratory of Inflammation and Nervous System Diseases
Department of Neuroscience
Mario Negri Institute for Pharmacological Research, Milan, Italy

Thesis submitted for the degree of
Doctor of Philosophy at the Open University of London, UK

Date of Submission: 28 September 201
Date of Award: 6 March 2013
Date of Award: 6 March 2013

ProQuest LLC.
789 East Eisenhower Parkway
P.O. Box 1346
Ann Arbor, MI 48106 – 1346

Pro veritate adversa diligere et prospera formidando declinare

(For the truth, love adversity and be cautious with the success)

san Gregorio Magno, *Regula Pastoralis*, VI century

Preface and Declaration

The work reported in this thesis has been performed at the Mario Negri Institute for Pharmacological Research, Milan, Italy and at the Strathclyde University of Glasgow and at the University of Glasgow, Glasgow, UK, during the years 2008-2012. I have been supervised by Dr. Maria-Grazia De Simoni, head of the Laboratory of Inflammation and Nervous System Diseases at Mario Negri Institute and by Prof. Paul Garside, Chair in Basic Immunology (Infection Immunity and Inflammation Medicine) at the University of Glasgow.

This thesis has not been submitted in whole or in part for a degree or diploma or other qualifications at any other University.

The experimental work here described and the original data obtained were performed by myself and includes also work performed in collaboration with the following persons: Carlo Perego (at the Mario Negri Institute), who contributed in section **6** by performing permanent ischemia model, and Jonathan A. Coles (at Strathclyde University), who contributed in section **7**, by providing two-photon microscope hardware set up.

Acknowledgements

I am grateful to Dr. Maria-Grazia De Simoni for the academic support that she always provided me during the years spent in her laboratory at the Mario Negri Institute.
I also thank Prof. Paul Garside for his useful help and advice during my Ph.D. period and during the months spent in Glasgow.

My sincere thanks to all my present and former colleagues at the Laboratory of Inflammation and Nervous System Diseases at Mario Negri Institute, Milan, Italy. A very special thank to Franca, Carlo, Elisa, Raffaella, and Fabrizio, for whom the definition 'colleagues' does not represent enough what they really are: good friends.
I also thank all the persons that I met during my period at the Strathclyde University of Glasgow, UK, and, especially: Hilary, Pasquale, Jonathan, Gary, Shalu and Fariborz.

Finally the super-special thank to my family: Guido, Marina and Andrea, for the support that you have always dedicated to me.

List of publications related to this thesis

Part of the data presented in section **5** have been published in:

Fumagalli S, Perego C, Ortolano F and De Simoni MG. CX3CR1 deficiency induces an early protective inflammatory environment in ischemic mice. *GLIA*, 2013 Epub 26th February 2013. DOI: 10.1002/glia.22474.

Part of the data presented in section **6** have been published in:

Perego C, Fumagalli S and De Simoni MG. Temporal pattern of expression and colocalization of microglia/macrophage phenotype markers following brain ischemic injury in mice. *Journal of Neuroinflammation*, 2011 Dec; 8:174.

Part of the data presented in section **7** have been published in:

Fumagalli S, Coles JA, Ejlerskov P, Ortolano F, Bushell TJ, Brewer JM, De Simoni MG, Dever G, Garside P, Maffia P and Carswell HV. In vivo real-time multiphoton imaging of T lymphocytes in the mouse brain after experimental stroke. *Stroke*, 2011 May; 42(5):1429-36.

INDEX

LIST OF FIGURES

LIST OF TABLES

ABBREVIATIONS

2-PM Two-Photon Microscopy

AD Alzheimer Disease

AID

AMPA alfa-Amino-3-Hydroxic-5-Methyl-4-isoxazole Propionate

ANOVA Analysis of Variance

AP Antero-posteriority

ASICs

ATP Adenosine TriPhosphate

BBB Blood Brain Barrier

BDNF Brain-Derive Neurotrophic Factor

CAD Capase-Activated Deoxyribonuclease

CaMKIV Ca^{2+} calmodulin-dependent protein kinase IV

CBP CREB binding protein

CINC Cytokine Induced Neutrophil Chemoattractant

CNS Central Nervous System

CRDs Carbohydrate Recognition Domains

CREB cyclic AMP response element binding protein

CSD Cortical Spreading Depression

CSF Cerebrospinal Fluid

CX3CL1 Chemokine (C-X3-C motif) Ligand 1

CX3CR1 Chemokine (C-X3-C motif) Receptor 1

d days

DCs Dendritic Cells

DNA Deoxyribonucleic Acid

DWI Diffusion-weighted Imaging

EAE Experimental Autoimmune Encephalitomyelitis

ERK extracellular signal regulated kinase

EU European Union

FASL Fas Ligand

FITC Fluorescein Isothiocyanate

FOXO forkhead box protein O

GDNF Glia-Derived Growth Factor

GFP Green Fluorescent Protein

h hours

IAP Inhibitor of Apoptosis Protein

IB4 *Griffonia simplicifolia* isolectin

ICAD Inhibitor of caspase-activated DNase

ICAM Intercellular Adhesion Molecule

ICH Intracerebral Haemorrhage

IGF-1 Insulin Growth Factor-1

IL InterLeukine

INF-γ Interferon-γ

iNOS inducible Nitric Oxide Synthase

Jacob juxtasynaptic attractor of caldenrin on dendritic boutons protein

LAMP Lysosomal/endosomal-Associated Membrane Glycoprotein

LCMV lymphocytic-choriomeningitis virus

LPS Lipopolysaccharide

M/M Microglia/Macrophages

MCA Middle Cerebral Artery

MCAo Middle Cerebral Artery occlusion

MCP-1 Monocyte Chemotactic Protein-1

MGlu Metabotropic Glutamate

MHC Major Histocompatibility Complex

min minutes

MMPs Matrix Metalloproteinases

MRI Magnetic Resonance Imaging

mRNA messenger Ribonucleic Acid

NA Numeric Aperture

NeuN Neuronal Nuclei

NIH National Institute of Health

NK Natural Killer

NMDA N-Methyl-D-Aspartate

NO Nitric Oxide

PANX pannexin family

PBS Phosphate Buffered Saline

pCO_2 partial CO_2 pressure

PET Positron Emission Tomography

PI Propidium Iodide

PID Peri-Infarct Depolarization

pMCAo permanent Middle Cerebral Artery occlusion

PO_2 partial O_2 pressure

PTEN phosphatase and tensin homolog deleted on cromosome 10

PWI Perfusion-weighted Imaging

RANKL Nuclear Factor-kappaB Ligand

RBC Red Blood Cell

RhITC Rhodamine Isothiocyanate

RNA Ribonucleic Acid

RNS nitrogen species

ROS Reactive Oxygen Species

SAH Subarachnoid haemorrhage

$TBXA_2$ Thromboxane

TCR T-cell Receptor

TGF-β Transforming Growth Factor-β

Th1 T-helper 1

Th2 T-helper 2

Th3 T-helper 3

TLRs Toll-like receptors

tMCAO transient Middle Cerebral Artery occlusion

TNF Tumor Necrosis Factor

TNFR Tumor Necrosis Factor Receptor

TORC transducer of regulated CREB activity

tPA tissutal Plasminogen Activator

TRAIL TNF-Related Apoptosis-Inducing Ligand

TRP transient receptor potential

TUNEL Terminal Deoxynucleotidyl Transferase dUTP Nick End Labeling

UK United Kingdom

US United States

XFPs X-Fluorescent Proteins (used for indicating genes encoding fluorescent proteins)

ABSTRACT

Mechanisms contributing to the inflammatory cascade, including vascular modifications and immune cell recruitment/activation, act with high dynamism within a three-dimensional space, thus being ideally investigated by *in vivo* two-photon microscopy (2-PM). In this thesis I applied *in vivo* 2-PM and quantitative bright field and confocal microscopy to explore cerebrovascular remodelling, immune cell dynamism and phenotype in two models of ischemia in mice achieved by transient or permanent middle cerebral artery occlusion. To specifically visualize microglia and T-cells, I used *cx3cr1*_eGFP and *hCD2*_eGFP mice, respectively.

I imaged animals before and at different time points after ischemia, and quantified blood flow velocity and extravasation in individual vessels. After reperfusion, blood flow exhibited >80% drop in most vessels and extravasation established as early as 20min after ischemia onset. In this ischemic territory, I analyzed motility and morphology of GFP+ microglia. Microglia were stationary and became ameboid at 24h after injury. The absence of fractalkine receptor (CX3CR1) prevented the ameboid switch and favoured a protective M2 microglia polarization, characterized by decreased CD68 and iNOS expression and increased Ym1 expression. To assess the temporal evolution of microglia/macrophage polarization in the ischemic brain, I investigated the expression and coexpression pattern of CD11b, CD45, CD68, Ym1, CD206 and iNOS after ischemia by conventional immunohistochemistry. Microglia/macrophages showed multiple polarization states, with a specific pattern of distribution and association with globular or ramified CD11b morphology. M2 microglia/macrophage peaked at 24h after injury, whereas M1 cells peaked at 48h. The phagocytic activity (CD68), mainly confined at the lesion borders at 6h-48h, dramatically increased and occupied all the ischemic territory at 7d.

I finally investigated T-cells dynamism within the ischemic territory by *in vivo* 2-PM. I described two populations characterized by different track velocities and found that motile cells preferentially moved along the perivascular space, where they contacted astrocytes and perivascular macrophages.

These data provide novel information on the inflammatory response after stroke and pave the way for developing strategies resulting in promotion of a protective inflammatory phenotype.

1. INTRODUCTION

1.1 Epidemiology of stroke

Ischemic brain injury is a global health problem, representing the third leading cause of morbidity and mortality in the Western countries. Globally there are 50 million stroke and transient ischemic attack survivors, whose 20% will suffer a subsequent stroke in the following 5 years and 15-20% suffer permanent disability (Adams et al. 1993; Lloyd-Jones et al. 2010).

In UK there are 110 000 all-cause strokes every year (Flynn et al. 2008). In Italy, recent data collected from registers on stroke incidence in different areas (distributed equally from Northern to Southern Italy), indicate that there are approximately 134 000 strokes per year (Sacco et al. 2011). The incidence rates increase linearly with age, peaking in subjects ≥85 years of age. This observation, along with the census data that show that the proportion of elderly people in Italy has been growing over the last three decades (ISTAT, 14° censimento, 21 October 2001, http://dawinci.istat.it/daWinci/jsp/MD/misc.jsp?p=2) suggests that the annual incidence of stroke is due to further increase.

The economic burden of stroke in Italy has been analyzed by the EcLIPSE study in 2005 (Gerzeli et al. 2005). The cost of stroke per patient for the first six-month period is equivalent to € 11 600, 53% of which are health care costs, 39% non-health care costs and the remaining 8% productivity losses (Gerzeli et al. 2005). Overall across the EU the cost of cerebrovascular disease for 2003, including those for informal care and productivity loss, were estimated at € 34 billion (Leal et al. 2006). In the US the estimated combined direct and indirect costs of stroke for 2007 were US$ 62.7 billion (Rosamond et al. 2007).

1.2 Pathophysiology of stroke

The brain is the most metabolically active organ in the body. While representing only 2% of the body's mass, it requires 15-20% of the total resting cardiac output to provide the necessary glucose and oxygen for its metabolism. Ischemic strokes result from events that limit or stop blood flow, such as embolism, thrombosis *in situ*, or relative hypoperfusion. As blood flow decreases, neurons cease functioning, and irreversible neuronal ischemia and injury begin at blood flow rates of less than 18 mL/100 mg/min (Doyle et al. 2008).

1.2.1 Classification

In humans, two different types of stroke exist: haemorrhagic stroke and ischemic stroke (Fatahzadeh and Glick 2006, Fig. 1.1).

1.2.1.1 Haemorrhagic stroke

Haemorrhagic stroke on the whole accounts for 10-15% of all strokes (Gebel and Broderick 2000) and is associated with higher mortality rates than cerebral infarctions. Haemorrhagic stroke can be divided in:

i. Intracerebral haemorrhage (ICH). In intracerebral haemorrhagic stroke (Aronowski and Zhao 2011; Qureshi et al. 2009) bleeding occurs directly into the brain parenchyma. The usual mechanism is thought to be leakage from small intracerebral arteries damaged by chronic hypertension. This kind of stroke has a predilection for certain sites in the brain, including the thalamus, putamen,

cerebellum, and brain stem. In addition to the area of the brain injured by the haemorrhage, the surrounding brain areas may be damaged by the pressure produced by the mass effect of the hematoma. Generally, with intracerebral haemorrhagic stroke, there is an increase in intracranial pressure.

ii. Subarachnoid haemorrhage (SAH). The term subarachnoid haemorrhage (SAH) refers to extravasation of blood into the subarachnoid space between the pial and arachnoid membranes. SAH comprises half of spontaneous atraumatic intracranial haemorrhages (Rhoney et al. 2010; Wong et al. 2010). SAH is a devastating condition with high morbidity and mortality. SAH occurs in various clinical contexts, the most common being head trauma. However, the familiar medical use of the term SAH refers to nontraumatic (or spontaneous) haemorrhage, which usually occurs in the setting of a ruptured cerebral aneurysm or arteriovenous malformation.

1.2.1.2 Ischemic stroke

Ischemic stroke is characterized by a sudden interruption of the cerebral blood flow due to an occlusion of a cerebral vessel and accounts approximately for 80% of all strokes (Stoll et al. 2008). There are 3 types of ischemic strokes:

i. Embolic stroke. Emboli may either be of cardiac or arterial origin. Cardiac sources include atrial fibrillation, recent myocardial infarction, prosthetic valves, native valvular disease, endocarditis, mural thrombi, dilated cardiomyopathy, or patent foramen ovale allowing passage of venous circulation emboli. Arterial sources can be atherothrombotic or cholesterol emboli that develop in the arch of the aorta and in the extracranial arteries (ie, carotid and vertebral arteries). Embolic strokes tend

to have a sudden onset. In these cases neuroimaging may demonstrate previous infarcts in several vascular territories or calcified emboli.

ii. Thrombotic stroke. Thrombotic strokes can be divided into large vessel, including the carotid artery system, or small vessel comprising the intracerebral arteries, including the branches of the Circle of Willis and the posterior circulation (lacunar stroke). The most common sites of thrombotic occlusion are cerebral artery branch points, especially in the distribution of the internal carotid artery. Arterial stenosis (ie, turbulent blood flow), atherosclerosis (ie, ulcerated plaques), and platelet adherence cause the formation of blood clots that occlude the artery. Any process that causes dissection of the cerebral arteries also can cause thrombotic stroke, such as trauma, thoracic aortic dissection, arteritis. The great majority of stroke are related to hypertension.

iii. Watershed stroke. These strokes, also known as border zone infarcts, develop from relative hypoperfusion in the most distal arterial territories and can produce bilateral symptoms. Frequently, this type of stroke occur perioperatively or in situations of prolonged hypotension.

In this thesis I will only discuss about ischemic stroke.

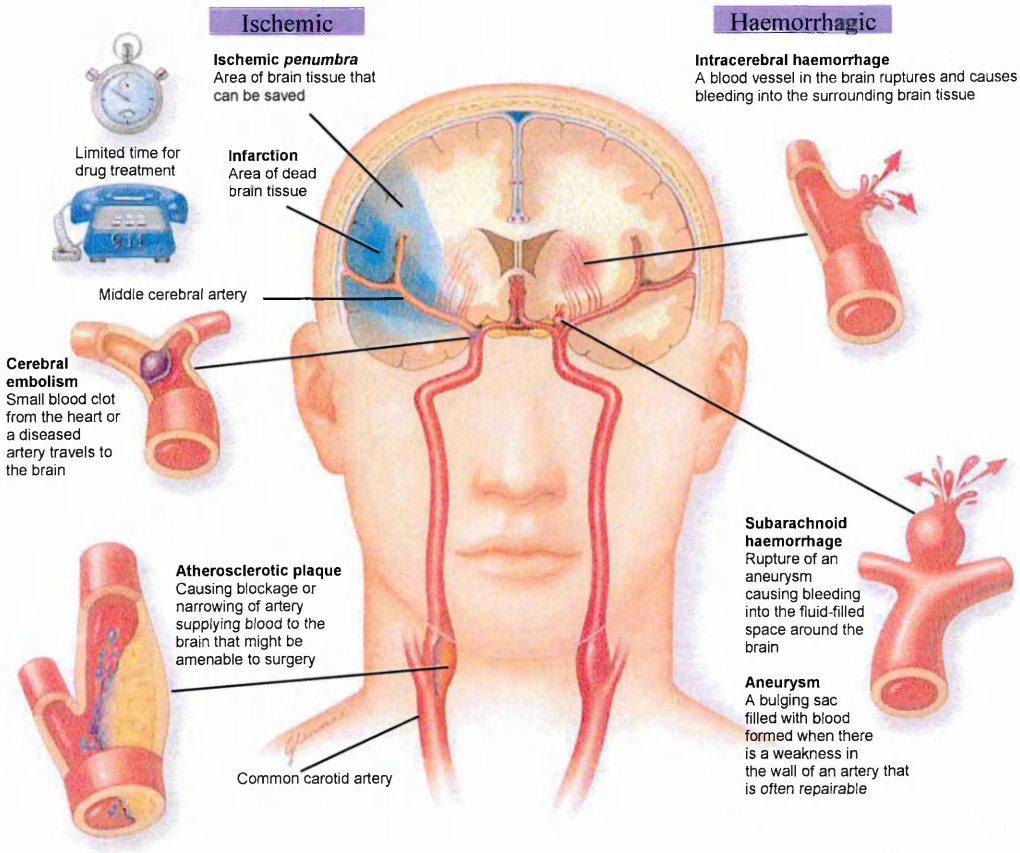

Figure 1.1 *The major types of stroke and cerebral accident* (Richard Green et al. 2003).

1.2.3 Molecular aspects

Ischemic strokes are characterized by an initial insult which is followed by a complex *sequelae* of events that evolve over time and space (Fig. 1.2). These events do not affect the ischemic territory homogeneously. The centre of perfusion deficit, where residual blood flow is 20% below normal, is defined as the core area (Fig. 1.2). In this area, permanent and anoxic depolarization develops minutes after the onset of ischemia and cells are killed rapidly by lipolysis and proteolysis due to the total bioenergetic failure. Between this lethally damaged core and the normal brain lies an area where perfusion is partially preserved and supports basal ATP levels and oxygen metabolism (Hossmann 1994;

Moskowitz et al. 2010; Obrenovitch 1995). This area, defined as ischemic penumbra, could be classified as an 'at risk' region being functionally impaired but still potentially salvageable. Given time and without treatment, the penumbra can progress to infarction owing to ongoing excitotoxicity (see below) or to secondary deleterious phenomena, such as spreading depolarization, post-ischemic inflammation and apoptosis (see below, Lo 2008b; Lo 2008a), and therapeutic opportunity is lost. It is, thus, evident that the prime goal of neuroprotection is to salvage the ischemic penumbra. Although there is ample evidence that the penumbra exists in human stroke patients (Read et al. 1998), the extent and temporal dynamics of this area are less well defined: it might be smaller and exist for a shorter time period in humans (Kaufmann et al. 1999).

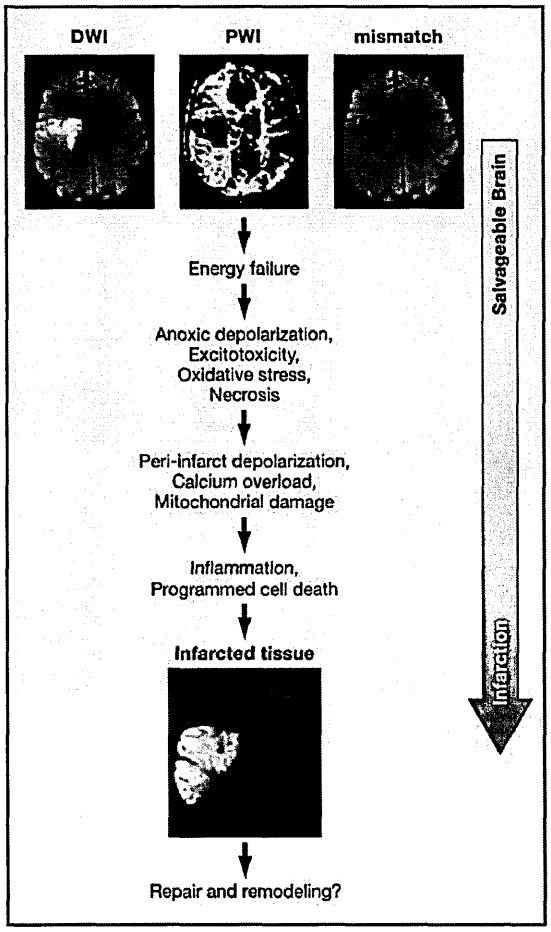

Figure 1.2 *Spatio-temporal evolution of the ischemic damage.*

Diffusion-weighted Imaging (DWI), on the top left image, shows the severely damaged ischemic core as an hyperintense area (white); Perfusion-weighted Imaging (PWI), top middle image, shows the spatial extent of the blood flow impairment. Top right image depicts the mismatch between the core area with a diffusion lesion (dark blue) and the large area with low perfusion (light blu). If no treatment is applied, over hours to days the core territory expands due to the physiopathological cascades that follow the initial insult. The resulting infarct is shown in the bottom image and is almost sized as the initial perfusion deficit (Moskowitz et al. 2010).

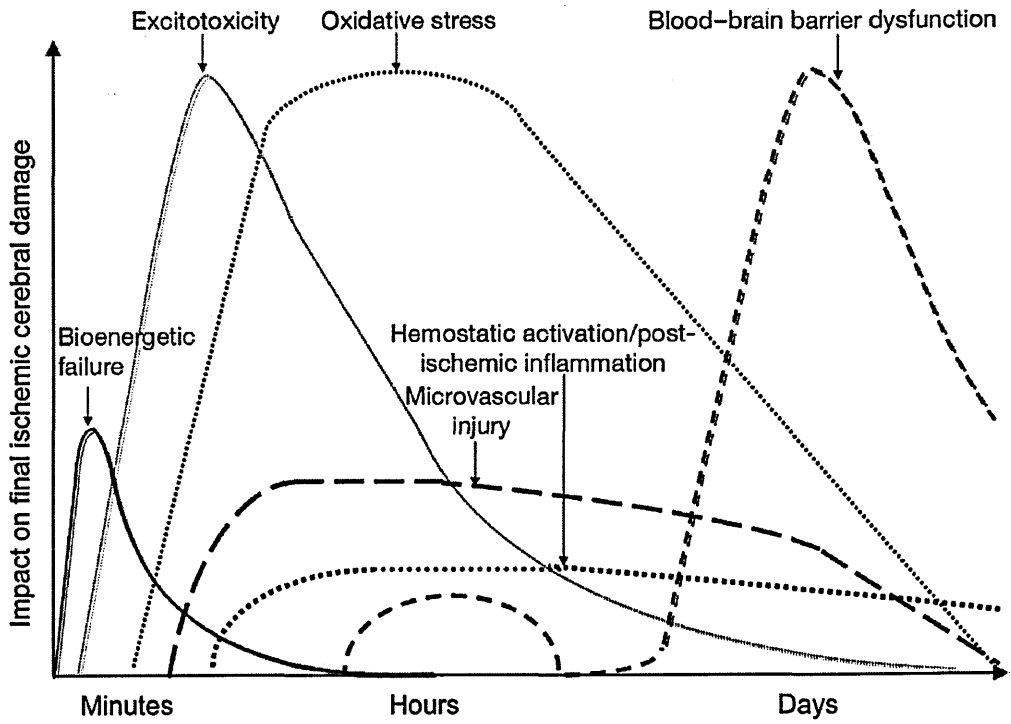

Figure 1.3 *Temporal cascade of the main pathogenetic events in stroke.*

Importantly, inflammation evolves in time, being a crucial clinical target (Saenger and Christenson 2010).

1.2.3.1 Excitotoxicity

The large amount of oxygen required by the brain is necessary to generate sufficient ATP by oxidative phosphorylation to maintain and restore ionic gradients. One estimate suggests that the Na+/K+ATPase found on the plasma membrane of neurons, consumes 70% of the energy supplied to the brain. This ion pump maintains the high intracellular K+ concentration and the low intracellular Na+ concentration necessary for the propagation of action potentials. After global ischemia, mitochondrial inhibition of ATP synthesis leads to ATP being consumed within 2 min, this causes neuronal plasma membrane depolarization, release of potassium into the extracellular space and entry of sodium into cells. Energy failure also prevents the plasma membrane Ca2+ ATPase from maintaining the very low

concentrations of calcium that are normally present within each cell. The extracellular calcium concentration is approximately 1.2 mM and most cellular processes regulated by calcium have a Km value in the range of 0.1-1μM. During ischemia intracellular calcium levels rise to 50-100μM, activating many, if not all calcium dependent proteases, lipases and DNases. Activation of these enzymes causes many cells in the ischemic core to die from simple catabolism. Because no ATP is available for the re-synthesis of cellular constituents these catabolic enzymes cause the necrosis of essential cellular structures. Membrane depolarization also leads to neurotransmitter release, with the release of the excitatory neurotransmitter glutamate playing a critical role in ischemic pathology. A large concentration gradient of glutamate is maintained across the plasma membrane by sodium-dependent glutamate transporters located on presynaptic and postsynaptic membranes. The synaptic glutamate concentration is in the micro molar range, whereas the cytosolic concentration of glutamate is approximately 10 mM. Membrane depolarization and accumulation of sodium inside cells during ischemia causes reversal of glutamate transporters and allows glutamate to exit cells along its concentration gradient. The effect of an increase in synaptic glutamate concentration is the activation of N-methyl-D-aspartate (NMDA) and AMPA receptors. NMDA receptors are calcium permeable and the opening of these channels leads to further membrane depolarization and greater calcium influx, exacerbating intracellular calcium overload (excitotoxicity, Olney and Sharpe 1969). AMPA receptors are not normally calcium permeable by virtue of their GluR2 subunit, however, this subunit is reduced after ischemia increasing the calcium permeability of these receptors by up to 18-fold, allowing AMPA receptors to contribute to delayed calciumdependent cell death (Liu et al. 2006). Blocking glutamate binding sites on NMDA and AMPA receptors has repeatedly been shown to provide robust neuroprotection in models of focal ischemia, where receptor blockade is thought to prevent calcium entry from reaching a toxic threshold. Recent findings indicate that NMDA receptors are also

involved in neuroprotective effects depending on their subcellular localization (Hardingham and Bading 2010; Tymianski 2011). Whereas stimulation of extrasynaptic NMDA receptors is deleterious via different pathways acting downstream, such as death-associated protein kinase 1 (DAPK1) and PTEN (phosphatase and tensin homolog deleted on cromosome 10), both associated with increased excitotoxicity (Ning et al. 2004; Tu et al. 2010), stimulation of synaptic NMDA receptors drives protective activity. Synaptic NMDA receptors activate several downstream pathways including the serine/threonine Akt (Hardingham 2006) and the transcription factor CREB (cyclic AMP response element binding protein). CREB is induced by nuclear Ca^{2+} signaling and, in turn, induces activity-regulated inhibitors of apoptosis (AID), brain-derived neurotrophic factor (BDNF) and other molecules that inhibit pro-apoptotic factors (Hardingham 2006; Hardingham and Bading 2010; Zhang et al. 2009). A scheme of the opposing effects of synaptic or extrasynaptic NMDA receptors is drawn in figure 1.4.

Metabotropic glutamate (mGlu) receptors also contribute to excitotoxicity. MGlu receptors are G-protein coupled receptors that modulate excitatory synaptic transmission. There are 8 subtypes divided into 3 groups. The group I mGlu receptors (mGlu1 and mGlu5) are predominantly found at the postsynaptic membrane of glutamatergic synapses where they increase neuronal excitability by modulating NMDA and AMPA receptors. Evidence that these receptors enhance the induction and progression of excitotoxic neuronal death is provided by the finding that pharmacologic blockade of group I mGlu receptors provides neuroprotection in *in vitro* and *in vivo* models of ischemia (Bruno et al. 2001). Group II (mGlu2 and mGlu3) and group III (mGlu4, mGlu6, mGlu7, mGlu8) mGlu receptors are predominantly found at presynaptic terminals where they inhibit the release of glutamate. Group II receptors are also widely expressed on astrocytes. Both group II and group III receptor agonists have been found to be neuroprotective by limiting the induction of excitotoxicty, however, group II receptor agonists also confer neuroprotection by

increasing production of neurotrophic factors such as nerve growth factor and TGF-β in astrocytes (Bruno et al. 2001).

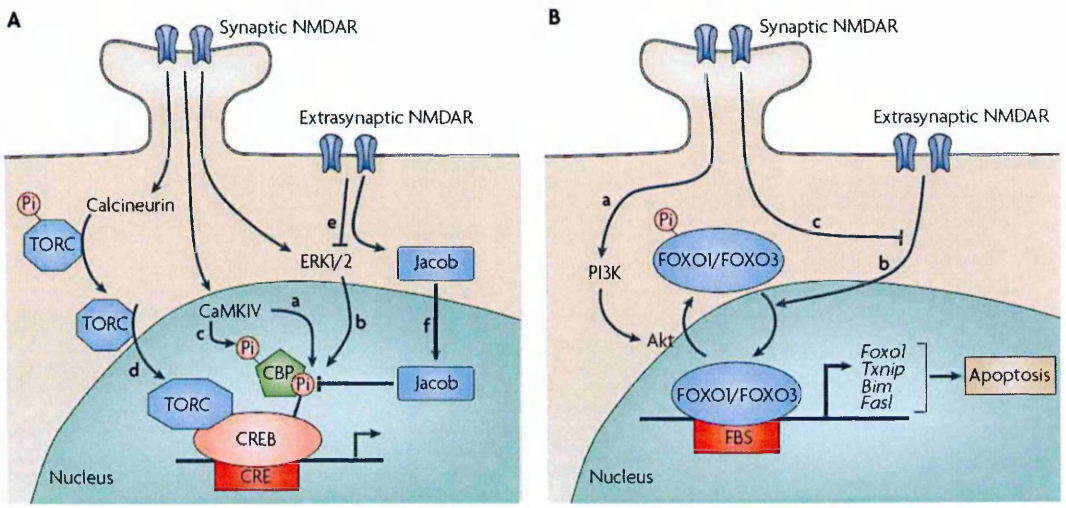

Figure 1.4 *Opposite effects of synaptic and extrasynaptic NMDA receptors.*

A: Activation of CREB by synaptic NMDA receptors is a multi-step process and needs the recrutiment of the co-activatory molecule CBP (CREB binding protein) via CREB phosphorylation. CREB phosphorylation is mediated by the activation of CaMKIV (Ca^{2+} calmodulin-dependent protein kinase IV) and ERK (extracellular signal regulated kinase) 1/2 pathway (Aa, Ab respectively) upon synaptic NMDA receptor signalling. CBP is subject to Ca2+-mediated transactivation by CaMKIV which phosphorylates CBP on serine 301 (Ac). Synaptic NMDA receptor signalling promote the nuclear import of TORC (transducer of regulated CREB activity) by TORC dephosphorylation mediated by calcineurin (Ad). TORC assists to CBP recruitment to favour CREB activation. Once activated, CREB promotes anti-apoptotic factors and neutrophic molecules. Extrasynaptic NMDA receptors are instead responsible for toxic effects via the inhibition of ERK 1/2 (Ae) and the nuclear translocation of Jacob (juxtasynaptic attractor of caldenrin on dendritic boutons protein) which dephosphorylates CBP (Af).

B: Synaptic NMDA receptors are also able to induce Akt production. Akt mediates phosphorylation and nuclear export of FOXO (forkhead box protein O) proteins (Ba). FOXOs are transcriptional factors for a number of pro-apoptotic genes. Akt-mediated phosphorylation is thus associated with anti-aptoptotic features via nuclear export of FOXOs. On the contrary, extrasynaptic NMDA receptors favour the nuclear import of FOXOs (Bb) and thus promote apoptosis. In some extent, the activity of extrasynaptic NMDA receptors can be blocked by synaptic receptors (Bc) even though this mechanism is largely unclear (Hardingham and Bading 2010).

More recent data suggest that glutamate receptors may be joined by several other mechanisms that are able to affect the deleterious consequences of ischemia and do not depend on glutamate signalling (Tymianski 2011). Among those are transient receptor potential (TRP) channels, and in particular the melastatin family (TRPM), a superfamily of nonselective Ca^{2+} permeable cation channels (Venkatachalam and Montell 2007). One element of this familiy, TRPM2, is strongly associated with toxic effects. TRPM2 is activated by excess of H_2O_2, arachidonic acid, ROS and nitrogen species (RNS), TNF and intracellular Ca^{2+} concentrations. The gene *trpm2* is upregulated in activated microglia and may confer to microglia toxic features (Fonfria et al. 2006).

The acid-sensing ion channels (ASICs) are activated by extracellular acidosis which accompanies brain ischemia. The final effect of ASICs is to increase Ca^{2+} intracellular influx, thus contributing to excitotoxicity in a glutamate-independent way (Allen and Attwell 2002; Giffard et al. 1990; Immke and McCleskey 2001; Yermolaieva et al. 2004).

Lastly, another mechanism that do not rely on glutamate metabolism is associated with activation of PANX protein (pannexin family). These proteins, although similar to the gap-junction forming proteins (innexins) are involved in the formation of large pores and may have a physiological function as well (MacVicar and Thompson 2010; Yen and Saier 2007). PANX1 is activated after oxygen glucose deprivation in cultured hippocampal and cortical pyramidal neurons, but their exact mechanism is unknown and their activation after ischemia is yet to be demonstrated in the *in vivo* setting (MacVicar and Thompson 2010; Thompson et al. 2006; Tymianski 2011).

1.2.3.2 Peri-infarct depolarisation

Cortical spreading depression (CSD) is a self-propagating wave of electrochemical activity that progresses through cortical tissue in intact brain. CSD causes sustained (1-5 min) cellular depolarization, depressed neuro-electrical activity, increased glutamate release and loss of membrane ionic gradients (Gonzalez et al. 1992). Peri-infarct depolarizations (PIDs) are spontaneous waves of depolarization with all of the characteristic features of CSD that propagate through the penumbra following focal stroke. PIDs may be caused by the release of potassium and excitatory amino acids from the ischemic core. Although CSD in the normally perfused brain does not lead to cell death, recurrent PIDs in the ischemic brain are associated with increased ischemic injury. Repeated depolarization in the penumbra may mediate tissue damage by allowing calcium to accumulate within neurons. A critical threshold of calcium could be reached in the case of PID due to the compromised energy supply of the tissue, thus causing damage in the case of PID but without evidence of lasting damage in the case of CSD. PIDs are known to occur in animal stroke models, where the incidence and duration of spreading depression correlates with infarct maturation (Strong et al. 2000). Recently Fabricius and colleagues demonstrated the existence of PIDs in the acutely injured human brain, which suggests that inhibition of spreading depression using a therapeutic approach such as hypothermia or glutamate receptor antagonism could be an important strategy to limit development of ischemic injury within the penumbra (Fabricius et al. 2006).

1.2.3.3 Inflammation

Inflammation rapidly establishes after ischemic injury and contributes to lesion evolution with long lasting effects. Many inflammatory events arise, including activation of resident immune populations (microglia and perivascular macrophages), recruitment of blood-borne cells (macrophages, lymphocytes, neutrophils and dendritic cells), activation of the complement system and development of cytokine/chemokine cascades. In patients with ischemic stroke chemokines such as monocyte chemoattractant protein-1 (MCP-1), and chemokine C-X-C motif ligand-1 are rapidly upregulated after stroke (Worthmann et al. 2010), suggesting that immune cells are quickly attracted to the ischemic area. The inflammatory response evolves over time and is characterized by an immediate reaction to acute injury, followed by acute and delayed phases, each involving specific cell types and effector molecules (see figure 1.5). The effect of individual components of the inflammatory cascade can be either detrimental or beneficial, depending on the stage of tissue injury, the magnitude of the response and whether the inflammatory component also activates neuroprotective pathways (Iadecola and Anrather 2011; Magnus et al. 2012). The inflammatory response is thus a composite process that involves many different cell types, inflammatory mediators and extracellular receptors, each with a specific function and timing of activation. As the main topic of this thesis is the study of the inflammatoy populations activated/recruited in the ischemic brain, I will provide thorough description of inflammation after stroke in section number **1.4.**

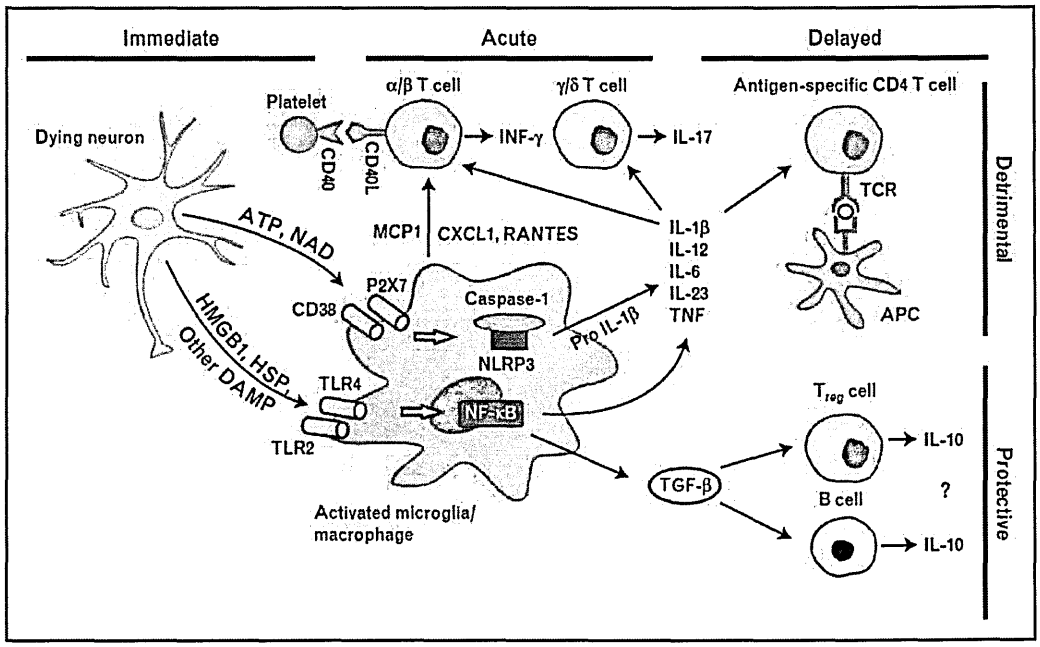

Figure 1.5 *Cascades of immune activation after stroke.*

Neurons die rapidly soon after initial acute injury. Danger signals (ATP, high-mobility group box 1 protein, HMGB1) are released and bind to P2X7 or Toll-like receptors (TLRs) on resident/early recruited immune cells. Microglia/Macrophages become activated upon sensing of danger signals and begin a downstream propagation of inflammatory molecules. The delayed response is characterized by the recruitment and activation of other immune cells (such as T-cells, here represented) that can drive either a detrimental or a protective inflammatory activity. In this phase microglia/macrophages continue to be important actors of the inflammatory cascade by changing their polarized state (see section **1.4.2.1**, Magnus et al. 2012).

1.2.3.4 Apoptosis

Mild ischemic injury preferentially induces cell death via an apoptotic-like mechanism rather than necrosis. Because the ischemic penumbra sustains milder injury and preserves ATP, apoptosis predominates in this region (Kerr et al. 1972). Triggers of apoptosis include oxygen free radicals, death receptor ligation, DNA damage, protease activation and ionic imbalance. The release of cytochrome c from the outer mitochondrial membrane plays a central role in mediating apoptosis in response to ischemia (Fig. 1.6). Release of

cytochrome c is caused by ionic imbalance and mitochondrial swelling or by formation of a pore in the outer mitochondrial membrane. The complex interplay of the Bcl-2 family of proteins either promotes (Bax, Bak, Bad, Bim, Bid) or prevents (Bcl-2, Bcl-XL, Bcl-w) pore formation. The pore is formed by oligomerization of Bax and/or Bak in the outer membrane, which in turn is activated by DNA damage. The anti-apoptotic Bcl-2 proteins, Bcl-2 and Bcl-XL, can form heterodimers with Bax, thereby preventing pore formation (Adams and Cory 2001; Edwards and Dean 1977; Hengartner 2000). Bad, Bim and Bid also influence pore formation, although the exact manner by which these molecules do so is unclear. Unlike Bax and Bak, Bid, Bad and Bim do not have the ability to directly mediate cytochrome c release by forming a pore. Instead they appear to function as sensors of cell stress that may promote apoptosis by heterodimerizing and antagonizing the function of anti-apoptotic Bcl-2/Bcl-XL and/or activating the function of Bax and Bak (Adams and Cory 2001; Edwards and Dean 1977; Hengartner 2000). Cytochrome c release activates downstream caspases of the intrinsic pathway through formation of the apoptosome, a complex of dATP, cytochrome c, procaspase 9 and Apaf1 (Fig. 1.6). Effector caspases 3 and 7 then target substrates that dismantle the cell by cleaving homeostatic, cytoskeletal, repair, metabolic, and cell signaling proteins. These caspases also cause further DNA fragmentation by activating capase-activated deoxyribonuclease (CAD) by cleaving the inhibitor protein ICAD. Caspase activation can be modulated by protein inhibitors of apoptosis (IAP) and indirectly by secondary mitochondria derived activator of caspase (Smac/Diablo). Activation of the extrinsic pathway of death receptors can induce caspase activation independent of the release of cytochrome c. Death receptor ligation results in activation of caspase-8 and caspase-10, which in turn can activate effector caspase 3 (Namura et al. 1998). Activation of death receptors such as Fas/CD95, TNFR1, and the TRAIL receptor is promoted by the TNF family of ligands, including

FASL, TNF, LT-alpha, LT-beta, CD40L, LIGHT, RANKL, and TRAIL, which are released as part of the inflammatory response to ischemia (Del Zoppo et al. 2000).

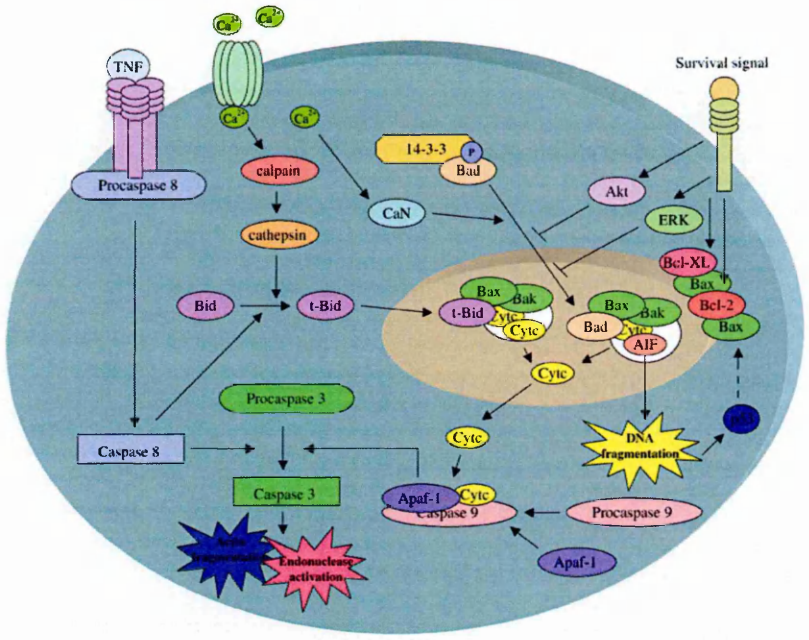

Figure 1.6 *Apoptosis in stroke.*

Cell death pathways relevant to apoptosis in cerebral ischemia. The release of cytochrome c (cyt c) from the mitochondria is mediated by the proapoptotic proteins Bax and/or Bak forming a pore in the mitochondrial membrane. Pore formation is facilitated by Bad and Bid. Calcium influx causes the dephosphorylation of Bad by calcineurin (CaN), which releases Bad from 14-3-3 and allows its translocation to the mitochondria. Calcium can also activate calpains, which can activate cathepsins that mediate the limited proteolysis of Bid, allowing truncated Bid (t-Bid) to translocate to the mitochondria. Caspase 8, which is activated by TNF receptor ligation, also mediates the limited proteolysis of Bid, allowing truncated Bid (t-Bid) to translocate to the mitochondria. Once present in the cytosol, cyt c forms the apoptosome complex by binding to Apaf-1 and procaspase 9. The apoptosome complex cleaves and activates caspase 3, which causes actin fragmentation, and endonuclease activation. Caspase 3 can also be activated by caspase 8. Apoptosis-inducing factor (AIF) can also be released from the pore created in the mitochondria, causing DNA degradation. DNA damage activates p53, which further increases Bax expression. The antiapoptotic proteins Bcl-XL and Bcl-2 prevent Bax-mediated pore formation and cyt c release. Various survival factors also prevent pore formation and cytochrome C release by activation of Akt and ERK pathways (Doyle et al. 2008).

1.3 Pharmacological treatment of stroke

Although more than three centuries elapsed from the first stroke description by Johan Jacob Wepfer (1620-1695), stroke is still an unmet medical need. The only therapy presently approved for clinical stroke is the administration of the thrombolytic agent tissue-type plasminogen activator (tPA), whose usage is however limited due to short time window of efficacy and to potential harmful side effects. The original 3h time window of tPA administration has been extended in 2008 to 4.5h as the European Cooperative Acute Stroke Study (ECASS) III trial (Hacke et al. 2008) provided evidence that a time window of 4.5h was both safe and effective. However, a further meta-analysis of all existing trials on intravenous tPA administration, showed that the proportion of patients achieving an excellent outcome of the modified Rankin Scale score declined significantly from an odds ratio of 2.4 when tPA was administered within 90 min, to 1.4 for tPA administered within 3h-4.5h time frame (Lees et al. 2010). Moreover, the beneficial effects of tPA administration at 6h after ischemic onset declined almost to zero.

Most trials of therapy indicate that tPA use was associated with risk of intracerebral hemorrhage with an odds ratio of 3.49 (Lees et al. 2010; Wardlaw et al. 2009). This rate did not increase significantly with time, even though at 6h the blood brain barrier (BBB) is potentially more porous (Lees et al. 2010). The recent meta-analysis (Lees et al. 2010) provides evidence of a little but significant increase of mortality over the 6h time window, possibly suggesting that nonhemorrhagic factors are also involved during this period. Predictors of risk and hemorrhage may include increasing age, early ischemic change on CT scan, high blood pressure, high blood glucose, high NIH Stroke Scale score, atrial fibrillation, weight (Wahlgren et al. 2008) and protocol violations (Katzan et al. 2000). There are other unwanted effects of tPA that contribute to the ischemic damage in different

ways: enhancing the excitotoxicity cleaving the NR1 or interacting with NR2 subunit of NMDA receptor; favouring the brain oedema formation; upregulating matrix metalloproteinases (MMPs); exacerbating the accumulation and the infiltration of inflammatory cells (such as lymphocytes, polymorphonucleates, leukocytes ecc.) from the periphery to the brain parenchyma (Kaur et al. 2004, Fig. 1.7).

Moreover, the use of thrombolysis for acute ischemic stroke is hampered by other reasons that are associated with low level of public awareness, poor recognition of symptoms, delays in emergency transport and a low level of expertise in tPA administration in many centres (Barber et al. 2001; Hoffman 2003; Hoffman and Schriger 2009; Kleindorfer et al. 2008; Kleindorfer et al. 2004; Kwan et al. 2004; Reeves et al. 2005). Overall, only 2-5% of eligible patients are effectively treated with thombolytic therapy in most centres, although this percentage increases in centres with a higher level of expertise (Kleindorfer et al. 2008; Nadeau et al. 2005). Thus major challenges for an effective use of the thrombolytic therapy remain, including further enhancement of its efficacy, extending the time window of administration, reducing its side effects and treating more patients within the 4.5h time window.

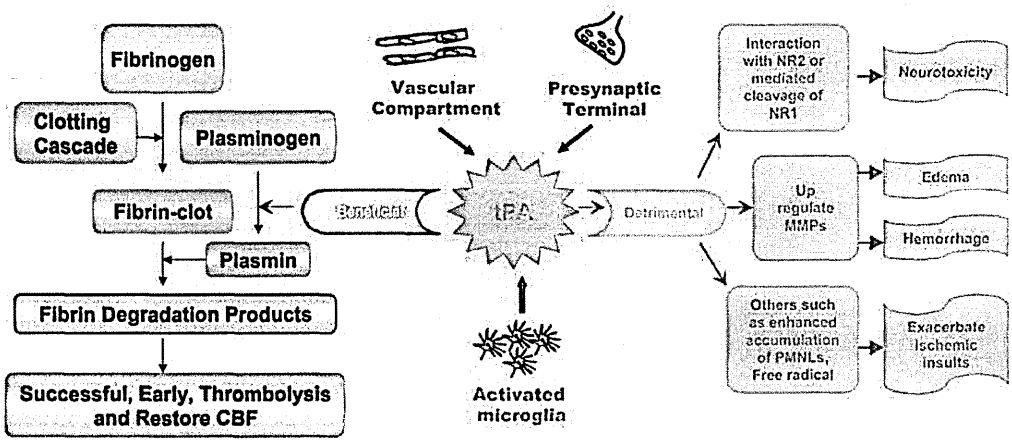

Figure 1.7 *Beneficial and detrimental effect of tPA following cerebral ischemia* (Kaur et al. 2004).

To enhance further the efficacy of the thrombolytic therapy, recent trials explored the use of bridging protocols, sonothrombosis or alternative thrombolytic agents. Bridging

protocols consist on a combined approach: after the initial intravenous injection of tPA, if recanalization is not demonstrated within a certain time frame, intra-arterial administration of tPA is also performed (International Mangement of Stroke, IMS, series of trials). IMS I and IMS II trials proved safety and feasibility of this approach in the early phase II (IMS Study Investigators 2007; IMS Study Investigators 2006; IMS Study Investigators 2004) and phase III is currently underway (Khatri et al. 2008). Sonothrombosis is based on the idea that ultrasound may enhance the effects of a thrombolytic agents, possibly by increasing drug transport to the clot (Alexandrov et al. 2004). At present, a phase II dose-ranging study indicated that a 1.4mL dose of ultrasound-activated perflutren lipid microspheres was safe and feasible, while increasing the dose was associated with increased incidence of intracerebral hemorrhage (Alexandrov et al. 2008; Molina et al. 2009). New thrombolytic agents are presently investigated. In particular, desmoteplase and tenecteplase have a longer half-life and are less associated with hemorrhagic risk (Liberatore et al. 2003; Reddrop et al. 2005; Tanswell et al. 2002). Whilst proven to be effective in phase II trials on MRI-based outcome measures, desmoteplase failed in phase III trial (Furlan et al. 2006; Hacke et al. 2009; Hacke et al. 2005). The rationale has been recently redesigned and a new phase III trial is still on course. Tenecteplase yielded encouraging results in a small pilot study (Parsons et al. 2009), being at least as effective as tPA and with no hemorrhagic effects when dosed at 0.1 mg/Kg. Bigger phase III trails are needed to substantiate these results but, unfortunately, a phase III trail in the USA terminated due to insufficient patient recruitment (Haley et al. 2010).

Many efforts have been done to extend the time window of efficacy of the thrombolytic therapy. However, to date, as previously discussed, 4.5h represents the time by which tPA must be administered to be effective. The recent IST-3 trial (Sandercock et al. 2012) provided evidence that patients treated up to 6h with tPA survived with less disability at 6 months, whilst no difference was observed in 6 month mortality. This study confirmed the

policy of treating patients as soon as possible, and supported the need of randomised trials of thrombolysis in patients more than 4.5h after stroke onset. Besides, IST-3 succeeded in extending the number of patients eligible for tPA treatment, including patients older than 80 years of age and excluding restriction of treatment on the basis of stroke severity or early ischemic changes in CT scans (Sandercock et al. 2012).

Another approach that could be useful to treat stroke patients consists in neuroprotective therapies. Differently from thrombolytic agents, neuroprotection refers to the use of therapies that reduce brain injury during acute stroke, generally through actions on the brain itself rather than by directly improving blood flow and perfusion through occluded cerebral vessels. Included in this group of therapies are a large number of medications, as well as strategies such as hypothermia designed to interfere more generally with adverse metabolic consequences of stroke (Sacco et al. 2007). Agents with several different mechanisms of action have been tested. For instance, minocycline have been demonstrated to reduce hemorrhagic effects of tPA treatment in experimental models acting via MMP9 (Machado et al. 2009; Machado et al. 2006; Murata et al. 2008) and to have broad anti-inflammatory proprieties (Fagan et al. 2010). Recently clinical trials using minocycline and tPA have been initiated (Fagan et al. 2010; Lampl et al. 2007). Other clinical trials have been performed using strategies aimed at interfering with the inflammatory response. A phase II placebo-controlled trial explored treatment with IL-1 receptor antagonist and found that blockade of IL-1 receptor reverses suppression of innate immune cytokine responses and attenuates the maintained elevation of plasma cortisol in stroke patients (Smith et al. 2012). The study is not yet completed and further and wider studies are needed to substantiate encouraging results.

Blocking antibodies against the adhesion molecule ICAM-1 or recombinant neutrophil inhibitory factors (Del Zoppo 2004) were unfortunately ineffective in the clinical setting,

while an indirect modulation of the immune activity via remote preconditioning has recently entered in an ongoing trial (Koch et al. 2011). Thus, although in many pre-clinical studies specific receptors and pathways related to the inflammatory response have been manipulated yielding promising results, none of the therapeutic interventions aimed at modifying the inflammatory response after stroke have been successful in humans (Iadecola and Anrather 2011). The possible reasons for these failures might be due to shortcomings in trial design rather than absence of efficacy of the agents tested (O'Collins et al. 2006), or to the fact that several aspects of brain immunity still need to be revealed. At present, however, acute stroke treatment guidelines do not advocate treatment with any neuroprotectant agent (Adams et al. 2005; Donnan et al. 2011; Sacco et al. 2007).

1.4 Inflammation in the Central Nervous System

In the late 19th century, Paul Ehrlich observed that a water-soluble viable dye injected into the peripheral circulation would stain all organs except the CNS, providing the first indication that the CNS was anatomically separated from the rest of the body. The idea that the brain was an unique anatomical compartment was further confirmed by Edwing Goldman that showed that a dye injected into the spinal fluid did not stain peripheral tissues. It is now well known that this is due to the presence of the blood brain barrier (BBB), that restricts acces to the brain to soluble factors, including 98% of antibodies, and immune cells (Ge et al. 2008; Hawkins and Davis 2005; Mrass and Weninger 2006). This feature along with the lack of lymphatic system, low constitutive levels of MHC class I and II molecules, local production of suppressive factors and limited number of professional antigen presenting cells, reinforces the concept of the CNS as an immuno-privileged site (Wilson et al. 2010). Thus in normal conditions presence and trafficking of immune cells

in the brain are negligible. Physiological homeostasis of the brain is ensured by microglia which are generally defined as the resident immune cells of the CNS (Kim and De Vellis 2005). These resident cells act mainly to stabilize the CNS by counteracting microdamages that possibly occur in the brain, such as small ischemic events, localized opening of the BBB, decline of neurons that must be removed (Hanisch and Kettenmann 2007).

In more severe diseased states, microglia as well as peripheral immune cells are recruited and activated to lesion sites. Microglia are well positioned throughout the brain to rapidly sense any disturbances (Denes et al. 2007), while peripheral immune cell recruitment is facilitated by the activation of endothelial cells and BBB associated cells (*i.e.* astrocytes) leading to reduced tight junction integrity and formation of transendothelial cell channels (Lossinsky and Shivers 2004; Raine et al. 1990; Wolburg et al. 2005). Several neurodegenerative disorders and infectious diseases are characterized by activation of inflammatory pathways whose effects could be of opposite nature. Although the ability to recognize infections and establish an inflammatory response in the CNS is required to limit pathogen replication, this response is not always beneficial. The classical features of inflammation, such as swelling and expansion, could be harmful given the presence of the rigid skull bone. Furthermore, although the immune system can contribute to the successful resolution of the tissutal damage associated with many CNS disorders (Byram et al. 2004; Simard et al. 2006), inflammation itself can drive multiple neurodegenerative conditions including Parkinson disease, Alzheimer disease and lysosomal storage diseases (Brochard et al. 2009). After brain ischemia, inflammation can have either protective or detrimental effects depending on timing of activation, populations involved, molecular signals released and location in respect to the lesion site. A clear understanding of the rules that govern brain immunity may inform the design of strategies aimed at augmenting the protective immune repsonses while minimizing collateral damage. The past two decades have seen remarkable advances in the comprehension of immune cell trafficking, activation and

functions within the CNS, but many aspects of brain immunity still remain to be fully elucidated.

1.4.1 Inflammation after stroke

1.4.1.1 Time dependent recruitment of immune cells to ischemic lesion site

After the ischemic insult immune populations are rapidly activated. These populations belong to both innate and adaptive responses and are recruited to the site of injury, where they further promote inflammatory signalling (Iadecola and Anrather 2011) with either detrimental or beneficial effects (Nawashiro et al. 2000; Zhang et al. 2000). Recruitment/activation of immune cells takes place in a time-dependent manner. As mentioned above, the inflammatory response is a composite process that involves many inflammatory cell types. The primary source of granulocytes and monocytes which are recruited to the ischemic brain is the bone marrow (D'Mello et al. 2009; McColl et al. 2008). Experimental evidence indicate that myeloid cells in the bone marrow respond very rapidly to ischemia, as suggested by the mobilization of Gr-1 (marker of myeloid cells) positive cells within 4h after MCAo (Denes et al. 2011). Within the first hours after ischemia, resident microglia are activated, undergo a morphological switch and begin producing inflammatory cytokines, including tumor necrosis factor α (TNFα) and interleukin (IL)-1β. After the early activation of microglia response, immune cell types coming from the peripheral immune system, such as neutrophils, macrophages, dendritic cells (DCs) and T-Lymphocytes, are recruited to the site of injury (Garcia et al. 1994) according to a well define time course (Gelderblom et al. 2009). Macrophages, DCs and T-lymphocytes accumulate soon after microglia activation, reaching their peak of presence

by the first 3-4 days after injury. The early accumulation of these immune cells favours the subsequent influx of neutrophils by the upregulation of cell adhesion molecules including intercellular adhesion molecule-1, vascular cell adhesion molecule-1 and E-selectin, thereby promoting neutrophil accumulation and migration into the brain parenchyma (Gelderblom et al. 2009; Huang et al. 2006). The transmigration of neutrophils through activated cerebral endothelium is capable to confer a neurotoxic phenotype to these cells (Allen et al. 2012). Neutrophil neurotoxicity develops rapidly after IL-1-induced transmigration and is characterized by the release of toxic proteases associated with de-condensed DNA (Allen et al. 2012). Neurotoxic neutrophils are endowed with the ability to kill neurons immediately after recruitment and to induce further cerebrovascular activation and leukocyte recruitment since they contain high levels of pro-inflammatory cytokines, such as KC, MCP-1 and RANTES (Allen et al. 2012).

Over the last years, growing attention has been payed to inflammatory mechanisms driven by microglia/macrophages and T-cells after ischemia, aimed at depicting the exact behavior of both resident and recruited immune cells in the ischemic context. These populations, altough participating in the pro-inflammatory cascades, are also capable of protective and regenerative functions (Iadecola and Anrather 2011; Magnus et al. 2012). However, many aspects of the behavior of these populations remain elusive, and further studies are needed to understand the complex inflammatory response induced by brain ischemia, in the view of developing strategies resulting in promotion of a protective inflammatory phenotype.

1.4.1.2 The cytokine inflammatory response

Cytokines and chemokines contribute to stroke-related brain injury (Gong et al. 1998). During ischemia, cytokines, such as IL-1, IL-6, TNF-α, TGF-β and chemokines such as CINC and MCP-1 are produced by a variety of activated cell types, including endothelial cells, microglia, neurons, platelets, leukocytes, and fibroblasts (Huang et al. 2006, Fig. 1.8). Production of IL-1 is increased after permanent or transient cerebral ischemia in microglia, astrocytes, and neurons. The exact role of IL-1 in propagating tissue damage is unclear, although possible deleterious effects of IL-1 include fever arachidonic acid release, enhancement of NMDA mediated excitotoxicity, and stimulation of nitric oxide synthesis (Huang et al. 2006). An additional role of IL-1 may be recruitment and adhesion of neutrophils. IL-1 has been shown to cause up-regulation of E-selectin, ICAM-1, ICAM-2, and VCAM-1 on cerebral endothelial cells and the induction of such adhesion molecules may explain why elevated IL-1 levels after ischemia increases neutrophil infiltration (Huang et al. 2006; Yamasaki et al. 1997). That the effects of IL-1 are deleterious was demonstrated by Garcia and Relton who showed that administration of recombinant IL-1 receptor antagonist reduces the severity of neurologic deficits and tissue necrosis in rats subjected to permanent MCAo (Garcia et al. 1995; Relton et al. 1996).

In rats subjected to permanent MCAo, IL-6 mRNA expression is up-regulated as early as 3h after occlusion, peaks at 12h, and continues for at least 24h (Wang et al. 1995). The biological activity of IL-6 overlaps with those of IL-1, and data from human studies suggest a pro-inflammatory role for IL-6 in stroke. Peripheral blood levels of IL-6 are higher in stroke patients and detectable within a few hours of stroke onset and higher CSF and serum levels of IL-6 correlate with larger infarct size and poorer clinical out come (Huang et al. 2006). However, in experimental models, IL-6 has been associated with anti-

apoptotic and anti-inflammatory properties due to its ability to induce IL-1 receptor antagonist synthesis (Relton et al. 1996). Thus, it is unclear whether the overall effect of IL-6 is beneficial or detrimental in the context of stroke.

Up-regulation of TNF-α mRNA parallels that of IL-1 and IL-6 mRNA within the first hours after ischemia (Huang et al. 2006). Both experimental and human data indicate a positive correlation between TNF-α and the extent of ischemic injury. For example, a study of 24 patients with ischemic stroke found that CSF levels of TNF-α were markedly increased within 24 h of ischemic stroke and that the levels of CSF and serum TNF-α were positively correlated with infarct volume (Zaremba et al. 2001). Like IL-1, TNF-α induces adhesion molecule expression in cerebral endothelial cells and promotes neutrophil accumulation and transmigration. In addition TNF-α stimulates acute-phase protein production, disrupts the blood-brain barrier and stimulates the induction of other inflammatory mediators. However, recent findings on animal models of brain diseases, including ischemia, indicate that TNF-α may be involved in protective mechanisms as well (Balosso et al. 2005; Fontaine et al. 2002; Genovese et al. 2008; Lambertsen et al. 2009; Quintana et al. 2005). This may be due to the ability of TNF-α to bind two different surface receptors, TNFR1 (p55) and TNFR2 (p75, MacEwan 2002; Wajant et al. 2003) which may result in opposite outcome. These receptors specifically bind TNF-α, but have different expression profile, ligand affinity, cytoplasmic tail structure and downstream signalling pathway activation. TNF-associated neuroprotection following cerebral ischemia has been shown to occur via the p55 receptor (Taoufik et al. 2008; Taoufik et al. 2007). A further work indicated that microglia are able to induce neuronal protection by TNF-α synthesis and release (Lambertsen et al. 2009). The molecular basis of the different role of TNF-α action in brain ischemia needs to be fully elucidated and could involve several aspects, including specific timing of activation, different binding affinities of TNF-α to each receptor, different expression of the two receptors in brain areas and/or selected cell

populations, and different ligand concentration. A further degree of complexity is represented by the existence of cross-talk between two receptor pathways.

Growing evidence suggests that TGF-β plays a neuroprotective role in the pathogenesis of stroke. In rodent models of cerebral ischemia, increased expression of TGF-β mRNA is demonstrated in ischemic tissues as early as 1-6 h after the ischemic event and remains elevated for up to 15-21 days (Wiessner et al. 1993). The effects of TGF-β upon stroke volume have been studied with intracarotid and icv administration and TGF-β has been found to be neuroprotective if administered before or after the ischemic insult (Huang et al. 2006). It is likely that the neuroprotective effect of TGF-β is the concerted result of the activation of several neuroprotective pathways. TGF-β1 has a concentration-dependent protective effect against neuronal injury caused by glutamate excitotoxicity *in vitro*, and recent evidence indicates that administration of a TGF-β1-blocking agent increases the extent of excitotoxic lesions after focal cerebral ischemia (Huang et al. 2006). Data also exist to supporting a role for TGF-β in diminishing ischemia-induced endothelial dysfunction (Lefer et al. 1993).

Increased expression of CINC and MCP-1 mRNA are detected in the brain of rats as early as 6 h after permanent MCAO, reach a maximal level at 12 h and are decreased by 24 h (Minami and Satoh 2003). CINC and MCP-1 expression attracts neutrophils to ischemic tissue, evidence for which comes from rodent experiments using transient ischemia, where CINC and MCP-1 are detectable in cerebral tissue before neutrophil infiltration (Huang et al. 2006). In rats, administration of anti-CINC antibody decreases cerebral edema and infarction, which further supports a role for CINC in mediating neutrophil infiltration and demonstrates another therapeutic opportunity (Yamasaki et al. 1997).

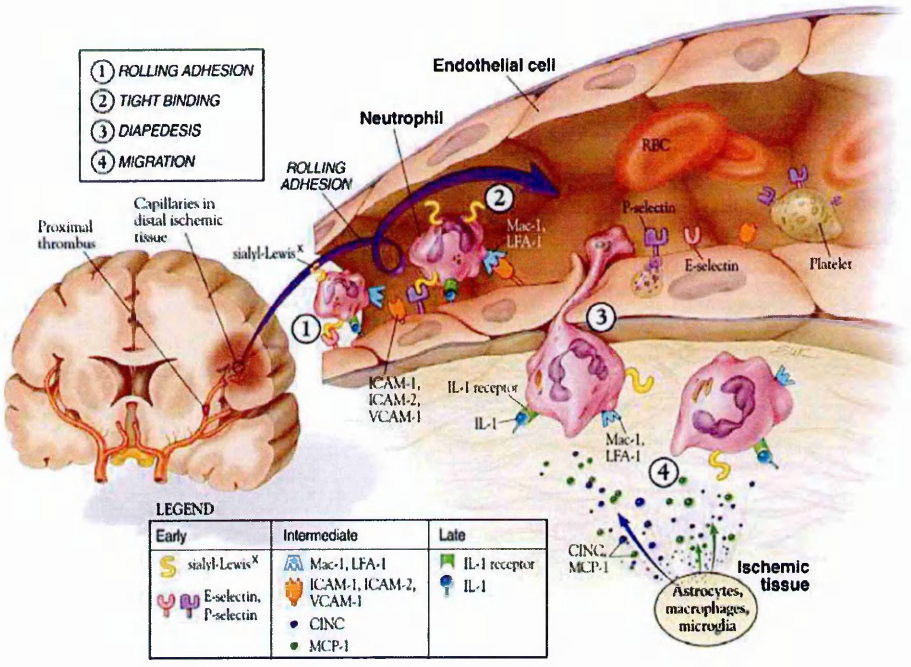

Figure 1.8 *Inflammatory cascades following vessel occlusion.*

Occlusion by a proximal thrombus leads to inflammatory cascades in the capillaries of distal ischemic tissue. P-selectin is released from preformed storage sites and, together with E-selectin, binds to sialyl–Lewis X moieties to promote rolling adhesion of neutrophils (1). Ischemia induces expression of IL-1 on endothelial cells that then induce expression of ICAM-1 on surface of endothelial cells. Integrins macrophage-1 antigen (Mac-1) and lymphocyte function-associated-1 antigen (LFA-1) on neutrophil surfaces binds intercellular adhesion molecule-1 and -2 (ICAM-1, ICAM-2), and vascular cell adhesion molecule-1 (VCAM-1) causing tight binding (2). Astrocytes, macrophages, and microglia in ischemic brain tissue release cytokine induced neutrophil chemoattractant (CINC) and MCP-1 in response to ischemically-driven cytokines. These chemokines signal neutrophil diapedesis and migration into the brain parenchyma, leading to tissue destruction (3 and 4, Huang et al. 2006).

1.4.2 Microglia/Macrophages and Lymphocytes: double-edged swords in ischemic damage evolution

1.4.2.1 Microglia/Macrophages

1.4.2.1.1 Ontogeny and activation

Microglial cells are considered the immune cells of the CNS (Kim and De Vellis 2005). It is now generally acknowledged that all CNS disorders are characterized by activation of microglia and that the progression and resolution of many diseases is contingent in part on the activity of microglia (Ransohoff and Cardona 2010). In the early 20th century, Cajal identified three cell populations composing the brain: neurons (which he called the first element), astrocytes (second element) and a third element characterized by small, round nuclei. Between 1919 and 1921, del Rìo-Hortega proposed that the third element comprised two distinct cell populations: oligodendrocytes (Gill and Binder 2007), more related to astrocytes and therefore belonged to the second element, and authentic third element cells, for which he firstly coined the term 'microglia'. He also suggested that these cells could transform themselves into migratory phagocytic cells.

Ontogeny of microglia has beeen a matter of debate for years and neuroscientists and neuroimmunologists have been working to understand how microglia fit in the overall scheme of mononuclear phagocytes, the category which microglia belong to. Current data indicate that they are of mesenchymal origin and invade the brain in two waves: the first during fetal development and the second in the early post-natal days, in both rodents and humans (Chan et al. 2007). Microglia have proprieties of monocytes and probably derive from myeloid-lineage progenitors (Fig. 1.9). As they set into the brain, microglia cells differentiate acquiring their typical phenotype characterized by small soma and highly

branched processes. At the end of development, microglia have populated all regions of the CNS, including the retina (Hanisch and Kettenmann 2007) representing the 20% of total glial populations within the brain. The rate of microglia turnover in the healthy adult brain is expected to be low, as a study on mouse retina reported a complete turnover in 6 months (Xu et al. 2007a). However this study was conducted using an experimental approach that included irradiation for depleting the intrinsic monocyte population prior to transplantation of bone marrow cells. Criticism of this approach regards the possible effects of irradiation itself on BBB integrity that may augment cell infiltration.

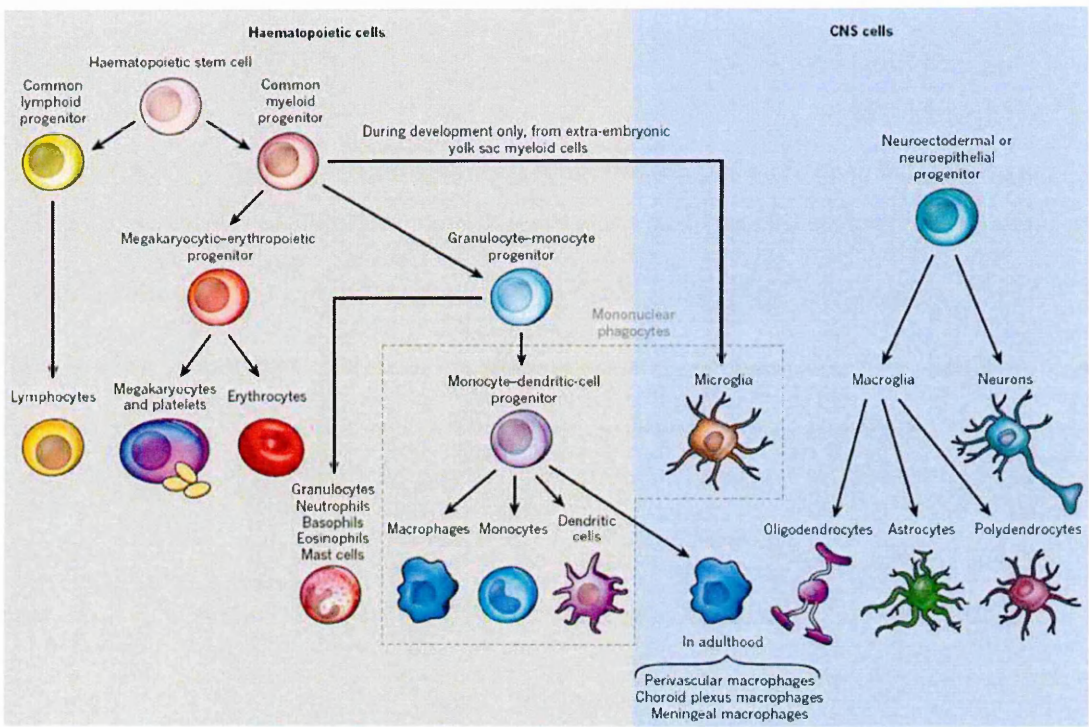

Figure 1.9 *Hematopoietic origin of microglia/macrophages.*

Arrows indicate lineage relatedness. Microglia and macrophages derive from common myeloid progenitors. Microglia settle within the CNS where they become the resident immune population of healthy CNS (Ransohoff and Cardona 2010).

There is also a population of perivascular cells that shares some features with immature microglia. These cells turn over more rapidly than parenchymal microglia (in 14 weeks) and probably turn over equally across different brain areas (Bechmann et al. 2001b;

Bechmann et al. 2001a). Surprisingly, little is known about heterogenity of microglia cells within different brain regions under physiological conditions. As mentioned above, parenchymal microglia are different from perivascular monocytes, nevertheless specifically adapted microglia cells may exist in specific CNS regions. White or gray matter location, proximity to vasculature, BBB features, biochemical microenvironment and substances released from neurons could impose specific adjustements of microglia phenotype (Binstadt et al. 2006; Galea et al. 2007). However subsets of microglia might exert different functions without being clearly distinguishable on the basis of morphology or single marker expression. There are few studies that indicate that hippocampal microglia express high levels of messenger RNA for TNFα which is associated with exacerbated hippocampal damage in TNFR knock-out mice in a model of Parkinson disease (Sriram et al. 2006). Evidence also exists for microglia subsets that can be distinguished on the basis of morphology and LPS response (Kuwabara et al. 2003). Some diversity in microglia basal activities could also be related to developmental adjustements as proliferative or phagocytic behavior changes with transition from embryonic to neonatal or postnatal stages until adulthood (Ladeby et al. 2005).

On the contrary, in response to a CNS disease, microglia activation shows a *plethora* of functional states, characterized by a specific pattern of receptor expression, released molecules and morphological features. The transition between resting and activated state should be considered a change in functional phenotype rather than an awakening. Microglia in resting state are not dormant, but do perform active surveillance of surrounding microenvironment (Davalos et al. 2005). Cells depart from surveillance mode and acquire a reactive profile to cope with altered homeostasis (Fig. 1.10). Reactive microglia have different functional states that reflect the complexity of these cells and their ability to differentiate towards a multitude of phenotypes that can result either in protective or detrimental effects.

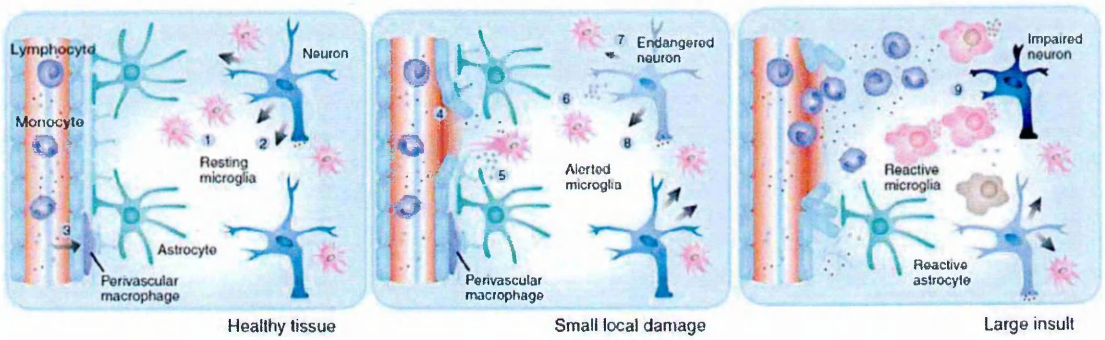

Figure 1.10 *States of microglia activation.*

Left: in the healthy tissue, microglia do perform microenvironmental sampling by continuos rebuilding of their processes (1). Microglia are equipped with receptors for a plethora of molecules to immediately sense signs of disturbed structural and functional integrity. Neurons may deliver signals keeping microglia in this surveillance mode (2). Besides the parenchymal microglia, there are also perivascular macrophages in closer association with blood vessels (3). Subsets of circulating monocytes may replenish perivascular cells, and to a much lesser extent also replenish the parenchymal microglia.

Middle: microglia rapidly re-organize their processes in response to a vascular or tissutal damage (4). Astrocytes do also participate in supporting the rapid microglial response (5). Microglia can produce neurotrophic factors to support endangered neurons (6). Disruption of ongoing communication through calming signals would allow an endangered neuron to call for microglial assistance (7). Such neurons can also emit signals indicating disturbed functions using molecules that are not usually released (at all or at critical concentrations (8). Microglial cells may be able to limit further damage and restore normal homeostasis.

Right: stronger challenges to the CNS cause a more drastic activation of microglia. Depending on the nature of the stimuli and their context, microglial cells acquire and adapt reactive behavior. Excessive acute, sustained (chronic) or maladaptive responses of microglia may lead to substantial impairment of neurons and glia (9). Failure of protection and an active contribution to damaging cascades have been attributed to activated microglia in many pathologic scenarios (Hanisch and Kettenmann 2007).

Macrophages are recruited to the brain as an injury occurs. They share with microglia a common myeloid progenitor and are defined as mononuclear phagocytes. Starting at the later stages of gestation, in which they are involved in the formation of blood vessels (Fantin et al. 2010), mononuclear phagocytes are continually renewed from the bone

marrow hematopoietic stem cells throughout life. They derive from a granulocyte-monocyte progenitor which is able to generate macrophages, monocytes and dendritic cells. Tissutal macrophages can be derived from blood monocytes or from circulating mononuclear phagocyte progenitors that settle in the brain originating perivascular, choroid plexus and meningeal macrophages (Ransohoff and Cardona 2010, Fig. 1.9). Their maintainance is due to either local self-renewal or influx of cells from the circulation. As an injury occurs, a further influx of macrophages into the brain is allowed by the increase of adhesion molecule expression on endothelial walls and by the leakage of the BBB. Once recruited to the brain, macrophages undergo activation leading to non-specific defense (innate immunity) as well as initiation of adaptive immunity. Similarly to what observed for microglia, macrophages exhibit a plastic nature, being able to exert either detrimental or protective functions upon activation (Porta et al. 2011; Porta et al. 2009).

Activated microglia and blood-born macrophages recruited to the injured ischemic brain are barely antigenically distinguishable and will be henceforth referred to as microglia/macrophages (M/M). After an insult to the CNS, including ischemia, M/M are able to switch their phenotype in a wide range of polarization activation states whose extremes are M1 detrimental phenotype and M2 protective phenotype.

1.4.2.1.2 M1-M2 extremes of M/M polarization

Among the inflammatory cells, M/M are major cellular contributors to post-injury inflammation (Graeber 2010; Ransohoff and Cardona 2010). After acute brain injury, a rapid activation with dramatic morphological and phenotypic changes of the resident microglial cells has been described. Within minutes after the insult, these cells migrate to and start surrounding the lesion site. This initial intrinsic response is followed by massive

expansion of activated microglia and by the recruitment of bloodborn macrophages which also migrate after a delay of several days into the injured brain parenchyma (Schilling et al. 2005). Typical morphological changes associated with activation of resident microglia include thickening of ramifications and of cell bodies followed by acquisition of a rounded amoeboid shape. This process is accompanied by expression of novel surface antigens and production of mediators that build up and maintain the inflammatory response of the brain tissue. Through the release of several harmful components such as IL-1β, TNF-α, proteases and ROS species (Hanisch 2002), microglia can affect neuronal function and promote neurotoxicity (Block et al. 2007). On the other hand, there is also growing evidence showing that under certain circumstances, these cells can be neuroprotective (Lalancette-Hébert et al. 2007; Neumann et al. 2006) and can also promote adult neurogenesis and lesion repair. Indeed, microglia has been proposed to be neurosupportive by several mechanisms including glutamate uptake (Nakajima et al. 2008), removal of cell debris (Stoll and Jander 1999) and production of neurotrophic factors such as IGF-1 (Thored et al. 2009), GDNF (Lu et al. 2005) and BDNF (Batchelor et al. 1999). Regarding macrophages, studies addressing their phenotypic changes in peripheral inflammation and immunity have shown that these cells can undergo two different forms of polarized activation. The first is the classic (or M1) activation, characterized by high capacity to present antigen, high production of NO and ROS and of proinflammatory cytokines. M1 cells act as potent effectors that kill micro-organisms and tumor cells and drive the inflammatory response and may mediate detrimental effects on neural cells. The second phenotype (M2) is an alternative apparently beneficial activation state more related to a fine tuning of inflammation, scavenging of debris, promotion of angiogenesis, tissue remodeling and repair. Specific environmental signals are able to induce these different polarization states (Porta et al. 2009). In particular, stimulation via TLR ligands and INF-γ induces classical M1 activation, while IL-4/IL-13 stimulation is able to favour the alternative M2 activation

(Sica and Mantovani 2012). A similar possibility has been also recently raised for microglia, by showing that these cells, under certain conditions, can indeed be pushed to both extremes of the M1 and M2 differentiation spectrum (Michelucci et al. 2009).

The revelation that macrophages, depending on the disease context, can become polarized to pro- and anti-inflammatory states that exhibit either harmful or protective/reparative proprieties, has been firstly obtained by research in non-CNS fields (bacterial and parasitic infections, non-neural tumors, David and Kroner 2011). M1 and M2 canonical definitions represent the extreme of macrophage polarized states as they have been documented by *in vitro* experiments (David and Kroner 2011). These states, under certain pathological conditions (parasite infections, allergy, cancer) are well mirrored *in vivo* (Sica and Mantovani 2012). However in neurodegenerative disorders M/M cells with mixed phenotypes have been also identified (Sica and Mantovani 2012), indicating the plastic nature of M/M, which have the ability of acquiring multiple phenotypes in response to signals received and time-dependent variations in the inflammatory melieu. A generally accepted classification of the M/M repertoire of polarized states indicates one M1 toxic polarization and three M2 polarization subtypes, namely M2a, M2b and M2c, each of which characterized by a specific pattern of marker expression and functionality (David and Kroner 2011), Table 1.1. M1 is associated with phagocytosis, ability to kill intracellular pathogens by iron restriction, acidification of phagosome and release of reactive oxygen species (Mantovani et al. 2004; Mantovani et al. 2002; Martinez et al. 2008; Martinez et al. 2006). M1 markers of phenotype include CD16, CD32, CD86, MHC II and iNOS. M2a polarized state is associated with immunity against parasites, recruitment of Th2 cells, tissue repair and growth stimulation. This state is characterized mainly by the expression of Arginase-1, Ym1 and Fizz (Gordon 2003; Gratchev et al. 2001; Hesse et al. 2001; Mantovani et al. 2004; Mantovani et al. 2002; Martinez et al. 2008; Martinez et al. 2006; Raes et al. 2005; Scotton et al. 2005; Stein et al. 1992; Villalta

et al. 2009). M2b has either pro- and anti-inflammatory functions and is associated with memory immune response (B cell class switch and recruitment of regulatory T cells). High levels of IL-10 expression, MHC II and costimulatory CD86 stand as M2b pattern of phenotype markers (Anderson and Mosser 2002a; Anderson and Mosser 2002b; Filardy et al. 2010; Gea-Sorlí et al. 2011; Goerdt and Orfanos 1999; Mantovani et al. 2004; Mantovani et al. 2002; Martinez et al. 2008). M2c is involved mainly in scavenging of cell debris, has pro-healing functions and is characterized by the expression of the markers Arginase-1, CD163 and CD206 (Bogdan et al. 1992; Goerdt and Orfanos 1999; Gordon 2003; Gratchev et al. 2001; Mantovani et al. 2004; Mantovani et al. 2002; Martinez et al. 2008; Valledor and Ricote 2004; Villalta et al. 2009).

The definition of M/M polarized states in CNS diseased states needs further studies using *in vivo* models of pathology. Events such as infiltration of leukocytes play an important role in orchestrating the polarization of M/M, making the *in vivo* studies far more instructive than *in vitro* models, in which the complete network of recruited/activated cells can not be reproduced (Sica and Mantovani 2012).

Subtype	Polarization	Cytokines	Chemokines	Phenotypic markers	Additionally expressed molecules	Function and mechanisms	Refs
M1	IFNγ and LPS–TLR4 signalling	IL-1, IL-6, IL-12, IL-15, IL-23 and TNFα	CCL8, CCL 15, CCL 19, CCL 20, CXCL9, CXCL 10, CXCL 11 and CXCL 13	CD16, CD32, CD86, MHCII and iNOS	• IL-2Rα, IL-15Rα, IL-7R, COX2 and CSPG	Phagocytosis, ability to kill intracellular pathogens by iron restriction, acidification of phagosome and release of ROI and NO	123,139 148,149
M2a	IL-4 or IL-13	TGFβ, IL-10, IL-1Ra, fibronectin 1, IGF1 and PDGF	CCL13, CCL14, CCL17, CCL18, CCL22, CCL23, CCL24 and CCL26	Arginase 1 (mouse), CD163, CD204, CD206, YM1 and Fizz 1	• COX2, CD302, CD209, CLEC4A (human), MS4A4A, MS4A6A and IL-1Ra • Fibrinogenic factors: βIG-H3, coagulation factor XIII and prothrombinase	Immunity against parasites, growth stimulation, tissue repair, collagen formation, and recruitment of T_H2 cells, basophils and eosinophils	123,139, 148–156
M2b	Immune complexes (binding of FcγR) and IL-1β or LPS	IL-10, TNFα, IL-1 β and IL-6	CCL1, CCL 20, CXCL1, CXCL2 and CXCL3	IL-10^{high}, IL-12^{low}, SPHK1, MHCII, CD86 and CD163	• Downregulation of IL-12	Pro- and anti-inflammatory function, B cell class switch and antibody production, recruitment of regulatory T cells (T_{Reg} cells). Phenotype can be induced by clearance of apoptotic neutrophils.	139,148, 149, 157–162
M2c	IL-10, TGFβ or glucocorticoids	None known	CCL16, CCL18 and CXCL13	Arginase 1, CD163, CD204 and CD206	• TLR8, TLR2, IL-21R • Polarization with IL-10: downregulation of TNFα, IL-6, IL-12 and MHCII • Polarization with TGFβ: downregulation of TNFα, IL-1 α, IL-18, CD163 • Polarization with glucocorticoids: downregulation of TNFα, IL-4, IL-5, IL-1, IL-6, IL-8, IL-12, iNOS, COX2 and CX3CR1, and increase of CD163	Debris scavenging, pro-healing function and iron sequestration	105,139, 140,148, 149,156, 157, 163–165

Table 1.1 *M1 and M2 classes of polarized states for microglia/ macrophages.*

The repertoire of M/M polarized states includes M1 and M2 subsets with a specific pattern of phenotype markers and cyto-, chemo- kines produced. Each subset has a peculiar function able to impact on acute damage evolution (David and Kroner 2011).

1.4.2.1.3 CX3CL1:CX3CR1 signalling pathway

CX3CR1 is the receptor for the chemokine Fractalkine (CX3CL1). In the CNS the CX3CL1:CX3CR1 pathway is involved in the communicaton between neurons and microglia, since neurons are the primary source of Fractalkine and CX3CR1 is almost exclusively expressed on microglia (Cardona et al. 2006). Under physiological conditions, CX3CL1 is released by neurons in a soluble form, probably by the activity of disintegrin-like metalloproteinases such as ADAM10 (Hundhausen et al. 2003). Upon binding with CX3CR1 on microglia, CX3CL1 determines the control of microglia activation, with suppressive functions (Zujovic et al. 2000). Following an acute insult, neurons

significantly decrease the release of fractalkine allowing the activation of microglia (Hundhausen et al. 2003; Lauro et al. 2006).

CX3CR1 is also present on a subset of CNS resident monocyes, characterized by a Ly-$6C^{low}$/CCR2-/CX3CR1+ phenotype. These cells patrol blood vessels to rapidly sense vascular damages. They become activated and cause early transient inflammatory bursts helping subsequent recruitment of effector cells prior to switch towards an M2-like phenotype (Geissmann et al. 2010; Prinz and Priller 2010).

In the periphery, CX3CL1 is present on endothelial cells and functions as an adhesion molecule and chemoattractant for leukocytes (Imai et al. 1997). Peripheral immune cells have been indeed shown to express CX3CR1 in an inducible way, even though their recruitment to the brain seems to rely mainly on CCR or CXC families of receptors (Ingersoll et al. 2011; Prinz and Priller 2010; Saederup et al. 2008). Circulating monocytes manifest a $Ly6C^{high}$/CCR2+/CX3CR1- phenotype and enter the brain via signalling by CCL2, a chemokine produced by reactive astrocytes (Ransohoff 2011). Once infiltrated, $Ly6C^{high}$ monocytes are induced to transform into macrophages by local cytokine and tissutal signals.

Resident microglia exhibit high levels of CX3CR1. Their turnover is due to the balance between apoptosis of senescent CX3CR1+ microglia and generation of new cells from CX3CR1+ local microglia progenitors (Ajami et al. 2011). In the inflamed CNS, microglia are activated and undergo morphological and phenotypical changes (Fig. 1.11).

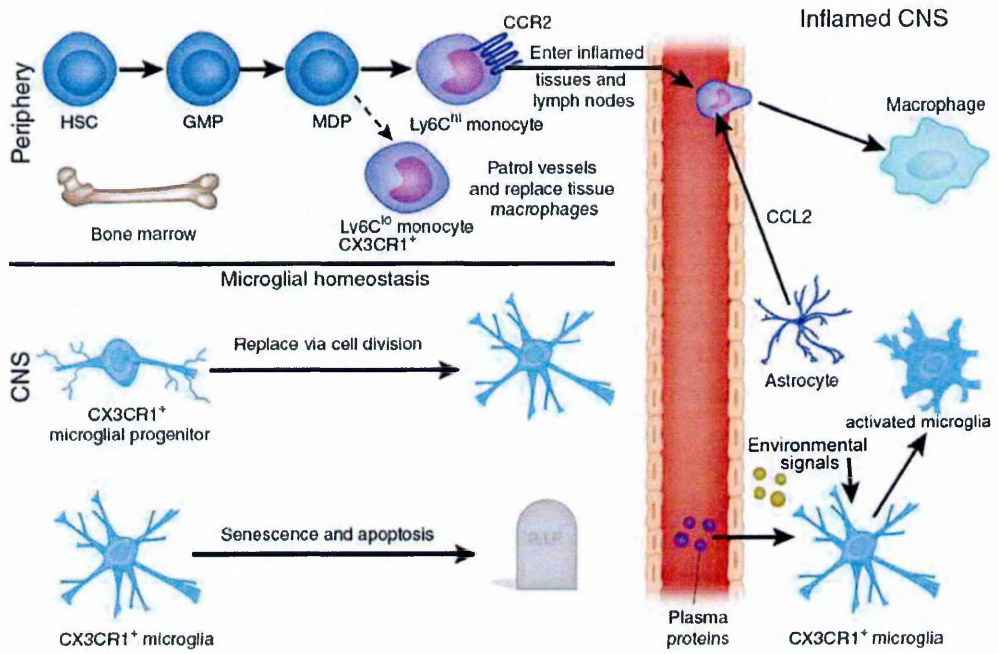

Figure 1.11 *Steady-state maintenance of monocytes and microglia.*

In adult life, monocytes (top) are generated in the bone marrow from HSCs that differentiate to GMPs and then to monocyte–dendritic cell progenitors. Mature Ly6Chi, CCR2+ 'inflammatory' monocytes are released into circulation, from which they are destined to enter inflamed tissues or lymph nodes. Ly6Clow, CCR2– 'resident' monocytes derive from the same progenitors, and patrol blood vessel walls and also replace tissue macrophages. Microglia (bottom) may senesce and undergo apoptosis at a low rate and then be replaced by cell division from CNS-resident CX3CR1+ progenitors. In the inflamed CNS, both monocytes and microglia can give rise to active macrophage/microglial cells during neuroinflammation. Reactive astrocytes produce the chemokine CCL2, which signals to receptor CCR2 on Ly6Chi monocytes, aiding their entry into the CNS parenchyma. Local cytokine and tissue signals can then induce transformation of monocytes to macrophages. Concurrently, inflammation can disrupt the blood-brain barrier, allowing plasma proteins to enter and activate microglia to adopt a macrophage activated phenotype; (modified from Ransohoff 2011).

The inhibition of the CX3CL1:CX3CR1 pathway has been demonstrated to determine different effects on chronic or acute diseases of the CNS. In models of chronic diseases such as lateral amyotrophic sclerosis (ALS, Cardona et al. 2006), Parkinson's disease (Pabon et al. 2011) and Alzheimer's disease (Cho et al. 2011b), the inhibition of the pathway has been associated with a worst outcome possibly be due to the lack of

fractalkine control of microglia activation leading to chronic pro-inflammatory function (Iadecola and Anrather 2011; Zujovic et al. 2000). Surprisingly enough, however, the inhibition of the CX3CL1:CX3CR1 pathway in acute injury models (transient and permanent ischemia, spinal cord injury) has been instead associated with a favourable outcome (Cipriani et al. 2011; Dénes et al. 2008; Donnelly et al. 2011; Soriano et al. 2002). Thus available data do not allow to draw a coherent picture of the role of fractalkine in brain injury and disease. Specifically, little information is available on CX3CL1:CX3CR1 pathway in the context of microglia activation following brain ischemia.

1.4.2.2 Lymphocytes

1.4.2.2.1 T-cell origin, recruitment and functions

T-lymphocytes originate from a common lymphoid progenitor derived from a hematopoietic stem cell (Fig. 1.09). They can be distinguished from other lymphocytes, *i.e.* B cells and NK cells, by the presence of a specific T-cell receptor (TCR) on cell surface. Their maturation takes place in the thymus and give origin to several subtypes (helper, cytotoxic, regulatory, memory and natural killer T-cells), each with a specific function.

T lymphocytes have been suggested to actively participate in the ischemic injury progression (Barone and Feuerstein 1999; Schroeter et al. 1994; Stoll et al. 1998). Recently a role for T lymphocytes has been highlighted, although the functional influence of these cells remains controversial. Some studies propose a deleterious role for lymphocytes (Hurn et al. 2007; Yilmaz et al. 2006) whereas others suggest that lymphocytes, and especially T cells, could exert a protective role promoting neuroprotection and repair (Becker et al. 2003; Becker et al. 1997). Number of infiltrating T-cells is supposed to be smaller if compared to other immune cell types recruited after ischemia (Gelderblom et al. 2009).

Nevertheless, T-cells may have multiple targets which direct their stimulatory function on, being thus able to amplify downstream the effects of their activity.

A number of data supports the idea that lymphocytes mediate an antigen non-specific inflammatory response after stroke. However whether an adaptive immune response occurs and its contribution to the progression of the lesion are not clear. The adaptive immune response is antigen-specific and requires an education of the immune response to a certain antigen. T lymphocytes become activated when an antigen in the context of the major histocompatibility complex and an additional costimulatory signal are provided. In general this activation leads to a Th1 immune response on subsequent encounters with the antigen. A Th1 response is characterized by the secretion of proinflammatory cytokines as IL-2, TNF-α and INF-γ that promote cellular immune response. A Th2/Th3 immune activation may also occur. This kind of response is characterized by the release of IL-4, IL-10 and TGF-β1, factors that may modulate the immune response in a protective fashion.

Under normal conditions CNS antigens are compartmentalized from the systemic immune system by the BBB and thus they are hidden to lymphocytes. When the BBB is disrupted like after stroke, the immune system comes into contact with CNS antigens that may induce T lymphocyte priming in the lymph nodes and subsequent recruitment to the lesion site. T-cell priming could lead to an autoimmune response which could switch towards tolerance if it does not receive an appropriate costimulatory signal. Several recent reports show that animals tolerized to CNS antigens show a decrease in infarct size after ischemia in comparision with non-tolerized animals (Becker et al. 1997). Another mechanisms by which T-cells may have protective impact on ischemic lesion progression is associated with Th2 cell subtype. Protective M/M belonging to the M2a polarization have been found to stimulate recruitment of Th2, which in turn, can further promote M/M protective features by the release of IL-4 (Butovsky et al. 2007; David and Kroner 2011). This cytokine has been demonstrated to lead microglia cells to express neural or dendritic-like

markers (Butovsky et al. 2007) and secrete neurotrophic factors in an event defined as protective autoimmunity (Hallenbeck et al. 2006).

1.5 Two-Photon Microscopy

1.5.1 Principles of two-photon excitation microscopy

The brain has a complex and dynamic structure. The spatial scales of interest to neurobiologists range from individual synapses (≈ 1μm) to neural circuits (centimeters) whilst timescales range from less than a millisecond (flickering of channels) to years (long term memory). Fluorescence microscopy offered a powerful tool to perform research within these spatial and temporal scales. Fluorescent objects can be selectively excited and visualized exploiting the properties of their specific light spectrum. Chemists have developed a wide range of fluorescent molecules that allow the labelling of multiple cellular structures of interest. Other fluorophores are sensitive to variation of Ca2+ and Na+ concentrations and membrane potential. Furthermore, the advent of genetically encoded fluorescent proteins (XFPs) allows the tagging of most cellular proteins (Tsien 1998). XFPs have been used to the study of intracellular signalling, *i.e.* kinase activation (Miyawaki 2005) and of specific subpopulations of cells (Feng et al. 2000; Gong et al. 2003; Lendvai et al. 2000).

A first advance of fluorescence microscopy was the introduction of confocal microscopy. This technique allowed to overcome the strong light scattering that causes signal degradation in wide-field fluorescence microscopy. Confocal microscopy uses a detector pinhole that serves to cut fluorescence from off-focus locations as well as photons scattered on their way out of the tissue (Svoboda and Yasuda 2006). Confocal microscopy

allows three-dimensional images at high-resolution. Image acquisition along the xyz dimensions introduced a fundamental step forward in the analysis of subcellular locations and co-localizations of proteins. Confocal microscopy, however, fails to detect fluorescent signals deep in tissue where it becomes wasteful in terms of signal photons (Centonze and White 1998; Conchello and Lichtman 2005). Compensating for signal loss increasing fluorescence excitation would cause massive photobleaching and phototoxicity (Svoboda and Yasuda 2006). For these reasons, confocal fluorescence microscopy is best applied to thin tissue specimens ($\approx 20\mu m$).

Two-photon microscopy (2-PM) represents a recent major advancement in the fluorescence microscopy techniques, providing high-resolution and high-sensivity fluorescence microscopy into intact tissues. This technique relies on the excitation of a fluorescent molecule by the cooperation of two low energy photons, able to generate an higher electronic transition in the target fluorophore. The first advantage of this kind of laser excitation is that fluorophores are excited almost exclusively in a tiny diffraction-limited focal volume. Indeed, in a focused laser, the intensity is highest in the vicinity of the focus and drops quadratically with above and below distance. Focusing the beam by a high numerical aperture (NA) objective makes the majority of fluorescence excitation to occur in a very small focal volume (Christensen and Nedergaard 2011). The very efficient localization of excitation allows to capture only useful fluorescence photons and to reach three-dimensional contrast and resolution without any spatial filters in the detection path (*i.e.* the pinhole in the confocal set up, Fig. 1.12).

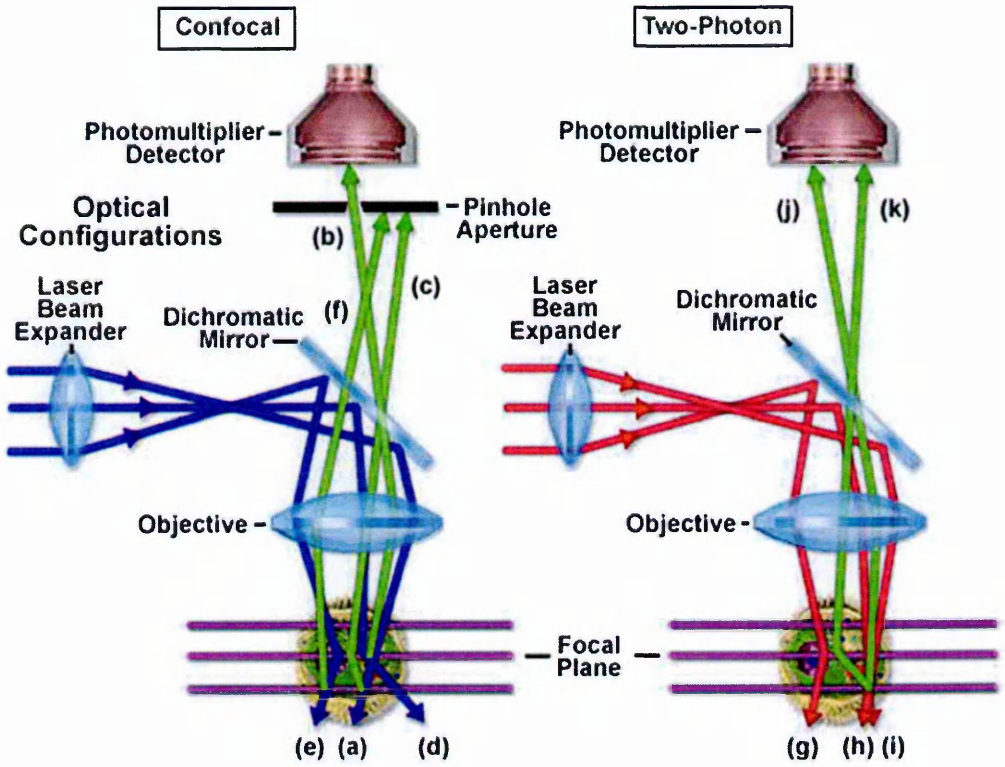

Figure 1.12 *Fluorescence microscopies compared.*

In a confocal microscope the excitation light (blue) is focused into the specimen (a), and the fluorescence (green) from that focal spot is captured by the objective lens, passes cleanly through the pinhole, and reaches the detector (b). This fluorescence light is the desired signal, but some of it can lost because scattered (c), absorbed (d) or scattered before it reaches the focus (e). Background signal can be also generated if the out-of-focus light is scattered into the pinhole, thus reducing image contrast. In the two-photon excitation method the excitation photons (red) can be scattered (g) as in the confocal system. However, the probability of two photons being scattered simultaneously to the same specimen location is essentially zero. In addition, a greater proportion of the excitation light reaches the focal plane (h and i) due the reduced out-of-focus absorption and the decreased scattering of the longer-wavelength two-photon excitation light (infrared). Importantly, the generated fluorescence (green), even if scattered, has an increased likelihood of being detected by the photomultiplier tube (j) because no pinhole is present to block it (k). This insensitivity to scattering effects and absence of out-of-focus absorption allow for the preservation of the full image contrast from considerable depth within specimens.

http://www.microscopyu.com/articles/fluorescence/multiphoton/multiphotonintro.html

2-PM provides several advantages compared to conventional fluorescence microscopy systems. Firstly, differently from conventional fluorescence microscopy that uses wavelenghts in the visible light spectrum, 2-PM uses excitation wavelengths near the infrared that penetrate efficiently in thick tissues due to reduced scattering and absorption by endogenous chromophores (Oheim et al. 2001; Svoboda and Block 1994; Yaroslavsky et al. 2002). Secondly, the non-linear nature of excitation determines non-appreciable fluorescence by scattered excitation photons. Thus, even deep into the tissue, under conditions in which most of the incidence photons are scattered, excitation still occurs in a narrow focal volume. Thirdly, as previously mentioned, all fluorescence photons constitute useful light signal when detected (in contrast, in wide-field and confocal microscopy scattered photons are either lost or cause increased background, (Centonze and White 1998). Finally, phototoxic events are reduced in 2-PM, allowing prolonged fluorophore excitation with limited signal loss.

Overall, due to its features, 2-PM has been successfully applied to time-lapse three-dimensional imaging in living animals, at the resolution of individual cells. In the next section I will provide a summary of the main applications of 2-PM to CNS studies, with a particular attention to the studies on brain ischemia.

1.5.2 Two-photon microscopy in CNS: study of vascular and cellular dynamism

2-PM has demonstrated its potential and suitability in the study of the CNS in different pathological states. Many events occurring in the diseased CNS, such as cerebrovascular modifications and immune cell trafficking, have a highly dynamic nature and require adequate systems of analysis. For years, the analysis of vascular and immune responses in the diseased brain has been mainly based on *post mortem* techniques, *i.e.*

immunohistochemistry and flow cytometry (Gelderblom et al. 2009), whose interpretation is limited by disruption and processing of tissue at defined time points. To get a reliable and effective picture of the dynamic processes involved in vascular and immune events in the CNS, real-time information *in vivo* is required. 2-PM represents a major qualitative advancement for *in vivo* imaging. This technique, indeed, allows high-resolution visualization of individual blood vessels and immune cells within a three-dimensional space over time (Ortolano et al. 2010; Svoboda and Yasuda 2006), overwhelming the major limitations in spatial resolution and three-dimensional acquisition that are associated with other *in vivo* imaging approaches (*i.e.* MRI, intravital microscopy). The 2-PM approach has been successfully used to dissect specific aspects of vascular and immune cell dynamism in the context of neurological diseases (Cordiglieri et al. 2010; Schaffer et al. 2006; Shih et al. 2012), yielding novel results that would have not been obtained with standard methods.

1.5.2.1 Dynamics of blood vessels

Blood flow distribution in the brain has been studied and measured *in vivo* for years using instruments such as laser Doppler (Nakase et al. 1997) and MRI (Nagaraja et al. 2008). These instruments focus over an area of interest sized hundreds of microns, yielding a measure that represents a mean value from the blood vessels pertinent to that area. MRI *in vivo* imaging is also limited by the long time delays between sequential images, thus hampering the acquisition of very fast dynamic events (Cho et al. 2011a). With the introduction of 2-PM, the possibility to image at sufficient spatial resolution and acquisition rate allowed to visualize single vessels and get parameters associated with vessel architecture (diameter, length, number of branching, topology of vessels), blood flow velocity, variations of O_2 concentrations, and to repeat same measures on same

individual vessel over time. Thus, 2-PM introduced the analysis of local and temporal variations of CNS vasculature, where 'local' means specific vessels and 'temporal' means in a before-after time scale.

Being brain ischemia a vascular pathology, most of these studies focus on the hemodynamic variations observed in different conditions modelling stroke. Stroke indeed induces a variety of vascular changes, including blood flow redistribution and blood brain barrier (BBB) leakage. These events trigger several pathophysiological cascades that evolve over time and space, leading to expansion of brain injury and standing as potential targets for therapy (Dirnagl et al. 1999). For its suitability to the study of dynamic events in the brain, 2-PM represented a fundamental tool to investigate previously unexplored aspects of cerebrovascular dynamics and functions (Denk et al. 1990; Svoboda and Yasuda 2006).

1.5.2.1.1 Parameters of blood flow dynamics, 2-PM quantitative analysis after localized occlusion of single vessels

Most of 2-PM studies on hemodynamics rely on the possibility to label blood vessels with a fluorescent dye (*i.e.* Rhodamine-Dextran, Q-dots) and measure blood flow velocity and direction in individual vessels, as firstly described by Chaigneau and colleagues (Chaigneau et al. 2003). Blood flow velocity in 2-PM experiments is measured on the basis of the time needed by a red blood cell (RBC) to travel over a certain distance within a blood vessel (RBC velocity, see methods for details). Being 2-PM capable to provide three-dimensional images of intact tissues (typically 250-600μm thick tissue stacks), it also allows to measure some parameters of the vascular architecture, such as diameter, length and branching of vessels (Cho et al. 2011a) and average blood volume flux (Shih et al. 2012). These measures have been applied to the study of vascular rearrangements in

models of stroke in rodents. The above listed output data from 2-PM experiments are important to draw a complete picture of vascular response after stroke, as the reliance on a single indicator of blood flow provides insufficient description (Pinard et al. 2002; Shih et al. 2009; Tasdemiroglu et al. 1992).

In most of the 2-PM studies on stroke, brain ischemia has been induced by a localized occlusion of one of the vessels pertinent to the visualized area. Being 2-PM easy to focus at tissue portions sized few microns, its laser beam can be directed exclusively to specific vessels and cause a laser induced cortical thrombosis (Nimmagadda et al. 2008). This model of thrombosis has been often used to occlude specific vessels and to study the induced changes in selected vessels downstream or upstream to the occlusion (Nimmagadda et al. 2008; Park et al. 2008; Schaffer et al. 2006). Due to the limitation of laser penetration into intact tissues (≈ 600 μm), these studies focused on the response of cortical microvessels, nevertheless revealing intriguing aspects of vascular dynamism after ischemia.

1.5.2.1.2 Hierarchical structure of the cerebrovascular network, mechanisms for blood flow maintainance in penetrating arterioles

The complex and often redundant network of cerebral vessels showed an active role in confering protection from an ischemic event, given the rapid re-organization of blood flow supply occurring after an occlusion. Schaffer and colleagues (Schaffer et al. 2006) demonstrated that the surface network of communicating arterioles appears to be well protected against single-point occlusions of surface arterioles by virtue of its architecture alone. Indeed blood flow downstream a targeted occlusion, as well as in MCAo ischemic models, does not stop, but is rather reestablished by a reversal in the direction of flow in one of the downstream branches (Schaffer et al. 2006). Occlusion of a single vessel is also

associated with a change in blood flow magnitude which is dependent on the topological relationship of a vessel to the clotted vessel, being reduced by less than half in the first downstream branch, whereas remaining close to baseline values in parallel and far downstream vessels (Schaffer et al. 2006). The rapid re-establishment of the new pattern of flow, about 1 second after clot formation, guarantees no major change in vessel diameter (Schaffer et al. 2006). Thus, cortical surface arterioles show persistent perfusion along with stability in vessel diameter without reaching the deficit in blood flow capable to cause irreversible neuropathology (Baron 2001; Hossmann 1994; Zhao et al. 1997). Indeed no downstream pathology has been observed after surface arteriole occlusion. On the contrary, occlusion of a penetrating arteriole has been associated with subsequent downstream neuropathology. Indeed penetrating arterioles can contribute significantly to blood flow supply over a cortical area extending up to 350μm radius and, in addition, collateral flow from neighboring penetrating arterioles is limited (Nishimura et al. 2007). After occlusion of a penetrating arteriole, RBC velocity is dramatically reduced as far as 10 branches distal to target vessel, being dropped to approximately 0.1-0.3 times baseline values (Nishimura et al. 2007).

Similar topological differences in blood flow redistribution have been observed for venules. While the occlusion of surface venules does not cause permanent drop of RBC, due to the redundancy of surface vessels, occlusion of cortical ascending venules causes a 20% blood flow decrease, potentially able to cause cognitive dysfunctions when protracted in time (Cho et al. 2011a). In particular, when a cortical ascending venule is occluded and a collateral venule is not present, capillaries one to four branches upstream to the target venule show dramatic decrease of RBC velocity, reversal of flow direction and diameter increase (Cho et al. 2011a). Venules present in the brain outnumber arterioles and, even sharing a similar pattern of capillary branching, their density is higher. For this reason the

occlusion of a venule affects RBC velocity up to a distance of 4 branchings, far shorter than the occlusion of an arteriole (up to 10 downstream branchings).

Overall, 2-PM studies on brain cortical vasculature clearly show the hierarchycal organization of the cerebral blood vessel network, based mainly on vascular geometry. Occlusions at different levels of vascular hierarchy yield different severity of ischemic damage, since vascular geometry has a fundamental role in redistributing blood flow. Surface vessels communicate by frequent connections and form a highly redundant network. In case of an occlusion, blood flow is rapidly re-established to pre-occlusion values by virtue of vessel geometry itself, with subsequent prevention of neuropathology. The network formed by penetrating vessels, on the contrary, is less redundant and, as a consequence of their architecture, penetrating vessels individually feed wide areas. After occlusion, alternative blood flow supply is limited in penetrating arterioles, resulting in tissutal damage. Thus, the redundancy of collateral networks observed for the surface blood vessels stands as a protective mechanism to assure sufficient perfusion of downstream penetrating arterioles, even during occlusions. Flow reversal indeed occurs in surface arterioles, but does not take place in penetrating arterioles (Shih et al. 2009), suggesting that the hierarchycal network is organized so to avoid eccessive variations in penetrating arteriole blood flow, whose occlusion would in turn cause pathology.

1.5.2.1.3 Blood flow regulation of neuronal activity

2-PM reaches sufficient spatial resolution to visualize finer structures than cerebral vasculature, such as neuronal dendrites and dendritic spines. *In vivo* imaging of these fine structures is limited by the intrinsic ability of infrared light to penetrate intact tissues and by the slight movements of the fluorescently labelled structures, due to heart/breathing rate and vasomotion, that may determine decreased resolution (Sigler and Murphy 2010). Most

of the 2-PM studies on dendritic plasticity have been thus conducted near to the pial surface, where dendrites of layer 5, 2 and 3 neurons curve and run almost parallel to pial vessels (Sigler and Murphy 2010). The main advantage of using 2-PM in the field of dendritic activity is the ability to image neurons in a before-after time frame. Investigators have altered sensory experience of animals under 2-PM imaging by whisker trimming or odorous stimuli, and recorded the elicited effects on the structural neuronal wiring. Data revealed that dendritic spines undergo a rapid turnover associated with enduring motor memories (Xu et al. 2009; Yang et al. 2009).

Dendritic plasticity has been also evaluated in relation with microcirculation during acute stroke (Sigler and Murphy 2010). 2-PM provided simultaneous visualization of cerebral vasculature and dendrites, thus revealing the effects of a vessel occlusion on the turnover of dendritic spines and to define the relationship between perfusion and dendritic structure (Fig. 1.13). Under normal conditions, the neuronal network is hard wired with minimum variations observed over time. Severe ischemia induced by the vasoconstrictor endothelin, dropping blood supply to 10% of normoperfused vessels, was able to cause a rapid loss of dendritic spines as early as 10 minutes from occlusion (Tsai et al. 2009; Zhang and Murphy 2007). If perfusion was re-established within 50 minutes, the dendritic and spine structures could be largely restored (Zhang et al. 2005). Dendritic spines are normally located at 13μm from blood vessels. During ischemia, as expected, many non perfused areas develop. In areas without flowing vessels, the dendritic structures could be maintained if distanced less than 80μm from the nearest perfused vessel (Zhang and Murphy 2007). In general, the differences in perfusion of vessels draw a sharp transition between intact and damaged dendritic structures, being vessels able to provide support for dendritic viability at a maximum distance of 80μm. In peri-infarct areas, where blood flow supply is maintaned over the critical values and redundant vascular architecture helps preserving perfusion, dendritic structures showed the highest plasticity, expecially at the

later stages of stroke pathogenesis. At 1-2 weeks after ischemia, the dendritic structures located within peri-infarct areas reached their maximal plasticity, as indicated by a 4-fold increase in spinogenesis, still detectable at 6 weeks (Brown et al. 2009; Brown et al. 2007). These changes were selectively associated with the neurons at the peri-infarct areas, since the spine turnover rates were not affected at the distal locations from the lesion (> 1.5mm).

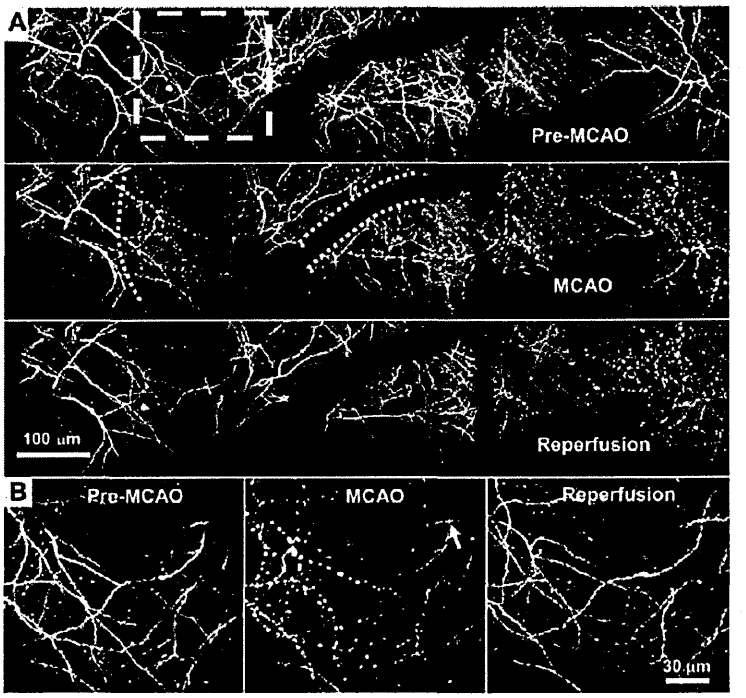

Figure 1.13 *View of local changes in dendritic structures before, during and after MCAo by 2-PM.*

A: 2-PM images taken from transgenic mice expressing GFP in neurons show the dendritic structure before ischemia (upper panel), during ischemia (middle panel) and after reperfusion (bottom panel). The dashed line in the left part of middle panel indicates the border of the structural damage, whitin which the dendritic damage is more evident. The dashed line in the centre of middle panel indicates a vessel with partial a perfusion that helped neurons to keep intact dendrites. A significant recovery of neuronal dendritic structures is observable after reperfusion.

B: Closer magnification of the rectangle indicated in A, upper panel. MCAo drives dendritic structure loss, while reperfusion induces significant recovery (Li and Murphy 2008).

1.5.2.1.4 Imaging of O_2 and blood flow

For a complete understanding of brain metabolism, the measure of the previously reported vascular parameters should be paralleled by the quantification of the amounts of oxygen that can be diffused to surrounding tissue (Raichle and Mintun 2006). Classical PO_2 measurements with electrodes (Lecoq et al. 2009; Ndubuizu and LaManna 2007) are limited by their invasivity and lack intravascular PO_2 sensivity (Lecoq et al. 2011). 2-PM offered a solution to these limitations. Recently the use of a phosphorescent probe, PtP-C343 (Finikova et al. 2007) was combined with 2-PM to get a simultaneous measure of PO_2 and blood flow in cerebral vessels up to 300µm of depth in rat brain (Lecoq et al. 2011). This probe proved enough sensivity to PO_2, decreasing its phosphorescence lifetime as PO_2 increased. This technique allows a very high resolution mapping of oxygen levels in the brain, enabling to measure vascular PO_2 inbetween two flowing RBC. Intriguingly, authors reported local increase of PO_2 associated with erythrocytes, as probe phosphorescence liftime was significantly shorter in the immediate vicinity of RBC than in the bulk plasma (Lecoq et al. 2011). Furthermore, they were able to generate local PO_2 variations by evoking odor stimulation. In particular odor triggers an increase of vascular PO_2 preceded by a dip in tissutal PO_2 (Lecoq et al. 2011).

1.5.2.2 Regulation of blood flow by cells of the neurovascular unit

1.5.2.2.1 Imaging of astrocytes enveloping the endothelium

As mentioned above, modifications to blood flow supply, BBB damage or microhemorrages are all capable to regulate the activity of both resident and recruited CNS cells. Neurons, astrocytes, pericytes and, in some extents, lymphocytes are in turn able to

affect blood flow, thus drawing a complex dynamic picture of cellular-vascular interplay. Local blood flow increases are needed for sustaining neuronal activity, in an event defined as neurovascular coupling. Evidence exists that local dilatation of capillaries takes place in response to whisker stimulation, allowing the needed metabolic support for neuronal activity (Stefanovic et al. 2008). Alteration to the vascular tone have been also observed in pathological conditions, such as ischemia or Alzheimer disease (Zlokovic 2005). The local control of blood flow supply is exerted by glial and neuronal cells proximal to vasculature and rely on different control mechanisms in respect to vascular autoregulation, the latter needed for ensuring constant blood flow in the brain. Local constriction or dilation of blood vessels depend on the activity of the smooth muscle cells associated with the endothelium. Smooth muscle cells are solely effector cells that regulate blood vessel diameter in response to signals received from astrocytic endfeet. Astrocytes are indeed located in an ideal situation to sense neuronal stimulation and transfer signal to smooth muscle cells, since astrocytes surround synapses and envelop blood vessels with their endfeet (Attwell et al. 2010). When astrocytes are activated upon sensing of neuron-released glutamate, they in turn release metabolites of arachidonic acid (prostaglandins and epoxyeicosatrienoic acids) causing relaxation of smooth muscle cells (Gordon et al. 2008; Metea and Newman 2006; Peng et al. 2004; Peng et al. 2002; Zonta et al. 2003). Interestingly, in contrast with these studies, a 2-PM study on brain slices from both rats and mice, provided evidence of vasoconstriction by astrocytes (Mulligan and MacVicar 2004). The authors investigated the effects of selective waves of increased Ca^{2+} concentrations at the astrocytic endfeet that were stimulated by localized flash photolysis of caged Ca^{2+} with 2-PM (Brown et al. 1999; Soeller and Cannell 1999). Upon increased $[Ca^{2+}]$ with propagation to the endfeet, astrocytes were able to cause vasoconstriction. The peak of $[Ca^{2+}]$ increase preceded vasoconstriction by 2.7±0.5 s, time enough for the syntesis and release of second messengers diffusing from astrocytic endfeet to smooth

muscle cells at the vascular walls. The authors identified the Ca^{2+}-sensitive photolipase A_2 to be responsible of the induced vasoconstrictions (Mulligan and MacVicar 2004).

Studies on brain slices provided contrasting results on the vascular control by astrocytes, having Zonta and colleagues proposed a role in vasorelaxation (Zonta et al. 2003) whilst Mulligan and MacVicar a role in vasoconstriction (Mulligan and MacVicar 2004). These studies are limited by the lack of blood perfusion in organotypic slice cultures, thus relying on potentially altered models in respect to intact animals. Takano and colleagues applied *in vivo* 2-PM to transgenic mice expressing GFP under the control of GFAP and demonstrated that photolysis of caged Ca^{2+} in astrocytic endfeet caused vasodilatation (Takano et al. 2007). They also showed that, at the early stages of Alzheimer disease, astrocytes have an abnormal activity characterized by spontanous increases of Ca^{2+} signalling that, in turn, causes repetitive cycles of vascular relaxation/constrictions. This astrocytic dysfunction and the subsequent abnormal microcirculation precede amyloid deposition and neuronal loss. Brain ischemia is also capable to induce variation in $[Ca^{2+}]$ in astrocytes. In a model of photothrombosis, repetitive and transient Ca^{2+} signals were detected starting from 20 minutes after clot formation (Ding et al. 2009). Photothrombosis caused increased amplitude and frequency of Ca^{2+} transients lasting up to 3h after occlusion onset. Antagonists for mGluR5 and $GABA_BR$ attenuated astrocytic Ca^{2+} signalling, suggesting a role of the two receptors in the elevation of Ca^{2+} stores (Ding et al. 2009).

1.5.2.2.2 Imaging of pericyte actions on brain capillaries

The studies on the control of vascular tone by astrocytes, in most cases conducted by *post mortem* analysis or in *in vitro* settings (Attwell et al. 2010), have suggested for years that the neurovascular coupling was mediated exclusively by smooth muscle cell activation.

Recently, a similar ability has been proposed for pericytes, whose presence and distribution along capillaries suggested their ability to regulate blood flow at the capillary level (Hamilton et al. 2010; Puro 2007; Shepro and Morel 1993). A number of studies demonstrated the ability of cultured pericytes to contract in response to arachidonic acid and neurotransmitters, further corroborating their role in blood flow regulation (Peppiatt et al. 2006; Puro 2007; Shepro and Morel 1993). Direct evidence of pericyte control of blood flow has been provided by a 2-PM study using GFP fluorescent mice (Fernández-Klett et al. 2010), as shown in figure 1.14. Under conditions of tissutal hypoperfusion caused by the topical administration of an agonist of $TBXA_2$, a mediator of vasoconstriction, local capillary constrictions were evident and more pronounced at pericyte bodies (Fernández-Klett et al. 2010). On the contrary, pericytes were not involved in capillary diameter increase after administration of bicucullin, a $GABA_A$ receptor antagonist able to induce recurring bursts of neuronal spike activity. Thus, in neurovascular coupling, capillaries dilate passively in response to increased pressure in upstream arterioles, and this process does not require pericyte functionality (Fernández-Klett et al. 2010). Pericyte contractile features are needed for vasoconstriction in response to an altered perfusion state, *i.e.* ischemia. During ischemia, pericytes constrict capillaries below a 5μm diameter, and the effects of the provoked vasoconstriction may be enhanced by blood cell trafficking. Red and white cells, indeed, have to deform considerably to flow through a 5μm diameter (Attwell et al. 2010) and, since ischemia significantly increases the number of circulating blood cells, collateral capillary clots may occur (no-reflow phenomenon, del Zoppo 1997) originating new, small non-perfused areas.

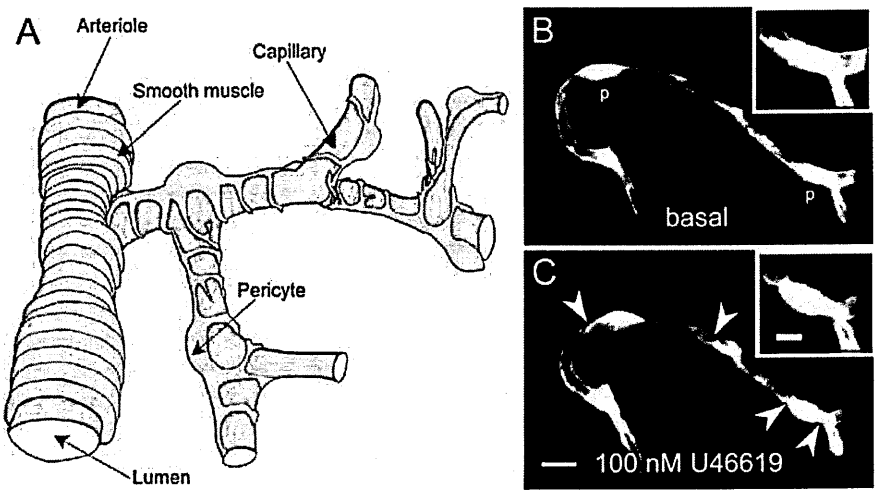

Figure 1.14. *Organisation of the capillary neurovascular unit and 2-PM vasualization of contractile pericytes.*

A: Pericytes send processes along and around capillaries, partially enveloping the vessels.

B: Using organotypic slice cultures from transgenic β-actin-GFP mice, pericytes (p) are clearly visible under 2-PM. C: The topical administration of an agonist of $TBXA_2$ (U46619, 100 nM) induces vasoconstriction, which is particularly evident at the pericyte bodies (arrowheads, modified from Fernández-Klett et al. 2010; Hamilton et al. 2010).

1.5.2.3 Dynamics of immune populations recruited and activated in the CNS

2-PM has been extensively used to study dynamics of immune cells behavior within CNS and revealed the ability of BBB components to instruct circulating immune cells prior to infiltration and the mechanisms of vascular alterations capable of activating resident microglia. All togheter these results depicted a new scenario on vascular-immune cell interaction within the CNS.

1.5.2.3.1 Two-photon imaging of T-Lymphocytes in CNS pathologies

As reported above, cells belonging to the immune system are recruited to brain in a time-dependent manner (Gelderblom et al. 2009). T-cells raised a particular interest as they play

a pivotal role in the progression of many autoimmune and inflammatory brain conditions, thus representing a potential therapeutical target.

Many CNS pathological conditions are often associated with a loss of BBB integrity, thus allowing passive T-cell infiltration. However, due to the complex cellular structure of the BBB, it is also conceivable that the BBB does not allow only a passive transfer of immune cells from blood stream to the brain once opened, but rather participate to their recruitment in an active manner. Owens and colleagues (Owens et al. 2008) elegantly described that extravasated T cells are likely to move in the perivascular space rather than in the brain parenchyma, and they possibly come into contact with the different cell types that compose the BBB to receive specific signals. Direct demonstration of this become only recently available, as, in different models of brain diseases, 2-PM observations clearly showed T-cells patrolling the perivascular space of CNS blood vessels prior to tissutal invasion.

Early 2-PM studies on T-cells behavior within CNS were conducted in rodent models of experimental autoimmune encephalitomyelitis (EAE, Bartholomäus et al. 2009; Flügel et al. 2007), and meningitis (Kim et al. 2009), both conditions characterized by a massive reactive T-cell recruitment. After collection of lymphocytes from donor animals, T-cells were fluorescently labelled and injected into recipient animals with pathology to be followed by 2-PM. In EAE, T-cell migratory behavior was investigated soon after transfer into recipient, where T-cells remained traceable for days. About 80% of injected T-cells were found to be crawling along blood vessel intraluminal side, with a crawling half-life of 15 minutes before extravasation (Bartholomäus et al. 2009). It is likely that T-cells move along blood vessel inner surface searching for a suitable place for completing tissutal entry. As the right spot to enter is found, the extravasation process takes approximately 10-20 minutes (Bartholomäus et al. 2009), during which integrins and G-coupled proteins on endothelial cells participate to allow either para- or trans-cellular migration (Bauer et al. 2009; Engelhardt 2006; Engelhardt and Wolburg 2004). Once passed through endothelium,

T-cells spend 80% of their time crawling on the abluminal space of vessels, a fundamental location for contacting various components of the BBB (Fig. 1.15). The encounter with perivascular resident cells stands as a crucial checkpoint prior to T-cell tissutal invasion. Motility of injected T-cells was affected by their ability to recognize a specific antigen. When immunized for ovalbumin, T-cells decreased their velocity upon administration of ovalbumin (from average 8.01±0.47 μm min^{-1} to 2.76±0.19 μm min^{-1}), and many arrested when in close contact with tetramethylrhodamine-dextran positive cells (meningeal and perivascular phagocytes (Odoardi et al. 2007).

A perivascular location was described also for T-cells in the model of meningitis (Kim et al. 2009). Naive GFP+ CD8+T-cells expressing a receptor able to recognize the lymphocytic-choriomeningitis virus (LCMV) were visualized in the brain after craniotomy. The number of T-cells increased significantly in 6 day symptomatic mice. The authors reported T-cell ability to recruit myelomonocytic cells which in turn caused vascular injury with subsequent BBB leakage (Kim et al. 2009). T-cell velocity was affected by their interaction with LCMV specific antigen. When this interaction was prevented, indeed, T-cells moved at an average speed of 5.16±0.46 μm min^{-1}, faster than their average 3.41±0.27 μm min^{-1} in the context of antigen presentation (Kim et al. 2009). Similarly, other works describe the ability of CD4+ T cells to slow down upon specific antigen encounter (Miller et al. 2002; Zinselmeyer et al. 2005). When primed and tolerized, CD4+ T-cells decreased their speed from 10 μm min^{-1} approximately to 4-5 μm min^{-1}. 2-PM thus well demonstrated that T-cells decrease their velocity when the immune synapse is formed and they receive priming/tolerization.

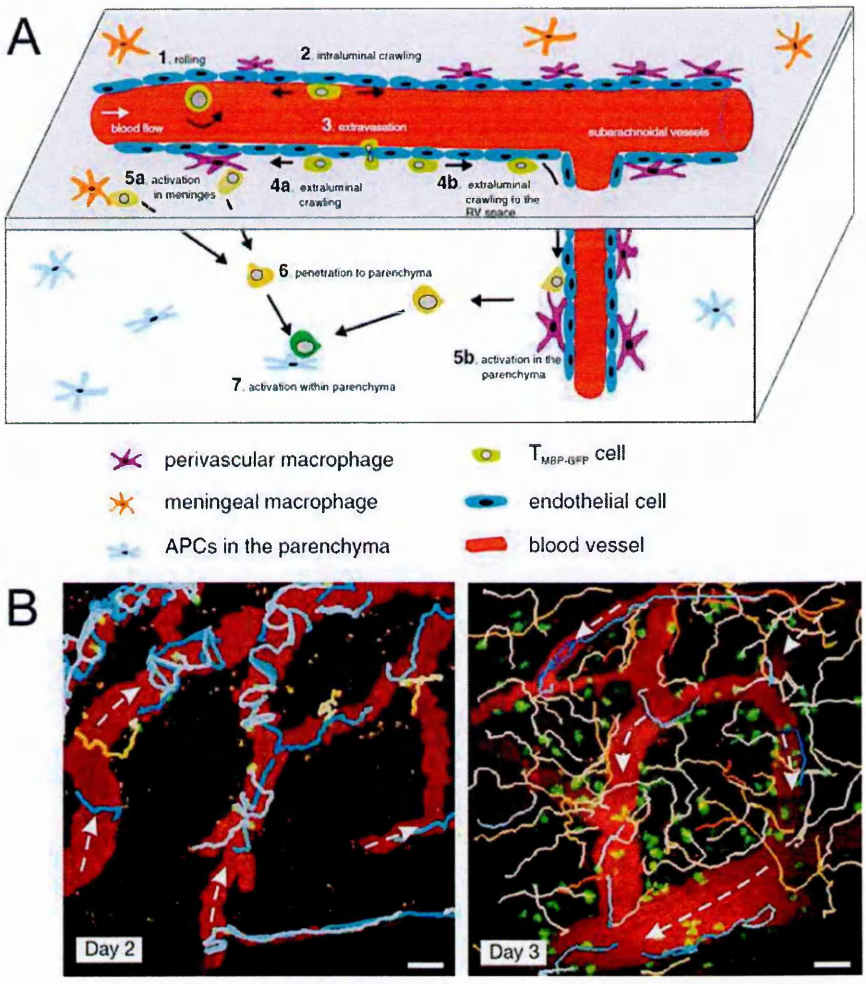

Figure 1.15. *Invasion steps of T-cells in brain parenchyma in EAE revealed by 2-PM.*

A: T-cells arrive at CNS leptomeningeal vessels and roll on endothelial cells (1). This is followed by intraluminal crawling directed both upstream and downstream of blood flow (2). After the extravasation (3), T- cells continue to crawl to the abluminal surface of vessels (4a). A part of T cells dive to the Robin Virchow space (RV; 4b). T cells meet local antigen-presenting cells at the perivascular space of leptomeningeal vessels (5a) or parenchyma (5b) and are activated. Activated T cells are allowed to penetrate within the CNS parenchyma (6). Finally, T cells can be further activated by antigen-presenting cells in the CNS parenchyma (7).

B: 2-PM images showing the migratory paths of moving T-cells over 30min of imaging either at day2 or day3 after EAE induction. Blood vessels are in red, T-cells in green. Arrows indicate the direction of blood flow, blue lines indicate paths of intravascular cells, while yellow lines indicate paths of extravascular cells (modified from Bartholomäus et al. 2009; Kawakami and Flügel 2010).

1.5.2.3.2 Two-photon imaging of microglia in CNS pathologies

Over the last years, microglia has been widely studied by *in vivo* 2-PM and time-lapse confocal microscopy using a transgenic mouse model expressing GFP under the control of fractalkine receptor (*cx3cr1*), which is costitutively expressed by resident microglia (Davalos et al. 2005; Liang et al. 2009; Masuda et al. 2011; Ohsawa and Kohsaka 2011). These studies revealed the high dynamic nature of microglia within CNS (Fig. 1.16). In physiological conditions, microglia extend and retrieve their processes to sample the surrounding microenvironment (Davalos et al. 2005) and make direct contact with other cell types present in the CNS, such as neurons (Wake et al. 2009) and perivascular astrocytes (Mathiisen et al. 2010). As an injury occurs, microglia become hypertrophic and retract their processes to acquire an ameboid active status. This event is triggered by the sensing of ATP (Davalos et al. 2005) through the adenosine receptor A_{2A} whose expression is increased in microglia cells soon after injury and is counterbalanced by decrease of $P2Y_{12}$ receptor expression (Haynes et al. 2006; Orr et al. 2009). This pathway is also responsible for increased microglia displacement after LPS stimulation (Ohsawa and Kohsaka 2011). However, the ability of microglia to travel over brain tissue seems to be dependent on the kind of danger signal received. In a model of spreading depression that causes loss of synaptic activity, microglia showed displacement by Lévy flight-like movements in response to decreased synaptic activity (Grinberg et al. 2011). On the contrary, in models of brain injury such as traumatic brain injury, photothrombotic stroke model and global ischemia, microglia did not show any body movement in response to damage (Davalos et al. 2005; Masuda et al. 2011). The observed lack of microglia displacement after ischemia could be related to the rapid decline of ATP levels due to vessel occlusion, being, as reported above, ATP needed for the cytoscheletal modifications exploited by microglia to migrate within the tissue (Davalos et al. 2005; Grinberg et al.

2011). The ability of microglia to rapidly modify their shape upon ischemic insult may need a lesser income of ATP, but it is dramatically affected by the residual capillary blood flow around their soma (Masuda et al. 2011). After complete loss of blood flow in their territory, microglia enter in a stalled status, unable to withdraw ramifications. Acquisition of the ameboid morphology requires a minimum level of blood flow and ATP supply by surrounding capillaries (Masuda et al. 2011). Resiliency of microglia is a key feature of this population, as they recover process activity once blood flow is re-established, even in the areas severely affected by transient occlusions (Masuda et al. 2011).

Cerebral vessels can determine activation of microglia also because of their bleeding, as a recent 2-PM study revealed (Rosidi et al. 2011). Cortical microhemorrages, while not producing acute stroke symptoms in aging brains (Cullen et al. 2005; Farrall and Wardlaw 2009), do cause activation of microglia cells up to 200μm from the origin of the bleeding (Rosidi et al. 2011). The area of microglia activation after microhemorrages (400 μm diameter) correlates to the extent of extravasated blood plasma, suggesting that blood plasma components trigger microglia activity (Rosidi et al. 2011). Since BBB leakage occurs soon after ischemia (Strbian et al. 2008), plasma components may be among the first activatory signals that elicit microglia response.

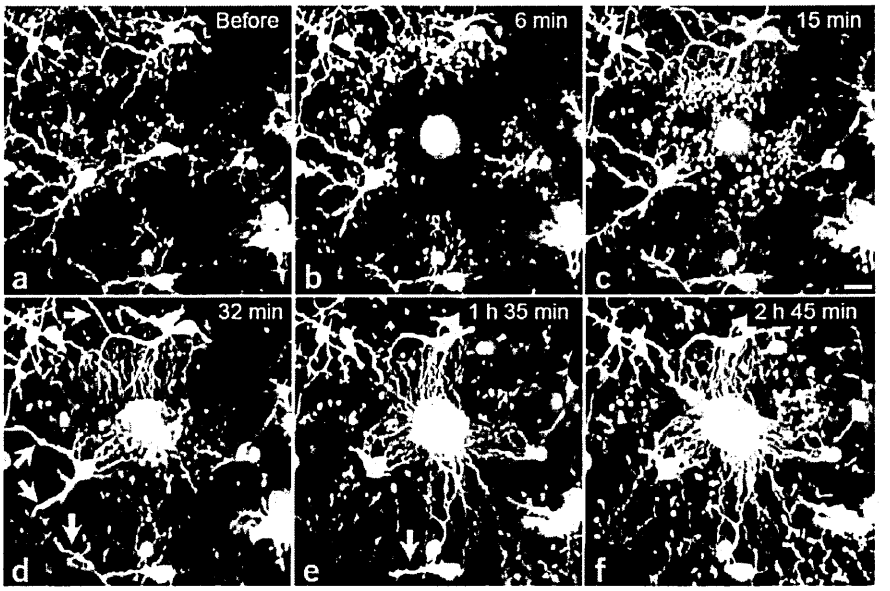

Figure 1.16. *Microglia sensing of a laser-induced injury.*

Microglia are normally present as ramified cells that explore their surrounding microenvironment (a). A laser-induced injury (white spot in b) causes rapid microglia activation. At 15min after injury microglia extend branches towards the site of injury (c), and at subsequent time points this event is paralled by retraction of branches that lay in direction opposite to the lesion site (arrows in d, e). At 2h 45min microglia processes almost completely surrounds the lesion (f, Davalos et al. 2005).

2. AIM OF THE STUDY

The main aim of this project has been to explore, in the ischemic brain: 1) the dynamics of vascular rearrangements; 2) the morphological and phenotypical changes associated with microglia/macrophage activation and 3) the dynamic behavior of T-cell recruited to the lesioned area. To these purposes, I used a model of transient and of permanent ischemia in mice and applied *in vivo* two-photon microscopy and *post mortem* quantitative histology.

To date, analysis of the pathogenetic mechanisms associated with brain ischemia has been mainly based on *post mortem* techniques, whose interpretation is limited by disruption and processing of tissue at defined time points. For a reliable and effective picture of the dynamic processes occurring in the central nervous system after an acute injury, such as vascular rearrangements and immune cell behavior, real-time information *in vivo* is required. There are currently a few *in vivo* imaging systems, among which 2-PM is a truly innovative tool for studying the brain. The 2-PM, indeed, introduced a new perspective to look at brain dynamism, given its ability to provide three-dimensional, high resoluted images over time. In this study, I applied 2-PM to visualize blood vessels, microglia and lymphocytes and to collect quantitative parameters associated with their dynamism after brain ischemia. To get insight into the phenotypical nature of the investigated immune populations, I also performed quantitative analysis of marker expression and evaluation of their co-expression, exploiting *post mortem* immunohistology and immunofluorescence followed by bright field or confocal microscopy.

I divided the study into four sections, whose rationale and specific aims are presented below.

1. Microvascular modifications after brain ischemia revealed by 2PM

A peculiar application of 2-PM is high-resolution angiography since both major vessels and microvasculature can be visualized and numerical data (*i.e.* vascular diameter, blood flow speed and flux volume) can be obtained as well. Studies using this approach have been focused on the vascular rearrangements occurring after permanent middle cerebral artery occlusion (pMCAo) or within 2 h after transient MCA occlusion (tMCAo), however, no studies are available describing blood flow dynamics at longer time points which are more applicable to intervention.

Specific aims of this part of the project included: 1) set up of a reliable method for repetitive *in vivo* imaging on the same animals (longitudinal study) up to 24h after injury; 2) identification of an area accessible to imaging and affected by MCAo; 3) obtaining information on the degree of blood flow velocity variations during MCAo and up to 1d after reperfusion; 4) measurement of the extent of extravasation (BBB damage).

2. *In vivo* imaging of microglia and protective features of CX3CR1-deficent microglia

Microglia/macrophages (M/M) are rapidly activated after brain ischemia and have a prominent role in ischemic damage progression. CX3CR1 is a receptor expressed by M/M cells, binds to neuron-secreted fractalkine and serves for control of M/M activation. Although widely studied in models of chronic diseases, the role CX3CR1:fractalkine pathway following brain ischemia has been scarcely addressed. Furthermore, available data on this pathway do not allow to draw a coherent picture of its function and the role of CX3CR1 after brain ischemia remains elusive.

The main aim of this part of the study has been to identify the consequences of CX3CR1 absence after brain ischemic injury, specifically addressing whether CX3CR1-deficent

M/M exhibited, compared with wt microglia: 1) different motility; 2) different morphological switch in response to injury; 3) alternative pattern of M/M marker expression (namely CD11b, CD68, CD45, Ym1, CD206 and iNOS); 4) lower susceptibility to ischemic brain injury.

In this part of the study, I used transgenic mice carrying GFP expression under the control of the promoter of the receptor of fractalkine (*cx3cr1*) to specifically image microglia by *in vivo* 2-PM. I have subjected transgenic mice to tMCAo and visualized GFP+ microglia by *in vivo* 2-PM before and up to 24h after ischemic injury, to measure motility and morphological parameters. At 24h after tMCAo, animals were sacrified and tissue collected for quantitative histology.

3. Temporal pattern of expression and colocalization of M/M

As previously mentioned, activated microglia and recruited macrophages can affect neuronal function and promote neurotoxicity through the release of several harmful components such as IL-1β, TNF-α, proteases and reactive oxygen and nitrogen species. On the other hand they also possess protective qualities and promote neurogenesis and lesion repair. Indeed, microglia have been proposed to be beneficial by several mechanisms including glutamate uptake, removal of cell debris and production of neurotrophic factors such as IGF-1, GDNF and BDNF. These functions are associated to specific patterns of phenotype markers, that confer M/M a given polarization state ranging from the toxic (M1) to the protective (M2) extremes. In spite of the large literature on inflammation after ischemia, information on M/M phenotype marker expression, their colocalization and temporal evolution in the injured brain is lacking.

Specific aims of this section included: 1) identification of the time course of expression of the selected M/M markers, with particular regard to the time of M1 and M2 polarization arousal; 2) understanding the tissutal location of M/M makers in relation to the ischemic site at distinct phases after injury; 3) definition of the pattern of co-expression of the selected M/M markers.

In this part of the study, I subjected mice to pMCAo and applied *post mortem* immunohistochemistry for selected M/M markers (CD11b, CD68, CD45, Ym1, CD206 and iNOS) followed by quantitative bright field microscopy. I then assessed the pattern of co-expression of the selected markers by using immunofluorescence followed by three-dimensional confocal analysis.

4. *In vivo* imaging of T-cell in the ischemic brain

T-cells play a pivotal role in the progression of many autoimmune and inflammatory brain conditions, thus representing a potential therapeutical target. Their gate to access the brain is vasculature, which is normally strictly closed to immune cell passage by the BBB, but may be permissive to cell infiltration after an injury, as BBB opens. The behavior of T-cells has been widely investigated by 2-PM in disease models that are associated with a huge recruitment of T-cells, such as experimental autoimmune encephalitomyelitis (EAE), toxoplasmic encephalitis and meningitis. The 2-PM approach allowed to describe T-cell behavior on the basis of motility parameters and route of trafficking. Despite stroke causes BBB leakage along with an increased expression of adhesion molecules, on the whole facilitating T-cell infiltration, there are far fewer T-cells in the brain after stroke compared with EAE, toxoplasmic encephalitis and meningitis. For this reason, time lapse *in vivo* imaging of T-cell dynamics in a model of stroke represents a major technical challenge.

Specific aims of this part of the project have been: 1) definition of the motility features of extravasated T-cells; 2) identification of the routes of T-cell trafficking within the ischemic area; 3) obtaining information on their crawling behavior on perivascular space.

In this part of the study I used adult male CBA/CaXC57F7BL/10 hCD2-GFP transgenic mice that express GFP specifically in T-cells under control of the hCD2 promoter. Transgenic mice have been subjected to pMCAo and T-cells have been visualized by *in vivo* 2-PM 3d after injury to obtain a quantitative description of T-cell motility.

3. MATERIALS AND METHODS

3.1 Animals

Procedures involving animals and their care were conducted in conformity with institutional guidelines that are in compliance with national (D.L. n.116, G.U. suppl. 40, 18 February 1992) and international laws and policies (EEC Council Directive 86/609, OJ L 358,1; Dec.12,1987; NIH Guide for the Care and Use of Laboratory Animals, U.S. National Research Council 1996). Animals (11 week old) at Mario Negri Institute were housed in an Specific Pathogen Free (SPF) *vivarium*, 5 per cage and kept at constant temperature (21 ± 1 °C) and relative humidity (60 %) with regular light/dark schedule (7 am-7 pm). Food (Altromin pellets for mice) and water were available *ad libitum.* Before beginning any procedure, mice were housed for at least 1 week in their home cages at the conditions described above.

All mice used at the Biological Procedures Unit, University of Strathclyde were maintained on a 12/12 h light/dark cycle with free access to food and water, and all the procedures performed in accordance with local ethical and UK Home Office regulations.

Strains used in the project were:

- Male 11 week old C57BL/6J mice (Harlan, Italy);
- Male 11 week old CBA/Ca×C57F7BL/10 that expressed GFP under control of the hCD2 promoter (kindly gifted by Dr. Dimitris Kioussis, NIMR, London, UK). GFP is expressed almost exclusively in thymocytes, and virtually all mature thymocytes express it (irrespective of CD4 or CD8 expression), peripheral B cells show about 1% of the GFP fluorescence of T cells (De Boer et al. 2003);

- Male 11 week old *cx3cr1*$^{GFP/+}$ and *cx3cr1*$^{GFP/GFP}$ mice (Jackson laboratories, CA, USA). These mice express the GFP under the control of the promoter of *cx3cr1*, which is costitutively expressed by microglia cells in the brain. To generate transgenic mice, the gene for *GFP* has been put on a substitution cassette, thus *cx3cr1*$^{GFP/GFP}$ do not express CX3CR1 and will be indicated in the text such as *cx3cr1*$^{-/-}$. Haplotype (*cx3cr1*$^{GFP/+}$) do express CR3CR1 and will be refereed to as *cx3cr1*$^{-/+}$ mice.

3.2 Experimental design and blinding

Mice were assigned to surgery and experimental groups with surgery distributed equally across cages and days. To minimize the variability, all surgeries were performed by the same investigator, blinded to the experimental groups. All subsequent evaluations were also done by blinded investigators.

3.3 Surgery protocols

3.3.1 Craniotomy for two-photon imaging

To image living mice under the 2-PM, animals were subjected to a craniotomy to expose the cortical area of interest at AP: -1 mm and L: -2.5 mm from bregma. Cranial window craniotomy was used for imaging blood vessels in chapter **4** (see details in section **4.2.2**), whilst skull thinning craniotomy was used for imaging microglia (chapter **5**) and T-cells (chapter **7**) as detailed in section **5.2.2** and **7.2.2**, respectively.

3.3.2 Transient middle cerebral artery occlusion (tMCAo)

Anesthesia was induced by 3% isoflurane inhalation in an N_2O/O_2 (70/30%) mixture and maintained by 1% to 1.5% isoflurane inhalation in an N_2O/O_2 (70/30%) mixture. Twenty-four hours after craniotomy and 45 min after the first imaging session, transient ischemia was induced by tMCAO (Gesuete et al. 2009). The right common carotid artery was exposed and the external carotid artery and its branches, including the occipital artery and the superior thyroid artery was isolated and cauterized. A silicone coated monofilament nylon suture (7-0, Doccol Corp, Redlands, CA), was introduced into the common carotid artery and advanced to the internal carotid artery so as to block its bifurcation into the MCA. At the end of the ischemic period, blood flow was restored by carefully removing the nylon filament. Mortality rate was 4%. Sham operated mice received a midline neck incision, and the subsequent exposure of the carotid sheath. The external carotid artery and its branches were isolated without being ligated or cauterized.

To confirm hypoperfusion and reperfusion in our model, blood flow was measured (n=3) during the entire tMCAo surgery and at the same post-reperfusion times of two-photon imaging (post and post24h) by laser doppler flowmetry (Perimed PF5010). We used a flexible 0.5 mm probe (Perimed, 407-1) positioned on the brain surface and secured with glue on the skull at the same coordinates of the cranial window: AP: -1 mm; L: -2.5 mm from bregma.

3.3.3 Permanent middle cerebral artery occlusion (pMCAo)

Permanent ischemia was obtained by pMCAO (Perego et al. 2011). Briefly, mice were anesthetized with Equitensin (pentobarbital 39 mM, chloral hydrate 256 mM, MgSO4 86 mM, ethanol 10% v/v, propyleneglycol 39.6% v/v) 100 µl/mouse administered by

intraperitoneal (i.p.) injection. A vertical midline incision was made between the right orbit and tragus. The temporal muscle was excised, and the right MCA was exposed through a small burr hole in the left temporal bone. The *dura mater* was cut with a fine needle, and the MCA permanently occluded by electrocoagulation just proximal to the origin of the olfactory branch. Intraoperative rectal temperature was kept at 37.0 ± 0.5°C using a heating pad (LSI Letica). Mortality rate was 8.5%. Sham-operated mice received identical anesthesia and surgical procedure without artery occlusion.

3.4 Two-photon microscope set up

3.4.1 Microscope used at Mario Negri Institute:

BX51WI microscope coupled to an FV300 scanner head (Olympus Corporation, Tokyo, Japan) and equipped with a multiphoton laser, Chamaleon ultra II (Coherent, Santa Clara, USA). A 20x magnification water immersion objective (XLUMPFL20X W/IR Objective with NA 0.95 WD 2.0 mm, Olympus, Tokyo) was used for multiphoton microscopy.

3.4.2 Microscope used at Strathclyde University:

A Ti-sapphire femtosecond laser (Chameleon, Coherent) provided pulsed infra-red light via a Radiance 2000 scanhead (BioRad) to an upright microscope (Eclipse, Nikon) with a large micrometer-driven stage. A Nikon Fluor 40x, NA 0.80 water immersion objective was used.

3.5 Cortical region compromised by ischemia

To check that the point on the skull with coordinates 2.5 mm lateral and 1 mm posterior to bregma was within the damaged area, we labeled the brain of one pMCAO wild type mice with Evans blue. A 29G needle was inserted at these surface coordinates to a depth of 1.5 mm through a craniotomy and 1 µL of Evans blue solution was injected. The mouse was then injected i.p. with equitensin to induce a deep anesthesia and transcardially perfused. Twenty-micron coronal brain sections were cut and stained with cresyl violet (Sigma Aldrich, MO, USA) to detect ischemic lesion as previously described (Capone et al. 2007; Perego et al. 2011). Images were acquired by an BX61 microscope managed by AnalySIS software (Olympus, Tokyo, Japan).

3.6 *In vivo* tracking of the ischemic region

The sites of imaging were identified by their relation to blood vessels and the stereotaxic coordinates (Fumagalli et al. 2011). The green autofluorescence of the skull bone was used to determine the underside of the skull, which we defined as z=0. To characterize the imaged brain area, 100 µL of a solution of propidium iodide (PI, Sigma-Aldrich; 1 mg/mL), which labels dead cells, was injected intravenously in *cx3cr1*$^{-/+}$ mice or wild-type mice 20 hours after tMCAO, or pMCAo, or sham surgery. The mice were imaged through the thinned skull 4 hours after the propidium iodide injection and 24h after tMCAo or 72h after pMCAo, along with respective sham animals. Excitation wavelength used for PI detection was: 767 nm, while GFP was excited at 844nm. Superimposed 350x350x50 µm thick volumes were obtained combining the two channels.

3.7 Brain transcardial perfusion

At selected time points, namely 24h after tMCAo and 6h, 12h, 24h, 48h, 3d and 7d after pMCAo, mice were deeply anesthetized with Equitensin (120 µl/mouse i.p.) and transcardially perfused with 20 ml of PBS, 0.1 mol/liter, pH 7.4, followed by 50 ml of chilled paraformaldehyde (4%) in PBS. After carefully removing the brains from the skull, they were transferred to 30% sucrose in PBS at 4°C overnight for cryoprotection. The brains were then rapidly frozen by immersion in isopentane at - 45°C for 3 min before being sealed into vials and stored at -70°C until use.

Animals returned to cages and had access *ad libitum* to food and water. No major deficits impairing autonomous feeding and water intake was observed after surgery at any time points (from 6h to 7d), so animals did not receive any further treatments.

3.8 Histology

3.8.1 Ischemic volume assessment

For lesion size determination, 20µm coronal brain cryosections were cut serially at 320µm intervals and stained with Cresyl Violet (Capone et al. 2007). Seven coronal brain slices were assessed, starting from AP=2.5mm and finishing at AP=4.5mm from bregma. On each slice, the infarcted area was assessed blindly and delineated by the relative paleness of histological staining tracing the area on a video screen. The infarcted area and the percentage of brain swelling for edema correction were determined by subtracting the area of the healthy tissue in the ipsilateral hemisphere from the area of the contralateral hemisphere on each section (De Simoni et al. 2003; Swanson et al. 1990). Infarct volumes

were calculated by the integration of infarcted areas on each brain slice as quantified with computer-assisted image analyzer and calculated by Analytical Image System (Imaging Research Inc., Brock University, St. Catharines, Ontario, Canada).

3.8.2 Immunohistochemistry

Immunohistochemistry was performed on 20μm brain coronal sections using anti-mouse antibodies as listed in Table 3.1. Positive cells were stained by secondary antibody coupling (see below, paragraph **3.12.7**) and reaction with 3,3 diaminobenzidine tetrahydrochloride (DAB, Vector laboratories, CA, USA). For negative control staining, the primary antibodies were omitted and no staining was observed.

3.8.3 Immunofluorescence

Immunofluorescence was performed on 20μm coronal sections according to the previously described method (Gesuete et al. 2009). Primary and secondary antibodies used are listed in Table 3.1 and in paragraph **3.8.4**. Appropriate negative controls without the primary antibodies were performed. None of the immunofluorescence reactions revealed unspecific fluorescent signal in the negative controls.

Specificity	Immunized species	Isotype	Dilution	Company
α-CD11b	Rat	IgG	1:800 1:30 000	Kindly provided by Dr. A. Doni
α-CD45	Rat	IgG	1:800	BD Biosciences Pharmingen, San Josè, CA, USA
α-CD3	Rat	IgG	1:200	BD Biosciences Pharmingen, San Josè, CA, USA
α-CD206	Rat	IgG	1:100	AbD Serotec, Kidlington, UK
α-CD68	Rat	IgG	1:200	AbD Serotec, Kidlington, UK
α-Ym1	Rabbit	IgG	1:400	Stem Cell Technologies, Vancouver, Canada
α-GFP	Rabbit	IgG	1:500	Molecular Probes, Life Technologies, Paisley, UK
α-GFAP	Mouse	IgG	1:2 000	Chemicon, Millipore, Billerica, MA, USA
α-iNOS /NOSII	Rabbit	IgG	1:50	BD Biosciences Pharmingen, San Josè, CA, USA

Table 3.1 *List of the primary antibodies used.*

3.8.4 Secondary antibody used for positive cell staining

For DAB staining, I used biotinylated α-rat or α-rabbit IgG antibodies, at 1:200 dilution (Vector Laboratories, Burlingame, CA, USA).

For fluorescent staining, I used fluorconjugated Alexa488 α-mouse, Alexa546 α-rat and Alexa594 α-rabbit (all 1:500, Invitrogen, Carlsbad, CA, USA). I also used biotinylated α-rat and α-mouse (1:200, Vector Laboratories, Burlingame, CA, USA) followed by flourescent signal coupling with streptavidine Alexa647 fluorconjugated (1:100,

Invitrogen, Carlsbad, CA, USA) or TSA amplification system kit (Cy5 1:300, Perkin Elmer, MA, USA).

Alexa488 fluoroconjugated *Griffonia simplicifolia* isolectin IB4 (marker of endothelium, microglia and perivascular macrophages, Invitrogen, Carlsbad, CA, USA) was used to identify cerebral vessels and perivascular macrophages or microglia.

3.9 Confocal analysis

Immunofluorescence was acquired using a scanning sequential mode to avoid bleed-through effects by an IX81 microscope equipped with a confocal scan unit FV500 with 3 laser lines: Ar-Kr (488nm), He-Ne red (646nm), and He-Ne green (532nm, Olympus, Tokyo, Japan) and a UV diode. Three-dimensional images were acquired over a 10μm z-axis with a 0.23μm step size and processed using Imaris software (Bitplane, Zurich, Switzerland) and Photoshop cs2 (Adobe Systems Europe Ltd).

3.10 Statistical analysis

Group comparisons have been done by appropriate analysis of variance and *post hoc* test, as indicated in each figure legend. Choice of parametric or non-parametric test has been done after normality Kolmorgov-Smirnov test to assess whether groups met normal distribution. Group size has been defined by the formula: $n=2\sigma 2f(\alpha,\beta)/\Delta 2$ (sd in groups=σ, type 1 error $\alpha=0.05$, type II error $\beta=0.2$, percentage difference between groups $\Delta=20$). Standard deviation for ischemic volume assessment has been calculated on a previous experiment in which $\sigma=18$, thus yielding $n=12.79$. Standard deviation for histological

evaluation of M/M markers between groups has been calculated on the bases of a previous experiment for CD11b marker expression quantification, where σ=14, thus yielding n=7.74. Statistical analysis was performed using standard software packages GraphPad Prism (GraphPad Software Inc., San Diego, CA, USA, version 4.0). All data are presented as mean and standard deviation (sd). p-values lower than 0.05 were considered statistically significant.

3.11 Experimental design

I performed *in vivo* 2-PM imaging to visualize blood vessels, microglia or T-cells in the ischemic tissue. I obtained different quantitative parameters relative to vascular or cellular dynamics, including blood flow velocity, extravasation, morphological complexity and parameters of cell motility.

I then combined 2-PM output data with histological analysis to confirm *in vivo* imaging data, to visualize the physical relationship between lymphocytes and the neurovascular unit and to define the phenotypical nature of the M/M population in respect to lesion progression.

The general experimental design included:

1) the opening of a craniotomy to uncover a cortical brain area to imaging;

2) *in vivo* 2-PM imaging at basal conditions (*i.e.* before ischemia) of a selected region of interest;

3) induction of transient or permanent ischemia;

4) *in vivo* 2-PM imaging of the selected region of interest during and at different time points after ischemia;

5) quantitative analysis of the three-dimensional time-lapse acquisitions obtained at the 2-PM (measurements of blood flow velocity, extravasation and parameters of motility and morphology).

6) Sacrifice of animals at selected time points to perform histological analysis (assessment of ischemic volume, quantification of apoptotic cells, viable neurons and marker expression, analysis of marker co-expression).

In the sections number **4**, **5**, **6** and **7** I will provide a more accurate description of the experimental plan for each part of the study.

4. MICROVASCULAR MODIFICATIONS AFTER BRAIN ISCHEMIA REVEALED BY 2-PM

4.1 Background

Ischemia determines major vascular effects (Morita et al. 1997; Watson et al. 2002; Wei et al. 1998), including blood flow redistribution and BBB leakage. These events trigger several pathophysiological cascades that evolve over time and space, leading to expansion of brain injury (Dirnagl et al. 1999). The initial onset and temporal evolution of vascular modifications following ischemia are still largely unknown. In this part of the project, I propose to study microvascular rearrangements in a model of tMCAo, by applying 2-PM at different time points from ischemic injury, namely before, during and 1h and 24h after occlusion onset. This part of my project also served for the set up of reliable protocols for preparing animals to 2-PM imaging, for visualizing vessels pertinent to an area affected by ischemia and for performing repeated imaging of the same ischemic area.

A peculiar application of two-photon microscopy is high-resolution angiography since both major vessels and microvasculature can be visualized and numerical data (*i.e.* vascular diameter, blood flow speed and flux volume, Helmchen and Kleinfeld 2008) can be obtained as well. This approach has been successfully applied to evaluate the effects of local vascular thrombosis and MCA occlusion (MCAo) in rats (Murphy et al. 2008; Nimmagadda et al. 2008; Park et al. 2008; Schaffer et al. 2006; Shih et al. 2009). These studies have been focused on the vascular rearrangements occurring after permanent MCA occlusion (pMCAo) or within 2 h after transient MCA occlusion (tMCAo), however, no studies are available describing blood flow dynamics at longer time points which are more

applicable to intervention. In my work I used 2-PM approach to assess *in vivo* blood flow redistribution in a clinically relevant model of tMCAo (Capone et al. 2007). Reperfusion, although ultimately contributing to brain tissue recovery, may also, in the early phases after injury, significantly participate in the pathogenesis by conveying inflammatory cells to the injured area and oxygen to cells unable to use it leading to increased oxygen radical formation (Lo et al. 2003). I examined and analyzed vascular dynamics during ischemia and over time in the same vessels up to 24 h after reperfusion. Furthermore, I provided information on the extent of extravasation in the exact same vessels, as an index of BBB damage, in ischemic conditions starting from very early time points from MCAo onset.

4.2 Specific methods in this chapter

4.2.1 Experimental plan

Experiments were conducted according to the plan detailed in Figure 4.1 A.

4.2.2 Cranial window for two-photon imaging (Mostany and Portera-Cailliau 2008)

During craniotomy, anesthesia of C57BL/6J mice was induced by 3% isoflurane in a N_2O/O_2 (70/30%) mixture and maintained by 1-1.5% isoflurane in N_2O/O_2 (70/30%) mixture. A cranial window was opened at AP: -1 mm and L: -2.5 mm from bregma to expose vessels lying in the region fed by the middle cerebral artery (MCA, Fig. 4.1 B,C). To this purpose, after a midline scalp incision, periostium was gently removed and a cranial window (circular, 1.8 mm in diameter, wide enough to uncover distal branches of the MCA) was created using an electric drill leaving the *dura mater* intact (drill tip by

Meisinger, Germany). A coverglass was placed on the craniotomy and the space between the glass and the brain was filled with agarose at 1.5% in sterile saline. Coverglass and a small nut were glued on the skull to permit animal immobilization under the microscope and a small well was created using epoxy glue to allow objective lens immersion in water during imaging. Craniotomized mice were given an overnight recovery before first imaging session.

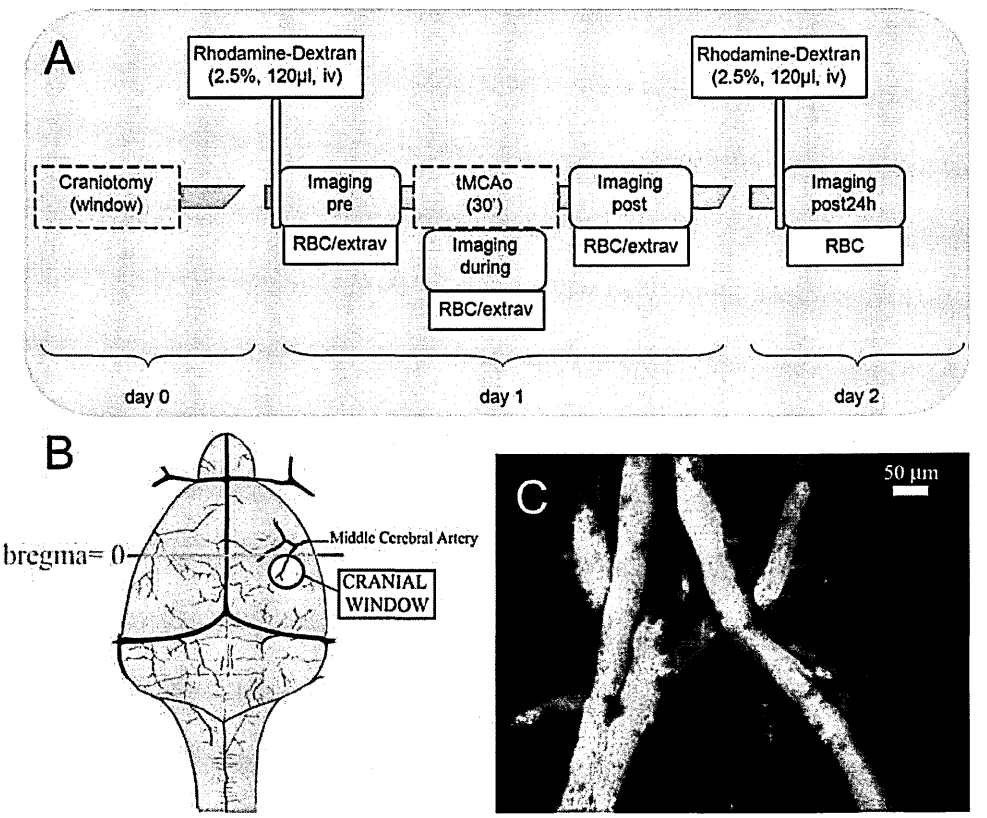

Figure 4.1 *Experimental plan and cranial window for imaging.*

Imaging was performed according to the plan showed in A. Cranial window was opened at day 0, while imaging was performed at day 1 and 2. *RBC* indicates the assessment of RBC speed, while *extrav* indicates the quantification of extravasated fluorescent signal. At pre, *RBC* and *extrav* were collected 30min and 20min before ischemia respectively. At during *RBC* and *extrav* were collected 10min and 20min after MCAo onset respectively. At post *RBC* and *extrav* were collected 40min and 50min after MCAo onset respectively. At post24h, only *RBC* was assessed. B) A distal branch of the MCA was exposed under the cranial window (image modified from: *The Anatomy of the Laboratory Mouse*, by Margaret J. Cook: http://www.informatics.jax.org/cookbook). C) Two-photon high-resolution angiography of the region lying under the cranial window and used for analysis. A mean of 6 vessels per brain were used to assess RBC speed and extravasation. After the first imaging session (pre) the analyzed vessels were labelled with a number on the angiography image obtained (Fig. 1C). This allowed to perform subsequent analysis on exactly the same vessels at each experimental time point. Scale bar= 25µm.

4.2.3 High-resolution angiography and extravasation measurement

A 20x magnification water immersion objective (XLUMPFL20X W/IR Objective with NA 0.95 WD 2.0 mm, Olympus, Tokyo) was used for high-resolution angiography. Tridimensional reconstructions over the z-axis were obtained at each time point of the observation and were used to measure extravasation. Image resolution was 800x600 pixels and distance between subsequent focal levels was 2 μm. Extravasation analysis was performed on each vessel used for RBC speed evaluation. It was identified by parenchymal accumulation of the fluorescent marker whose transendothelial transport is negligible under physiological conditions due to its molecular weight (70 kDa, Deli). All the images lying on the same focal stack of a vessel were collected and included into the analysis. Integrated pixel density over the selected stack was calculated inside (intra-vascular) and nearby (extra-vascular) a vessel. ImageJ software (http://rsbweb.nih.gov/ij/) was used for the analysis and extravasation was expressed as ratio between intra-vascular and extra-vascular mean pixel density over the z axis.

4.2.4 Blood flow speed measurement

Blood flow speed was calculated as red blood cell (RBC) speed according to the line-scan method (Fig. 4.2, Nimmagadda et al. 2008; Schaffer et al. 2006). Imaging was performed over a 250 μm thick cortical region, where most vessels lie horizontal to the cortical surface. Line-scan acquisition was performed at a rate of 830 Hz, positioning the acquisition line at the centre of the vessel where blood flow speed is supposed to reach its maximum value (Schaffer et al. 2006). The determination of RBC speed from the streaks in the space-time line-scan data was performed over 6 second epochs, divided into short subset epochs of 300ms each. Three 300ms epochs per image were then rotated to yield

horizontal RBC streaks and speed was calculated by assessing the mean $\Delta x/\Delta t$ slope value for each vessel (Nimmagadda et al. 2008). A negative value for speed accounts for inversion in blood flow direction in comparison to the baseline condition.

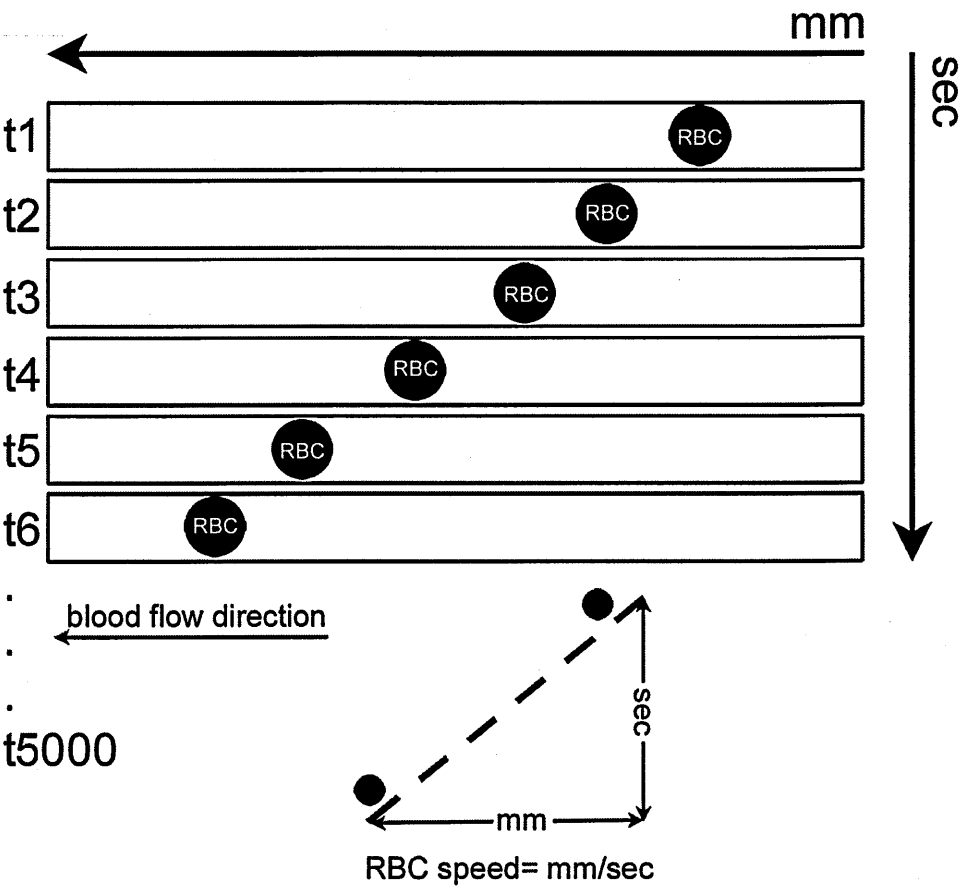

Figure 4.2 *Method for RBC speed calculation.*

RBC can be visualized as round-shaped black objects in the blood stream as they do not take up the fluorescent dye. Five-thousands linescans over 6 seconds are acquired and piled up to yield an image whose side lengths corresponds to distance (mm) and time (sec). RBC, by flowing within the vessel according to blood flow direction, form diagonal streaks. Slopes of streaks are calculated to obtain RBC speed as mm/sec.

4.2.5 Histological assessment of extravasation

To verify our *in vivo* extravasation method, we additionally assessed extravasation via well established post-mortem histological technique (Marcon et al. 2009). Extravasation was evaluated at post experimental time point. Briefly, after skin incision, mice were

transcardiacally perfused with a fluorescent dye solution (FITC-albumin, 10 mg/ml in buffered saline, Sigma-Aldrich) at 1 ml/min (10 ml/kg, Marcon et al. 2009). Five minutes after injection, mice were killed by decapitation and their brains were immersion-fixed for 48h in 4% paraformaldehyde in 0.1 M PBS, pH 7.4, cryoprotected overnight in 30% sucrose in PBS, frozen at −45 °C in isopentane and stored at −20 °C. Coronal sections (20 μm) were cut on cryostat and collected on gelatin-coated slides and coverslipped using Fluorsave to preserve fluorescent signal (Calbiochem, Germany).

Z-stacked images from cortical regions at -0.58 and -1.22 mm from bregma were collected with the confocal microscope Olympus IX81 equipped with an Olympus confocal scan unit FV500 and managed by Fluoview software (Olympus Tokyo, Japan).

4.2.6 Blood gas analysis

Craniotomized ischemic mice were prepared for blood gas analysis in order to establish whether the anesthesia and surgery protocol affected physiological parameters. After anesthesia induction and at the experimental time points shown in Fig. 4.1 A, mice were subjected to right carotid artery exposure and 100 μL of blood was withdrawn and loaded on cartridges. Blood gas analysis was then performed by the i-STAT 1 analyzer (i-STAT Corporation, East Windsor, NJ).

4.3 Results

4.3.1 RBC speed

Assessment of pH and pCO_2 values revealed that anesthesia and surgery procedures did not significantly affect physiological parameters (Table 4.1).

Table 4.1 *Physiological parameter analysis*

parameter	pre	during	post	post24h
pH	7.3±0.03	7.3±0.08	7.2±0.02	7.4±0.08
pCO^2	39.4±4.41	37.4±8.13	35.2±2.17	36.4±8.95

Data for pH and pCO^2 (mm Hg) are showed for each experimental time point, n=4.

A total of 24 vessels visualized in 4 different ischemic mice were analyzed and pre-ischemic baseline RBC speed for each vessel ranged from 0.438 to 8.000 mm/s (Table 4.2), with a mean value of 3.130±2.121 (mm/s, mean±sd). Each vessel represented an independent biological unit for statistical analysis in this result section.

During MCAo mean RBC speed dropped to 0.287±0.411 mm/s. Blood flow was completely blocked in 4/24 (0 mm/s) while the remaining vessels were still perfused, albeit to different extents. Perfusion in 11/24 vessels was largely inadequate ranging from 0.025 to 0.069 mm/s (during, Table 4.2). Blood flow was found to be slightly preserved only in 6/24 vessels ranging from 0.258 to 0.982 mm/s, which represents a percentage drop of 85% in comparison to pre values. Notably, in 3/24 vessels blood flow was inverted, reaching a mean speed of -1.170±0.207 mm/s. The temporal profile of RBC speed for each vessel is illustrated in figure 4.3 A,C.

When reperfusion was allowed, 10 min after reperfusion, RBC speed showed a mean value of 0.403±0.523 mm/s. 2/24 vessels exhibited zero flow and 7/24 showed a poor perfusion

ranging from 0.025 to 0.055 mm/s (Table 4.2). In 11/24 vessels blood flow was restored ranging from 0.147 to 0.778 mm/s corresponding to a reduction of 80% in RBC baseline speed. Blood flow was restored to higher levels (1.487 to 1.767 mm/s, representing a 64% drop) only in three vessels belonging to the same mouse, while reverted flow was preserved in only 1 vessel (-0.162 mm/s).

Twenty-four hours after ischemia RBC speed averaged 0.471±0.751 mm/s. The total number of blocked or inadequately perfused vessels did not vary in comparison with post. Interestingly, as illustrated in Table 4.2, these vessels were not necessarily the same which were blocked or poorly perfused at the previous time point and, vice versa, some vessels that showed a flow soon after reperfusion were not able to preserve it 24 h later.

Notably, in one mouse, 24 h after reperfusion, blood flow was completely prevented in three vessels, although these vessels were not blocked either during ischemia or 10 min after reperfusion. RBC speed in the vessels in which blood flow was re-established at post24h showed a reduction of 70% compared to pre values. No vessel exhibited a reverted blood flow 24 h after reperfusion, indicating that the endogenous flow reversal in response to an occlusion is a transient event.

I did not observe any significant variation in RBC speed of the four sham-operated mice (22 vessels were analyzed) during the whole experiment (Fig. 4.3 B,D).

Table 4.2 *Red Blood Cell speed values*

	pre	during	%	post	%	post24h	%
mouse 1							
	2.608	0.982	37.653	0.147	5.637	0.000	0.000
	3.355	-1.232	-36.721	-0.162	-4.829	0.000	0.000
	3.046	0.325	10.670	0.043	1.412	0.009	0.295
	5.078	0.025	0.492	0.000	0.000	0.057	1.122
mouse 2							
	2.078	0.064	3.080	0.037	1.781	0.011	0.529
	3.043	0.039	1.282	0.021	0.690	0.031	1.019
	3.241	0.058	1.790	0.325	10.028	0.178	5.492
	2.656	0.052	1.958	0.161	6.062	0.076	2.861
	4.799	0.032	0.667	0.055	1.146	0.036	0.750
	4.478	0.000	0.000	0.190	4.243	0.053	1.184
	6.731	0.386	5.735	0.769	11.425	0.219	3.254
mouse 3							
	2.714	0.000	0.000	0.570	21.002	0.702	25.866
	7.218	-1.339	-18.551	1.767	24.480	2.798	38.764
	3.030	0.470	15.512	1.487	49.076	2.367	78.119
	4.799	0.368	7.668	1.608	33.507	1.177	24.526
	0.871	0.064	7.348	0.373	42.824	0.217	24.914
	2.134	0.258	12.090	0.778	36.457	0.684	32.052
	0.736	0.068	9.239	0.288	39.130	0.158	21.467
	1.157	0.061	5.272	0.392	33.881	0.066	5.704
mouse 4							
	1.086	0.068	6.262	0.037	3.407	0.714	65.746
	0.911	0.069	7.574	0.046	5.049	0.285	31.284
	0.438	0.000	0.000	0.000	0.000	0.000	0.000
	8.000	-0.939	-11.738	0.402	5.025	1.306	16.325
	0.914	0.000	0.000	0.025	2.735	0.151	16.521

Absolute RBC speed values expressed as mm/s and their % compared to pre are reported for each analyzed vessel.

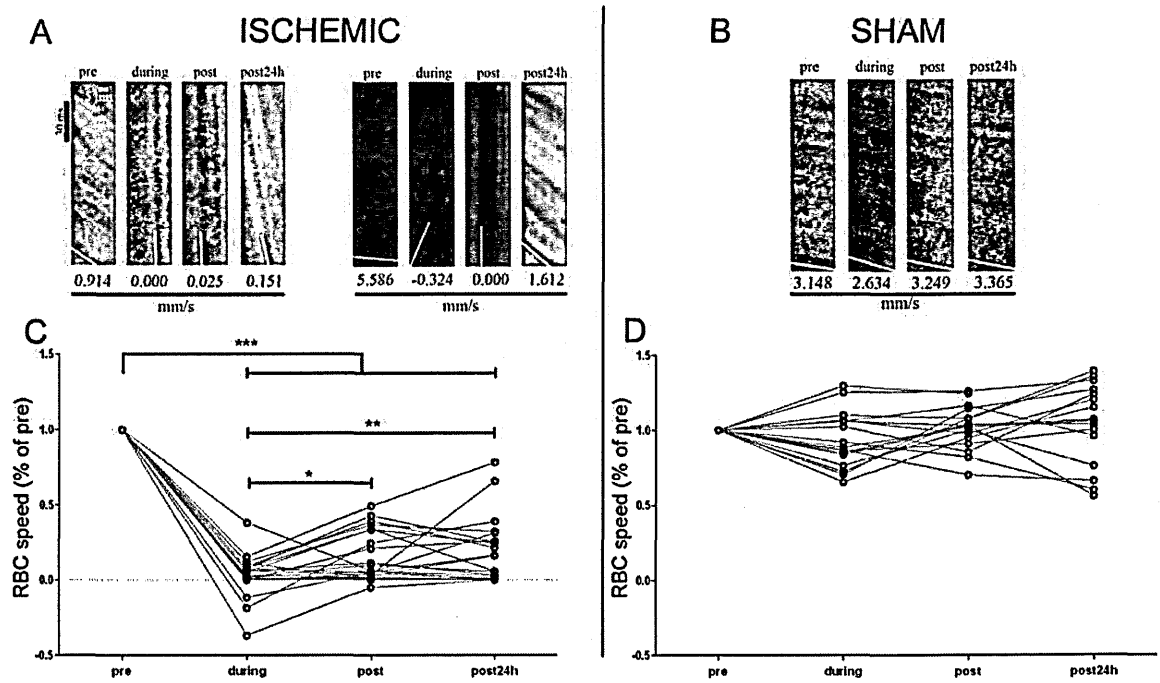

Figure 4.3 *RBC speed measurements.*

A) Representative ischemic mouse: RBC streaks (white lines) obtained from the line-scan acquisition over a 135 ms period, change their slope revealing blood flow slowing down during ischemia and at post. RBC speed remains slow at post24h, indicating an inadequate reperfusion. Scale bar= 14μm. B) Representative sham-operated mouse: the slopes of RBC streaks (white lines) do not vary over the four experimental time points. C) RBC speed fold-change compared with pre in 4 ischemic mice showing a significant reduction in RBC speed during tMCAo. At post and post24h blood flow appears to be only weakly restored. Calculated fold-change values for speed in sham-operated animals are plotted in D. Each line corresponds to an individual vessel. One-way ANOVA for repeated measures; post-hoc Tukey's test; *$p<0.05$, **$p<0.05$, ***$p<0.001$.

4.3.2 Laser Doppler measurements

To exclude the possibility that poor blood flow re-establishment was due to an experimental artifact (e.g. lack of reperfusion of MCA or increased blood density after dextran injection), we performed a laser Doppler analysis at the same stereotactic coordinates of the cranial window (AP: -1 mm; L: -2.5 mm from bregma). Mice were

subjected to the same anesthesia regimen of imaging sessions and injected with fluorescent-dextran prior to ischemia. Laser Doppler measurement revealed blood flow restoration, although incomplete, both 10 min and 24 h after ischemia (n=3, Fig. 4.4 showing a representative mouse).

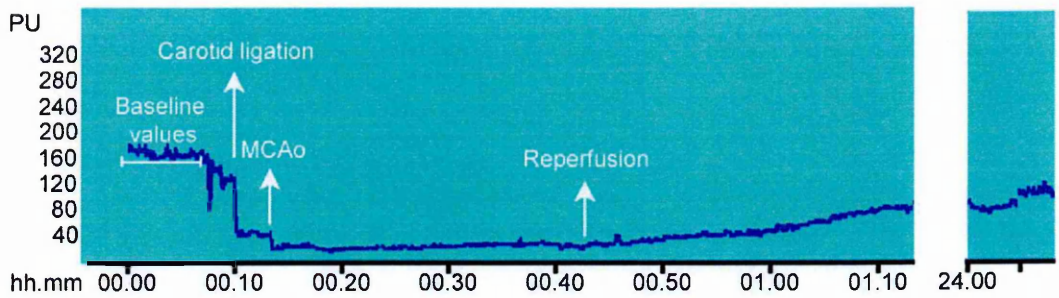

Figure 4.4 *Laser Doppler tracking of a mouse subjected to tMCAo.*

Blood flow (blue track) dropped significantly (over 70%) after MCAo compared with baseline values in the area measured by the laser Doppler (2.5 mm lateral and 1 mm posterior to bregma). When reperfusion was allowed, blood flow re-established to levels that were kept at 24h after MCAo. PU = perfusion units; time scale indicates hours:minutes.

4.3.3 Extravasation

Extravasation was assessed by parenchymal accumulation of the fluorescent marker which normally does not cross the barrier due to its molecular dimension (70 kDa). Extravasation was measured 20 min after the ischemic onset and 20 min after reperfusion. Since imaging at post24h was obtained following a new fluorescent dextran administration, comparable extravasation data at this time point could not be provided.

Fluorescent dextran presence in the parenchyma was significantly increased 20 min after MCA occlusion onset (Fig. 4.5 A-C, G) suggesting a rapid appearance of extravasation. In contrast to ischemic mice, sham-operated mice did not show any significant extravasation, indicating that imaging in normal conditions did not affect vessel viability (Fig. 4.5 D-F). A mild, not statistically significant, increase of integrated density ratio between extra- and

intra-vascular pixels was also apparent in the sham animals (Fig. 4.5 G). This was probably due to either a progressive loss of performance of the laser during imaging or to the physiological clearance of the dextran over time, which leads to a gradual decrease of intravascular concentration of the fluorescent dye. It is important to note that this technical bias did not hamper the visualization of vessels, therefore fluorescent signal was not enhanced by laser intensity or photomultiplier adjustment over time.

To further validate the *in vivo* method to detect extravasation and exclude any false positive results due to the technical bias, we performed a *post-mortem* analysis through a well established histological method (Marcon et al. 2009). By transcardiac injection of FITC-albumin, we were able to confirm that extravasation was present at post in the ischemic region and that surrounding cortical areas did not reperfuse (Fig. 4.5 H,I). Contra-lateral side was used as control and showed a uniform perfusion in the cortex with no signs of extravasation (Fig. 4.5 L,M).

Extravasation was found to be associated with morphological changes in the vessel profiles, possibly due to the incipient BBB damage. The alterations were evident during ischemia and lasted at every time point considered (Fig. 4.6 A-D). In the sham-operated mice vessel edges preserved their straight and regular shape (Fig. 4.6 E-H).

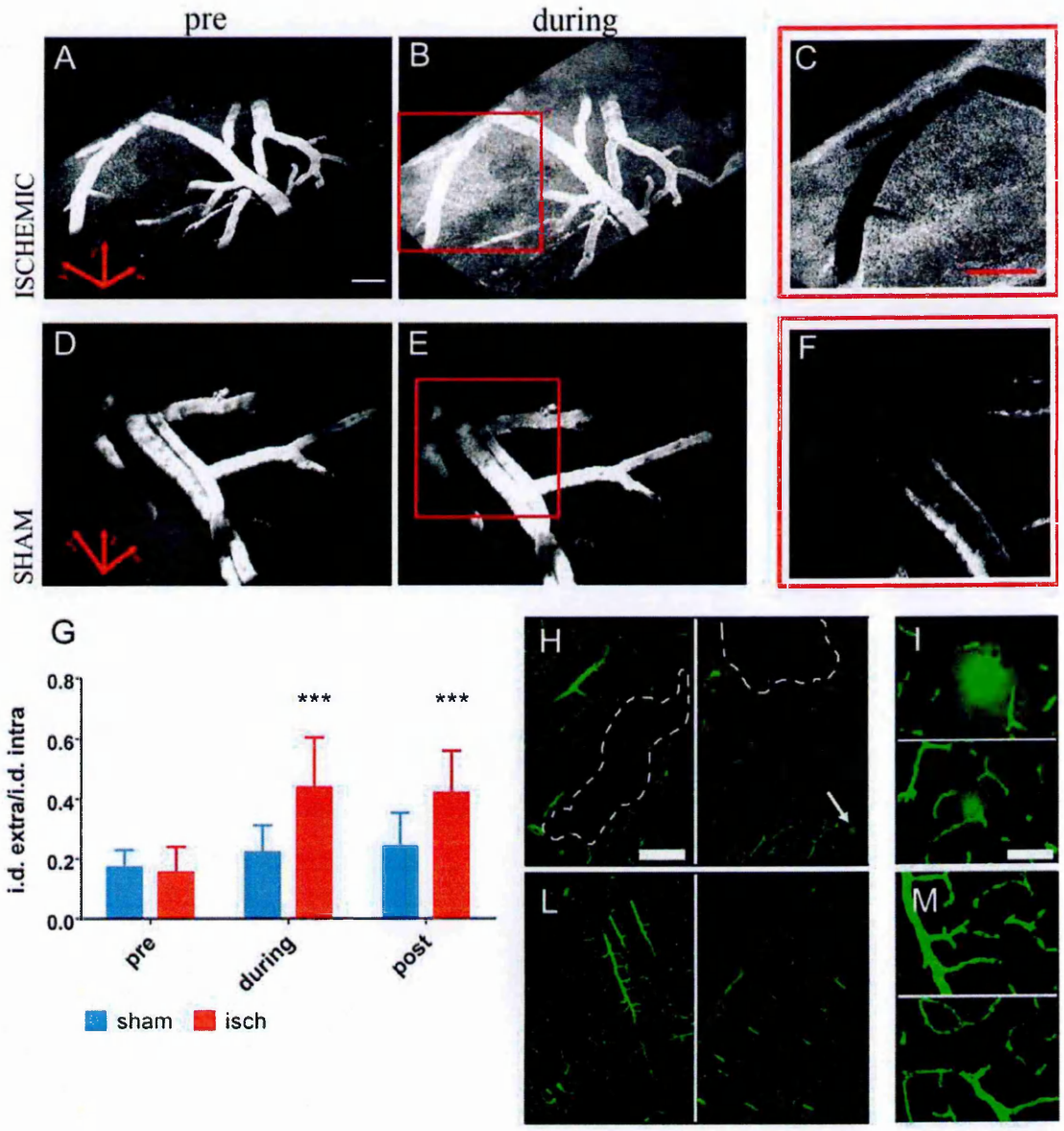

Figure 4.5 *Extravasation assessment at the different experimental time points.*

Extravasation became evident as early as 20 minutes after the occlusion onset. At baseline (A) the fluorescent marker signal was confined into the vessels, with a minimum background noise widespread in the parenchyma. During tMCAo (B) the fluorescent signal was also clearly visible outside the vessels indicating that extravasation occurred. A differential image of the red insert was obtained by subtracting image A to image B. The resulting image (C) shows the parenchymal accumulation of dextran. In sham-operated mice (D, E and F) no extravasated fluorescent signal was detectable, and the apparent signal in the differential image in F is due to a slight misalignment of the vessels. Bars= 100 μm.

G) Integrated density ratio between extra- and intra- vascular dextran. In the ischemic mice extravasation is significantly increased as early as 20 minutes after the occlusion onset. Data from the same mice that were calculated for RBC speed and expressed as mean+sd, n=24 vessels for ischemic mice and n=22 vessles for

sham-operated animals. Two-way ANOVA ($p<0.0001$) followed by *post-hoc* Bonferroni test: ***$p<0.001$ vs sham. H) Post-mortem histological analysis of extravasation (FITC-Albumin) at post reaveals vast cortical areas with no-reperfusion in the ischemic mice (dashed areas) and some extravasation (white arrow); scale bar= 200μm. At higher magnification (I) extravasation is clearly visibile; scale bar= 50μm. Contra-lateral side appears entirely perfused and does not show any visible extravasated fluorescent dye (L, M).

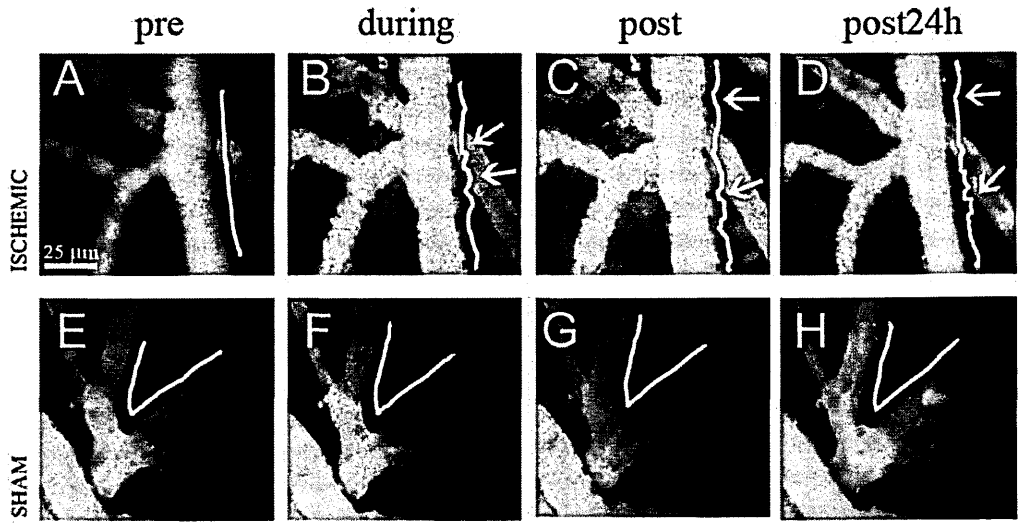

Figure 4.6 *Morphological changes in the vessel edges accompanies extravasation.*

At baseline (A) vessel borders appear to be straight and regular, while during tMCAo (B) they became markedly irregular possibly due to the incipient BBB damage (white arrows). During the first minutes of reperfusion (C) and at longer times (D), BBB damage is still present, being the irregular shape always visible. In a sham-operated mouse, no alteration in the vessel morphology is apparent at any time point analyzed (E, F, G and H). Scale bar= 25μm.

4.4 Discussion

In this part of the project, I have: 1) set up and applied an *in vivo* 2-PM protocol for investigating temporal vascular and hemodynamic events in individual cerebral vessels after ischemia/reperfusion; 2) used the protocol to obtain data on blood flow speed, extravasation and vascular morphology.

During occlusion we consistently observed a massive blood flow decrease in the cortical region fed by MCA. Notably, in a few branches, blood flow reversion occurred. This phenomenon that had been previously described following permanent ischemia could be the result of redundancy in the cortical vascular architecture that acts as endogenous protective response to occlusions (Schaffer et al. 2006). We found that extravasation appeared within the first 20 min after tMCAo onset, rapidly contributing to edema formation. This data is consistent with the observations by Strbian *et al.* (Strbian et al. 2008) who studied gadolinium extravasation in a rat model of transient ischemia by means of MRI and found that extravasation is present at 25 min after ischemia (Strbian et al. 2008). Compared with MRI, 2-PM provides a higher level of resolution, allowing monitoring of morphology and blood flow changes over time in each individual vessel. Notably, analyzing vascular morphology, we could observe that the vessel edges became markedly irregular during ischemia indicating that the microvascular structure was rapidly affected by ischemia. In sham-operated mice vascular borders kept their regular and straight shape during the whole session of imaging and this was regarded as an index of a healthy state. These results in the sham-operated mice show that 2-PM is a suitable technique to study intact tissues over time. Indeed, the fluorescent signal was clearly detectable at each time point analyzed and, moreover, exposure to the laser beam did not impair vessel viability.

We could observe that reperfusion did not result in an adequate re-establishment of blood flow at post, in line with what observed by Shih *et al.* (Shih et al. 2009). We could also show that this lack of reperfusion persisted up to 24 h after the occlusion removal, although the laser Doppler analysis showed that reperfusion was there at both time points. The apparent inconsistency between laser Doppler and two-photon analysis can be explained as while laser Doppler measures the general blood flow in an area beneath the probe

including large vessels, 2-PM allows the study of small individual vessel contribution to perfusion with an higher anatomical resolution.

The existence of an incomplete re-establishment of blood flow following reperfusion in small vessels had been previously proposed on the basis of *post-mortem* analysis and defined as 'focal no-reflow' (Del Zoppo and Mabuchi 2003). It suggests the existence of further pathogenetic mechanism, induced by the occlusion, affecting vascular viability. It is possible that rapidly established edema causes an increased parenchymal pressure leading to a relevant vascular compression able to affect flow recovery in the microvasculature. Furthermore, even if the number of inadequately perfused vessels did not vary either 10 min or 24 h after ischemia, the analysis of each individual vessel showed that not every perfused vessel at post was able to maintain perfusion later on, and vice versa. This observation corroborates the idea that mechanisms driven by edema prompted the vasculature to a further rearrangement during reperfusion, impairing, thereby, a complete and effective blood flow re-establishment.

Massive rearrangements in blood flow and morphological changes of vessels along with early extravasation following tMCAo confirm that cerebral vasculature responds to an altered CNS state with high dynamism (Del Zoppo and Mabuchi 2003). CNS vascular architecture forms a highly interconnected network which has been hypothesized to assure a source of collateral flow in the event of a vessel occlusion (Brozici et al. 2003; Vander Eecken and Adams 1953; Wei et al. 1995). In this respect 2-PM represents a unique tool to study rapid vascular rearrangements and to follow them for several hours after ischemic injury.

In this study we have analyzed, for the first time, the effects of reperfusion on vascular dynamics following ischemia up to 24 h after injury. This is relevant since reperfusion leads to massive recruitment of immune cells that significantly contribute to the ischemic damage pathogenesis. At this time point I could show that blood flow is not fully restored,

possibly as a consequence of extravasation effects, and that flow reversal is not present any longer.

It has been recently reported that anesthesia regimen may influence blood flow analysis with 2-PM (Tétrault et al. 2008). Our data clearly show that haemogas parameters were not significantly affected by the chosen anesthetic regimen across groups, excluding the hypothesis that anesthesia *per se* could be responsible for RBC speed changes through mechanisms that are independent from MCA occlusion. Fluorescent-dextran clearance may represent an additional bias that affects extravasation measurements possibly originating false positive data. We confirmed the occurrence of extravasation by a conventional confocal analysis on frozen sections from FITC-Albumin perfused brains. The histological analysis also revealed that vast not-perfused areas were present in the cortical regions affected by ischemia. This data is in line with the lack of reperfusion that we observed by *in vivo* imaging. Interestingly, since not-perfused areas on the sections were spread all over the injured cortex and were present also beyond the imaged area, we can further rule out the possibility of any local artefact in the area assessed *in vivo* due to either the cranial window or the laser irradiation.

4.5 Conclusions

We established a reliable model to study the effects of ischemic/reperfusion injury at different time points and up to 1 day after the ischemic onset, thus providing a detailed time course of the events in the same animal. We showed a massive reduction in blood flow measured as RBC speed during ischemia and an inadequate re-establishment of flow after reperfusion. This focal no-reflow in the area fed by the MCA can be explained by

mechanisms driven by rapid extravasation which causes microvessel compression and impairs reperfusion. Indeed extravasation could be shown as early as 20 minutes after the MCA occlusion. Furthermore, we showed that reversion in blood flow is a transient event since it is not present 1 day after ischemia.

In humans, the degree of reperfusion after brain ischemia, if present, is highly variable (Caplan et al. 2011; Lo 2008b). However, in the future the number of patients undergoing reperfusion is likely to increase, since the time window for thrombolytic therapy has been recently widened from 3 to 4.5 h (Davis and Donnan 2009). Thus, the exact comprehension of vascular dynamics at the level of the individual vessel *in vivo* when reperfusion is allowed represents a crucial issue for stroke therapy and improved recovery.

5. *IN VIVO* IMAGING OF MICROGLIA AND PROTECTIVE FEATURES OF CX3CR1-DEFICIENT MICROGLIA

5.1 Background

In physiological conditions, microglia perform micro-environmental patrolling by the extension/withdrawal of ramifications (Davalos et al. 2005; Hanisch and Kettenmann 2007). Activation of microglia in response to a pathological status drives a switch in phenotype along with change in cell morphology. Following ischemia, activated microglia can potentially exert either protective or detrimental effects suggesting that these cells may acquire different phenotypes belonging to the 'classical' (M1) or to the 'alternative' (M2) active status which have been described for macrophage-driven immunity (David and Kroner 2011; Michelucci et al. 2009). Specific environmental signals, including effector molecules, timing of activation and degree of injury may induce these different polarization states (Porta et al. 2009; Zanier et al. 2011). As a direct consequence of their commitment, microglia can worsen the final outcome or promote tissue recovery.

Over the last years, a particular interest raised for fractalkine, a chemokine responsible for deregulating microglia activity (Lauro et al. 2006; Prinz and Priller 2010). Fractalkine binds to its unique receptor CX3CR1, which is expressed on resident brain microglia/macrophages and on peripheral immune cell populations (Prinz and Priller 2010). Binding of fractalkine to CX3CR1 is needed for neuron-microglia communication. In normal conditions, neurons continuosly release fractalkine keeping microglia inactive. Following an acute insult, neurons significantly decrease the release of fractalkine allowing the activation of microglia (Hundhausen et al. 2003; Lauro et al. 2006). Animals in which

the *cx3cr1* gene is substituted with the gene for the green fluorescent protein (GFP) on both alleles ($cx3cr1^{GFP/GFP}$), thus being defective for the receptor of fractalkine (henceforth referred to as $cx3cr1^{-/-}$ mice), have been used to assess the importance of the fractalkine:CX3CR1 pathway in neurological disorders (Cardona et al. 2006; Corona et al. 2010; Dénes et al. 2008; Donnelly et al. 2011). In models of chronic diseases such as lateral amyotrophic sclerosis (ALS, Cardona et al. 2006) Parkinson's disease (Pabon et al. 2011) and Alzheimer's disease (Cho et al. 2011b), the absence of CX3CR1 has been associated with a worst outcome possibly be due to the lack of fractalkine control of microglia activation leading to chronic pro-inflammatory function (Iadecola and Anrather 2011; Zujovic et al. 2000). Surprisingly enough, however, the absence of CX3CR1 in acute injury models (transient and permanent ischemia, spinal cord injury) has been instead associated with a favourable outcome (Cipriani et al. 2011; Dénes et al. 2008; Donnelly et al. 2011; Soriano et al. 2002). Thus available data do not allow to draw a coherent picture of the role of fractalkine in brain injury and disease. Specifically, little information is available on fractalkine:CX3CR1 pathway in the context of microglia activation following brain ischemia.

In this part of the study, using a murine model of transient focal ischemia (tMCAo), I explored the consequences of CX3CR1 absence on microglia phenotype. I analyzed microglia morphology and motion *in vivo* by two-photon microscopy before, 1h and 24h after transient brain ischemia in $cx3cr1^{-/-}$ and in $cx3cr1^{-/+}$ mice. In these two strains I also assessed the expression of the microglia/macrophage (M/M) markers CD11b, CD68, CD45, Ym1, CD206 and iNOS by quantitative immunohistochemistry. Lastly, I determined the susceptibility to ischemic injury.

5.2 Specific methods in this chapter

5.2.1 Experimental plan

Experiments were conducted according to the plan shown in Fig. 5.1.

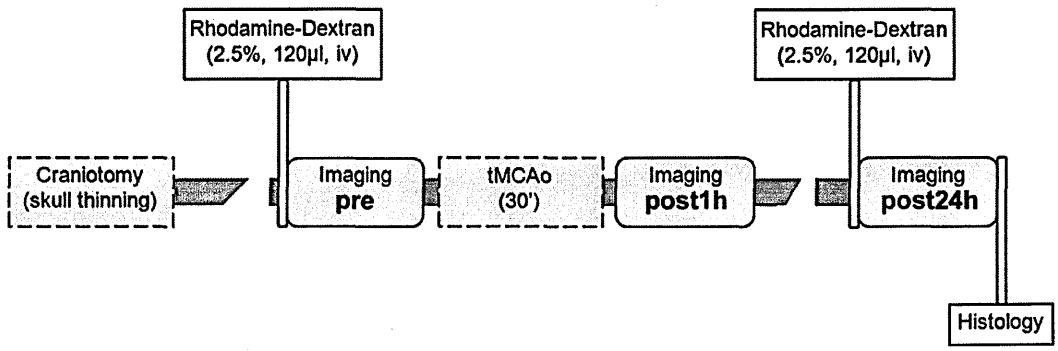

Figure 5.1 *Experimental plan.*

Mice were subjected to skull thinning craniotomy. After one overnight recovery, they received iv Rhodamine dextran to label the vessels and underwent two-photon imaging at baseline (pre), 1h and 24h after tMCAo (post1h and post24h respectively). Each imaging session lasted approximately 30 min including animal positioning under the objective, RBC speed acquisition and 20min time-lapse recording. Mice were sacrificed at 24h for histological analysis.

5.2.2 Thinned skull craniotomy for two-photon imaging (Fumagalli et al. 2011)

At Mario Negri Institute, Milan, Italy: The blood was labeled by injecting a red fluorescent marker in a tail vein, rhodamine B isothiocyanate-dextran (RhITC-dextran, 70 kD, Sigma; 5% in PBS, 150 µL) prior to imaging. Mice (n=5) were isoflurane-anesthetized with rectal temperature maintained at 37°C and positioned on a stereotactic frame (KOPF, CA, USA). The left parietal skull was exposed and dried; a point near 2.5 mm lateral, 1 mm posterior to the bregma was marked. Under a dissecting microscope, the skull was thinned using a dental drill with a diamond burr (Meisinger, Neuss, Germany). When the pial vasculature

could be clearly seen, a sterile absorbable gelatin sponge with hemostatic effect was applied on the thinned skull for the control of the bleeding of skull microvessels (Curaspon, Cura Medical, Assendelft, The Netherlands). A stainless M3 nut was positioned on the contra-lateral side of the skull and glued with epoxidic glue. This served to firmly position the animal under the microscope during the whole imaging sessions. A small well was prepared around the thinned skull with the epoxidic glue to allow objective immersion in water for image acquisition. Craniotomized mice were given an overnight recovery before first imaging session.

5.2.3 Imaging of GFP+ microglia

5.2.3.1 GFP signal detection

We imaged cortical volumes sized 350x350x30 μm in mice receiving a previous intravenous injection of RhITC-dextran, 70 kDa, Sigma; 2.5% in sterile water, 150 μL. RhITC-dextran and GFP were simultaneously excited at 844nm, and emission wavelengths were separated through a 500nm dichroic mirror and conveyed to two external photomultipliers (Hamamatsu Photonics, Japan).

5.2.3.2 Image acquisition and processing

The location (centroid) of each GFP+ cell within each 3-dimensional image stack was determined manually by the operator. To quantify GFP+ cell displacement rate we calculated, for each cell, the straight line distance from the first location in the track to the last and divided by the time it was tracked (Fig. 5.2 A). Where needed, image shift over

time was corrected in the 3-dimensional space using vessel geometry as reference points. Displacement rate was expressed as μm/minute (Fumagalli et al. 2011).

Sholl analysis (Gensel et al. 2010) was used for measuring cell morphology on the basis of frequency and length of ramifications. Each GFP+ cell was visualized in orthogonal view mode, selected and put into a field formed by concentric circles whose smallest had a 5μm radius and biggest a 40μm radius. Distance between each circle was 0.5μm. The frequency of each circle touching by cell ramifications was counted (Fig. 5.2 B). Mean number of cell touchings per cell from 5 to 10 μm, 10 to 20 μm and 20 to 30 μm from cell controid were plotted into graphs and used for statistical analysis.

Post-acquisition processing was performed by using Imaris software (Bitplane, Switzerland) and ImageJ (http://rsbweb.nih.gov/ij/). Five animals per group underwent imaging session and 18-20 GFP+ cells per imaged volume were detectable at each time point.

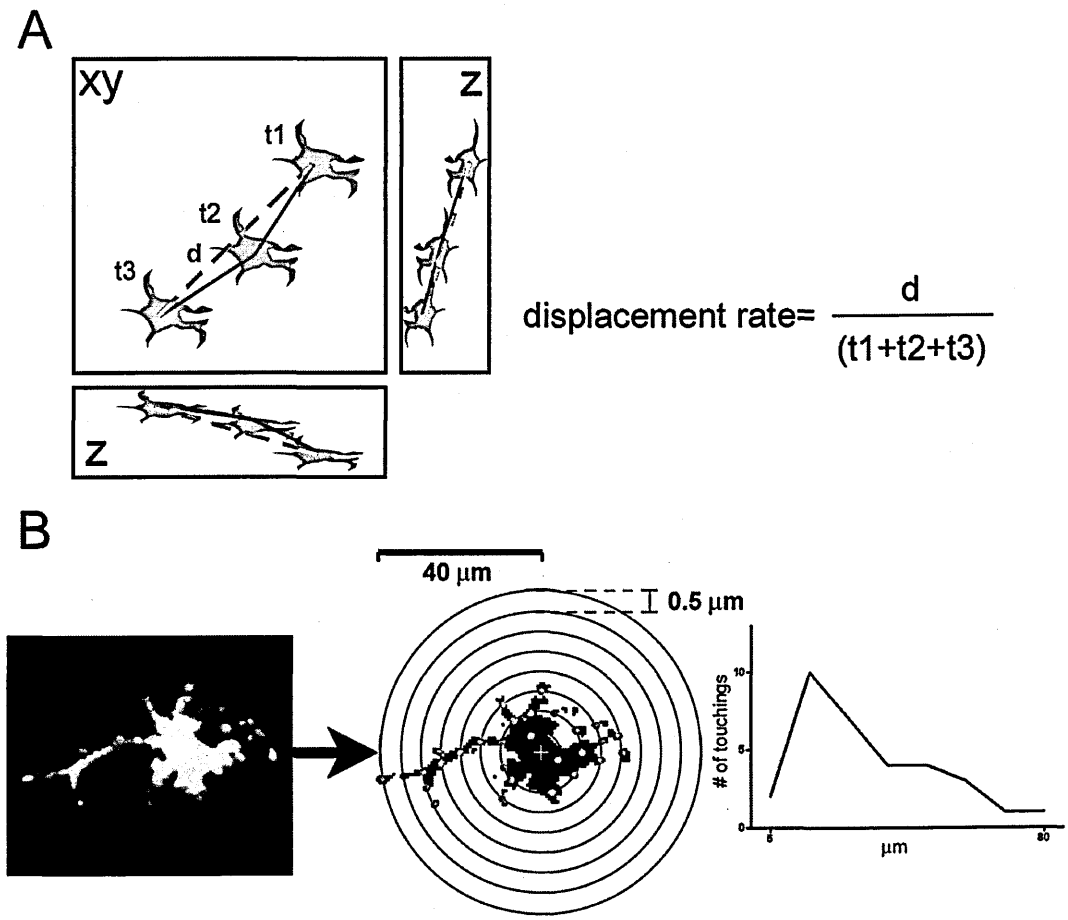

Figure 5.2 *Methods for quantification of cell displacement and Sholl analysis.*

To calculate cell displacement rate, xyz coordinates of cell centroid for a given cell were connected between subsequent time points (t1…t3). Linear distance between first and last time points was calculated and divided by the total time in which the cell was imaged (t1+t2+t3+…+tf= 20 minutes, A). Sholl analysis was performed for each visible cell in the imaged field (B). Isolated cells were put into a field made by concentric circles with increasing radius (ranging from 5 to 40µm, 0.5µm interval). Number of ramification touchings per circle was quantified and graphed.

5.2.4 Slices selection and quantitative analysis

The coronal sections used for marker quantification in ischemic areas were:

cortex: -1mm from bregma, corresponding to the cortical area beneath the craniotomy (Fumagalli et al. 2011). 13 frames at 40x magnification, distancing their centres 270 µm horizontally and 360 µm vertically;

striatum: +0.6, 0 and – 0.6 mm from bregma, 10 frames at 40x magnification per section. Centres of frames were distanced 450μm for horizontally aligned frames and 400μm for vertically aligned frames.

Positioning of the frames is detailed in Fig. 5.3.

Quantifications were performed using ImageJ software (http://rsbweb.nih.gov/ij/) and expressed as positive pixels/total assessed pixels (staining percentage area), or cells/mm^2 (cell density) for subsequent statistical analysis (Perego et al. 2011).

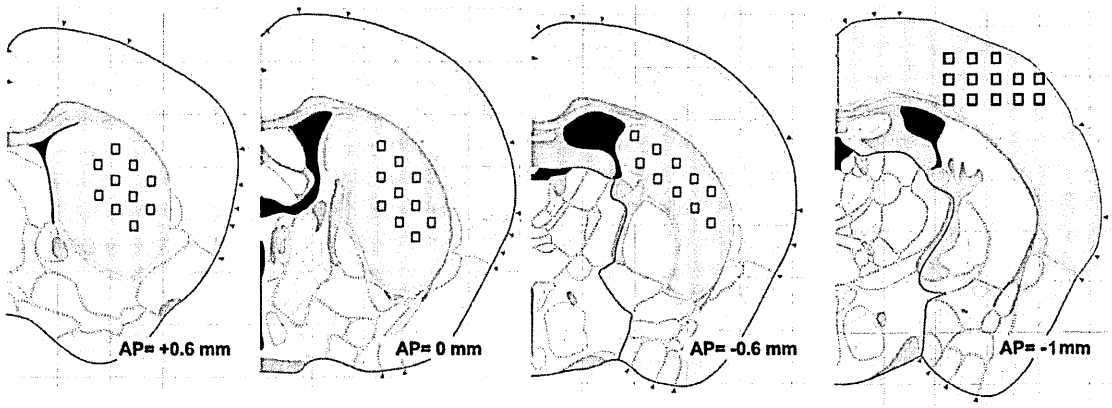

Figure 5.3 *Slice selection for immunohistological measurements.*

Three brain coronal slices were chosen for striatal quantification, namely AP=+0.6, 0 and -0.6mm from bregma; one brain coronal slice was chosen for cortical quantification at AP=-1mm from bregma, just beneath the craniotomy for 2-PM. Fields at 40x magnification were positioned as detailed in the figure (black boxes).

5.3 Results

5.3.1 Characterization of the imaged area

The cranial window through skull thinning exposed the area susceptible to MCA occlusion (Fig. 5.4 A, Fumagalli et al. 2011). RBC speed significantly decreased in all the animals

tested 1h after tMCAo when compared to baseline values (pre, Fig. 5.4 B). In *cx3cr1*$^{-/+}$ mice, RBC speed dropped from 4.7±2.8 mm/s (mean±sd, n=19-23 vessels from 5 mice per group) at pre, to 1.2±0.9 mm/s at post1h, and in *cx3cr1*$^{-/-}$ mice RBC speed dropped from 5.4±3.5 mm/s at pre to 1.9±1.7 mm/s at post1h. Intravenous injection of PI in selected animals was used to detect the presence of dying cells (Unal Cevik and Dalkara 2003). The observation that no PI positive cells were present in sham-operated mice, showed that thinning of the skull did not cause cell death or compromise the blood– brain barrier integrity (Fig. 5.4 C, Hussain et al. 1985). On the contrary, a great number of PI positive cells appeared to be labelled after MCAo, showing that in the ischemic areas where GFP+ cells were imaged, PI extravasated from vessels and penetrated inside cells (Fig. 5.4 D) indicating leakage of the blood– brain barrier and debility of the stained cells after MCAo (Fumagalli et al. 2011).

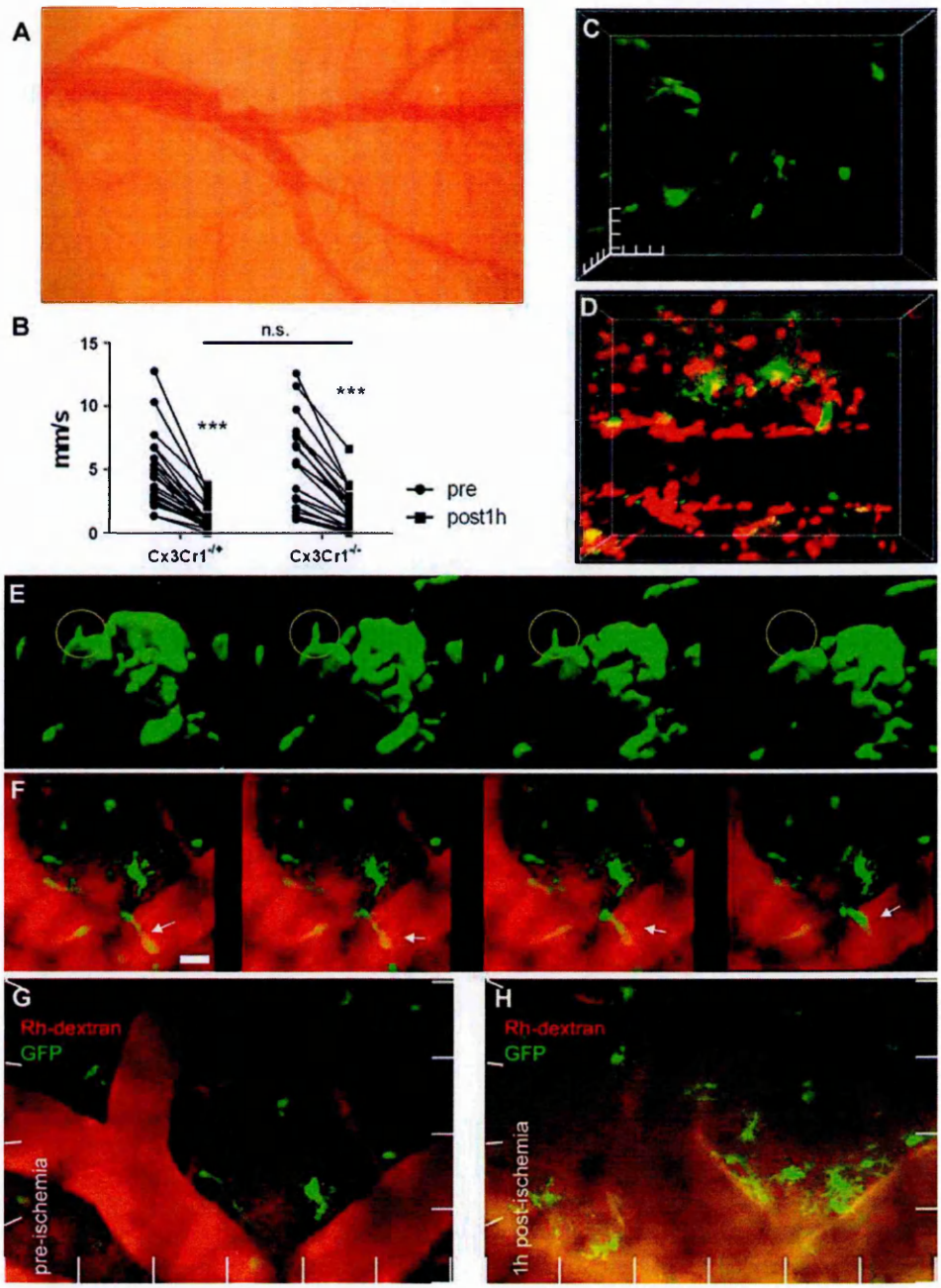

Figure 5.4 *Characterization of the cortical area subjected to two-photon imaging before and after tMCAo.* Thinned skull allows direct inspection of main cerebral blood vessels under light microscope (A). RBC speed is significantly reduced at post1h in the vessels belonging to the imaged area across the entire experimental group, with no significant differences between *cx3cr1*$^{-/+}$ and *cx3cr1*$^{-/-}$ mice (B). n=19-23 vessels from 5 mice per group, two-way ANOVA for repeated measures followed by Bonferroni's post hoc test: ***p<0.001 pre vs post1h. Propidum iodide uploaded *in vivo* into cell nuclei reveals the presence of dying cells in the visualized region of ischemic animals (D, red: propidium iodide positive cells; green: GFP+ cells), but not in sham animals (C). Tick interval = 10μm. GFP+ cells display an intense explorative activity by branch protruding/withdrawal at baseline point (E, 3D rendering). Microglia often take contact with blood vessels

(F, arrow, scale bar = 20μm), during a 10 min acquisition. During imaging before ischemia (pre), rhodamine-dextran (red) is confined into blood vessels and GFP+ cells (green) are clearly detectable in the brain tissue (G). One hour after ischemia (post1h), Rhodamine-dextran extravasates due to blood-brain barrier damage and GFP+ cells show a ramified shape (H). Tick interval = 50μm.

5.3.2 In vivo time-lapse imaging and immunophenotyping of GFP+ cells

When *in vivo* imaging was performed at pre, an intense activity of microenvironment exploration by ramification protruding/withdrawal was detected in microglia GFP+ cells (Fig. 5.4 E). As illustrated in Fig. 5.4 F, microglia cells were located close to blood vessels and often wrapped their ramifications around the vessel surface. A dramatic change in GFP+ cell shape was observed 1h following ischemia when GFP+ cells presented new ramifications or thickened the existing ones in both *cx3cr1*$^{-/+}$ (Fig. 5.4 G, H) and *cx3cr1*$^{-/-}$ mice (data not shown). Images in figure 5.4 document the leakage of rhodamine-dextran 1h after tMCAo (Fig. 5.4 G, H) indicating an early damage to the blood-brain barrier.

To explore GFP+cell phenotype, we performed *post mortem* immunophenotyping (Fig. 5.5). *cx3cr1*$^{-/+}$ mice subjected to *in vivo* imaging were sacrificed at 24h after tMCAo and immunofluorescence assays for CD11b, CD45, CD3 and CD206 were performed on frozen 20μm coronal brain sections. GFP+ cells were evaluated by confocal microscopy exploiting the native protein fluorescence emission. GFP+ cells co-localized with ramified CD11b+ cells, whilst no co-localization was detected with round-shaped CD11b+ cells, CD45^{high}+ leukocytes (Stein et al. 2007) and CD3+ lymphocytes (Fig. 5.5 A-C). Also perivascular macrophages (CD206+, Galea et al. 2005) appeared to express GFP fluorescent protein (Fig. 5.5 D). We then assessed the presence of GFP in the peripheral immune system. In spleen, immune cells expressing CD11b, CD45 or CD3, were found to be partially positive for GFP (Fig. 5.5 E-G). As *GFP* is controlled by the promoter of the

fractalkine receptor gene (*cx3cr1*), the absence of GFP signal in CD45^{high}+ cells in the brain tissue and their presence in the spleen indicates that the monocyte/macrophage subset recruited in the inflammed brain does not express *cx3cr1* similarly to what reported in other organs (Ingersoll et al. 2011). Thus *in vivo* analysis based on GFP positivity in the brain was referred to resident microglia. Similar findings were obtained in *cx3cr1*$^{-/-}$ mice (data not shown).

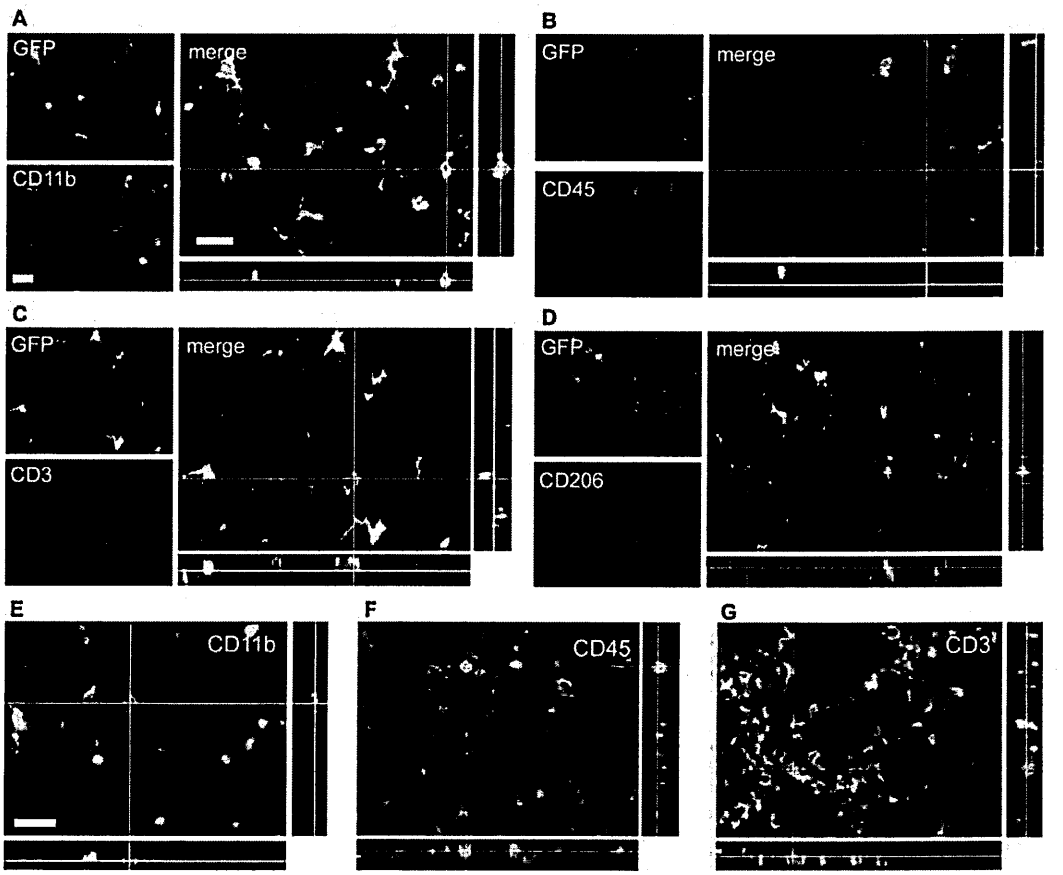

Figure 5.5 *Coexpression of CD11b, CD45, CD3 or CD206 with GFP in cerebral cortex and spleen of cx3cr1*$^{-/+}$ *mice 24h after tMCAo.*

Photomicrographs of cortical brain region ipsilateral to the lesion (A-D). GFP co-localizes exclusively with CD11b ramified cells (A). Round-shaped CD11b+ (A), CD45+ (B) and CD3+ (C) cells do not express GFP, suggesting that infiltrating cells in the brain do not express CX3CR1. Perivascular macrophages (CD206+) express GFP (D). At variance with cortex, immune cells in spleen (E-G) expressing CD11b (E), CD45 (F) or CD3 (G) are partially positive for GFP. Scale bars = 20μm.

5.3.3 Quantification of microglia cell displacement

Microglia did not show any significant motility within the imaged volume at pre, post1h and post24h acquisitions. Cell bodies remained almost still over the 20 min time-lapse imaging recordings in both *cx3cr1*$^{-/+}$ and *cx3cr1*$^{-/-}$ strains (Fig. 5.6 A-C, D-E). In fact, when a stack obtained at the beginning of post1h acquisition (green) was superimposed to one from the same area obtained 20 min later (red), a good overlay (yellow) with minor shift at the level of cell bodies was obtained, indicating an almost null displacement. The same finding was obtained from pre and post24h acquisitions (data not shown). Displacement rate was calculated throughout the experimental time points in both strains used. We found that mean displacement rates were always below the threshold for cell motility (1μm/min, Cordiglieri et al. 2010, Fig. 5.6 G), being 0.32±0.30, 0.47±0.49 and 0.80±0.75 μm/min (mean±sd, n≈100 cells per time point, 5 mice per group) at pre, post1h and post24h respectively in *cx3cr1*$^{-/+}$ mice and 0.35±0.34, 0.52±0.47 and 0.39±0.50 μm/min at pre, post1h and post24h respectively in *cx3cr1*$^{-/-}$ mice. This confirmed that microglia was not motile. No significant difference in cell displacement rates were found comparing the two mouse strains.

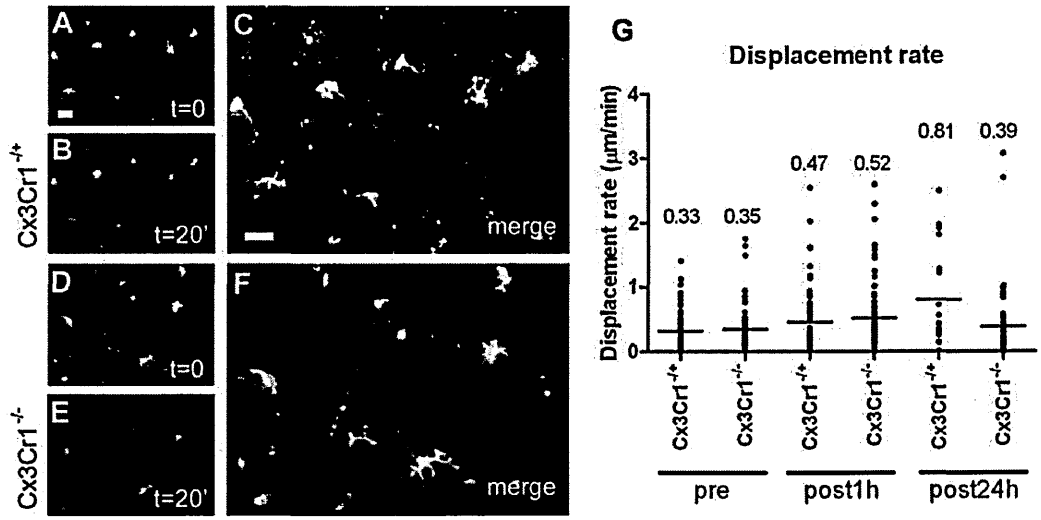

Figure 5.6 *Analysis of GFP+ cell displacement by two-photon microscopy.*

Superimposition of image stacks from time-lapse recording acquired at the beginning of the post1h imaging session (A, D) and 20 min later (B, E). In the overlay image (C, F) GFP+ cell bodies co-localize (yellow) with only a minor shift over the time span acquired. Scale bars = 20µm. Mean values of displacement rate are below the threshold for cell motility (1 µm/min) at every time point analyzed and in both strains (lines at the indicated mean values, n≈100 cells per time point, 5 mice per group (G), thus confirming that GFP+ do not move in this time window (20 min). Two-way ANOVA for repeated measures was applied and did not yield any significant difference.

5.3.4 Analysis of microglia morphology

Since microglia displayed active morphological dynamism rather than variation of motility, morphological features of microglia were analyzed in both strains at pre, post1h and post24h time points. In *cx3cr1*$^{-/+}$ mice microglia sprouted new ramifications at post1h and subsequently acquired a hypertrophic morphology characterized by numerous and short ramifications at post24h (Fig. 5.7 A). In *cx3cr1*$^{-/-}$ mice microglia were still able to sprout new ramifications at post1h, but they did not acquire the hypertrophic morphology with short branches at post24h (Fig. 5.7 B). Sholl analysis was applied to quantify cell complexity on the basis of frequency and length of branches emerging from cell bodies (Gensel et al. 2010, Fig. 5.2). At pre and post24h time points Sholl curves of complexity

were unmatched when *cx3cr1*$^{-/+}$ and *cx3cr1*$^{-/-}$ mice curves were compared (Fig. 5.7 C, E) whilst they were similar at post1h (Fig. 5.7 D). Cell complexity was statistically analyzed by considering, for each time point the frequency of short, intermediate and long ramifications (see methods for Sholl analysis in section **5.2.3.1**). *cx3cr1*$^{-/-}$ mice displayed a significant 2.0 fold increase in intermediate ramifications at pre time point (Fig. 5.7 F), equal length and frequency of branches at post1h (Fig. 5.7 G) and a significant 1.7 fold increase of intermediate ramifications and 3.1 fold increase of long distance ramifications at post24h (Fig. 5.7 H) when compared to *cx3cr1*$^{-/+}$ mice. It should be noted that the majority of long ramifications emerge directly from cell soma, thus contributing to the value of short ramification frequency. The fact that this value did not vary between the two strains indicates a similar number of total ramifications emerging from cell body at any time points. The different values found for intermediate and long ramifications are instead indicative of a different length of ramifications between the two strains. On the whole these results indicate that at 24h after tMCAo, in *cx3cr1*$^{-/+}$ mice microglia evolved towards an amoeboid shape in response to ischemia (Fig 5.7 A), while in *cx3cr1*$^{-/-}$ mice they failed to withdraw their longer branches and to acquire an amoeboid phenotype (Fig. 5.7 B).

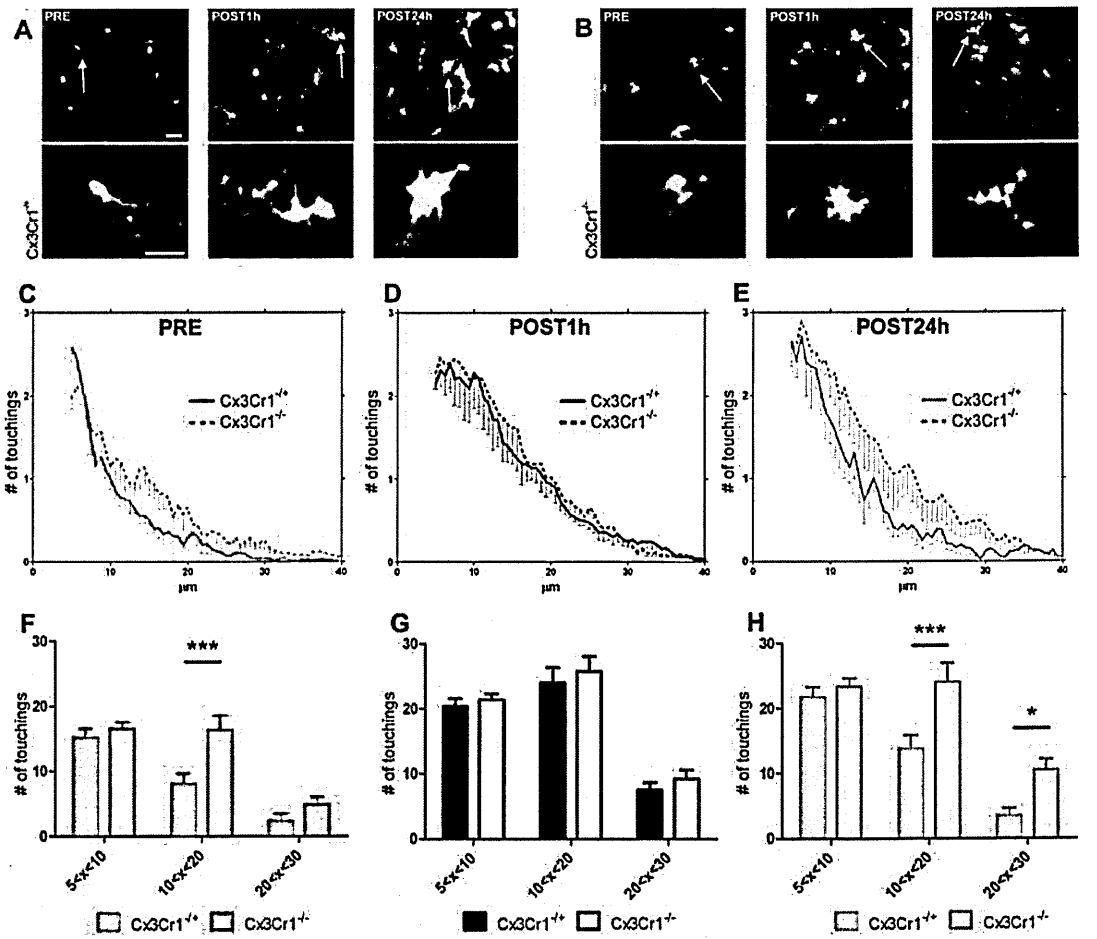

Figure 5.7 *Quantification of morphological complexity by Sholl analysis.*

cx3cr1$^{-/+}$ and *cx3cr1*$^{-/-}$ mice show a different evolution of microglia morphology over time. In *cx3cr1*$^{-/+}$ mice microglia increase number and length of ramifications at post1h and subsequently acquire a hypertrophic morphology by shortening ramifications at post24h (A). On the contrary, microglia in *cx3cr1*$^{-/-}$ mice increase number and length of ramifications at post1h and leave them unaltered at post24h (B). Arrows indicate cells showed in the higher magnification fields, scale bars=20µm. When the two strains are compared directly, *cx3cr1*$^{-/-}$ mice reveal increased touchings at pre, equal touchings at post1h and increased touchings at post24h compared with *cx3cr1*$^{-/+}$ mice (C,D,E: Sholl curves; F,G,H: statistical analysis between the two strains comparing frequency of ramifications at short (5 to 10µm), intermediate (10 to 20µm) and long (20 to 30µm) distance from cell centroid). Mean -/+ sd, n=90-100 cells per time point, 5 mice per group, two-way ANOVA followed by Bonferroni's post hoc test: *p<0.05, ***p<0.001.

Sham operated *cx3cr1*$^{-/+}$ mice (n=75 cells from 4 mice) did not show any significant difference in microglia morphology at the three time points assessed. The number of short

ramifications was 17.8±10.5 (mean±sd), 18.5±9.8 and 22.1±12.5, that of intermediate was 10.9±13.6, 9.1±12.3 and 8.8±9.6, that of long was 2.1±5.2, 0.9±3.1 and 0.6±2.5 at pre, post1h and post24h, respectively (Fig. 5.8).

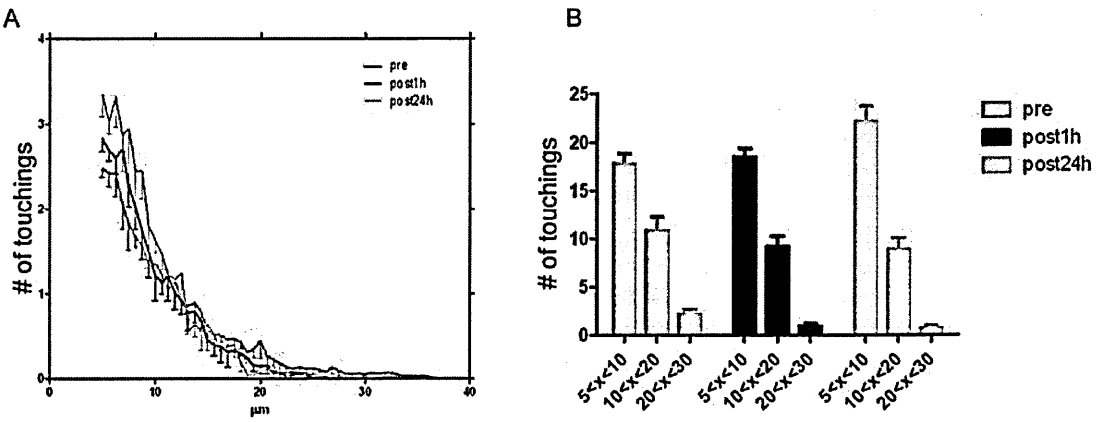

Figure 5.8 *Quantification of morphological complexity by Sholl analysis in sham animals.*
Analysis of Sholl applied to *cx3cr1*$^{-/+}$ sham mice revealed that no variations in cell complexity was observable over the three time points considered, thus confirming that imaging procedure itself does not induce microglia morphological changes.

5.3.5 Quantification of immunostainings for CD11b, CD68, CD45, Ym1, CD206 and iNOS

At post24h, coronal brain sections were stained and quantified for CD11b (marker of microglia/macrophages), CD68 (marker of active phagocytosis, (De Beer et al. 2003; Ramprasad et al. 1996), CD45^{high} (recruited macrophages), CD45^{low} (resident microglia) (Gesuete et al. 2009; Perego et al. 2011; Stein et al. 2007), Ym1 and CD206 (markers of M2 polarization) and iNOS (M1 polarization) expression. Immunohistological analysis was performed both in cortex and striatum, the latter representing the ischemic core area. At 24h after ischemia, CD11b+ cells in *cx3cr1*$^{-/+}$ mice showed hypertrophic morphology upon activation in both cortex and striatum (Fig. 5.9 A, B). In *cx3cr1*$^{-/-}$ mice these cells appeared highly ramified and did not show the same hypertrophic appearance (Fig. 5.9 A,

B). Quantification of the stained area revealed that CD11b expression was decreased in *cx3cr1*$^{-/-}$ ischemic mice compared to *cx3cr1*$^{-/+}$ mice at 24h after tMCAo in both cortex (3.54±1.76 vs 6.79±2.30 % stained area, mean±sd, n=6, Fig. 5.9 A) and striatum (8.69±1.44 vs 10.88±1.61, Fig. 5.9 B). Expression of CD68 was induced 24h after tMCAo, in *cx3cr1*$^{-/-}$ and *cx3cr1*$^{-/+}$ mice (Fig. 5.9 C, D), but to a lesser extent in striatum of *cx3cr1*$^{-/-}$ mice compared to the same area of *cx3cr1*$^{-/+}$ mice (1.25±0.40 vs 2.00±0.53 % stained area, Fig. 5.9 D). CD45^{high}+ and CD45^{low}+ cells were quantified separately. Massive recruitment of CD45^{high}+ cells occurred at 24h after tMCAo in both cortex and striatum (Fig. 5.9 E, F). The number of CD45^{high}+ cells was significantly higher in *cx3cr1*$^{-/-}$ compared to *cx3cr1*$^{-/+}$ mice (cortex: 108.97±100.31 vs 25.64±21.18 cells/mm^2; striatum: 65.56±12.24 vs 41.87±23.77, Fig. 5.9 E, F). CD45^{low}+ cells were present both in sham and ischemic *cx3cr1*$^{-/-}$ and *cx3cr1*$^{-/+}$ mice with no significant difference in cell density across the groups (Fig. 5.9 E, F). Ym1 expression was induced after ischemia (Fig. 5.10 A, B) in both strains. No significant difference could be detected in cortex (Fig. 5.10 A) whilst Ym1 appeared to be increased in striatum of *cx3cr1*$^{-/-}$ compared to *cx3cr1*$^{-/+}$ mice (0.31±0.11 vs 0.18±0.04 % stained area, Fig. 5.10 B). CD206+ cell density was increased after ischemia in both *cx3cr1*$^{-/-}$ and *cx3cr1*$^{-/+}$ mice with no significant difference between the two strains (Fig. 5.10 C, D). iNOS expression was induced after tMCAo with no difference between the two strains in cortex, whilst, in striatum, it showed to be significantly upregulated in *cx3cr1*$^{-/-}$ compared to *cx3cr1*$^{-/+}$ mice (0.08±0.05 vs 0.19±0.10 % stained area, Fig. 5.10 E,F).

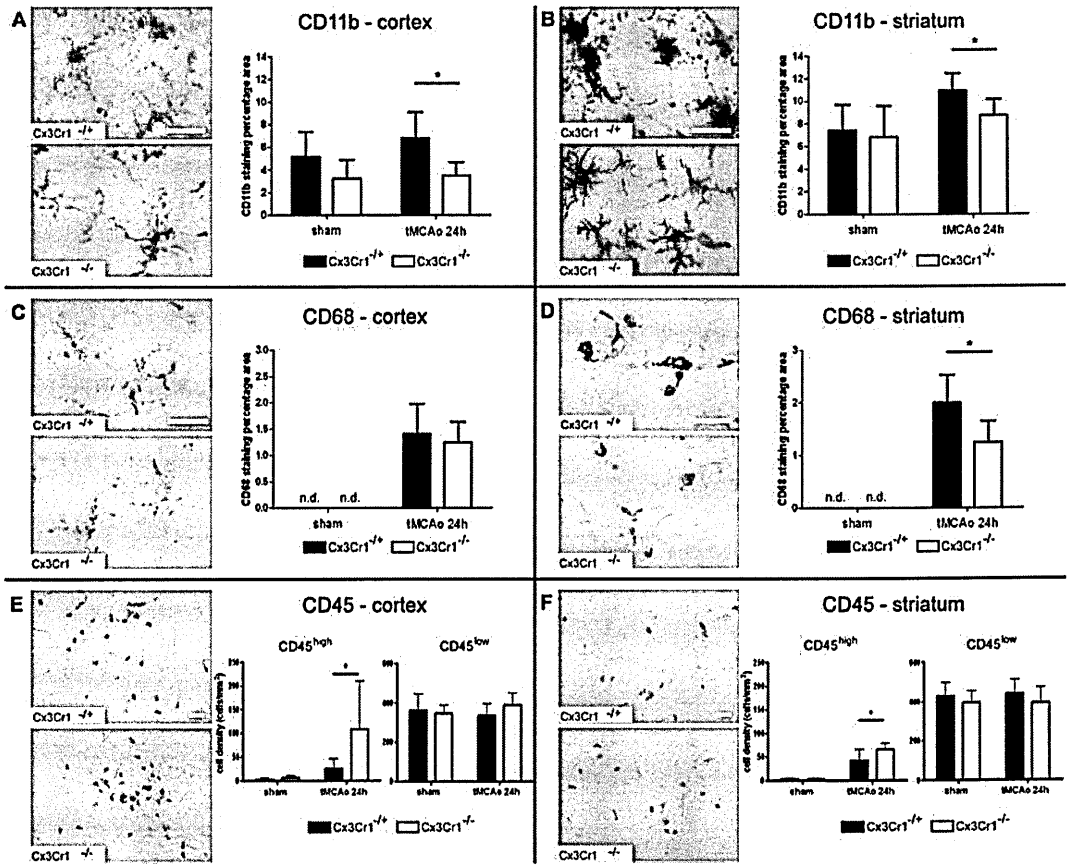

Figure 5.9 *Immunostainings and quantitative analysis for CD11b, CD68 and CD45 expression in cortex and striatum at 24h after tMCAo.*

CD11b+ cells (A, B) show a different morphology between the two strains, being hypertrophic and ameboid in *cx3cr1*$^{-/+}$ mice and highly ramified in *cx3cr1*$^{-/-}$ mice. Quantitative analysis reveals that in both cortex (A) and striatum (B), CD11b stained area is significantly decreased in *cx3cr1*$^{-/-}$ mice after ischemia. Phagocytic activity (CD68+ cells) is unchanged in cortex (C), but it is significantly reduced in striatum (D) of *cx3cr1*$^{-/-}$ mice. Differential count for CD45^{high}+ cells (arrows in E) and CD45^{low}+ cells (arrowheads in E) reveals a significant increase of round-shaped CD45^{high}+ cells in both cortex and striatum of *cx3cr1*$^{-/-}$ mice (E, F) and no changes in ramified CD45^{low}+ cells. No significant differences are detectable comparing sham animals for the assessed markers. Scale bars = 20µm. Mean+sd, n=6, Two-way ANOVA followed by Bonferroni's post hoc test for CD11b and CD45. Since CD68 was not detectable in sham animals, sham groups were excluded from statistics. Mann-Whitney test was used for CD68. *p<0.05, n.d. = not detectable.

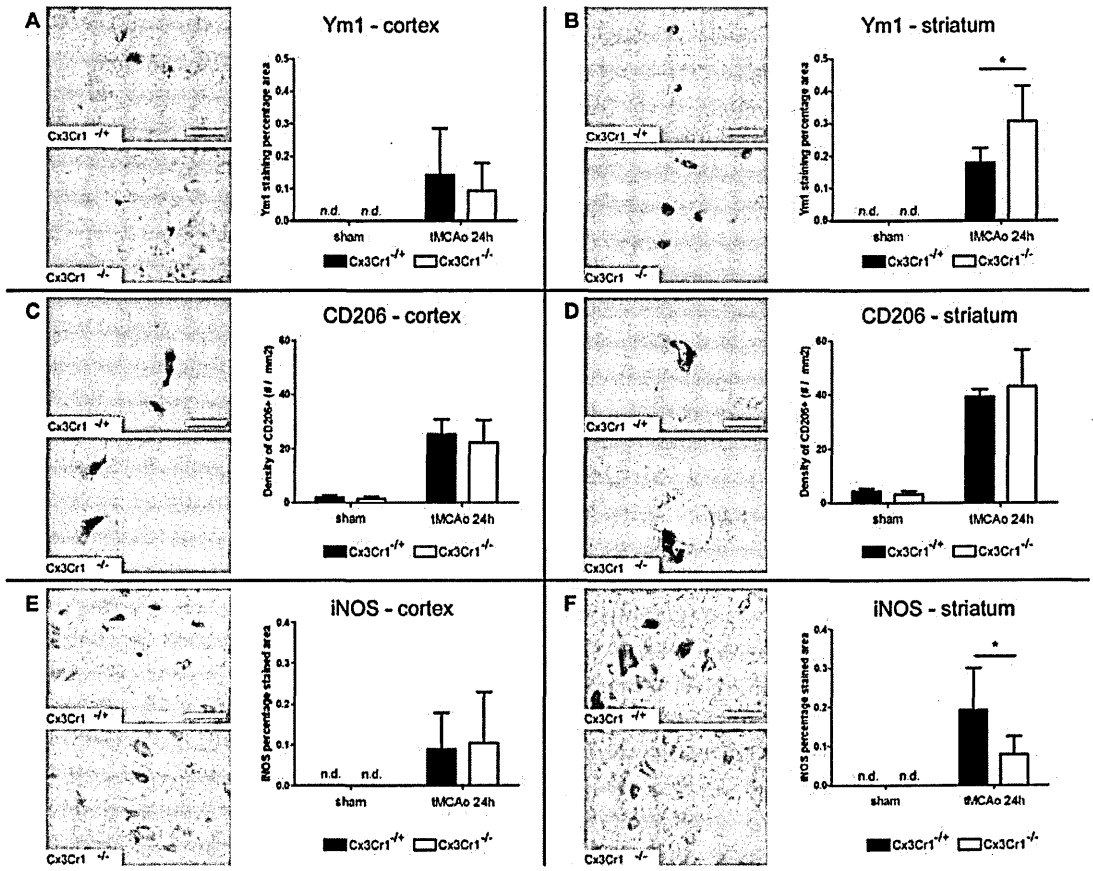

Figure 5.10 *Immunostainings and quantitative analysis for M2 polarization markers Ym1 and CD206 and M1 polarization marker iNOS in cortex and striatum at 24h after tMCAo.*

The expression of Ym1 remains unchanged in cortex (A), whilst it is significantly increased in striatum of *cx3cr1-/-* mice after ischemia (B). No Ym1 positivity is detectable in sham animals. The density of CD206+ cells do not change in both cortex (C) and striatum (D) comparing sham and tMCAo *cx3cr1*$^{-/+}$ and *cx3cr1*$^{-/-}$ mice. iNOS expression, whilst not changing in cortex (E), is significantly decreased in striatum of *cx3cr1*$^{-/-}$ mice (F). Scale bars = 20µm. Mean+sd, n=6, Mann-Whitney test: *p<0.05, n.d. = not detectable.

5.3.6 Assessment of lesion volume at 24h after tMCAo

tMCAo induced a comparable decrease of RBC speed values in both strains (Fig. 5.4 B) with no significant difference in flow reduction (1.9±1.7 mm/s in *cx3cr1*$^{-/-}$ mice and 1.2±0.9 mm/s in *cx3cr1*$^{-/+}$ mice). Histological evaluation of ischemic lesion revealed that at 24h after ischemia *cx3cr1*$^{-/-}$ had a smaller ischemic volume compared to *cx3cr1*$^{-/+}$ mice

(29.32±6.76 vs 39.33± 7.39 mm^3, mean±sd) corresponding to a 25.5% reduction in lesion size in mice defective for *cx3cr1* (Fig. 5.11).

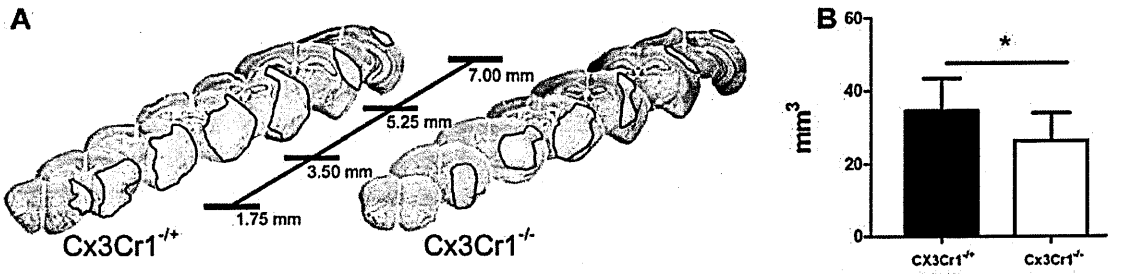

Figure 5.11 *Ischemic volume assessment.*

Representative distribution of the lesion 24h after tMCAo in typical *cx3cr1*$^{-/+}$ and *cx3cr1*$^{-/-}$ mice (A). Quantification of the lesion shows a significant reduction (by 25.5%) in *cx3cr1*$^{-/-}$ compared to *cx3cr1*$^{-/+}$ mice. Mean+sd, n=12, Mann-Whitney test: *p<0.05.

5.4 Discussion

I used a murine model of transient brain ischemia and advanced two-photon *in vivo* imaging techniques in combination with *post mortem* phenotype analysis to reveal the early effects of CX3CR1 deficiency after ischemia. I demonstrated that CX3CR1 deficiency leads microglia to express an early protective phenotype. In particular, 24h after ischemia: 1) microglia displayed an increased number of ramifications and lack of ameboid morphology; 2) the expression of M/M markers CD11b and CD68 was reduced in the ischemic area, indicating a lower level of activation and decreased phagocytic function; 3) the recruitment of $CD45^{high}$ cells was enhanced; 4) the expression of Ym1 was increased in striatum, indicating a shift towards a M2 polarization within the ischemic environment. All these changes were associated with a 25.5% decrease of ischemic volume.

The transgenic model based on GFP expression under the control of the promoter of *cx3cr1* has been widely used to assess microglia behavior *in vivo* in different models of neurological conditions (Cardona et al. 2006; Cipriani et al. 2011; Corona et al. 2010; Davalos et al. 2005; Dénes et al. 2008; Donnelly et al. 2011). Most of these studies refer to GFP+ cells as microglia although other cell types may express *cx3cr1* (Prinz and Priller 2010). While at baseline only resident monocytes (microglia and perivascular macrophages) are present in the brain (Hanisch and Kettenmann 2007), after ischemia, infiltration of immune cells from the periphery occurs with a specific pattern of tissutal invasion (Gelderblom et al. 2009). Thus to obtain information on the phenotype of GFP+ cells after brain ischemia, we analyzed *cx3cr1*-expressing cells exploiting native GFP emission. At 24h after tMCAo, GFP was expressed exclusively by CD11b+ ramified (microglia) and CD206+ (perivascular macrophages) cells. None of the cells presenting the features of infiltrating immune cells, expressed GFP in the brain, being round-shaped CD11b+, $CD45^{high}$+ and CD3+ cells all negative for native GFP. These cell types were instead found to be partially GFP+ in the spleen. Constitutive expression of *cx3cr1* is typical of resident monocytes (and microglia), while it is inducible in peripheral immune cells (Huang et al. 2001; Prinz and Priller 2010). Circulating monocytes have been divided into two subsets, each with a specific pattern of chemokine receptor expression and trafficking activity (Geissmann et al. 2003; Sunderkötter et al. 2004; Ziegler-Heitbrock 2007). Monocytes belonging to the classical subsets express the CCR family receptors and are more prone to tissutal invasion upon recruitment (Ingersoll et al. 2011; Prinz and Priller 2010; Saederup et al. 2008). On the contrary, those belonging to the nonclassical subsets express CX3CR1, demonstrate a patrolling behavior along blood vessel walls and accumulate into peripheral tissues as spleen, lung and liver (Auffray et al. 2007; Geissmann et al. 2003; Ingersoll et al. 2011). The nonclassical CX3CR1 subsets may be recruited in the brain at later stages after acute injury, and thus may not be present at the

early time points after insult that we analyzed. Overall, these data corroborate the observation that infiltrated immune cells were negative for GFP, allowing us to refer to GFP+ cells, in the used ischemic model, at the considered time points, as microglia.

Variations of cell morphology or cell displacement are related to the specific activity of microglia (Soltys et al. 2005), being specific shapes or motility rates strongly associated with function. Analysis of cell dynamics over time can thus provide information on microglia activity status. We exploited *in vivo* 2-PM to assess microglia dynamism and morphology over time. We used a thin skull craniotomy approach, which has minor effects on the cortical tissue beneath, leaving the density of dendritic spines unchanged and avoiding inflammatory response (Fumagalli et al. 2011; Xu et al. 2007b; Yang et al. 2010). In the cortical area selected for imaging we could confirm *in vivo* both the decrease in blood flow (RBC speed) and the presence of dying cells (PI administration) as a consequence of MCAo.

We assessed microglia cell body displacement within the imaged volume. The ability of microglia to travel over long distances seems to be dependent on the danger signal received. In models of brain injury such as traumatic brain injury, photothrombotic stroke model and global ischemia, microglia did not show any body movement in response to damage (Davalos et al. 2005; Masuda et al. 2011). On the contrary, in a model of spreading depression that causes loss of synaptic activity, microglia showed Lévy flight-like movements in response to decreased synaptic activity (Grinberg et al. 2011). In our tMCAo model, microglia were almost completely stationary within the imaged volume at any time point considered. Indeed, during the 20min imaging sessions, for both *cx3cr1*$^{-/+}$ and *cx3cr1*$^{-/-}$ mice, mean displacement rate calculated for cell centroid was below 1μm/min, which is the minimum threshold for immune cell motility in the central nervous system (Cordiglieri et al. 2010; Fumagalli et al. 2011). The observed lack of microglia displacement could be related to the rapid decline of ATP levels due to tMCAo, being ATP

needed for the modifications of the cytoskeleton exploited by microglia to migrate within the tissue (Davalos et al. 2005; Grinberg et al. 2011). To analyze cell morphology, we measured cell complexity on the basis of ramification frequency and length (Gensel et al. 2010). At baseline, *cx3cr1*$^{-/+}$ and *cx3cr1*$^{-/-}$ mice showed a distinct cell complexity having *cx3cr1*$^{-/-}$ animals a higher number of intermediate distance (10 to 20 µm from centroid) ramifications. Thus, at baseline, the lack of fractalkine receptor prevents fractalkine, which is continously shed from neurons, from keeping a low number of ramifications, *i.e.* low level of microglia activity (Prinz and Priller 2010). At 24h after ischemia, in *cx3cr1*$^{-/+}$, but not in *cx3cr1*$^{-/-}$ mice, microglia switch towards a hypertrophic morphology characterized by numerous, short and thick ramifications indicating that fractalkine is a key factor in inducing microglia ameboid, hypertrophic shape.

We then assessed if these morphological differences were associated to a different expression of markers of M/M phenotype, namely CD11b, CD68 and CD45. CD11b staining revealed that in both cortex and striatum ramified microglia was hypertrophic with numerous, short and thick branches in *cx3cr1*$^{-/+}$ mice, and highly ramified with long protrusions in *cx3cr1*$^{-/-}$ mice, coherently with the results obtained by *in vivo* imaging. The observed increase in ramified microglia in *cx3cr1*$^{-/-}$ mice was associated with a reduction of infarct size. In a recent paper, Vinet and colleagues (Vinet et al. 2012) showed a protective role of ramified microglia in excitotoxicity-induced neurodegeneration. Our observations are coherent with the suggestion made by these authors that ramified microglia not only survey their microenvironment but also contribute to protection of neurons under pathological conditions. CD11b stained area was significantly reduced in *cx3cr1*$^{-/-}$ mice suggesting a different/defective activation of M/M. The ameboid shape of M/M has been associated with their phagocytic function, which can be assessed by CD68 staining (De Beer et al. 2003; Ramprasad et al. 1996). *cx3cr1*$^{-/-}$ mice showed a decrease in CD68 stained area compared to *cx3cr1*$^{-/+}$ mice in striatum, in line with the different cell

morphology described for the two strains. The phagocytic activity was thus significantly reduced at 24h after tMCAo in the absence of the fractalkine receptor, suggesting the involvement of the fractalkine:CX3CR1 pathway in the activation of the innate phagocytic functions of microglia. Similar changes in microglia phenotype and CD11b and CD68 expression had been previously reported following other protective manipulations such as stem cells infusion or ischemic preconditioning, where the observed protective effects were associated to a decrease of ameboid CD11b/CD68 positive cells and to a decrease of CD68 expression (Longhi et al. 2011; Zanier et al. 2011).

The expression of CD45 was then assessed by a differential count of microglial $CD45^{low}$+ cells and leukocyte-like round-shaped $CD45^{high}$+ cells (Gesuete et al. 2009). The frequency of $CD45^{low}$+ cells was not different between *cx3cr1*$^{-/+}$ and *cx3cr1*$^{-/-}$ mice, indicating that the absence of CX3CR1 did not alter the number of microglia cells present in the ischemic areas, possibly due to the absence of displacement. Leukocyte-like $CD45^{high}$+ cells were instead significantly more numerous in *cx3cr1*$^{-/-}$ mice in line with an increased recruitment from blood. This picture may be different at longer time points when recruitment of CX3CR1-dependent pathway monocytes takes place (Nahrendorf et al. 2007). Indeed a reduced infiltration of immune cells in ischemic brains of *cx3cr1*$^{-/-}$ mice has been reported 3 days after injury (Dénes et al. 2008). Overall these observations suggest that immune cell infiltration is somehow anticipated in *cx3cr1*$^{-/-}$ mice and perhaps occurs over a narrower time window compared to *cx3cr1*$^{-/+}$ mice, the latter being also exposed to the late wave of CX3CR1-dependent pathway monocyte infiltration. At 24h after tMCAo, in the absence of CX3CR1, the increased/anticipated infiltration of $CD45^{high}$ cells could be associated to an alternative M2 polarization of M/M. Indeed infiltrated leukocytes, among which are polarized T-cells (Th1, Th2 and Tregs) have been documented to be key orchestrators of M/M polarized activation (Biswas and Mantovani 2010; Sica and Mantovani 2012) with the ability to drive a protective phenotype (Butovsky et al. 2007). I observed an increase of

Ym1 expression in *cx3cr1*$^{-/-}$ mice but not that of the other M2 marker CD206 indicating that M2 polarization *in vivo* may show multiple M/M phenotypes (Perego et al. 2011; Sica and Mantovani 2012). Interestingly the upregulation of protective Ym1 marker is paralleled by significant decrease of the expression of the marker of toxic M1 polarization iNOS. This observation may indicate that CX3CR1 deficency leads to different M1/M2 balance in the ischemic territory, and, in particular, that M/M switch towards the M2 protective polarization is enhanced and favoured.

5.5 Conclusions

Overall the results obtained in the present study, together with the literature data allow to propose a different role for fractalkine and its receptor in the control of microglia in different circumstances. Under physiological conditions in mice defective for CX3CR1, the suppressive function of fractalkine is prevented and this determines a chronic activation state of microglia displaying a highly ramified morphology (present study). This state has been associated to decreased hippocampal neurogenesis and cognitive deficits (Bachstetter et al. 2011; Rogers et al. 2011; Tremblay et al. 2011). Early after acute injury, chronically activated microglia enhance the ramified morphology, downregulate the phagocytic activity and acquire protective features typical of the M2 polarization that result in decreased susceptibility to the ischemic injury (present study). This response may be transient, and, as evidenced above, at longer times other events may take place dramatically changing the impact of CX3CR1 deficiency. Among these, recruitment of macrophages belonging to the CX3CR1-dependent pathway (non classical monocyte subset) has been associated with beneficial effects as this population is capable of tissue healing (Nahrendorf et al. 2007). CX3CR1 deficiency would impair the recruitment of this

protective population thus resulting in a detrimental phenotype, as strongly supported by the wide literature on *cx3cr1*$^{-/-}$ mice in chronic CNS diseases (Prinz and Priller 2010).

Thus blocking the fractalkine:CX3CR1 pathway inhibits the detrimental activity of microglia and enhances/anticipates their protective functions early after ischemia. Inhibition of this pathway at later times, preventing fractalkine physiological control of microglia activation may result in a toxic phenotype.

6. TEMPORAL PATTERN OF EXPRESSION AND COLOCALIZATION OF MICROGLIA/MACROPHAGE MARKERS

6.1 Background

Microglia, the major cellular contributors to post-injury inflammation, have the potential to act as markers of disease onset and progression and to contribute to neurological outcome of acute brain injury. After acute brain injury, these resident cells are rapidly activated and undergo dramatic morphological and phenotypic changes (Davalos et al. 2005; Iadecola and Anrather 2011; Yenari et al. 2010). Microglial response is associated to recruitment of blood-born macrophages which migrate into the injured brain parenchyma (Jin et al. 2010; Schilling et al. 2005). This process is accompanied by expression of novel surface antigens and production of mediators that build up and maintain the inflammatory response of the brain tissue. Activated microglia and recruited macrophages (which are antigenically not distinguishable, henceforth referred to as M/M), can affect neuronal function and promote either neurotoxicity or neuroprotection.

Studies addressing phenotypic changes occurring in macrophages in peripheral inflammation and immunity have shown that these cells can undergo different forms of polarized activation. One is the classic or M1 activation, characterized by high capacity to present antigen, high production of NO and ROS and of proinflammatory cytokines. M1 cells act as potent effectors that kill micro-organisms and tumor cells, drive the inflammatory response and may mediate detrimental effects on neural cells. The second phenotype (M2) is an alternative apparently beneficial activation state, more related to a fine tuning of inflammation, scavaging of debris, promotion of angiogenesis, tissue remodeling and repair. Specific environmental signals are able to induce these different

polarization states (Porta et al. 2009). A similar possibility has been also recently raised for microglia, by showing that these cells, under certain conditions, can indeed be pushed to both extremes of the M1 and M2 differentiation spectrum (David and Kroner 2011; Michelucci et al. 2009). More studies are needed to substantiate these observations.

In this frame, this part of study aims at getting insight on previously unexplored aspects of microglia phenotype changes induced by cerebral ischemia, namely, the presence of specific phenotype markers, their temporal expression, whether or not they are concomitantly expressed by the same subpopulation, whether they are expressed at distinct phases or locations in relation to the ischemic lesion. I focused on a few molecules that are known to be expressed by macrophages in peripheral inflammation and that have been associated to different functions. They include: CD11b, a marker of M/M activation/recruitment, CD45 expressed on all nucleated hematopoietic cells (Penninger et al. 2001), CD68 a marker of active phagocytosis, Ym1 a secretory protein that binds heparin and heparin sulphate, CD206 a C-type lectin carbohydrate binding protein, both of them expressed by alternatively activated macrophages and associated to recovery and function restoration (Bhatia et al. 2011; Raes et al. 2002) and iNOS, a cytokine-inducible nitric oxide synthase that has been associated with classical activated macrophages (David and Kroner 2011).

6.2 Specific methods in this chapter

6.2.1 Experimental plan

Experiments were conducted according to the plan detailed in Figure 6.1 A.

6.2.2 Slice selection and quantitative analysis

The coronal sections used for marker quantification in ischemic areas were: +1.54, +0.50 and – 0.94 mm from bregma, 24 fields at 20x or 33 fields at 40x magnification. The first row of fields at 40x was positioned at the lesion edge, spacing each field by 572.5μm (distance between centres of the fields). Further rows of fields were positioned distanced by 389.3μm each. 20x magnification fields were separated by 572.5μm (distance between centres of fields), while distance between each row was 389.3μm.

Field selection was performed using a BX61 Olympus microscope equipped with a motorized stage acquiring the same focal plan throughout the samples (Donnelly et al. 2009; Perego et al. 2011). Positioning of the frames is detailed in Fig. 6.1 B.

Quantifications were performed using ImageJ software (http://rsbweb.nih.gov/ij/) and expressed as positive pixels/total assessed pixels (staining percentage area), or cells/mm^2 (cell density) for subsequent statistical analysis (Perego et al. 2011).

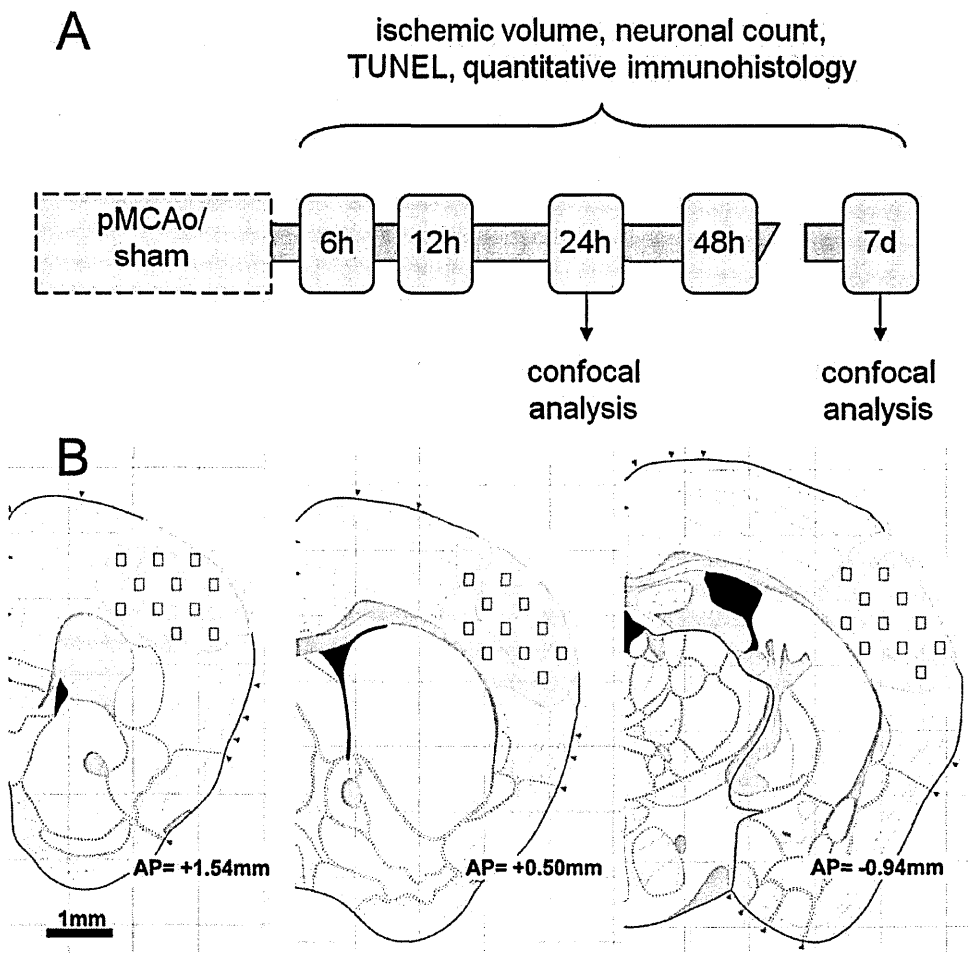

Figure 6.1 *Experimental plan, selection of slices and tissue sampling for neuronal counts, TUNEL and quantification of immunostained area.*

Mice subjected to pMCAo or sham surgery were sacrified at the indicated time points for assessment of ischemic volume, neuronal count, TUNEL and quantitative immunohistology (A). Fields for neuronal counts, TUNEL evaluation and quantification of stained area were positioned within the ischemic territory at defined distances (B, see methods for details). The regions sampled pertained to the ischemic territory (B, yellow) at the time points considered (6h, 12h, 24h, 48h and 7d).

6.2.3 Neuronal Count

Cresyl Violet stained brain sections were used for neuronal count. Thirty-three fields at 40x were analyzed for each mouse. The amount of neuronal loss was calculated by pooling the number of stained neurons in the three ipsilateral sections and expressed as percentage

of those in sham- operated animals. Fields were analyzed using ImageJ software (http://rsbweb.nih.gov/ij/) and segmentation was used to discriminate neurons from glia on the basis of cell size.

6.2.4 TUNEL staining

To assess the presence of injured cells showing DNA damage, terminal deoxynucleotidyl transferaseYmediated dUTP nick end labeling (TUNEL) staining was performed on 20-μm sections by *in situ* cell death detection kit (Roche, Mannheim, Germany) according to the manufacturer instructions, as previously described (Ortolano et al. 2009a). DNase-treated sections were used as a positive control. After staining, the sections were visualized using fluorescent microscopy (Olympus IX70 Olympus Tokyo, Japan). Images of the area of interest were acquired using AnalySIS software (Olympus, Tokyo, Japan). For each mouse twenty-four fields at 20x were analyzed. TUNEL-positive cells were counted using ImageJ software (http://rsbweb.nih.gov/ij/) and expressed as number per mm^2 for subsequent statistical analysis (Longhi et al. 2011).

6.2.5 Three-dimensional renderings of immunofluorescent stainings

Images from confocal microscope were managed by Imaris software (Bitplane, Switzerland) and processed. Briefly, image files were uploaded with the *surpass* mode on software. A color channel was selected and a color threshold applied so to specifically remove background noise signal. Isosurfaces were then created by using same threshold in the algorhitm for creating surfaces. Algorhitm was applied for each color channel. Resulting isosurfaces were merged and rotated on the screen so to choose the right orientation prior to export snapshot images.

6.3 Results

6.3.1 Comparison of microglia distribution after transient or permanent ischemia

The degree of reperfusion in the clinical setting is highly variable (Caplan et al. 2011; Lo 2008b), and thus pre-clinical research should consider the use of both transient and permanent models of brain ischemia. *In vivo* imaging studies of microglia reported in the result section **5** refer to a transient model of ischemia (tMCAo). In this and in the following section (number **7**), in addition to tMCAo, I will also use a model of permanent ischemia, achieved by the permanent occlusion of the MCA (pMCAo) through electrocoagulation (see methods **3.3.3**).

Cx3cr1$^{GFP/+}$ mice were subjected to tMCAo or pMCAo and compared for distribution of microglial cells at 24h after injury, exploiting the native GFP emission. Interestingly, the presence/absence of reperfusion had a huge effect on GFP+ microglia distribution in relation to the lesion (Fig. 6.2). After tMCAo, microglia in the ischemic area, that include both striatum and cortex (dashed red line in Fig. 6.2 A), mostly survived and activated as suggested by their hypertrophism in both areas (Fig. 6.2 B, C) compared with the contra-lateral side (Fig. 6.2 D). After pMCAo, instead, GFP+ microglia almost completely disappeared in the ischemic area, which is located in cortex (dashed red line in Fig. 6.2 E), where only sparse residual fluorescent signal could be detected (Fig. 6.2 F). At the borders of the lesion area, microglia were still present and showed the hypetrophic shape (Fig. 6.2 G), differently from the highly ramified microglia visualized in the contra-lateral side (Fig. 6.2 H). Overall, these results confirm that microglia need residual or quickly re-established blood flow to become activated (Masuda et al. 2011) after sensing an injury, and indicate that the prolonged absence of blood supply leads to microglia cell death within 24h.

The ischemic area of pMCAo mice is rapidly replenished by immune cells positive to CD11b, most of which are negative to GFP (Fig. 6.2 I) and may be recruited from the periphery (see section **5.3.2**). Resident microglia (GFP+/CD11b+) seem to settle preferentially around the lesion (Fig. 6.2 J) and only few cells can survive and activate within the core area. To study both resident and recruited CD11b after pMCAo, I chose to perform *post mortem* imaging at different time points and analyze microglia/macrophage phenotype on the basis of temporal and topological distance from the injured area.

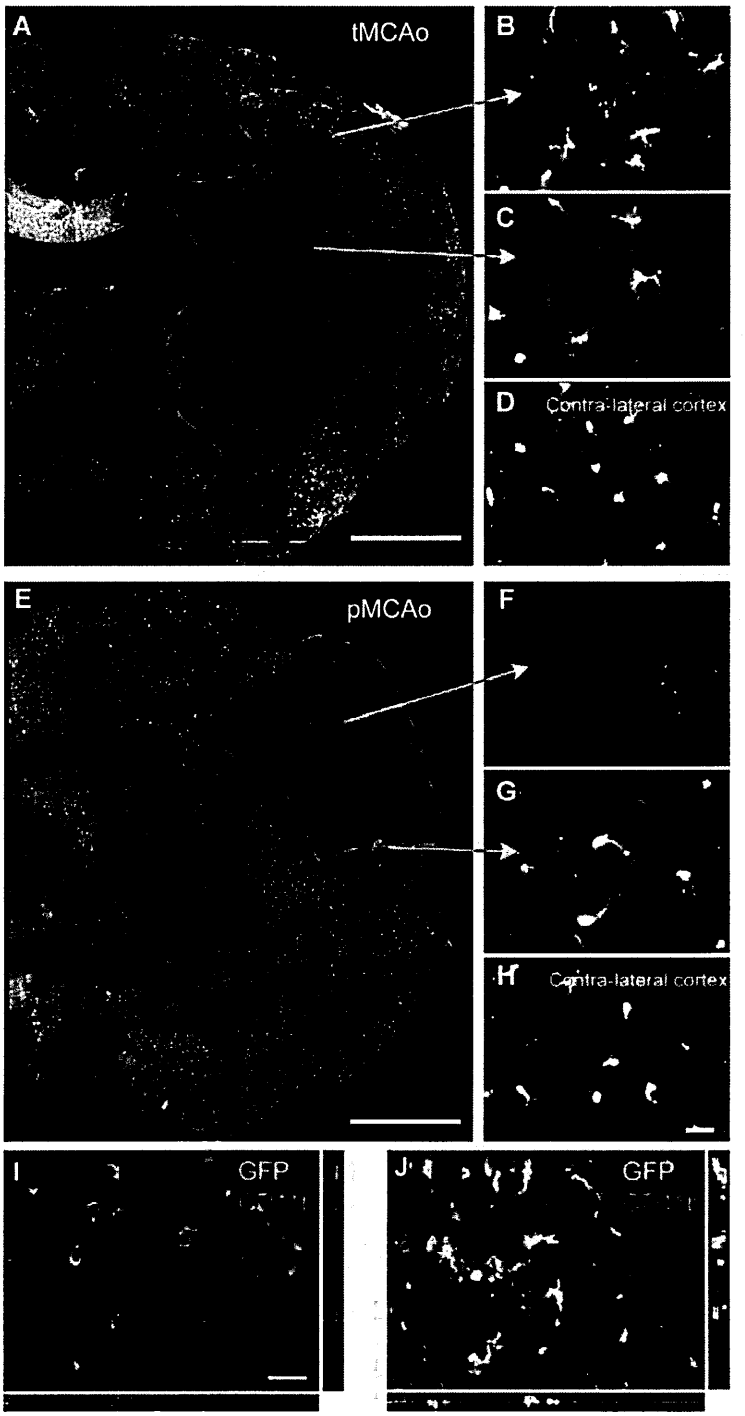

Figure 6.2 *Distribution of GFP+ microglia in transient (tMCAo) or permanent (pMCAo) ischemia.*

A: microglia are distribuited in all ischemic areas (dashed red line, traced according to cresyl violet staining of adjacent slice) 24h after tMCAo. Microglia are hypertrophic in both cortex (B) and striatum (C), whilst they are high ramified with thin branches in contra-lateral side (D).

E: microglia are almost not present in the ischemic area (dashed red line, traced according to cresyl violet staining of adjacent slice and F) 24h after pMCAo. At the border of the lesion microglia show hypertrophic morphology (G), whilst they are high ramified with thin branches in contra-lateral side (H). The ischemic

area in E is replenished by many GFP-/CD11b+ cells (I); GFP+/CD11b+ resident microglia are mainly located at the borders of the lesion (J). Scale bars in A,E=1mm, scale bar in B-D, F-H=20μm.

6.3.2 Histopathological findings at different time points from pMCAO

Histological analysis were performed according to the experimental plan shown in figure 6.1 A and by sampling the ischemic area as shown in figure 6.1 B. We specifically quantified lesion progression on the basis of ischemic volume assessment, viable neuronal count and apoptotic cell count. We measured the expression of selected M/M markers (CD11b, CD68, CD45, CD206 and Ym1) by quantification of immunostained area or positive cell density. These measures have been performed at different time points after pMCAo, namely at 6h, 12h, 24h, 48h and 7d.

pMCAO induced an infarcted area in the ipsilateral cortex (Fig. 6.3 A) as expected (Gesuete et al. 2009; Storini et al. 2006). The lesion, evaluated as relative paleness of cresyl violet staining and corrected for edema, at 6h, 12h, 24h, 48h and 7d, had a volume of $12.5mm^3 \pm 5.8$, $12.4mm^3 \pm 5.7$, $23.8mm^3 \pm 5.1$, $22.1mm^3 \pm 3.3$ and $9.6mm^3 \pm 4.7$, respectively (Fig. 6.3 B).

Cortex, the brain area involved in the ischemic lesion was considered for neuronal count (Fig. 6.3 C). Six hours after ischemia, neuronal count performed in the ipsilateral cortex revealed a significant cell loss when compared to the corresponding area in the sham-operated group (84.9%). Neuronal counts progressively but slowly decreased reaching 64.9% at 7d. No significant difference was found between ispilateral and contralateral side in sham-operated animals (data not shown).

At 6h after pMCAO rare TUNEL-positive cells were present in the injuried cortex indicating the presence of few dying cells (30.2±14.2, expressed as cell density per mm^2, Fig. 6.3 D). Number of dying cells progressively increased at 12, 24 and 48h post ischemia (278.6±51.1, 589.7±77.3 and 708.8±30.2, respectively). Seven days after ischemia still several TUNEL-positive cells were present (343.6±120.0) indicating the persistence of dying cells at this time point. Positive TUNEL staining was not apparent in any sham-operated mice at any time points.

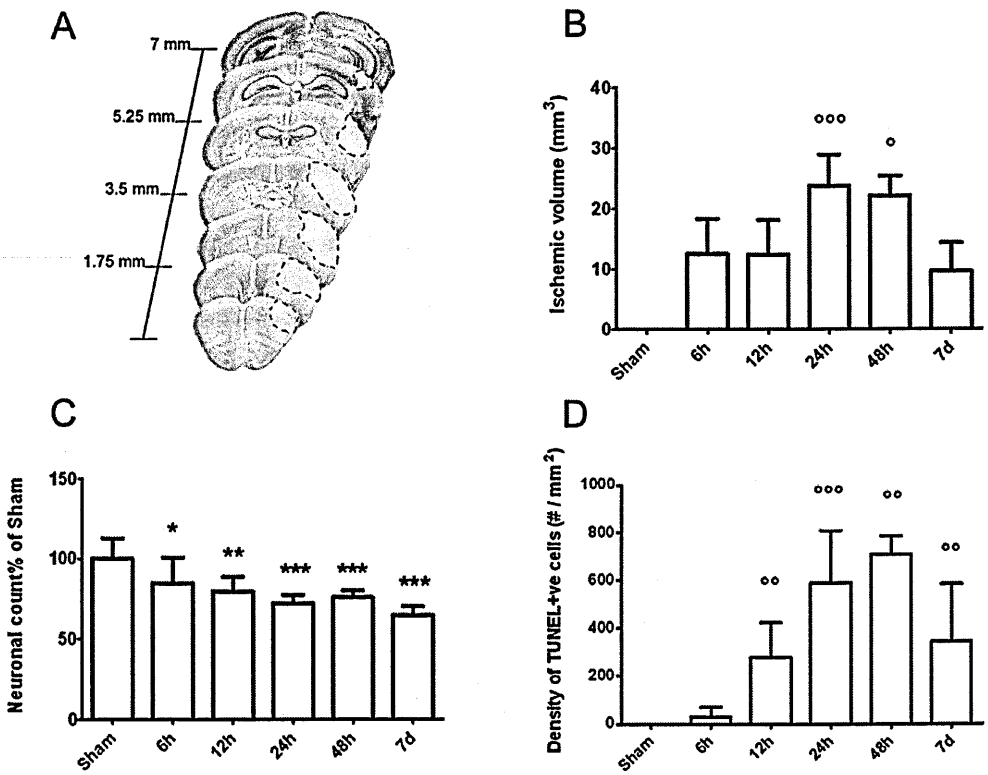

Figure 6.3 *Histopathological findings at different time points from pMCAO.*

A: representative brain coronal sections obtained 24h after pMCAO. Pale demarcated areas depict the ischemic lesion. Quantification of ischemic volume (B), neuronal counts (data obtained from the mean of 33 frames/mouse and expressed as % of sham groups, C) and TUNEL-positive cells (D) in the cortex of sham and ischemic mice at different times after pMCAO. Data are reported as mean+sd, n=8. *p<0.05,**p<0.01, ***p<0.001 versus sham; °p<0.05, °°p<0.01, °°°p<0.001 versus 6h, Bonferroni's Multiple Comparison Test.

6.3.3 Time-course of expression of M/M markers: CD11b, CD45, CD68, Ym1, CD206 and iNOS

The M/M marker expression was analyzed within the ischemic area based on the tissue sampling represented in Fig. 6.1 B. At each time point, the sampled cortical area pertained to the ischemic territory, being the number of neurons in this region decreased compared to sham animals at every time points (Fig. 6.3 C).

CD11b, a constitutive marker of microglia and macrophages was expressed at every time point considered as well as in sham-operated mice (5.6±1.9, percent of stained area). Starting from 6h the immunoreactivity increased and remained elevated at every subsequent time point considered, with no major differences throughout the experimental groups (9.5±1.5, 11.7±1.6, 10.1±1.7, 13.1±2.8, 13.0±0.1, respectively at 6h, 12h, 24h, 48h and 7d, Fig. 6.4 B).

Outside the lesion, CD11b staining revealed thin ramifications and small soma (Fig. 6.4 A/C). CD11b immunoreactivity was associated with a different morphology in relation to the cell localization in the lesioned area. Two main areas were identified, namely a lesion border showing CD11b+ highly ramified cells (Fig. 6.4 A,D) and an ischemic core showing both CD11b+ ameboid cells and cells with hypertrophic soma endowed with thick branches (Fig. 6.4 A,E).

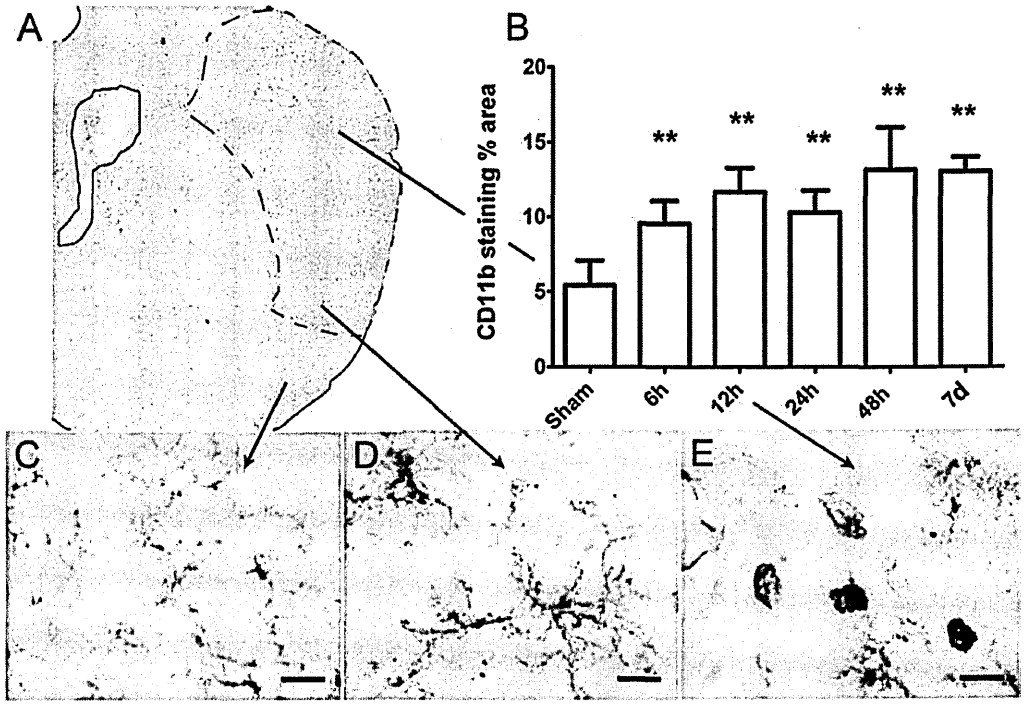

Figure 6.4 *Immunohistochemical analysis and quantification of the microglial marker CD11b.*

A: representative micrographs of CD11b immunostaining in the injured cortex at 24hours after pMCAo. CD11b-positive cells display different morphology depending on their localization in the ischemic area (C: outside the lesion, D: border zone, E: ischemic core). B: quantification of CD11b immunostaining at different times after pMCAo. Data are expressed as mean+sd of 33 frames/mouse, n=8. One way Anova: $p<0.0001$. **$p<0.01$ vs sham; Bonferroni's Multiple Comparison Test. Scale bars=10μm.

No CD45-positive cells ($CD45^{high}$ cells, see methods, Fig. 6.5 A) could be observed in sham-operated mice and in the contralateral hemisphere of ischemic mice. Six hours after ischemia these cells were clearly visible in the area considered (0.4±0.2 percent of stained area). The immunoreactivity was further increased 12 and 24h after ischemia (0.6±0.2 and 1.1±0.3, respectively). No further increase could be observed at 48h (1.1±0.4). CD45 staining was still present at 7d (0.9±0.4, Fig. 6.5 A).

CD68 immunoreactivity was undetectable in sham-operated mice and appeared 6h after ischemia (0.3±0.2 percent of stained area). It progressively increased at every time point

considered (0.6±0.2 at 12h; 1.7±0.2 at 24h; 3.7±0.8 at 48h). Notably, further increase in the CD68 stained area could be observed at 7d (7.4±1.4, Fig. 6.5 B).

Ym1 immunoreactivity was detectable starting from 12h (0.04±0.02 percent of stained area). This marker was maximally expressed at 24h (0.84±0.16) and markedly decreased at later time points (0.37±0.10 at 48h and 0.23±0.15 at 7d, Fig. 6.5 C).

CD206 positive cells were present in sham-operated mice (7.3±0.9 cell/mm^2). They could be observed 6h after pMCAO (12.2±6.2) and significantly increased progressively up to 24h (23.6±5.3 at 12h and 40.0±14.9 at 24h). A significant number of CD206 positive cells was still present at 48h (30.5±10.5) and 7d (32.7±8.8, Fig. 6.5 D).

iNOS positive cells were present starting from 6h after pMCAo (194.3±41.4 cells/mm^2). At 12h their number did not change significantly (191.5±124.8), while started to increase at 24h 273.4±107.1) and reached a peak at 48h (528.2±149.1). At 7d their number was reduced to the lowest value measured (105.2±99.9, Fig. 6.5 E).

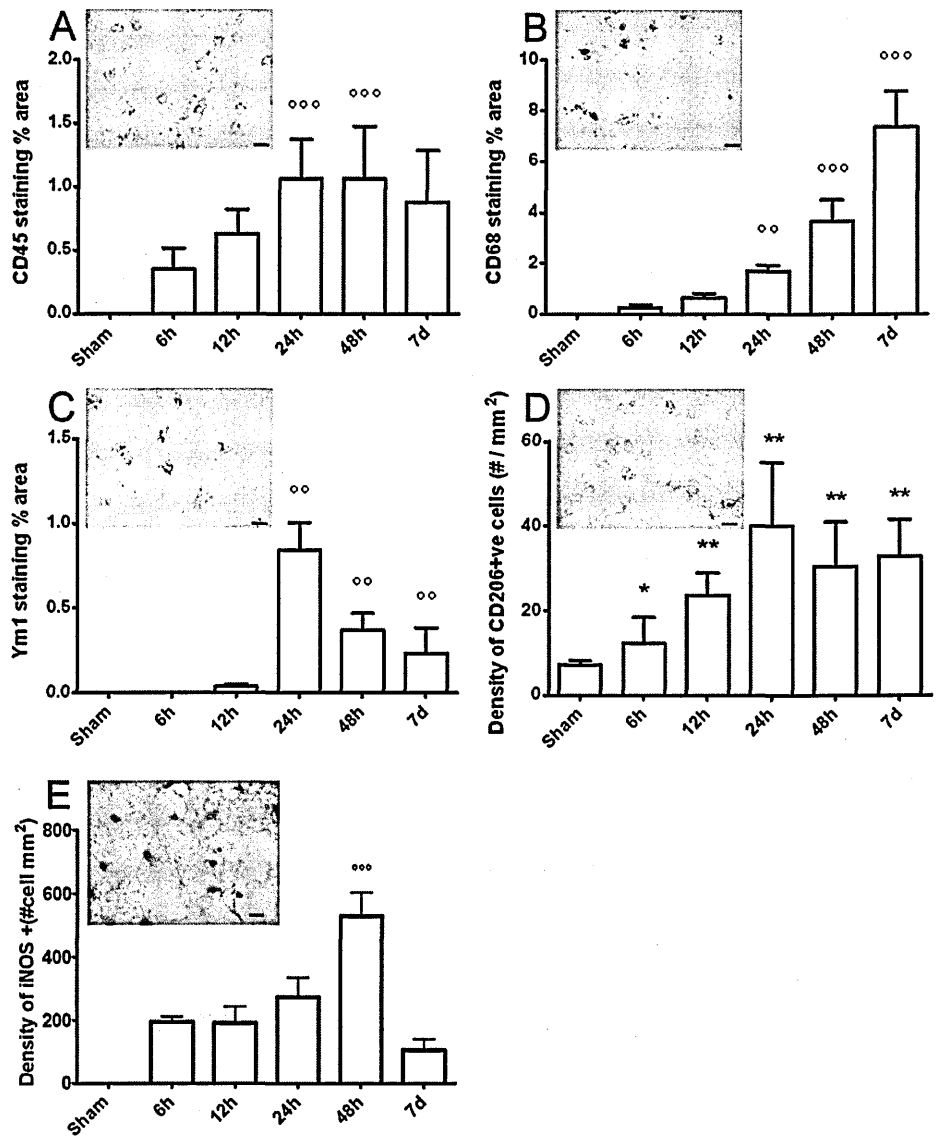

Figure 6.5 *Immunohistochemical analysis and quantification of the microglial markers CD45, CD68, Ym1, CD206 and iNOS.*

Representative micrographs of CD45 (A), CD68 (B), Ym1 (C), CD206 (D) and iNOS (E) immunoreactivity at 24hours after ischemia, and related quantifications at different times after pMCAO (Bar 10μm). Data are expressed as mean+sd of 33 frames/mouse (24 frames/mouse for CD45, TUNEL, CD206), n=8. One way Anova: $p<0.0001$. *$p<0.05$, **$p<0.01$ vs sham; °°$p<0.01$, °°°$p<0.001$ vs 6h (12h for Ym1). Bonferroni's Multiple Comparison Test.

6.3.4 Localization of M/M markers with respect to the lesion

Twenty-four hours after pMCAO, the immunoreactivity for CD11b appeared to be evenly distributed in the ischemic area, being present both in the lesion border and in the ischemic core (Fig. 6.6). At the same time CD45 staining showed a similar distribution being present throughout the entire ischemic area (Fig. 6.6). CD45 cells visible at 10x magnification (Fig. 6.6) did not reveal the presence of $CD45^{low}$ cells (corresponding to ramified microglia) appearing in the CD11b staining microphotograph. Conversely CD68 appeared to be mainly concentrated in the border zone, with rare cells present in the ischemic core. Notably, at longer time points (7d) along with the great increase of its expression (Fig. 6.5 B), CD68 appears both in the border and in the core areas (Fig. 6.10). Ym1 at 24h after pMCAO appeared exclusively expressed in the ischemic core, similarly to CD206 (Fig. 6.6). With the exception of CD68, all the markers considered showed a similar distribution at every time point (data not shown).

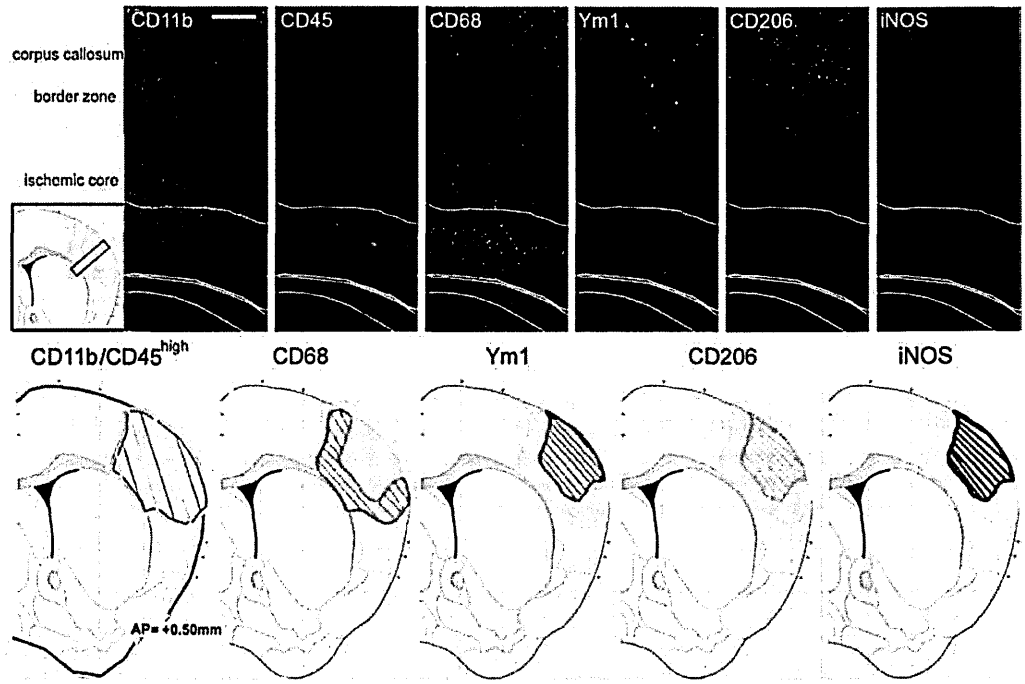

Figure 6.6 *Distribution of the selected M/M markers inside the ischemic lesion at 24h from the injury.* Representative immunostaining micrographs show spatial distribution of M/M phenotype markers (CD11b, CD45, CD68, Ym1, CD206 and iNOS) into the ischemic area at 24h after ischemia. Bar=250μm. Drawings representing the immunostaining data. Only immunoreactivity for CD11b could be observed outside the lesioned area in basal conditions (sham-operated mice). In the lesion, CD11b+ cells showing a ramified to globular morphology could be observed going from the border zone to the ischemic core (red). CD45 staining was present throughout the entire ischemic area (pink). Conversely CD68 appeared to be strongly concentrated in the border zone. Ym1, CD206 and iNOS were exclusively expressed in the ischemic core.

6.3.5 Coexpression of M/M markers at 24h and 7d after pMCAO

Twenty-four hours after ischemia CD68 was expressed in hypertrophic ameboid CD11b cells present in the ischemic core and in ramified microglia in the border zone where CD68 positive cells were mostly located (Fig. 6.6 and 6.7 A-B). A similar pattern of coexpression could be observed at 7d. At this time point the expression of CD68 was greatly increased both in globular CD11b+ cells in the ischemic core and in ramified CD11b cells laying in the border zone (Fig. 6.6 and Fig. 6.7 C-D).

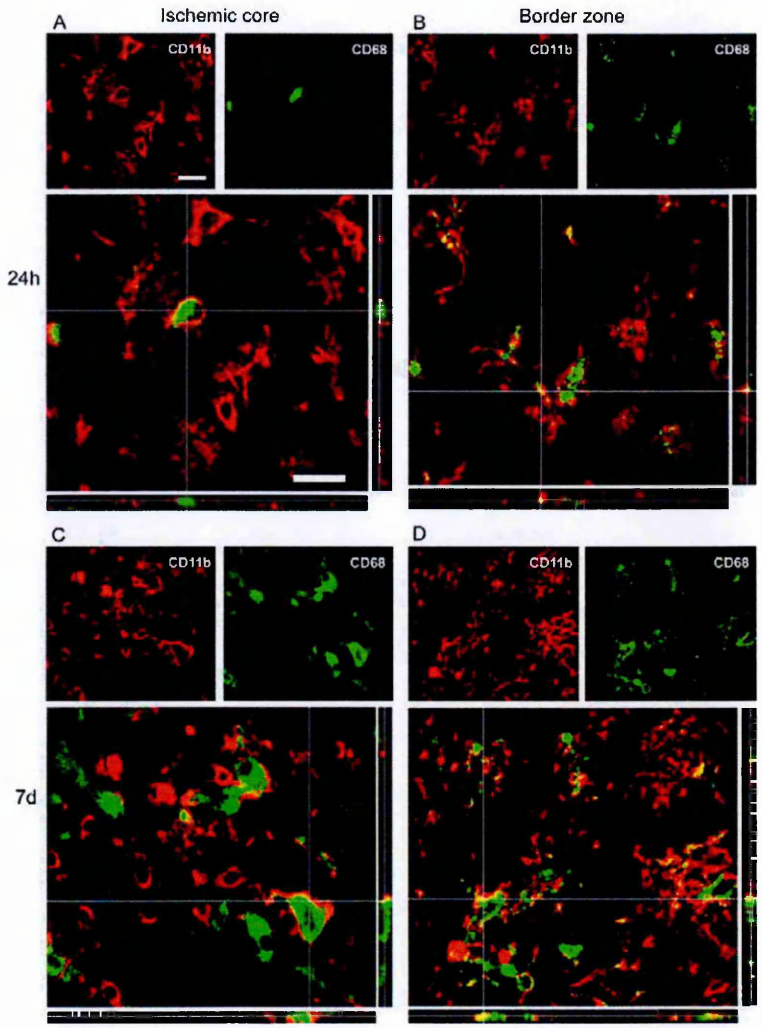

Figure 6.7 *Coexpression of CD11b (red) and CD68 (green) 24h (A-B) and 7d (C-D) after pMCAO.*

In the ischemic core at 24h CD11b positive cells are prevalently globular and some of them are positive to CD68 (A). In the border zone (B) CD11b cells display rounded cell bodies and ramified processes positive to CD68. Globular CD11b cells in the lesioned area 7d after ischemia mostly express CD68 marker (C). A high number of CD11b cells displaying different morphology colabel with CD68 in the border zone (D). Data are representative of 3 independent experiments. Bars: 20μm.

At 24h after pMCAO Ym1 positive cells co-labeled with CD11b globular cells within the ischemic core, where they were exclusively located (Fig. 6.6 and Fig. 6.8 A-B-E-F). Seven days after ischemia Ym1 and CD11b coexpression pattern was similar to that observed at 24h (Fig. 6.8 C-D-G-H).

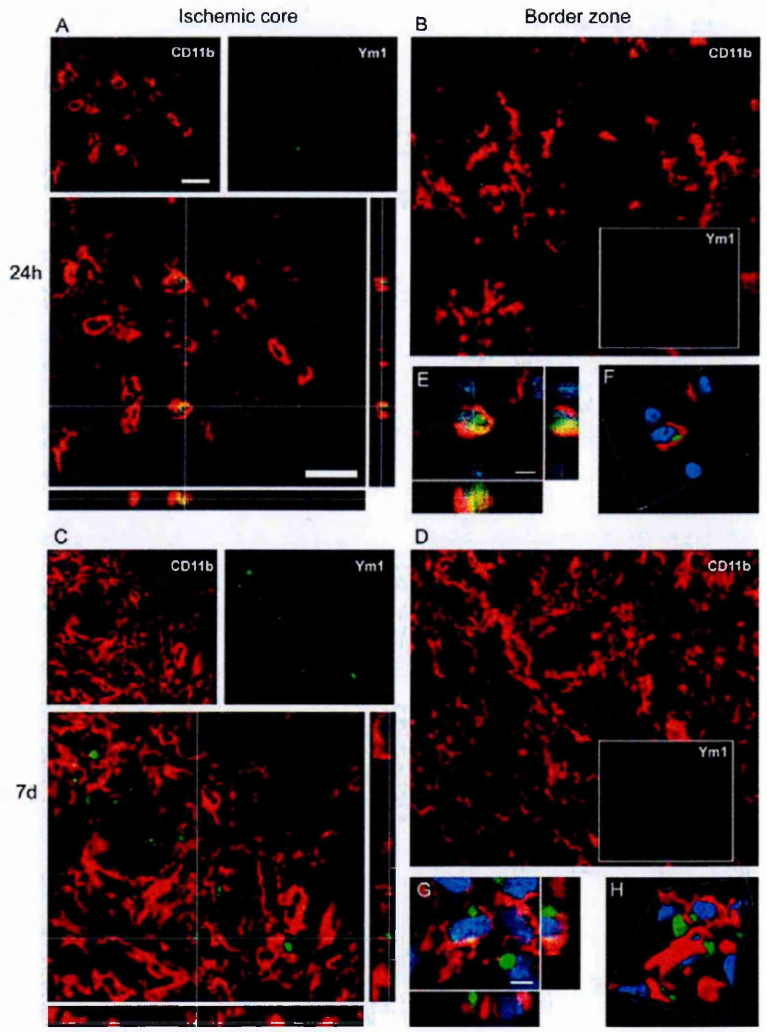

Figure 6.8 *Coexpression of CD11b (red) and Ym1 (green) at 24h (A-B-E-F) and 7d (C-D-G-H) after pMCAO.*

Ym1 positive cells co-label with globular CD11b postive cells at both time points (A,C). High magnifications (E-G) and 3D rendering (F-H) show colabeling of markers further highlighting the coexpression (blu=nuclei, bar: 5µm). Consistent with the observation that no Ym1 cells are present in the border zone (fig. 6.6), no immunostaining for Ym1 at neither time points could be observed in this area (B, D). Data are representative of 3 independent experiments. Bars: 20µm.

CD206 at 24h was present exclusively in the ischemic core (Fig. 6.6) where it colocalized with globular CD11b positive cells (Fig. 6.9 A-B-E-F). The same pattern of coexpression was observed at 7d (Fig. 6.9 C-D-G-H).

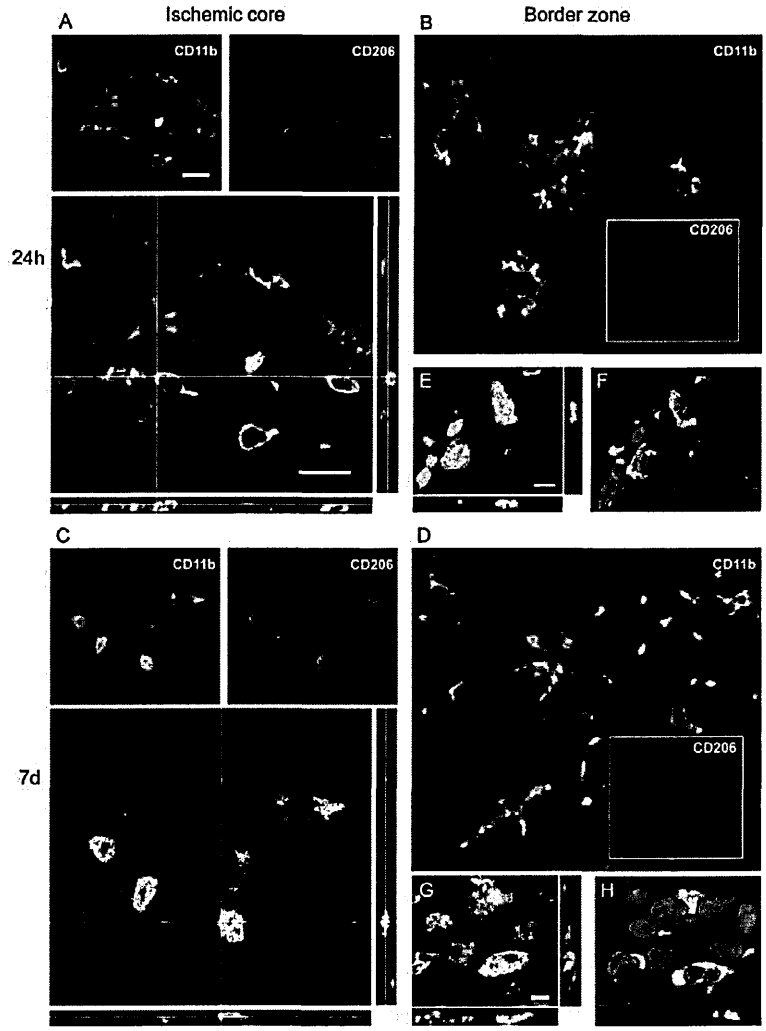

Figure 6.9 *Coexpression of CD11b (red) and CD206 (green) at 24h (A-B-E-F) and 7d (C-D-G-H) after pMCAO.*

At 24 h after ischemia some globular CD11b cells co-label with CD206 marker in the ischemic core (A). Seven days after ischemia CD11b cells are prevalently globular in the ischemic core and are highly positive to CD206 (C). High magnifications (E-G) and 3D rendering (F-H) show colabeling of markers further highlighting the coexpression (blu=nuclei, bar: 5μm). Consistent with the observation that no CD206 cells are present in the border zone (fig. 6.6), no immunostaining for this marker at neither time points could be observed in this area (B, D). Data are representative of 3 independent experiments. Bars: 20μm

At 24h after pMCAO, the few CD68+ cells found in the ischemic core did not colocalize with Ym1+ cells that were present exclusively in this area (Fig. 6.6 and Fig. 6.10 A-B). In the magnification of Fig. 6.10 E-F it is possible to observe that even when these markers

appear closely related, they actually belong to distinct cells. At longer times (7d) Ym1 cells not colocalizing with CD68 are still present, however coexpression with CD68 can also be seen (Fig. 6.10 C-D-G-H).

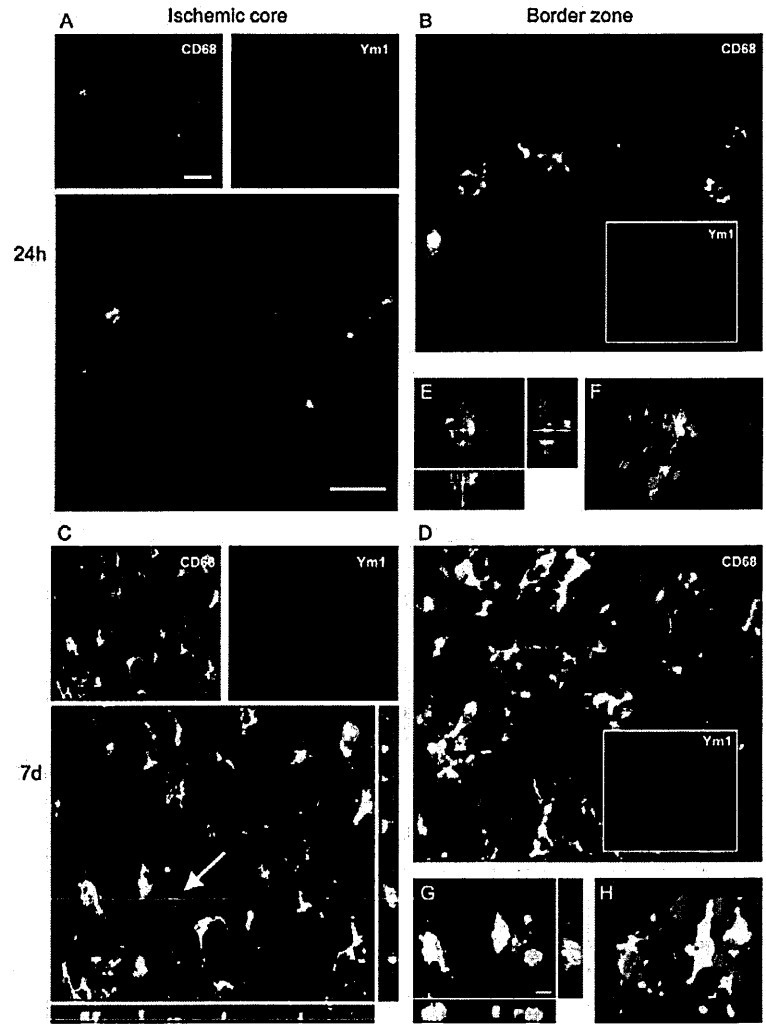

Figure 6.10 *Coexpression of CD68 (red) and Ym1 (green) at 24h (A-B-E-F) and 7d (C-D-G-H) after pMCAO.*

At 24h CD68 positive cells found in the ischemic core do not co-localize with Ym1 positive cells (A). In high magnifications panels (E-F) the two markers appear to belong to different cells although in close contact (blu=nuclei). Seven days after ischemia, when CD68 immunoreactivity is greately increased, Ym1 appears to be expressed also, but not exclusively in CD68 positive cells (C). Note the presence of one Ym1 positive cells (arrow) that does not co-localize with CD68. High magnifications (G) and 3D rendering (H) show colabeling of markers further highlighting the coexpression (blu=nuclei). Consistent with the observation that no Ym1 cells are present in the border zone (fig. 6.6), no immunoreactivity for this marker could be observed at either time points in that area (B, D). Data are representative of 3 independent experiments. Bars: 20μm. High magnifications and 3D rendering bar: 5μm.

A small fraction of CD206 positive cells show coexpression with CD68 at 24h after ischemia in the ischemic core (Fig. 6.11 A-E-F). Similar situation is observed at 7d after pMCAO when a dramatic increase in CD68 positive cells is apparent in the ischemic core (Fig. 6.11 C-G-H). CD206 marker is not present in the border zone at both time points (Fig. 6.11 B-D).

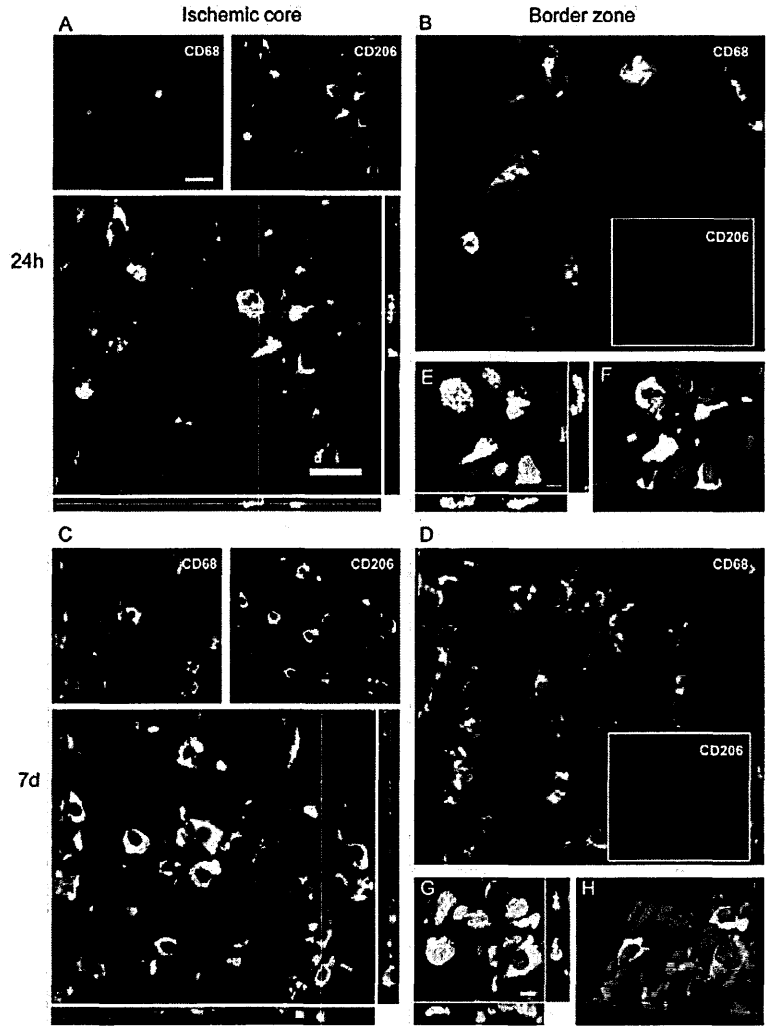

Figure 6.11 *Coexpression of CD68 (red) and CD206 (green) at 24h (A-B-E-F) and 7d (C-D-G-H) after pMCAO.*

At 24h and 7d after ischemia, a minor part of CD68 positive cells found in the ischemic core colocalize with CD206 (A, C). High magnification (E-G) and 3D rendering (F-H) show both single- and double-positive cells in the ischemic core (blu=nuclei, bar: 5μm). Consistent with the observation that no CD206 cells are present in the border zone (fig. 6.6), no immunoreactivity for this marker could be observed at neither time points in that area (B, D). Data are representative of 3 independent experiments. Bars: 20μm.

Ym1 and CD206 appeared to be coexpressed in the ischemic core both at 24h (Fig. 6.12 A-C-D) and 7d (Fig. 6.12 B-E-F) after pMCAO. None of the two markers was present in the border zone at both time points considered (Fig. 6.6).

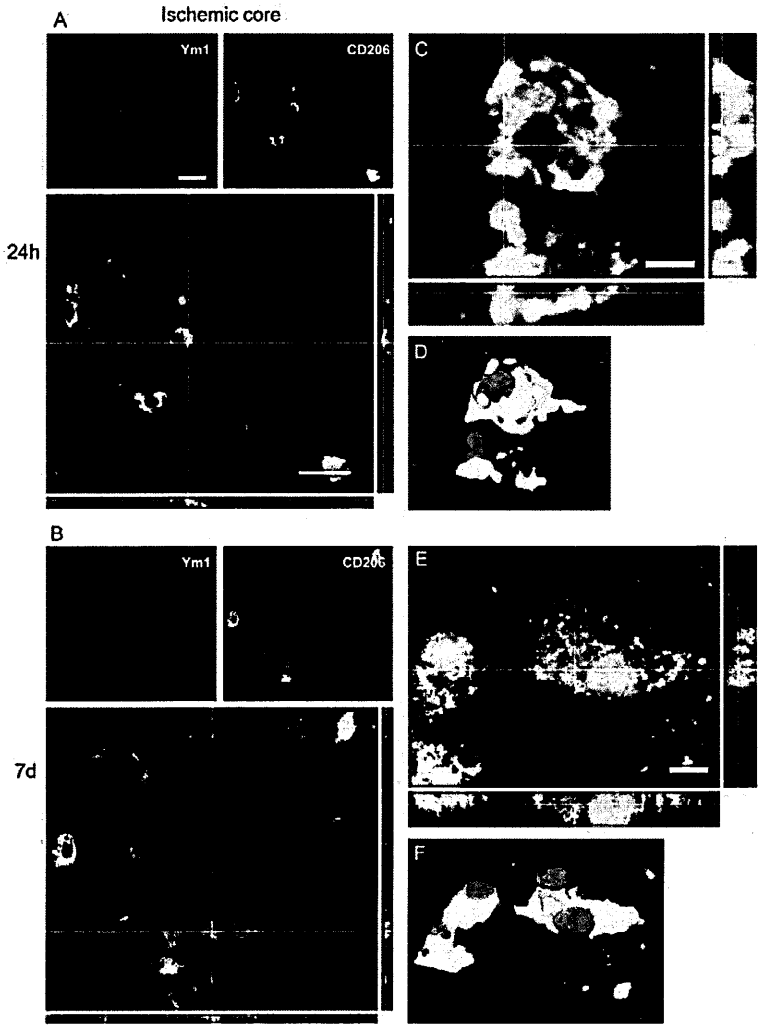

Figure 6.12 *Coexpression of Ym1 (red) and CD206 (green) at 24h (A-C-D) and 7d (B-E-F) after pMCAO.* At 24h and 7d after ischemia Ym1 positive cells co-label with CD206 positive cells in the ischemic core (A-B) Bars: 20μm. High magnification (C-E) and 3D rendering (D-F) show coexpression of markers with the same cell nucleus (blu). Bar: 5μm. Consistent with the observation that neither Ym1 cells nor CD206 cells are present in the border zone (fig. 6.6) no immunostaining for these markers could be observed at neither time pointsi in this area (data not shown). Data are representative of 3 independent experiments.

As expected all CD11b globular, CD68 globular, Ym1 and CD206 positive cells were all positive for $CD45^{high}$ in both ischemic core and border zone (data not shown), being CD45 a common marker for immune cell populations (Sedgwick et al. 1991; Stein et al. 2007).

A summary of M/M markers coexpression 24h and 7d after the ischemic lesion is reported in Fig. 6.13.

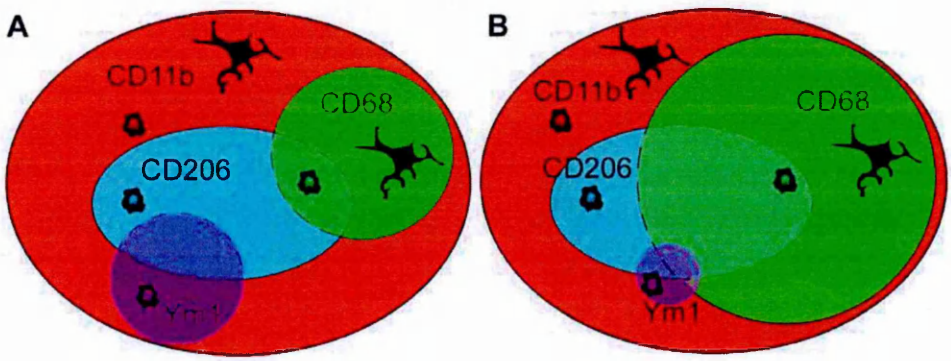

Figure 6.13 *Summary of M/M markers coexpression 24h and 7d after the ischemic lesion.*

At 24h after injury (A) immunoreactivity for CD11, which is readly increased after ischemia, is expressed in ramified and globular cells. CD68 is present in a percentage of both globular and ramified CD11b+ cells. Ym1 and CD206 that are present mostly in the core of the lesion, are expressed by a fraction of globular CD11b+ cells and can present on the same cells. A few cells coexpressing CD206 and CD68 can be found in the area between the core and the border zone where the two markers are mainly located respectively. At 7d after injury (B) Ym1 decreases while CD68 expression greatly increases and from the border zone where it was at earlier times it invades the ischemic core (see also data in Fig. 6.3). A few CD68+ cells appear now to express Ym1.

Lastly, to provide additional details on the functional status of M/M, we assessed their relationship with neurons (NeuN+). We analyzed CD11b/CD68 and CD11b/Ym1 double positive cells as these populations showed to increase at different time points, thus suggesting distinct functional states. CD11b stain of M/M membranes was chosen for documenting the morphology of M/M when contacting neurons. Neurons were found to be often enwrapped by CD11b positive cells in both ischemic core and border zone at both 24h and 7d (Fig. 6.14). In most cases CD11b cells surrounding neurons were positive for

CD68 at both zones (Fig. 6.14 A-B-C-D), suggesting an active phagocytosis. None of the CD11b/Ym1 double positive cells at 24h appeared to be engaging a phagocytic interaction with neurons, being these cells never in contact with NeuN positive cells (Fig. 6.14 E). At 7d, a few CD11b/Ym1 double positive cells showed a phagocytic appearance enveloping neurons (Fig. 6.14 G), coherently with their partially CD68 positive phenotype at this time point (Fig. 6.10). In the border zone, at both time points, Ym1 was not detectable and only single CD11b positive cells did envelop neurons (Fig. 6.14 F-H).

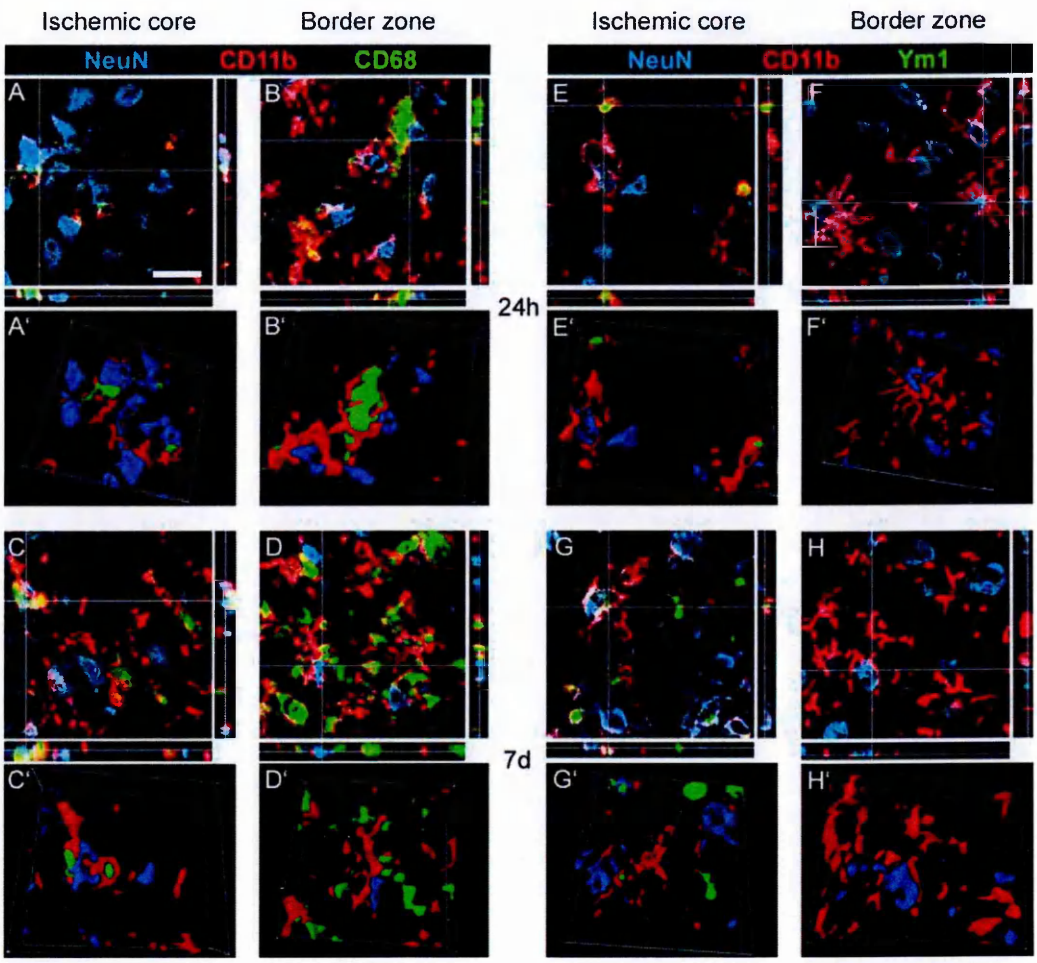

Figure 6.14 *Coexpression of CD11b (red) and NeuN (blue) with CD68 (green) at 24h (A-A'-B-B') and 7d (C-C'-D-D') or with Ym1 at 24h (E-E'-F-F') and 7d (G-G'-H-H') after pMCAO.*

In the ischemic core CD11b/CD68 double positive cells envelop NeuN positive cells, possibly indicating phagocytosis of neurons (A; 3D rendering in A'). The same interaction was observed in the border zone (B-B'). At 7d after ischemia, when CD68 expression is enhanced (Fig. 6.5) in both ischemic core and border zone, CD11b/CD68 double positive cells enwrap neurons, suggesting active phagocytosis also at this time point (C-C'-D-D'). At 24h after pMCAO in the ischemic core, where Ym1 positive cells are exclusively located, CD11b/Ym1 double positive cells do not appear involved in a phagocytic interaction with neurons (NeuN positive cells, E; 3D rendering on E'). CD11b single positive cells in both ischemic core (E-E') and border zone (where Ym1 is not expressed, F-F') surround neurons. At 7d after ischemia part of CD11b/Ym1 double positive cells engage a phagocytic appearance by enveloping neurons in ischemic core (G-G') coherently with their partially CD68 positive phenotype at this time point (Fig. 6.10). In the border zone at 7d (Ym1 is absent) CD11b single positive cells still enwrap neurons (H-H'). Data are representative of 3 independent experiments. Bar: 20μm.

6.4 Discussion

This part of the project shows that the ischemic lesion is accompanied by activation of specific M/M phenotype that presents distinctive spatial and temporal features. I have demonstrated that: 1) the ischemic lesion induces the expression of the selected M/M markers that develop over time, each with a specific pattern; 2) the selected markers are associated with globular or ramified CD11b morphology, 3) each marker has a given localization in the lesioned area with no apparent major changes during time, with the exception of CD68, 4) M2 polarized cells have a peak at 24h after injury, while M1 cells peak at 48h.

We have firstly determined the histopathological features of the lesion induced by pMCAO. From the analysis of the temporal evolution of the lesion it appears that the percentage of neuronal loss is somehow stable from 24h up to 7d although the persistence of TUNEL-positive cells at this late point indicates that some cells may still be in degeneration at that late time. It should be noted that assessing the lesion volume by the paleness of the cresyl violet staining may lead to misleading conclusions since, as detailed below, invading inflammatory cells may contribute to the apparent reduction of the lesioned area at 7d. Actually the quantification of the CD11b and $CD45^{high}$ immunoreactivity indicates that inflammatory cells rapidly increase in number and/or size early after the injury and at every time point considered.

M/M play a pivotal role in surveillance and response to altered CNS conditions (Davalos et al. 2005; Jin et al. 2010; Yenari et al. 2010). An emerging concept is that, similarly to what happens for peripheral macrophages, these cells can exert different antithetic functions depending on environmental signals, acting as major players in the pro-inflammatory cytotoxic response, but also participating in the immunosuppressive and self-repair processes (Block et al. 2007; Colton 2009; Lambertsen et al. 2009). The phenotype

markers considered here include classical markers of M/M activation (CD11b and CD45) and markers expressed by alternatively activated macrophages (CD68, Ym1 and CD206). Although evidence of M2 activation state in the brain has been reported in M/M in AD models (Reed-Geaghan et al. 2010; Shin et al. 2011), following global ischemia (Ohtaki et al. 2008), in models of experimental autoimmune encephalomyelitis (Ponomarev et al. 2007) or spinal cord injury (David and Kroner 2011; Kigerl et al. 2009), information on M2 marker expression, coexpression and temporal evolution in the injuried brain is lacking. We could observe that these phenotype markers are exclusively expressed by CD11b cells and that each of them shows distinct features in terms of time course of activation and localization in relation to the ischemic lesion.

CD11b is expressed on the surface of many leukocytes and is a widely used marker of M/M. It belongs to a family of cell surface receptors known as integrins. It is covalently bound to a beta 2 subunit to form integrin $\alpha_M\beta_2$ (Mac-1, CD11b/CD18) which is implicated in diverse responses including cell-mediated killing, phagocytosis, chemotaxis and cellular activation. CD11b has the ability to recognize a wide series of ligands such as fibrinogen, iC3b fragment of the third complement component, ICAM-1, denaturated products, blood coagulation factor X (Solovjov et al. 2005). My data show that CD11b staining increases at early time points after ischemia, rapidly reaching a plateau of activation. Notably, CD11b positive cells display a different morphology in relation to the lesion, namely they are ramified in the border zone and ameboid in the ischemic core. Similarly to CD11b, also $CD45^{high}$ cells increase rapidly after ischemia. These cells, display a rounded morphology and most probably correspond to recruited macrophages, neutrophils and lymphocytes (Gelderblom et al. 2009; Gesuete et al. 2009; Stein et al. 2007). This study does not specifically address the question of differentiating between invading macrophages and resident microglia. An important future direction will be to identify specific molecular/phenotypical markers for these two cell populations, since there

is evidence that they may play a different role in the progression of brain injury (Ajami et al. 2011; Lalancette-Hébert et al. 2007; Lambertsen et al. 2009).

CD68 or macrosialin is a member of the lysosomal/endosomal-associated membrane glycoprotein (LAMP) family and a member of the scavenger receptor family which recognizes a wide range of anionic macromolecules such as oxidatively modified lipoprotein, apoptotic cells and cell surface antigens of microorganisms. Its localization and predominance in phagocytic macrophages implicates CD68 in phagocytosis (De Beer et al. 2003; Ramprasad et al. 1996). We observed that the early increase in CD68 immunoreactivity is concentrated in the border zone and expressed in ramified CD11b positive cells. At later time points a dramatic increase in CD68 expression appears both in the border zone and the ischemic core and is apparent in globular CD11b cells. At both time points and in both zones, CD11b/CD68 double positive cells appear to physically interact with neurons and show a phagocytic-like morphology characterized by neuron engulfment. The phagocytic activity of alternatively activated M/M is associated to clearance of cells debris, of damaged or dying cells and of infiltrating neutrophils thus resulting in the elimination of several potentially cytotoxic substances (Denes et al. 2007; Jayadev et al. 2011; Jin et al. 2010; Michelucci et al. 2009; Raes et al. 2002). However the overall functional meaning of phagocytosis in acute brain injury is still an open question. Actually the protective effect of manipulations such as stem cell infusion may be associated with a decrease in CD68 expression (Zanier et al. 2011).

Ym1 belongs to the lectin family and is constitutively expressed by liver, lung and bone marrow, consistently with the fact that these are the original sources of myeloid cells (Chang and Karin 2001). It is synthesized and secreted by activated macrophages during inflammation and exhibits a pH-dependent, specific activity towards GlcN oligomers and heparin. Ym1 may control leukocyte trafficking by competing with them for binding sites on local extracellular matrix, an action resulting in down-regulation of inflammation. Our

findings show that, similarly to what reported in peripheral macrophages, Ym1 is activated transiently suggesting that it may be involved in the establishment of an inflammatory management control of the injured region (Chang and Karin 2001). Its expression is restricted to the ischemic core and it colocalizes with CD11b globular cells and with some CD68 cells at later times only. None of the CD11b/Ym1 double positive cells is associated with phagocytosis of neurons at 24h, whilst at 7d some of them show a phagocytic appearance and envelop neurons, coherently with their partially CD68 positive phenotype at this time point. An increase in Ym1 expression has been associated to the beneficial effect of stem cell infusion in mice subjected to global ischemia (Ohtaki et al. 2008), in line with a protective role in acute brain injury.

Another marker of alternatively activated macrophages is CD206 or mannose receptor (Jayadev et al. 2011; Porcheray et al. 2005). This is an endocytic receptor that binds both microbial glycans and self glycoproteins carrying terminal mannose, fucose and N-acetylglucosamine by interaction with its carbohydrate recognition domains (CRDs). Its known function is related to recognition and endocytosis of the carbohydrate portion of antigens for processing and presentation (Linehan et al. 2005). My results show that CD206 expression significantly increases over time and colocalizes with Ym1 positive cells and with a fraction of CD68 positive cells that increase at later time points.

We then assessed the presence of iNOS, a well defined marker of the classical activation of M/M. iNOS is a cytokine-inducible nitric oxide synthase produced in M/M. iNOS is involved in the immune response upon binding to calmodulin and produces large amounts of NO that may have detrimental effects after ischemic injury. Its expression is induced as early as 6h after pMCAo and has a peak at 48h after injury, thus trailing the peak of expression of the M2 marker Ym1 (24h).

Lastly, our data have been obtained in a model of permanent ischemia and may not be extended to an ischemia with reperfusion paradigm. Notably the present data and previous results obtianed in our lab (Gesuete et al. 2009) indicate that the ratio of $CD45^{high}/CD45^{low}$ is dramatically different in these two conditions, being much higher after pMCAO. This may be due to either a higher number of infiltrating cells and/or a lower survival of resident cells, thus indicating that in transient ischemia the composition of the specific M/M populations in the lesioned area is different.

6.5 Conclusions

In the ischemic lesion M/M express markers that show distinct temporal expression, distribution and association with a definite cell morphology suggesting that different M/M populations are acting at the site of injury according to well defined phenotype, time of activation and pattern of localization. Conceivably, at 24h after insult, ramified and phagocytic M/M surround the lesion, possibly acting as a barrier against further expansion of the lesion, whilst globular M/M committed to a protective phenotype (*i.e.* expressing Ym1 and CD206 or iNOS) populate the ischemic core with the primary function of resolving inflammation and promoting wound healing. Interestingly, the peak of Ym1 and CD206 expression is observable at 24h, whilst that of iNOS is shifted to 48h after injury. At later time points (7d) the phagocytic behavior of M/M becomes prevalent in the whole lesioned area with numerous globular phagocytic M/M invading the core territory. The observed switch towards the phagocytic phenotype is accompanied by the progressive reduction of the expression of the protective Ym1.

At 24h protective Ym1 positive cells do not appear to be involved in neuron phagocytosis, differently from CD68 positive cells that show a close physical interaction with neurons.

At 7d, when neuronal damage becomes irreversible in the core area, Ym1 positive cells decrease and start to show phagocytic behavior being partially co-localized with CD68. These cells now show the ability to envelop neurons in a phagocytic-like manner. Overall this effect suggests that endogenous protective mechanisms take place soon after injury (24h-48h) and last at least up to 7d when phagocytosis of neurons and debris removal are prevalent. Whether this effect is beneficial or detrimental cannot be clearly established. Phagocytosis (CD68 positive cells) can result in a protective function if properly balanced. In normal brain, phagocytic function of microglia have been suggested to support neurogenesis (Sierra et al. 2010). After an acute injury microglia are supposed to remove cellular parts, as well as whole cells (Kettenmann 2007), an action that might be necessary to remove irreversibly damaged cells to make space for new neuronal projections and fresh connections or newly generated neurons.

The different states of M/M in the ischemic lesion reflect the complexity of these cells and their ability to differentiate towards a multitude of phenotypes depending on the surrounding microenvironmental signals that can change over time. The inflammatory response that follows cerebral ischemia is regarded as a promising target for stroke therapy. The data presented in this study provide a basis for understanding this complex response and for developing strategies resulting in promotion of a protective inflammatory phenotype.

7. *IN VIVO* IMAGING OF T-CELLS IN THE ISCHEMIC BRAIN

7.1 Background

T lymphocytes have been recently revealed as potential therapeutic targets in brain ischemia. Mice deficient in lymphocytes have been shown to exhibit reduced infarct volume after tMCAo by an intraluminal filament (Hurn et al. 2007; Yilmaz et al. 2006) and after pMCAO by electrocoagulation (Liesz et al. 2009). Infarct volume after tMCAo has also reportedly been reduced by the immunosuppressant FTY720, which blocks T-cell infiltration into the brain (Shichita et al. 2009). Despite the deleterious effect of T-cells on stroke, subpopulations of T-cells may be harnessed to reduce tissue damage. Neuroprotective mucosal immunization is mediated by inducible regulatory lymphocytes (Gee et al. 2008) and regulatory T-cells have indeed been shown to be protective against delayed infarct expansion after both pMCAO and transient middle cerebral artery occlusion (Liesz et al. 2009).

Over the last years, a few *in vivo* imaging systems to study T-cell dynamism become available and have been applied to models of CNS diseases. In particular, the introduction of 2-PM allowed high-resolution visualization of T-cells within a three-dimensional space over time. This technique can image the movements of single T-cells at depths of hundreds of microns into living tissue (Helmchen and Denk 2005) and could provide fundamental insight into how T cells and antigen-presenting cells access and behave within the ischemic brain. This technique provided new information on T-cell dynamism in superfused slices of ischemic brain *ex vivo* and detailed quantitative measurements of the movements of T-cells (Ortolano et al. 2010; Ortolano et al. 2009b; Rush et al. 2009; Zinselmeyer et al. 2005). However, immune cell mobility and activation are drastically altered in brain slice

cultures, where the vascular system is not preserved. 2-PM has recently been used to image T-cell behavior *in vivo* in the lower spinal cord in models of cerebral autoimmune disease (Bartholomäus et al. 2009; Flügel et al. 2007; Smorodchenko et al. 2007). However, considering the difficulties in localizing the ischemic area of interest and that there are far fewer T cells extravasated in stroke compared with autoimmune disease, this *in vivo* approach has to date never been applied to image T-cells after stroke.

I here report real-time *in vivo* 2-PM imaging and quantitative tracking of endogenous T-cell dynamics in the brain after a focal cerebral ischemic insult using transgenic mice whose T-cells express green fluorescent protein (GFP). To study T cells in the pMCAO model, it was necessary to image in and near the territory of the middle cerebral artery. To avoid performing a craniotomy, which has been shown to have pathological effects (Xu et al. 2007b), I imaged through the thinned skull (Yang et al. 2010). The imaging was performed 72 hours after pMCAO, because the results of Jander (Jander et al. 1995) and Schroeter (Schroeter et al. 1994) and my preliminary data suggested that the population of infiltrated T-cells was near its peak at this time point.

7.2 Specific methods in this chapter

7.2.1 Experimental plan

Experiments were performed according to the plan shown in figure 7.1.

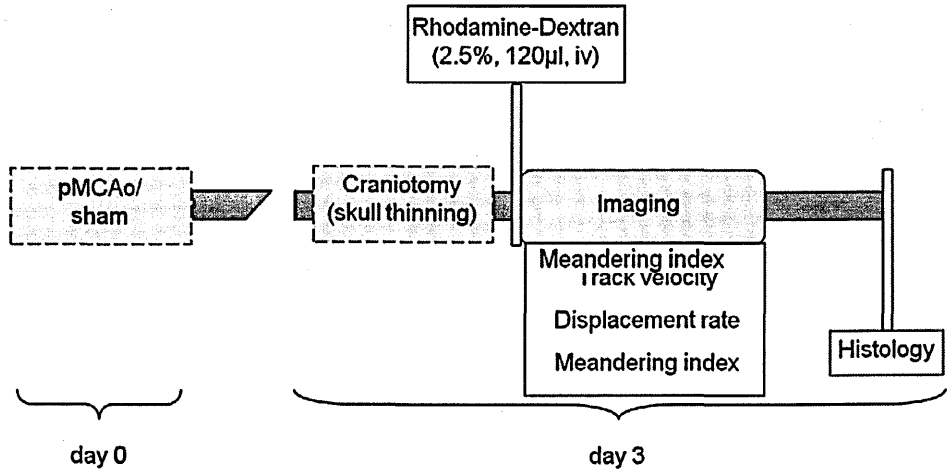

Figure 7.1 *Experimental plan.*

Mice with GFP+ T-cells were subjected to pMCAo or sham surgery and subsequently, after 3d, to craniotomy and in vivo 2-PM. Mice were sacrified at the end of imaging for immunofluorescence.

7.2.2 Thinned skull craniotomy for two-photon imaging (Fumagalli et al. 2011)

At Strathclyde University, Glasgow, UK: Seventy two hours post-MCAO the blood was labeled by injecting a red fluorescent marker in a tail vein, rhodamine B isothiocyanate-dextran (RhITC-dextran, 70 kD, Sigma; 5% in PBS, 150 µL). The mice (n=6) were anesthetized with isofluorane in oxygen and its rectal temperature maintained at 36.2 - 37°C by an electrically heated plate. The left parietal skull was exposed and dried, a point near 2.5 mm lateral, 1 mm posterior to the bregma was marked with a felt tip pen and the coordinates of the mark measured. A stainless steel plate 0.4 mm thick with a 5 mm hole was glued to the skull with its centre over the mark. Initial adhesion was with a cyanoacrylate glue (Vetbond, 3M); a two-component rapid epoxy glue was then used to fill gaps and allowed 15 min to harden. The plate was clamped between two supports on a base plate. Under a dissecting microscope the skull was thinned using a NSK Vmax Volvere dental drill (Wright Cottrell) with a diamond bur (Diama Labcraft). When the pial

vasculature could be clearly seen, the mouse on its base plate was moved to the imaging microscope. Imaging was performed soon after the craniotomy was created.

7.2.3 Imaging of GFP+ T-cells

7.2.3.1 GFP signal detection

To image GFP-expressing T cells we used the longest available excitation wavelength, 940 nm. The blood marker used (RhITC-dextran) absorbs more strongly at 830 nm than at 940 nm, therefore in few cases the vasculature was imaged separately from the T cells. In tests, the image shifted laterally by at a maximum of 3.1 μm over 1 hour. When the vasculature and T cells were imaged separately, the imaging period was usually less than 30 min. Although a single snapshot of a T cell did not always establish with certainty that it was extravascular, time series of images that included several cells left no doubt that they were indeed extravascular.

7.2.3.2 Image acquisition and processing

To track extravascular T cells, time series of z-stacks were obtained, *i.e.*, x-y planes were imaged at a series of depths to give a 3D image and this was done repeatedly to give 4D. Typically, the area imaged was 284 μm x 284 μm at 512 x 512 pixels and 500 lines per sec, the z step was 2.0 μm, with a total depth of 16-20 stacks, and the repetition rate for the stacks was 34 sec per stack. 4D reconstructions were analyzed using Volocity 5 software (Improvision, UK) and Excel (Microsoft).

The location (centroid) of each GFP positive cell within each 3D image stack was determined manually by the operator. The x and y coordinates of the cell were determined

in an extended focus view and the z coordinate was determined by examination of single planes. T cell movements were tracked in 3D by linking the consecutive xyz coordinates of the same object. T cell velocity was computed as the distance between xyz coordinates (cell centroids) in successive stacks, divided by the interstack time interval. Only tracks with at least 3 time points were included in the analysis. To quantify T cell behaviors, we calculated, for each cell, its mean velocity as it moved along its track, length covered, displacement (straight line distance from the first position in the track to the last), displacement rate (total displacement during the period of tracking divided by the time it was tracked) and meandering index (displacement rate/velocity, which provides a measure of a track's deviation from a straight line. A meandering index of 1 indicates that the track is a perfect straight line; the smaller the value of the meandering index, the greater the meandering of the track). Figure 7.2 illustrates the tracking of T-cells over time and space. Images were processed using Adobe® Photoshop® CS3 (Adobe Systems Europe Ltd, United Kingdom).

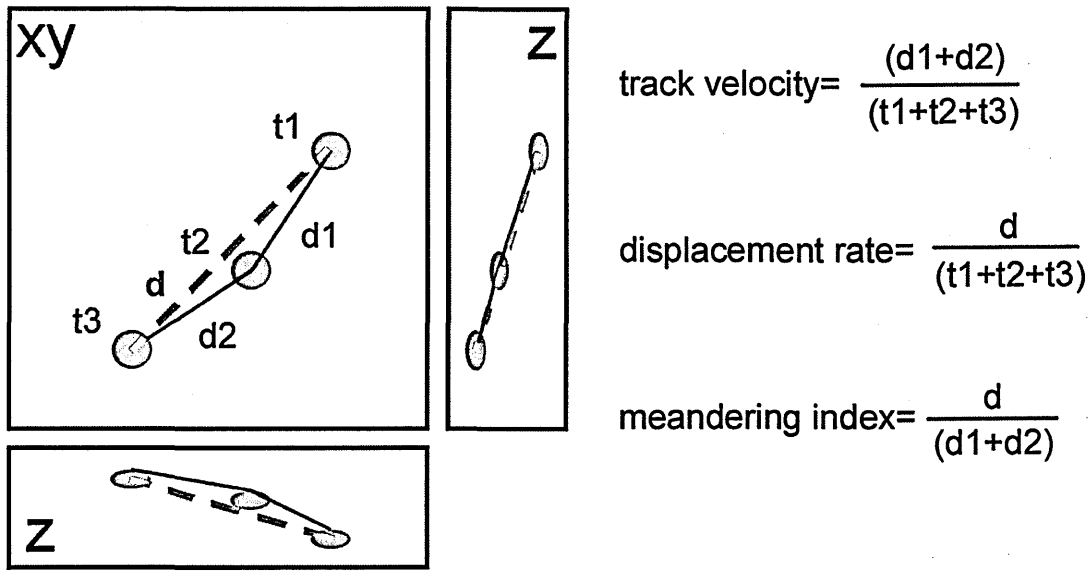

Figure 7.2 *Tracking of T-cells by post-acquisition analysis.*

To calculate track velocity, displacement rate and meandering index, xyz coordinates of cell centroid for each cell present in the imaged volume were identified. Centroids belonging to subsequent time points (t1...t3) were connected. Motility parameters were calculated as shown in figure: track velocity=total distance moved/ total time of cell imaging; displacement rate=linear distance between first and last time points/ total time of cell imaging; meandering index=linear distance between first and last time points/ total distance moved.

7.3 Results

I performed imaging through the thinned skull. To determine the coordinates of each recording site, I took photographs through the dissecting microscope. The sites of imaging were identified by their relation to blood vessels and the stereotaxic coordinates (Fig. 7.3). The green autofluorescence of the skull bone was used to determine the underside of the skull, which I defined as z=0.

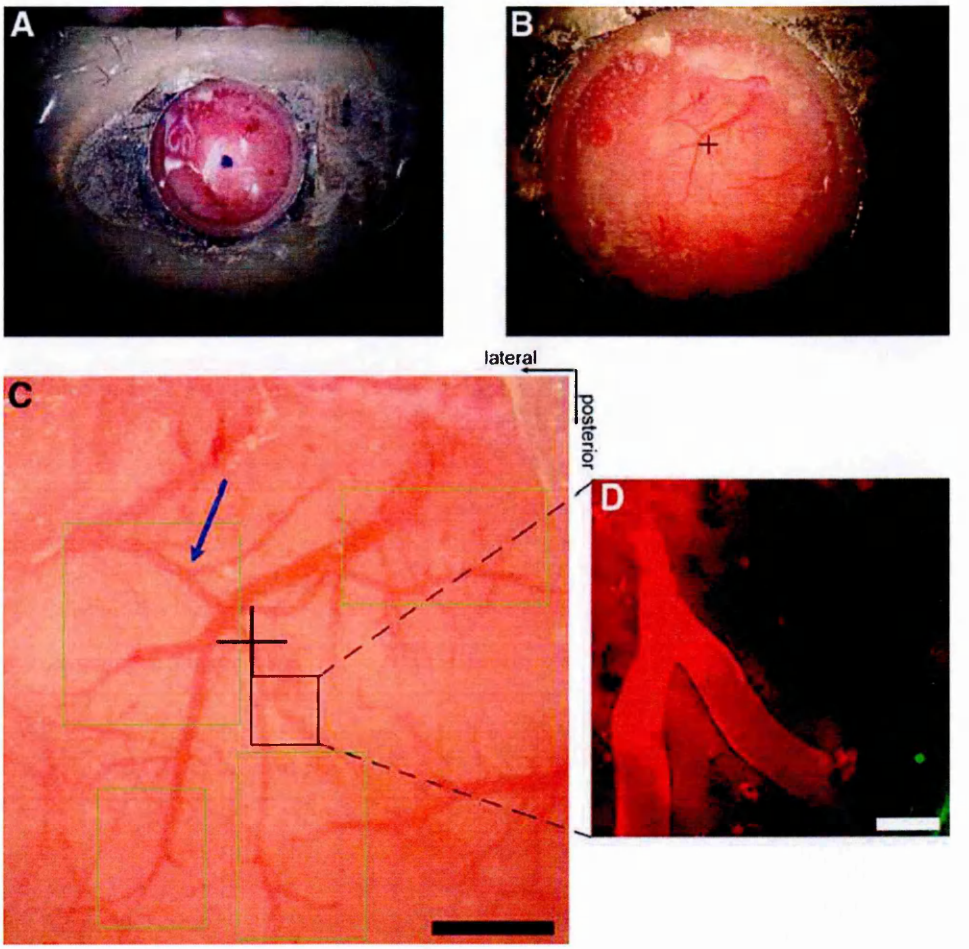

Figure 7.3 *In vivo brain imaging protocol for location of imaging fields.*

A: coordinates are defined by an ink dot on the skull (2.5 mm lateral, 1.0 mm posterior to bregma), and the stainless steel plate is glued to the skull. A template constructed from A is used to determine the position corresponding to the ink dot on the vasculature seen through the thinned skull (cross in B). C: imaging coordinates of T-cells in a representative sham animal; blue arrow indicates middle cerebral artery (MCA). No T-cells were observed in the extensive areas indicated by the green rectangles. The black cross indicates the standard coordinate position. D: high resolution two-photon image of blood vessels from the black rectangle in C. Scales: (A. B) hole in plate is 5 mm diameter. Bars = 0.5 mm in C and 50 μm in D.

7.3.1 Characterization of the imaged area

As expected, a significant area of lesion was observed at 72 hours after pMCAO (Fig. 7.4 H). It was our aim to perform *in vivo* 2-PM imaging through the skull in an area not too far from the midline but within the lesioned zone. We confirmed that the surface coordinates

2.5 mm lateral, 1.0 mm posterior to bregma met these requirements. Intravenous injection of propidium iodide was used to label dead cells (Unal Cevik and Dalkara 2003) and produced little labeling of cells in sham-operated mice, showing that the procedure of thinning the skull caused no cell death or did not compromise the blood– brain barrier (Fig. 7.4 A, Hussain et al. 1985). After pMCAO, numerous cells were stained, particularly near the central coordinate point (Fig. 7.4 B-D). These results show that in the areas where T cells were imaged after pMCAO, propidium iodide could extravasate from perfused vessels and cross the membranes of many cells. This indicates opening of the blood– brain barrier and, perhaps, debility of the stained cells (Unal Cevik and Dalkara 2003). In addition, *in vivo* Evans blue staining at the image site (1 µL of Evans blue injected at 1 mm posterior, 2.5 mm lateral from bregma and 1.5 mm ventral to the skull, 72 hours after pMCAO) was colocalized with the autofluorescence produced by the injured tissue providing clear confirmation that the imaging site is present inside the compromised area (Fig. 7.4 E-I).

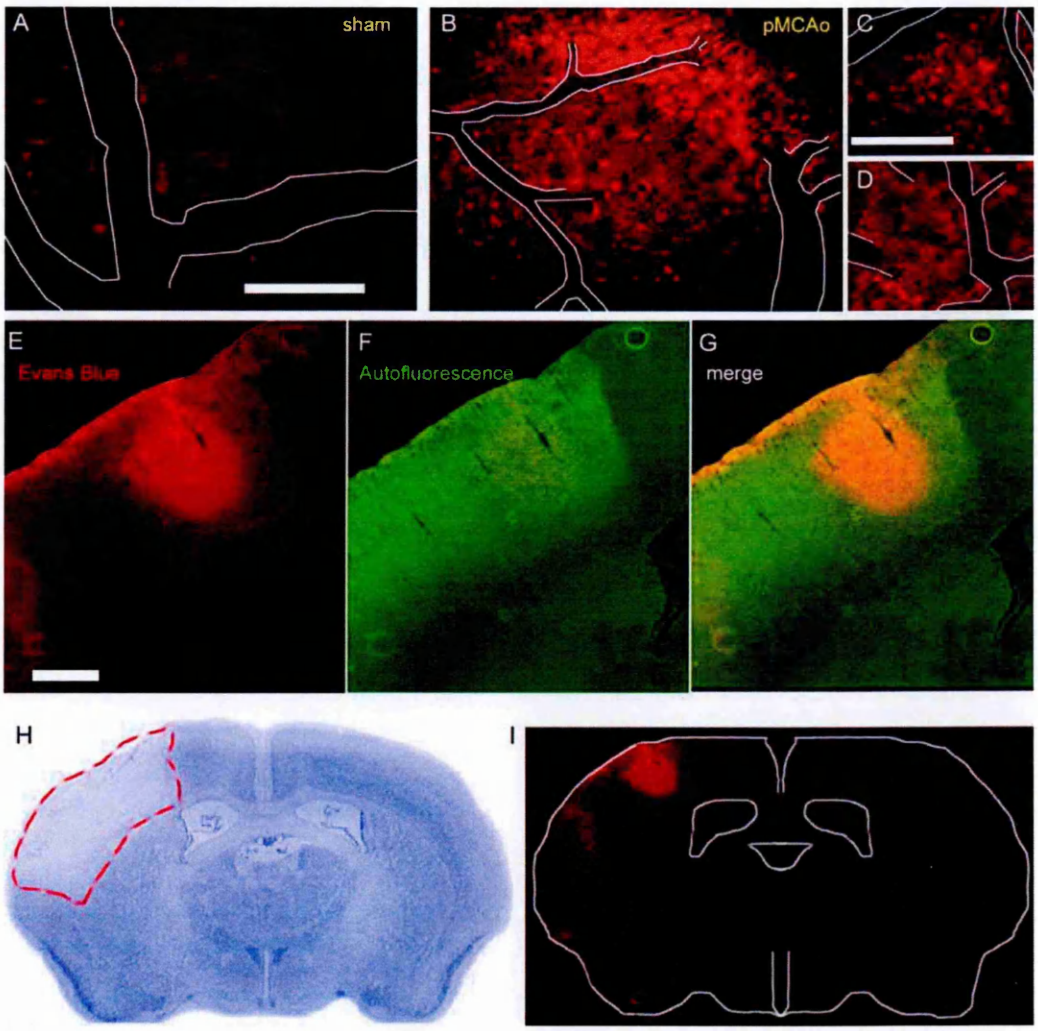

Figure 7.4 *Confirmation of imaging over cortical area compromized by pMCAo.*

A: sparse dead cells after sham injury. B: After pMCAo, many PI-labeled cells were visualized at the center of the area examined by 2-PM, and in other areas under the craniotomy (C, D) indicating many necrotic cells all over the exposed area to imaging. Bars= 150μm. E-G: signal from the intraparenchymal injection of Evans Blue at reference coordinates (E) and green autofluorescence caused by the ischemic damage (F) showed co-localization (G). H: representative image of cresyl violet staining showing coronal topography of infarct (dashed line) at the level of septal nucleus (0.145 mm from bregma) and (I) adjacent section showing coronal topography of Evans Blue staining overlapping the lesioned area.

7.3.2 Visualization of T-cells and quantification of their motility

Many areas scanned in sham mice revealed no T-cells or rarely more than 1 to 2 extravascular T-cells per imaging volume and these were close to the skull (within 20 μm; Fig. 7.5 A, C). In contrast, in pMCAO mice, extravascular T-cells were observed in virtually all areas where the blood marker was present (Fig. 7.5 B, D). The number of extravascular T cells observed in each imaging field were normalized for the volume of the field and averaged for each mouse. The mean T-cell density was significantly ($P<0.05$) higher in pMCAO mice (5.1±1.2 thousand/mm3, n=6) compared with sham-operated mice (sham; 1.9±0.4 thousand/mm3, n=6). Note that the true ratio of the T-cell populations is greater than these numbers suggest, because the volumes in shams with no T-cells (green areas in Fig. 7.3) were not imaged and therefore excluded. With rare exceptions (1 animal in 6 analyzed), the sparse extravascular T-cells in sham animals moved slowly and meandered so that their displacement was small (Fig. 7.5 A, C). After pMCAO, most of the numerous T-cells (Fig. 7.5 B, D) patrolled up and down the perivascular surfaces of blood vessels (Fig. 7.5 E), sometimes moving from 1 vessel to another, and few T-cells were remote from blood vessels. T cells, detected in the bloodstream, moved with a similar velocity as erythrocytes (Fig 7.5 F,G). After pMCAO, some vessels were poorly perfused, as shown by an absence of fast-moving cells (Fig 7.5 G). Very few T-cells were observed on the luminal surface of the vascular endothelium in perfused vessels.

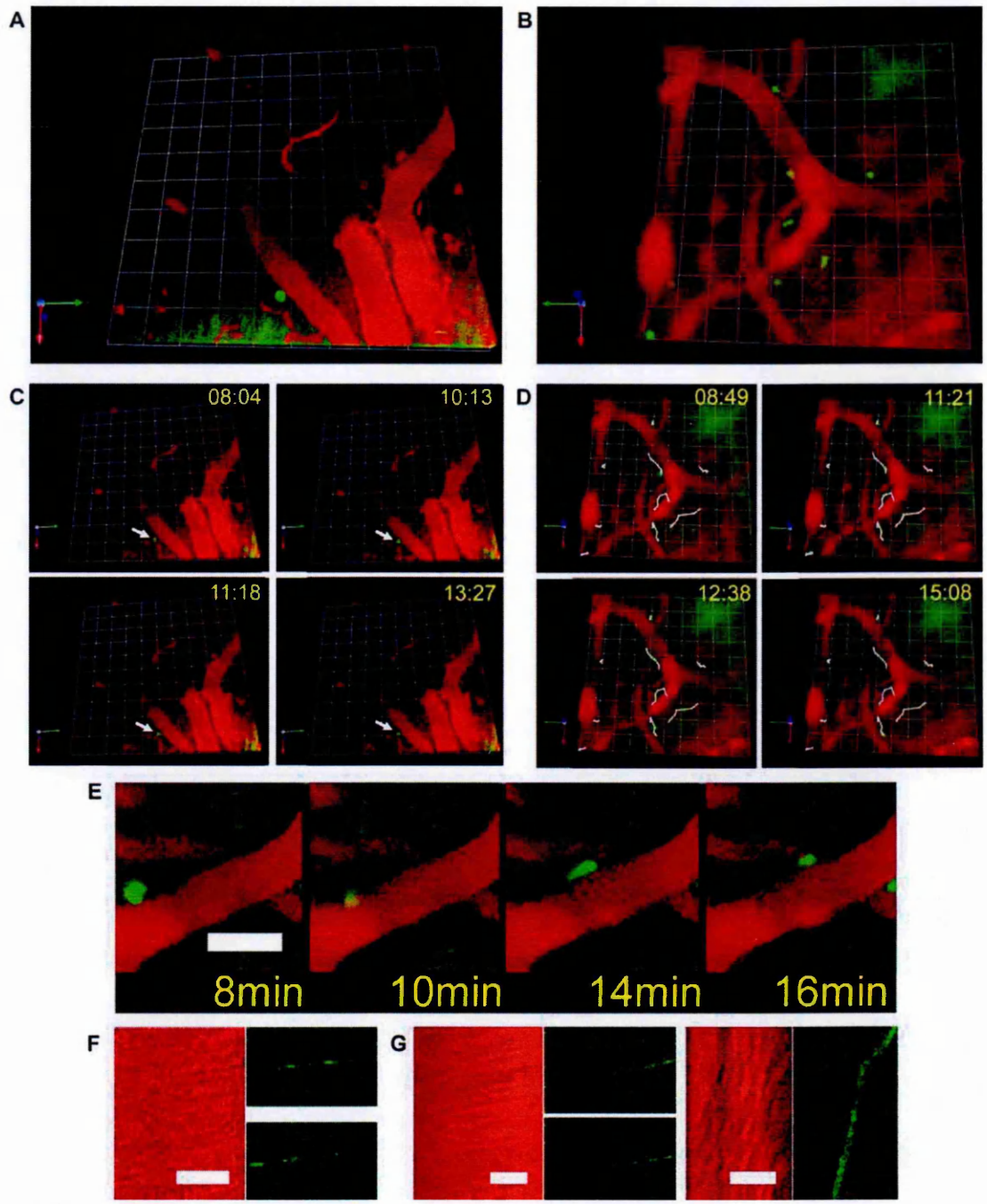

Figure 7.5 *Three-dimensional reconstructions showing extravasated T-cells.*

A typical imaging volume includes only 1 T-cell after sham (A) and several cells after pMCAo (B). The cell in A hardly moved (C, time markers indicate minutes:seconds). Successive positions of the cells in B were joined by white lines and images at 4 time points are shown in (D). 1 grid unit = 28.47 µm. E: in pMCAo mice T-cells often crawled along blood vessel abluminal space. F, G: T-cells found in the blood vessels flowed at the same velocity of RBC in both sham (F) and ischemic (G, left panel: normo-perfused vessel; right panel: ischemic vessel).

For each mouse, all available T-cell tracks were displayed in a single volume (Fig. 7.6, right panels). In the 6 sham-operated mice, the cell movement was generally confined within a radius of approximately 10 μm (Fig. 7.6), although a few longer displacements were seen. This behavior is also evident when the tracks were plotted so that their origins coincided (lefthand panels in Fig. 7.6). In contrast, T cells that moved over 10s of microns were observed in all 6 pMCAO mice (Fig. 7.7), although a subpopulation of almost stationary T-cells was also observed.

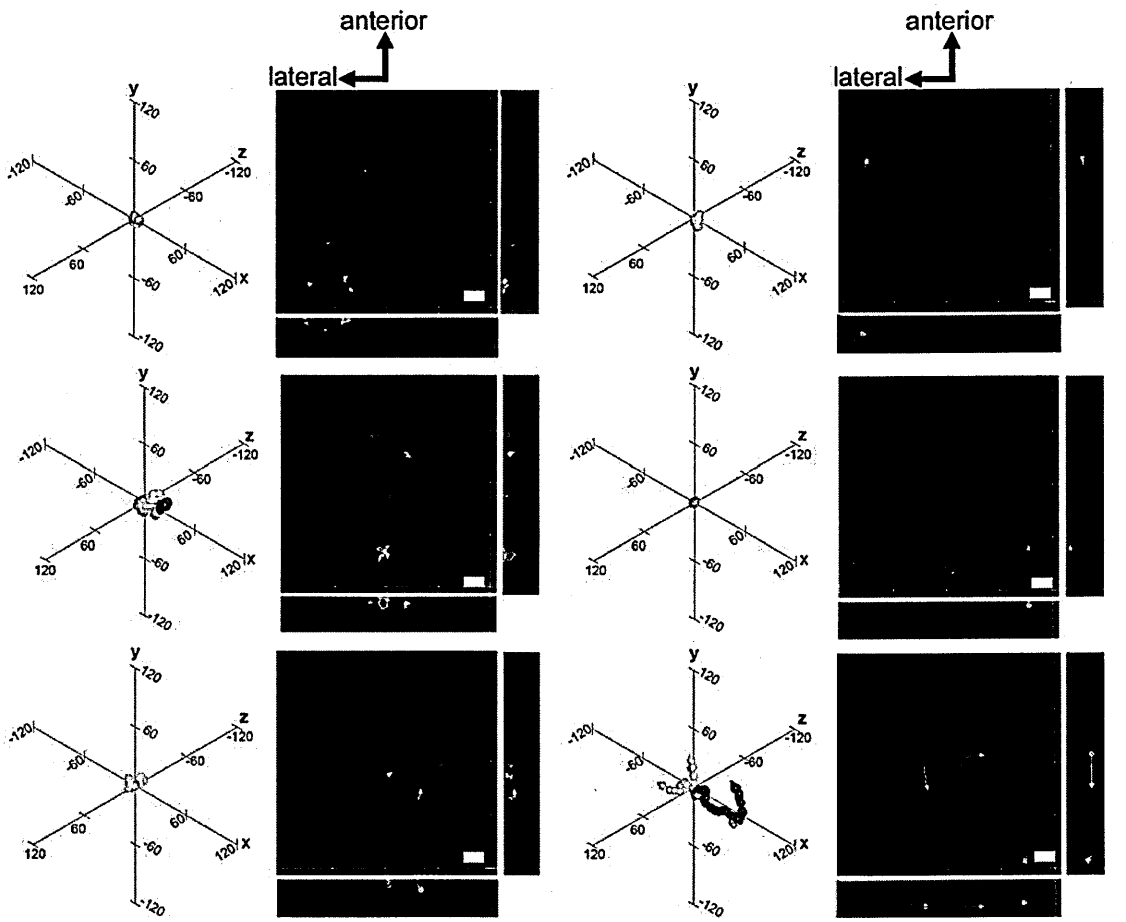

Figure 7.6 *Three-dimensional plots of T-cell movements in sham mice.*

T-cell tracks from each imaged animal are presented in figure. The right-hand panels show the tracks in extended focus seen from above and from the posterior and medial sides of the imaging volumes. The plots in the left-hand panels were generated by putting the starting point of each track at the origin of the axes. The cells have been labeled with individual colors. The tracks show that scarce T-cells were found and in most cases they moved over little distances. Left-hand panels: axis lengths are expressed in microns. Scale bars=25 μm, z projections=40 μm.

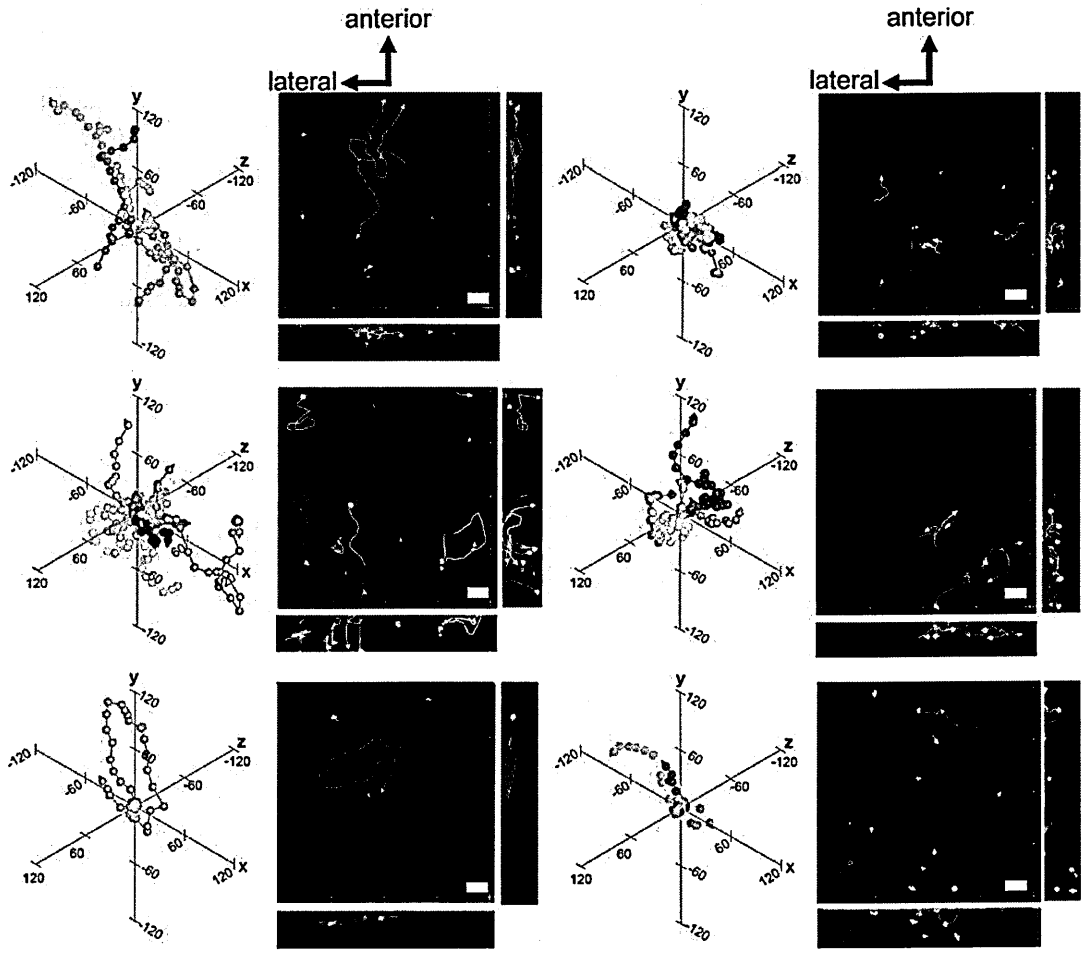

Figure 7.7 *Three-dimensional plots of T-cell movements in pMCAo mice.*

T-cell tracks from each imaged animal are presented in figure. The right-hand panels show the tracks in extended focus seen from above and from the posterior and medial sides of the imaging volumes. The plots in the left-hand panels were generated by putting the starting point of each track at the origin of the axes. The cells have been labeled with individual colors. The tracks show that many T-cells were present in ischemic mice. Part of the cells moved over long distances in both xy plane and z axis. Also stationary cells with minimum displacement were found. Left-hand panels: axis lengths are expressed in microns. Scale bars=25 μm, z projections=40 μm.

In sham animals, cells moved with an average velocity of 4.78±0.63 μm/min (n=23 T-cells) with 39% of them stationary (velocity <2 μm/min, Miller et al. 2002; Zinselmeyer et al. 2005). Two main populations were found in pMCAO animals (Fig. 7.8 A); 1 population was almost stationary (1.74±0.11 μm/min, n=23 T-cells, Population 1) and the other

population was quickly moving (8.21±0.10 μm/min, n=25 T-cells, Population 2). In addition to exhibiting significantly increased track velocity (Fig. 7.8 B), Population 2 showed significantly increased displacement rate (Fig. 7.8 C) compared with Population 1 ($P<0.001$) and sham ($P<0.01$) and a higher meandering index (Fig. 7.8 C) compared with Population 1 ($P<0.001$) but not sham. Interestingly, Population 1 showed significantly lower ($P<0.01$) track velocity and displacement rate compared with sham (Fig. 7.8 B,C).

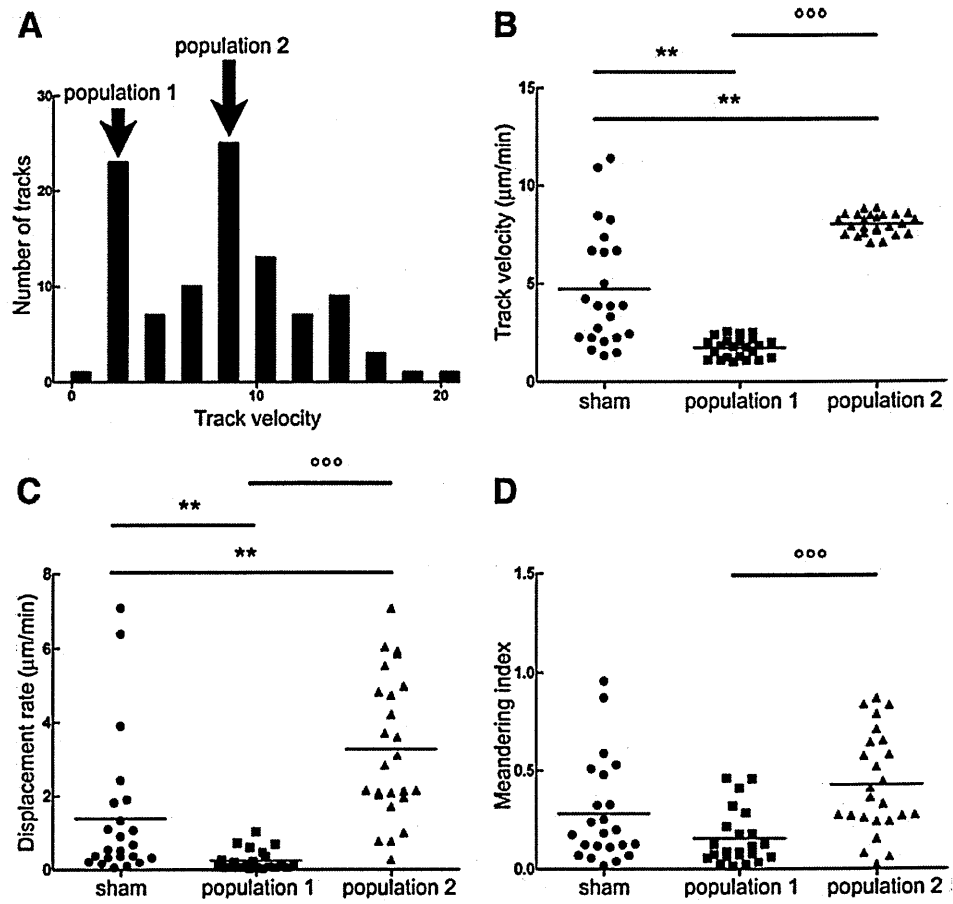

Figure 7.8 *Quantitative analysis of T-cell dynamics.*

Two main populations (arrows in A) as track velocity (µm/min) were found in pMCAo mice (A), one near stationary (population 1) and one quickly moving (population 2). B: population 1 exhibited significanlty lower track velocity compared with sham and populations 2. Population 2 had significantly higher values compared with sham and population 1. Population 1 showed also significantly lower displacement rate (C) and meandering index (D) compared with population 2. Population 1 had also significantly lower displacement rate compared with sham (C). Populations 2 had significantly higher values compared with sham in all assessed parameters. Single data point and mens (bars) are presented. One-way ANOVA followed by Dunn's post hoc test; **$p<0.01$ vs sham; °°°$p<0.001$ vs pMCAo Population 1.

Finally, by using conventional *post mortem* immunofluorescence and confocal microscopy, we confirmed T-cell location in the perivascular space of vessels in contact with components of the neurovascular unit such as astrocytes (glial fibrillary acidic protein-positive) and perivascular macrophages (IB4+/CD11b+; Fig. 7.9).

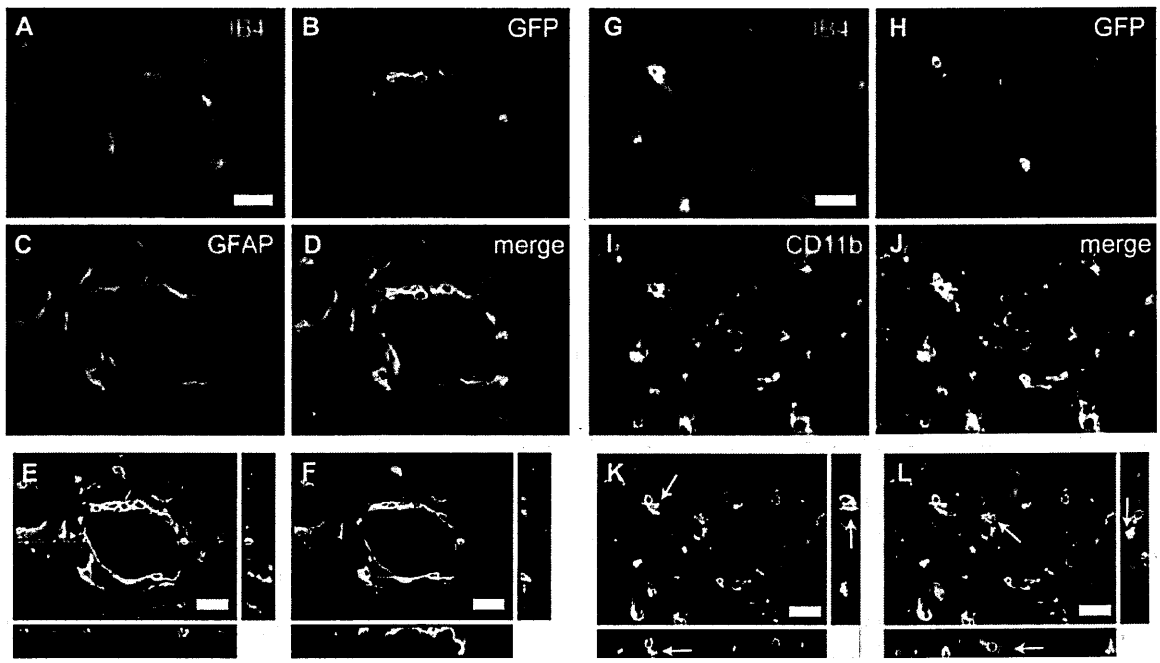

Figure 7.9 *Post mortem confocal images of immunofluorescence showing T-cells in the perivascular space.* A-F: immunofluorescence was performed for the markers IB4 (red, endothelium), GFP (white, T-cells) and GFAP (green, astrocytes). Single plan views with projections of the z axis (E, F) showed that T-cells were located between the endothelium (red) and astrocytic endfeet (green). G-L: immunofluorescence was performed for the markers IB4 (red, endothelium), GFP (white, T-cells) and CD11b (green, microglia/macrophages). Single plan views with projections of the z axis (K, L) showed that T-cells made contact with microglia/macrophages (IB4/CD11b double positive, yellow) in the perivascular space. An extravasated T-cell distant from blood vessels (L) interacted with microglia/macrophage cell (arrow in L) as evidenced in bottom projection. Bars = 20 μm.

7.4 Discussion

In this part of my project, I succedeed to visualize, define, and quantitatively analyze the movement and behavior of T-cells *in vivo* in real time after stroke. Specifically, I observed a higher number of extravasated T-cells in the subarachnoid space after pMCAO than sham and 2 distinct T-cell populations in pMCAO mice, 1 that was almost stationary and the second showing higher track velocity and displacement than sham. Infiltrated T-cells

were observed to patrol along the perivascular surfaces of cerebral vessels. 2-PM technology has been previously exploited in infection or autoimmune diseases. Several 2-PM studies describe the dynamics of T cells participating in the development of pathology such as experimental autoimmune encephalomyelitis (Bartholomäus et al. 2009; Flügel et al. 2007; Kim et al. 2010), toxoplasmic encephalitis (Wilson et al. 2009), and acute viral meningitis (Kim et al. 2009). These studies have provided important information on how T-cells access the central nervous system and factors that regulate their behavior once in the central nervous system. However, challenges lie ahead for providing insight into neurological diseases such as stroke.

The brain is unique in its development of inflammation because it has no lymphatic system and the blood– brain barrier limits antibody and immune cell entry (Cserr and Knopf 1992; Wilson et al. 2010). Therefore, T-cell access is tightly regulated and rare in the normal brain, and despite an increased expression of adhesion molecules during ischemia that facilitates T-cell infiltration, there are far fewer T-cells in the brain after stroke compared with autoimmune disease (Flügel et al. 2007). To the best of my knowledge, realtime *in vivo* T-cell movements after stroke have never been successfully visualized and analyzed. We observed a high number of extravascular T-cells 72 hours after pMCAO and only a few T-cells after sham. I cannot exclude that the sham procedure (anesthesia, skull thinning) may have induced recruitment of these cells. On the contrary, increased T-cell infiltration after stroke is consistent with *post mortem* immunohistochemistry or flow cytometry studies (Frenkel et al. 2003; Stevens et al. 2002), although such techniques are limited by the removal, disruption, and processing of tissue at defined time points. A key observation from the 2-PM approach is the significant differences in motility, namely track velocity, displacement, and meandering, of extravasated T-cells between pMCAO and sham mice. Interestingly, 2 main populations were found in pMCAO mice; both populations showed significantly different dynamics compared with T-cells in sham mice.

One population showed a mean displacement of 0.25±0.06 μm/min, the other population 3.26±0.39 μm/min, and sham 1.4±0.4 μm/min. Cordiglieri and colleagues defined in the central nervous system motile cells with displacements >1 μm/min and stationary cells with displacements <1 μm/min (Cordiglieri et al. 2010); therefore, we consider Population 1 stationary. On the contrary, Population 2 showed track velocity in the range of data already shown in other models of neuroinflammation (Bartholomäus et al. 2009; Kim et al. 2009). The reported differences in track velocities between Population 1 (1.74 μm/min) and Population 2 (8.21 μm/min), in the model here analyzed, are extremely relevant if compared with T-cell velocity in secondary lymphoid organs. It has been shown (Miller et al. 2002; Zinselmeyer et al. 2005) that naı¨ve CD4 T-cells move at an average velocity 10 μm/min. Both primed and tolerized T-cells show slower velocity of approximately 4 to 5 μm/min and cells with velocities <2 μm/min are essentially stationary due to factors like centroid movement. Thus, the observed differences between Populations 1 and 2 and sham in my setting could clearly depend on the different activation status of these cells. The different motility of the 2 cell populations could reflect the evolution of T-cell response from a naı¨ve population to effector/memory cells and/or the behavior of T-cells that, after antigen encounter, display an altered profile of adhesion molecules and chemokine receptors. One limitation of my experiments is that GFP expression was not restricted to a specific population of T-cells and therefore it is impossible to distinguish which T-cell subset was stationary or motile or if this was related to their antigen specificity. Interestingly, recent real-time imaging during recall responses in the lymph node have shown that, in contrast to CD4 T-cells, which show slower migration (Rush et al. 2009), memory CD8 T-cells move more rapidly than naı¨ve cells (Chtanova et al. 2009), suggesting that faster migration could be a defining characteristic of CD8 versus CD4 memory T-cells. Also key to my findings are the paths of these cells once extravasated and we could reveal 3 key locations: perivascular, moving from 1 vessel to another, and remote

from vessels. The perivascular location of T-cells is in line with previous data by Owens (Owens et al. 2008) who elegantly describes the transmigration of immune cells into the perivascular space and movement of extravasated T-cells are likely to be in the perivascular space rather than in the brain parenchyma. We observed T cells patrolling up and down the perivascular surfaces of blood vessels. The object of their survey is unclear, but direct contact of T-cells with cellular components of the neurovascular unit has been shown in other inflammatory central nervous system conditions (Bartholomäus et al. 2009) and the perivascular space seems to be a location where immune cells could interact with potential antigen-presenting cells (Owens et al. 2008). The immunologic synapse could be formed with astrocytic end feet or perivascular phagocytes, all of which have the capacity to act as antigenpresenting cells (Fierz et al. 1985; Kivisäkk et al. 2009). We have attempted to shed further light on these cellular interactions using immunofluorescence. Although this analysis was performed deeper in the parenchyma compared with the imaged area, we could confirm T-cells' location between the endothelium and astrocytic end feet in the perivascular space with a direct contact among astrocytes, macrophages/microglial cells, and T-cells. Whether this direct contact is associated with the reported role of the neurovascular unit in stimulating inflammatory responses after stroke (Del Zoppo 2009) is yet to be elucidated, but this would explain the reason for some T-cells moving from 1 vessel to another after pMCAO. Lastly, I observed T-cells remote from blood vessels in the *in vivo* imaging and again using immunofluorescence, we observed extravasated T-cells quite far from vessels interacting with a microglial cell. Whether T-cells' contribution to cerebral ischemia depends on antigen recognition is still under debate (Kleinschnitz et al. 2010); therefore, a deeper understanding of the cellular interactions between T-cells to astrocytes and microglia would help to clarify this issue. By measuring parameters that are likely to influence the character of immune responses (eg, location of T-cell activation, location of immune cell interactions, duration and number of interactions, etc) and relating

these to the parallel determination of immunologic parameters (eg, cytokine and costimulatory molecules production), a 2-PM strategy could help to analyze these interactions *in vivo* and hopefully help to elucidate the role of immune cells in stroke.

7.5 Conclusions

I have provided previously unavailable information on the dynamics of T lymphocytes recruited by the ischemic brain, which could reveal important mechanisms of immune surveillance after stroke. In addition, the imaging approach represents a major technical advance and an important research tool for the understanding of the complex interactions between the brain and immune cells after ischemia. Combining the development of strategies to deplete specific cell populations/subsets or modify their function and the application of available fluorescent reporters for antigen presenting cells should allow a dissection of how the behavior of immune cells relates to their function in the ischemic brain. It is hoped that these advances in imaging of immune cells after stroke could provide important information for the development and use of specific therapies for a better management of the immune response in the ischemic brain.

8. GENERAL CONCLUSIONS

It has long been recognized that brain ischemia induces a neuroinflammatory response that involves both the recruitment of circulating inflammatory cells into the CNS and the activation of resident microglia. Vascular remodelling and a direct involvement of the BBB are also part of the inflammatory process, as they can influence the recruitment of circulating cells (Bartholomäus et al. 2009; Owens et al. 2008) as well as determine the modification of the active status of resident microglia (Masuda et al. 2011). Vascular modifications, blood flow variations and motility of immune cells are all mechanisms acting in a very dynamic fashion (ranging from milliseconds to minutes) within a three-dimensional space (the brain). Obviously, these events require the action of solid objects, such as blood vessels and cells, which exert their specific function in intact tissues, where a complex network of interactions exists. Most of the information associated with spatial motility, time-dependent dynamics and tissue integrity (*i.e.* contemporary presence of all the cell types involved in the biological effect) is lost with conventional biochemical, biomolecular or histological techniques. The application of 2-PM to neurobiology offered a new perspective to tackle previously unexplored mechanisms in physiological or pathological conditions, due to its ability to provide a three-dimensional, high-resolution representation of the CNS over time in living animals.

Inflammation after brain ischemia stands as a promising therapeutical target. It is indeed early induced after injury and has long-lasting effects, thus having a prominent role in damage evolution over time. Believed for years to have only detrimental effects, over the recent past inflammation has been demonstrated to exert also beneficial effects. In particular two inflammatory populations, microglia/macrophages and T- lymphocytes, caught the attention of neurobiologists, provided that these populations, although

participating in the pro-inflammatory cascades, are also capable of protective and regenerative functions (Iadecola and Anrather 2011; Magnus et al. 2012). A detailed comprehension of the inflammatory mechanisms after brain ischemia is needed in order to develop future pharmacological tools to revert a detrimental inflammatory phenotype into a beneficial regenerative one. Such a pharmacological approach may be coupled with the thrombolytic therapy in order to ameliorate the ischemic outcome in patients by acting on long lasting secondary pathogenetic mechanisms.

The past two decades have seen remarkable advances in the comprehension of immune cell trafficking, activation and functions within the CNS, and many molecules involved in the protective functions have been identified. *In vitro* evidence for phenotype switching in response to different types and different degrees of injury has been indeed obtained (Häusler et al. 2002; Lai and Todd 2008; Magnus et al. 2001). This phenomenon has been little studied in a systematic way in appropriate *in vivo* models, that are certainly more informative. For this reason and for the complex nature of the inflammatory network, to date, many aspects of brain immunity still remain to be fully elucidated.

Great attention has been dedicated to microglia that gained increasing consideration as potential therapeutic targets. However, available information may be not transferred in a straighforward way to clinical settings yet, as many aspects of microglia functions remain elusive. The exact contribution to ischemic injury evolution of resident microglia versus that of recruited macrophages still needs to be determined. Microglia share with macrophages same myeloid origin, marker expression and ability of acquiring a polarized phenotype, however, new evidence on organotypic slice cultures indicate that M2 polarized microglia have protective functions, whilst macrophages act in a cytotoxic way regardless of their polarization (Girard et al. 2013). This observation needs confirmation in the *in vivo* setting, in which, however, methodological limitations applies to properly distinguish the two populations.

Data presented in my thesis rule out the detrimental function of the fractalkine:CX3CR1 pathway in ischemic damage evolution. Other pathways able to influence polarization of microglia have been also identified in different models and by different strategies (Ransohoff and Prinz 2013). However there is still little transferibility of this information to the clinical setting, as 1) characterization of microglia function in humans is lacking; 2) availablilty of molecules specifically targetting microglia polarization is limited.

Similar observations may apply to T-cells. They participate to ischemic injury development by either toxic or protective action. While their toxic behavior does not seem to need a proper priming (Kleinschnitz et al. 2010), protective effects are due to tolerization or T-reg maturation (Liesz et al. 2009). However as far as their specific role in pre-clinical and human studies is not completely understood, direct transferibility of this information to clinical setting remains limited.

It should be stressed that inflammatory mechanisms after brain ischemia are still widely unknown, thus hampering the effective development of a therapeutic stategy. Most of pre-clinical studies focus on a specific mechanism, whilst it is clear that inflammation involves many different events and cell types, often with overlapping functions, that evolve over time. Furthermore, the impact of inflammatory states already in place before ischemia is often underestimated in animal models. Evidence that systemic inflammation is able to enhance ischemic damage has been provided in leptin deficient obese (ob/ob) mice (Terao et al. 2008). In humans, stroke is preceded by a variety of risk factors, many of those co-exist. Most of co-morbidities are associated with the dysregulation of systemic inflammatory processess and imply either chronic or acute inflammation (Murray et al. 2013). In future, animal model studies should consider the use of more clinically-relevant paradigms, which incorporate commonly recognized risk factors.

In this thesis *in vivo* 2-PM and *post mortem* histochemical and immunohistochemical techniques were applied to dissect specific aspects related to vascular remodelling, immune cell dynamism and expression of markers of M/M polarization in two models of focal brain ischemia.

Key to the project has been to set up a reliable protocol for *in vivo* longitudinal 2-PM imaging. Animals should indeed be surgically prepared to imaging by the exposure of a cortical area of interest. Methods to expose brain to 2-PM imaging rely on the opening of a craniotomy that may be of two different kind: cranial window (Mostany and Portera-Cailliau 2008) and skull thinning (Yang et al. 2010). While cranial window allows a deeper laser penetration compared to skull thinning due to limited scattering effects, the surgical procedure for window preparation is invasive enough to induce synaptic rearrangements and inflammation (Xu et al. 2007b). For this reason cranial window was used to imaging of blood vessels, whereas skull thinning was used for imaging of GFP+ immune populations. Once selected the best option for craniotomy, a further major requirement to fullfil has been to verify whether the exposed area was affected by MCAo. The imaged area was actually ischemic, being: 1) the blood flow significantly reduced in the vessels pertinent to that area and 2) necrotic cells present all over the observed tissue after MCAo. Moreover imaging of the same area could be repeated on a same mouse at different time points from MCAo and up to 24h after insult.

In humans, the degree of reperfusion after brain ischemia, if present, is highly variable (Caplan et al. 2011; Lo 2008b). For this reason pre-clinical studies should consider the use of both transient and permanent models of brain ischemia. In the future, the number of patients undergoing reperfusion is likely to increase, since the time window for thrombolytic therapy has been recently widened from 3 to 4.5 h (Davis and Donnan 2009)

and clinical studies are presently underway to further widen time window and patients' accessibility to thrombolytic therapy (Sandercock et al. 2012). Thus, the exact comprehension of vascular dynamics at the level of the individual vessel *in vivo* during occlusion and when reperfusion is allowed represents a crucial issue for stroke therapy and improved recovery. The data presented in this thesis on vascular remodelling confirmed that, during ischemia, a massive blood flow decrease in the cortical region fed by MCA occurs, notably associated in few cases with blood flow reversion. This phenomenon, that had been described following permanent ischemia, could be the result of redundancy in the cortical vascular architecture that acts as endogenous protective response to occlusions (Schaffer et al. 2006). Extravasation appears as early as 20min from ischemic onset, and is accompanied by an irregular morphology of vessel edges. Single vessel analysis revealed that after reperfusion blood flow is incompletely re-established at 24h, and in some small vessels it is completely prevented. This suggests the existence of further pathogenetic mechanisms, induced by the occlusion, affecting vascular viability. Among these it is possible that the rapidly established edema causes increased parenchymal pressure leading to a relevant vascular compression, able to affect flow recovery in the microvasculature.

As discussed above, vasculature has a prominent role in regulating the recruitment and activation of immune populations, which, in turn, participate to the evolution of ischemic lesion. Immune cells act through a *plaetora* of different mechanisms, whose final effects can be of opposite nature.

In view of a therapeutic modulation of immunity after stroke, recent pre-clinical studies applied strategies aimed either at limiting the propagation of pro-inflammatory signals (Orsini et al. 2012; Pradillo et al. 2012) or at favouring the protective functions of immune cells (Lalancette-Hébert et al. 2007). Unfortunately, to date, all the attempts to translate the encouraging pre-clinical results on inflammatory modulation to the clinical setting have

failed (Iadecola and Anrather 2011; del Zoppo 2004). One possible reason of these failures stands in the fact that many aspects of immunity after stroke still remain elusive.

In my research project, I focused on M/M, whose modulation has been proven to confer protection after experimental stroke (Lalancette-Hébert et al. 2007; Lambertsen et al. 2009). After tMCAo, resident microglia rapidly change their morphology to become hypertrophic/ameboid at 24h after insult and macrophages are recruited to lesion site. Within the lesioned area, the expression of markers of active M/M, such as CD11b, CD68, CD45, Ym1, CD206 and iNOS significantly increases, indicating that both M1 and M2 polarization states are present in the ischemic territory. I found that deletion of CX3CR1 prevents microglia from acquiring an ameboid phenotype, in association with decreased CD11b and CD68 immunoreactivity. Under these circumstances, the balance between toxic M1 and protective M2 polarization changes and, in particular, the absence of CX3CR1 favours the M2 polarization being Ym1 significantly increased and iNOS significantly decreased in *cx3cr1*$^{-/-}$ mice at 24h after tMCAo. This effect results in a protective outcome, being the ischemic volume 25.5% lower in *cx3cr1*$^{-/-}$ mice compared to control mice.

Although M/M polarization markers have been extensively studied in many models of CNS diseases, such as AD (Reed-Geaghan et al. 2010; Shin et al. 2011), global ischemia (Ohtaki et al. 2008), EAE (Ponomarev et al. 2007) or spinal cord injury (David and Kroner 2011; Kigerl et al. 2009), information on M/M polarization marker expression, coexpression and temporal evolution in the ischemic brain is lacking. Aa model of pMCAo was used to provide a characterization of the time course of activation and localization of a few M/M markers, either related to the M1 or the M2 polarization.

Different states of M/M activation are present in the ischemic lesion, reflecting the complexity of these cells and their ability to differentiate towards a multitude of phenotypes depending on the surrounding microenvironmental signals that can change

over time. Detrimental M1 and protective M2 phenotypes have been classified on the basis of *in vitro* studies or in many cancer models that yielded the canonical definition of M1-M2 phenotypes. In the ischemic brain *in vivo*, activated M/M may escape the classical phenotypical categorization, due to the complex molecular and cellular network established soon after injury and evolving over time. The work presented here provides evidence of the different patterns of M/M polarization after brain ischemia, and suggests that they have a specific distribution which is dependent on time and distance from the lesion. A protective M2 polarization is rapidly activated (Ym1 expression peaks at 24h), precedes M1 polarization (iNOS expression peaks at 48h), but it is short-lasting, being significantly reduced as early as 48h after injury.

Phagocytosis is a key feature of M/M. Differently from other M/M markers, the phagocytic activity does not seem to be clearly linked to a specific M1 or M2 polarization state. Phagocytosis is needed to remove cell debris and dying cells, thus limiting the propagation of 'eat-me' signals, that can further exacerbate damage progression. Cells belonging to the M2c class of protective polarization as well as M1 toxic cells are endowed with phagocytic functions (David and Kroner 2011), suggesting that phagocytosis can serve either for scavenging of debris (protection) or killing cells (toxicity). The phagocytic activity was assessed by cell positivity to CD68. At early time points after pMCAo (6h-48h), the expression of CD68 is preferentially located at the ischemic borders, while at 7d after injury CD68 expression dramatically increases and involves all ischemic areas. Interestingly, this event is accompanied by the progressive reduction of the expression of the protective M2 marker Ym1. Moreover after tMCAo, *cx3cr1*$^{-/-}$ mice show significantly decreased CD68 expression and protection from ischemic injury (see above). These observations imply that phagocytosis may be needed for limiting the propagation of danger signals, but an excess of phagocytosis is detrimental if not counteracted early after injury. Actually, a similar decrease in CD68 expression has been previously reported following

other protective manipulations such as stem cells infusion or ischemic preconditioning, where the observed protective effects were associated to a decrease of ameboid CD11b/CD68 positive cells (Longhi et al. 2011; Zanier et al. 2011).

Phagocytosis involves many molecules. Altough CD68 is expressed by phagocytic cells, it may provide a partial picture of the phagocytic events that take place within the brain. Further studies addressing the exact role of phagocytosis should also consider the use of different markers or different techniques, such as the measure of phagocytosed opsonized beads (Daigneault et al. 2010).

In the final part of the project I focused on T-cells recruited to the ischemic brain. T lymphocytes have been recently proposed as potential therapeutic targets in brain ischemia, proven that they have toxic effects and mice deficient in lymphocytes exhibit reduced ischemic infarct volume (Hurn et al. 2007; Kleinschnitz et al. 2010; Yilmaz et al. 2006). However, T-cells may have also protective effects, by releasing IL-4 (Butovsky et al. 2007) or by priming to T-regulatory cells (Liesz et al. 2009). In a clinical perspective, to modulate T-cells and promote their protective behavior, a deeper knowledge of the mechanims of T-cell recrutiment and activation after brain ischemia is needed.

T-cells were successfully visualized by *in vivo* 2-PM 3d after pMCAo and obtained information on their dynamic behavior after extravasation. T-cells increase significantly in number in the ischemic territory visualized and split into two distinct populations on the basis of their track velocity: one that was almost stationary and the second showing higher track velocity and displacement. Infiltrated T-cells patrol along the perivascular surfaces of cerebral vessels, where they come into contact with components of the BBB, such as astrocytic endfeet and perivascular macrophages, that may have 'instructive' functions to T-cells prior to invasion.

9. FUTURE PERSPECTIVES

This study may be limited by the short analysis of immune populations after brain ischemia, since 2-PM has been applied in a time frame ranging from before to 3d after ischemia. This limitation is due mainly to concerns related craniotomy, being very difficult to keep it clean for periods longer than 3d with no further surgery. 2-PM studies at later stages after ischemia should consider re-opening the craniotomy or avoiding baseline imaging (prior to ischemia) or opening the craniotomy only at the experimental time point of interest. In this study, where possible, I preferred to perform *in vivo* 2-PM at baseline in order to achieve a more reliable longitudinal study (each animal represented its own control).

The analysis of inflammation and immune cell behavior/phenotype at later stages of ischemic damage would be very informative. As discussed in section **5**, events different from the ones here described may take place, including recruitment of a population of protective macrophages (Nahrendorf et al. 2007), further modifications of microglia morphology/phenotype and peak expression of adaptive immune responses, all able to deeply impact on ischemic damage evolution. Thus, possible future experiments could include the investigation on events at later time points from ischemia.

As discussed above, the use of more clinically-relevant animal models including common stroke risk factors should be considered. In this view, the project may be expanded by analyzing M/M behavior in aging or in ob/ob mice, in order to assess whether presence of M1 or M2 polarization markers differ depending on age or co-morbidities.

While M/M have been extensively studied in animal models, information on their activation and functions in humans needs to be widened. In humans imaging of M/M is possible by Positron Emission Tomography (PET), which remains limited for its elevated costs and long time of execution. In clinical scenarios MRI shows promises because, by

magnectic spectroscopy, it is possible to detect metabolic patterns associated with specific cellular functions. However, while some specific patterns for neuronal damage and gliosis have already been set up, information on the metabolic pattern associated with M/M activation is still lacking. A unit for MRI is available at Mario Negri Institute, thus future developments of the project may regard the identification of new metabolic fingerprints of M/M activation that could be visualized by MRI, in view of their application to patients' imaging.

As previously discussed, the immune response can be modulated by different approaches capable of yielding protection after ischemia. To translate effectively the promising pre-clinical studies on inflammatory modulation to the clinical setting, however, a deeper knowledge of the complex network of inflammatory molecules and effector cells is needed. In this view, future development of this project would include simultaneous *in vivo* imaging of microglia and T-cells. Upon activation, T-cells give origin to a Th1 or a Th2/Th3 response, responsible respectively for the secretion of proinflammatory cytokines such as IL-2, TNF-α and INF-γ that promote toxic inflammation, or the release of IL-4, IL-10 and TGF-β1, that may favour protective brain immunity. Th2 have been described to activate microglia via IL-4, possibly pushing microglia towards a protective phenotype (Butovsky et al. 2007). *In vivo* 2-PM may help elucidating the dynamic interaction between these two immune populations and, in particular: 1) whether and to what extent they interact (*i.e.* time of contact); 2) ability of microglia to influence T-cell motility; 3) microglia morphological response to T-cell interaction; 4) effects of CX3CR1 deletion or of immunomodulatory strategies. Since *in vivo* 2-PM does not provide phenotype information, it should be paralleled by *post mortem* analysis of M/M phenotype, to investigate how T-cells may influence M/M polarization state.

Other peripheral immune populations have been demonstrated to have a role in ischemic injury progression. Among those, neutrophils have been clearly identified as neurotoxic cells, able to infiltrate the brain after ischemia and to exert a detrimental function. Neutrophils are mediators of the toxic effects elicited by IL-1, whose targeting has been already shown to be protective (Allen et al. 2012; Pradillo et al. 2012). It has been proposed that microglia protective functions may be also associated with phagocytosis of infiltrated neutrophils (Denes et al. 2007). Future developments of this project should consider the role of neutrophils and whether peaks of protective microglia polarization are associated with decreased IL-1 production or neutrophil presence in the ischemic brain. This will also help to better define the role of phagocytic microglia since, as discussed in the thesis, phagocytic behavior may not be linked to a specific polarization state straightforwardly.

Overall my study adds new insight on immunity after stroke, having: 1) investigated the dynamic behavior of M/M and T-cells within the ischemic brain; 2) provided information on M/M polarization after tMCAo and pMCAo. These data add previously unavailable information on the complex inflammatory response after stroke and may pave the way for developing strategies resulting in promotion of a protective inflammatory phenotype.

10. BIBLIOGRAPHY

Adams H, Adams R, Del Zoppo G, Goldstein LB (2005) Guidelines for the early management of patients with ischemic stroke: 2005 guidelines update a scientific statement from the Stroke Council of the American Heart Association/American Stroke Association. Stroke 36:916–923. doi: 10.1161/01.STR.0000163257.66207.2d

Adams HP Jr, Bendixen BH, Kappelle LJ, et al. (1993) Classification of subtype of acute ischemic stroke. Definitions for use in a multicenter clinical trial. TOAST. Trial of Org 10172 in Acute Stroke Treatment. Stroke 24:35–41.

Adams JM, Cory S (2001) Life-or-death decisions by the Bcl-2 protein family. Trends Biochem Sci 26:61–66.

Ajami B, Bennett JL, Krieger C, et al. (2011) Infiltrating monocytes trigger EAE progression, but do not contribute to the resident microglia pool. Nat Neurosci 14:1142–1149. doi: 10.1038/nn.2887

Alexandrov AV, Mikulik R, Ribo M, et al. (2008) A pilot randomized clinical safety study of sonothrombolysis augmentation with ultrasound-activated perflutren-lipid microspheres for acute ischemic stroke. Stroke 39:1464–1469. doi: 10.1161/STROKEAHA.107.505727

Alexandrov AV, Molina CA, Grotta JC, et al. (2004) Ultrasound-enhanced systemic thrombolysis for acute ischemic stroke. N Engl J Med 351:2170–2178. doi: 10.1056/NEJMoa041175

Allen C, Thornton P, Denes A, et al. (2012) Neutrophil cerebrovascular transmigration triggers rapid neurotoxicity through release of proteases associated with decondensed DNA. J Immunol 189:381–392. doi: 10.4049/jimmunol.1200409

Allen NJ, Attwell D (2002) Modulation of ASIC channels in rat cerebellar Purkinje neurons by ischaemia-related signals. J Physiol (Lond) 543:521–529.

Anderson CF, Mosser DM (2002a) A novel phenotype for an activated macrophage: the type 2 activated macrophage. J Leukoc Biol 72:101–106.

Anderson CF, Mosser DM (2002b) Cutting edge: biasing immune responses by directing antigen to macrophage Fc gamma receptors. J Immunol 168:3697–3701.

Aronowski J, Zhao X (2011) Molecular pathophysiology of cerebral hemorrhage: secondary brain injury. Stroke 42:1781–1786. doi: 10.1161/STROKEAHA.110.596718

Attwell D, Buchan AM, Charpak S, et al. (2010) Glial and neuronal control of brain blood flow. Nature 468:232–243. doi: 10.1038/nature09613

Auffray C, Fogg D, Garfa M, et al. (2007) Monitoring of blood vessels and tissues by a population of monocytes with patrolling behavior. Science 317:666–670. doi: 10.1126/science.1142883

Bachstetter AD, Morganti JM, Jernberg J, et al. (2011) Fractalkine and CX 3 CR1 regulate hippocampal neurogenesis in adult and aged rats. Neurobiol Aging 32:2030–2044. doi: 10.1016/j.neurobiolaging.2009.11.022

Balosso S, Ravizza T, Perego C, et al. (2005) Tumor necrosis factor-alpha inhibits seizures in mice via p75 receptors. Ann Neurol 57:804–812. doi: 10.1002/ana.20480

Barber PA, Zhang J, Demchuk AM, et al. (2001) Why are stroke patients excluded from TPA therapy? An analysis of patient eligibility. Neurology 56:1015–1020.

Baron JC (2001) Perfusion thresholds in human cerebral ischemia: historical perspective and therapeutic implications. Cerebrovasc Dis 11 Suppl 1:2–8. doi: 49119

Barone FC, Feuerstein GZ (1999) Inflammatory mediators and stroke: new opportunities for novel therapeutics. J Cereb Blood Flow Metab 19:819–834. doi: 10.1097/00004647-199908000-00001

Bartholomäus I, Kawakami N, Odoardi F, et al. (2009) Effector T cell interactions with meningeal vascular structures in nascent autoimmune CNS lesions. Nature 462:94–98. doi: 10.1038/nature08478

Batchelor PE, Liberatore GT, Wong JY, et al. (1999) Activated macrophages and microglia induce dopaminergic sprouting in the injured striatum and express brain-derived neurotrophic factor and glial cell line-derived neurotrophic factor. J Neurosci 19:1708–1716.

Bauer M, Brakebusch C, Coisne C, et al. (2009) Beta1 integrins differentially control extravasation of inflammatory cell subsets into the CNS during autoimmunity. Proc Natl Acad Sci USA 106:1920–1925. doi: 10.1073/pnas.0808909106

Bechmann I, Kwidzinski E, Kovac AD, et al. (2001a) Turnover of rat brain perivascular cells. Exp Neurol 168:242–249. doi: 10.1006/exnr.2000.7618

Bechmann I, Priller J, Kovac A, et al. (2001b) Immune surveillance of mouse brain perivascular spaces by blood-borne macrophages. Eur J Neurosci 14:1651–1658.

Becker K, Kindrick D, McCarron R, et al. (2003) Adoptive transfer of myelin basic protein-tolerized splenocytes to naive animals reduces infarct size: a role for

lymphocytes in ischemic brain injury? Stroke 34:1809–1815. doi: 10.1161/01.STR.0000078308.77727.EA

Becker KJ, McCarron RM, Ruetzler C, et al. (1997) Immunologic tolerance to myelin basic protein decreases stroke size after transient focal cerebral ischemia. Proc Natl Acad Sci USA 94:10873–10878.

De Beer MC, Zhao Z, Webb NR, et al. (2003) Lack of a direct role for macrosialin in oxidized LDL metabolism. J Lipid Res 44:674–685. doi: 10.1194/jlr.M200444-JLR200

Bhatia S, Fei M, Yarlagadda M, et al. (2011) Rapid host defense against Aspergillus fumigatus involves alveolar macrophages with a predominance of alternatively activated phenotype. PLoS ONE 6:e15943. doi: 10.1371/journal.pone.0015943

Binstadt BA, Patel PR, Alencar H, et al. (2006) Particularities of the vasculature can promote the organ specificity of autoimmune attack. Nat Immunol 7:284–292. doi: 10.1038/ni1306

Biswas SK, Mantovani A (2010) Macrophage plasticity and interaction with lymphocyte subsets: cancer as a paradigm. Nat Immunol 11:889–896. doi: 10.1038/ni.1937

Block ML, Zecca L, Hong J-S (2007) Microglia-mediated neurotoxicity: uncovering the molecular mechanisms. Nat Rev Neurosci 8:57–69. doi: 10.1038/nrn2038

De Boer J, Williams A, Skavdis G, et al. (2003) Transgenic mice with hematopoietic and lymphoid specific expression of Cre. Eur J Immunol 33:314–325. doi: 10.1002/immu.200310005

Bogdan C, Paik J, Vodovotz Y, Nathan C (1992) Contrasting mechanisms for suppression of macrophage cytokine release by transforming growth factor-beta and interleukin-10. J Biol Chem 267:23301–23308.

Brochard V, Combadière B, Prigent A, et al. (2009) Infiltration of CD4+ lymphocytes into the brain contributes to neurodegeneration in a mouse model of Parkinson disease. J Clin Invest 119:182–192. doi: 10.1172/JCI36470

Brown CE, Aminoltejari K, Erb H, et al. (2009) In vivo voltage-sensitive dye imaging in adult mice reveals that somatosensory maps lost to stroke are replaced over weeks by new structural and functional circuits with prolonged modes of activation within both the peri-infarct zone and distant sites. J Neurosci 29:1719–1734. doi: 10.1523/JNEUROSCI.4249-08.2009

Brown CE, Li P, Boyd JD, et al. (2007) Extensive turnover of dendritic spines and vascular remodeling in cortical tissues recovering from stroke. J Neurosci 27:4101–4109. doi: 10.1523/JNEUROSCI.4295-06.2007

Brown EB, Shear JB, Adams SR, et al. (1999) Photolysis of caged calcium in femtoliter volumes using two-photon excitation. Biophys J 76:489–499. doi: 10.1016/S0006-3495(99)77217-6

Brozici M, Van der Zwan A, Hillen B (2003) Anatomy and functionality of leptomeningeal anastomoses: a review. Stroke 34:2750–2762. doi: 10.1161/01.STR.0000095791.85737.65

Bruno V, Battaglia G, Copani A, et al. (2001) Metabotropic glutamate receptor subtypes as targets for neuroprotective drugs. J Cereb Blood Flow Metab 21:1013–1033. doi: 10.1097/00004647-200109000-00001

Butovsky O, Bukshpan S, Kunis G, et al. (2007) Microglia can be induced by IFN-gamma or IL-4 to express neural or dendritic-like markers. Mol Cell Neurosci 35:490–500. doi: 10.1016/j.mcn.2007.04.009

Byram SC, Carson MJ, DeBoy CA, et al. (2004) CD4-positive T cell-mediated neuroprotection requires dual compartment antigen presentation. J Neurosci 24:4333–4339. doi: 10.1523/JNEUROSCI.5276-03.2004

Caplan LR, Arenillas J, Cramer SC, et al. (2011) Stroke-related translational research. Arch Neurol 68:1110–1123. doi: 10.1001/archneurol.2011.99

Capone C, Frigerio S, Fumagalli S, et al. (2007) Neurosphere-derived cells exert a neuroprotective action by changing the ischemic microenvironment. PLoS ONE 2:e373. doi: 10.1371/journal.pone.0000373

Cardona AE, Pioro EP, Sasse ME, et al. (2006) Control of microglial neurotoxicity by the fractalkine receptor. Nat Neurosci 9:917–924. doi: 10.1038/nn1715

Centonze VE, White JG (1998) Multiphoton excitation provides optical sections from deeper within scattering specimens than confocal imaging. Biophys J 75:2015–2024. doi: 10.1016/S0006-3495(98)77643-X

Chaigneau E, Oheim M, Audinat E, Charpak S (2003) Two-photon imaging of capillary blood flow in olfactory bulb glomeruli. Proc Natl Acad Sci USA 100:13081–13086. doi: 10.1073/pnas.2133652100

Chan WY, Kohsaka S, Rezaie P (2007) The origin and cell lineage of microglia: new concepts. Brain Res Rev 53:344–354. doi: 10.1016/j.brainresrev.2006.11.002

Chang L, Karin M (2001) Mammalian MAP kinase signalling cascades. Nature 410:37–40. doi: 10.1038/35065000

Cho EE, Drazic J, Ganguly M, et al. (2011a) Two-photon fluorescence microscopy study of cerebrovascular dynamics in ultrasound-induced blood-brain barrier opening. J Cereb Blood Flow Metab 31:1852–1862. doi: 10.1038/jcbfm.2011.59

Cho S-H, Sun B, Zhou Y, et al. (2011b) CX3CR1 protein signaling modulates microglial activation and protects against plaque-independent cognitive deficits in a mouse model of Alzheimer disease. J Biol Chem 286:32713–32722. doi: 10.1074/jbc.M111.254268

Christensen DJ, Nedergaard M (2011) Two-photon in vivo imaging of cells. Pediatr Nephrol 26:1483–1489. doi: 10.1007/s00467-011-1818-9

Chtanova T, Han S-J, Schaeffer M, et al. (2009) Dynamics of T cell, antigen-presenting cell, and pathogen interactions during recall responses in the lymph node. Immunity 31:342–355. doi: 10.1016/j.immuni.2009.06.023

Cipriani R, Villa P, Chece G, et al. (2011) CX3CL1 is neuroprotective in permanent focal cerebral ischemia in rodents. J Neurosci 31:16327–16335. doi: 10.1523/JNEUROSCI.3611-11.2011

Colton CA (2009) Heterogeneity of microglial activation in the innate immune response in the brain. J Neuroimmune Pharmacol 4:399–418. doi: 10.1007/s11481-009-9164-4

Conchello J-A, Lichtman JW (2005) Optical sectioning microscopy. Nat Methods 2:920–931. doi: 10.1038/nmeth815

Cordiglieri C, Odoardi F, Zhang B, et al. (2010) Nicotinic acid adenine dinucleotide phosphate-mediated calcium signalling in effector T cells regulates autoimmunity of the central nervous system. Brain 133:1930–1943. doi: 10.1093/brain/awq135

Corona AW, Huang Y, O'Connor JC, et al. (2010) Fractalkine receptor (CX3CR1) deficiency sensitizes mice to the behavioral changes induced by lipopolysaccharide. J Neuroinflammation 7:93. doi: 10.1186/1742-2094-7-93

Cserr HF, Knopf PM (1992) Cervical lymphatics, the blood-brain barrier and the immunoreactivity of the brain: a new view. Immunol Today 13:507–512. doi: 10.1016/0167-5699(92)90027-5

Cullen KM, Kócsi Z, Stone J (2005) Pericapillary haem-rich deposits: evidence for microhaemorrhages in aging human cerebral cortex. J Cereb Blood Flow Metab 25:1656–1667. doi: 10.1038/sj.jcbfm.9600155

D'Mello C, Le T, Swain MG (2009) Cerebral microglia recruit monocytes into the brain in response to tumor necrosis factoralpha signaling during peripheral organ inflammation. J Neurosci 29:2089–2102. doi: 10.1523/JNEUROSCI.3567-08.2009

Daigneault M, Preston JA, Marriott HM, et al. (2010) The identification of markers of macrophage differentiation in PMA-stimulated THP-1 cells and monocyte-derived macrophages. PLoS ONE 5:e8668. doi: 10.1371/journal.pone.0008668

Davalos D, Grutzendler J, Yang G, et al. (2005) ATP mediates rapid microglial response to local brain injury in vivo. Nat Neurosci 8:752–758. doi: 10.1038/nn1472

David S, Kroner A (2011) Repertoire of microglial and macrophage responses after spinal cord injury. Nat Rev Neurosci 12:388–399. doi: 10.1038/nrn3053

Davis SM, Donnan GA (2009) 4.5 hours: the new time window for tissue plasminogen activator in stroke. Stroke 40:2266–2267. doi: 10.1161/STROKEAHA.108.544171

DELI MA The role of blood-brain barrier in neurodegenerative diseases. http://cat.inist.fr/?aModele=afficheN&cpsidt=18315992. Accessed 27 Feb 2012

Dénes A, Ferenczi S, Halász J, et al. (2008) Role of CX3CR1 (fractalkine receptor) in brain damage and inflammation induced by focal cerebral ischemia in mouse. J Cereb Blood Flow Metab 28:1707–1721. doi: 10.1038/jcbfm.2008.64

Denes A, McColl BW, Leow-Dyke SF, et al. (2011) Experimental stroke-induced changes in the bone marrow reveal complex regulation of leukocyte responses. J Cereb Blood Flow Metab 31:1036–1050. doi: 10.1038/jcbfm.2010.198

Denes A, Vidyasagar R, Feng J, et al. (2007) Proliferating resident microglia after focal cerebral ischaemia in mice. J Cereb Blood Flow Metab 27:1941–1953. doi: 10.1038/sj.jcbfm.9600495

Denk W, Strickler JH, Webb WW (1990) Two-photon laser scanning fluorescence microscopy. Science 248:73–76.

Ding S, Wang T, Cui W, Haydon PG (2009) Photothrombosis ischemia stimulates a sustained astrocytic Ca2+ signaling in vivo. Glia 57:767–776. doi: 10.1002/glia.20804

Dirnagl U, Iadecola C, Moskowitz MA (1999) Pathobiology of ischaemic stroke: an integrated view. Trends Neurosci 22:391–397.

Donnan GA, Davis SM, Parsons MW, et al. (2011) How to make better use of thrombolytic therapy in acute ischemic stroke. Nat Rev Neurol 7:400–409. doi: 10.1038/nrneurol.2011.89

Donnelly DJ, Gensel JC, Ankeny DP, et al. (2009) An efficient and reproducible method for quantifying macrophages in different experimental models of central nervous system pathology. J Neurosci Methods 181:36–44. doi: 10.1016/j.jneumeth.2009.04.010

Donnelly DJ, Longbrake EE, Shawler TM, et al. (2011) Deficient CX3CR1 signaling promotes recovery after mouse spinal cord injury by limiting the recruitment and activation of Ly6Clo/iNOS+ macrophages. J Neurosci 31:9910–9922. doi: 10.1523/JNEUROSCI.2114-11.2011

Doyle KP, Simon RP, Stenzel-Poore MP (2008) Mechanisms of ischemic brain damage. Neuropharmacology 55:310–318. doi: 10.1016/j.neuropharm.2008.01.005

Edwards EA, Dean LM (1977) Effects of crowding of mice on humoral antibody formation and protection to lethal antigenic challenge. Psychosom Med 39:19–24.

Engelhardt B (2006) Molecular mechanisms involved in T cell migration across the blood-brain barrier. J Neural Transm 113:477–485. doi: 10.1007/s00702-005-0409-y

Engelhardt B, Wolburg H (2004) Mini-review: Transendothelial migration of leukocytes: through the front door or around the side of the house? Eur J Immunol 34:2955–2963. doi: 10.1002/eji.200425327

Fabricius M, Fuhr S, Bhatia R, et al. (2006) Cortical spreading depression and peri-infarct depolarization in acutely injured human cerebral cortex. Brain 129:778–790. doi: 10.1093/brain/awh716

Fagan SC, Waller JL, Nichols FT, et al. (2010) Minocycline to improve neurologic outcome in stroke (MINOS): a dose-finding study. Stroke 41:2283–2287. doi: 10.1161/STROKEAHA.110.582601

Fantin A, Vieira JM, Gestri G, et al. (2010) Tissue macrophages act as cellular chaperones for vascular anastomosis downstream of VEGF-mediated endothelial tip cell induction. Blood 116:829–840. doi: 10.1182/blood-2009-12-257832

Farrall AJ, Wardlaw JM (2009) Blood-brain barrier: ageing and microvascular disease--systematic review and meta-analysis. Neurobiol Aging 30:337–352. doi: 10.1016/j.neurobiolaging.2007.07.015

Fatahzadeh M, Glick M (2006) Stroke: epidemiology, classification, risk factors, complications, diagnosis, prevention, and medical and dental management. Oral Surg Oral Med Oral Pathol Oral Radiol Endod 102:180–191. doi: 10.1016/j.tripleo.2005.07.031

Feng G, Mellor RH, Bernstein M, et al. (2000) Imaging neuronal subsets in transgenic mice expressing multiple spectral variants of GFP. Neuron 28:41–51.

Fernández-Klett F, Offenhauser N, Dirnagl U, et al. (2010) Pericytes in capillaries are contractile in vivo, but arterioles mediate functional hyperemia in the mouse brain. Proc Natl Acad Sci USA 107:22290–22295. doi: 10.1073/pnas.1011321108

Fierz W, Endler B, Reske K, et al. (1985) Astrocytes as antigen-presenting cells. I. Induction of Ia antigen expression on astrocytes by T cells via immune interferon and its effect on antigen presentation. J Immunol 134:3785–3793.

Filardy AA, Pires DR, Nunes MP, et al. (2010) Proinflammatory clearance of apoptotic neutrophils induces an IL-12(low)IL-10(high) regulatory phenotype in macrophages. J Immunol 185:2044–2050. doi: 10.4049/jimmunol.1000017

Finikova OS, Troxler T, Senes A, et al. (2007) Energy and electron transfer in enhanced two-photon-absorbing systems with triplet cores. J Phys Chem A 111:6977–6990. doi: 10.1021/jp071586f

Flügel A, Odoardi F, Nosov M, Kawakami N (2007) Autoaggressive effector T cells in the course of experimental autoimmune encephalomyelitis visualized in the light of

two-photon microscopy. J Neuroimmunol 191:86–97. doi: 10.1016/j.jneuroim.2007.09.017

Flynn RWV, MacWalter RSM, Doney ASF (2008) The cost of cerebral ischaemia. Neuropharmacology 55:250–256. doi: 10.1016/j.neuropharm.2008.05.031

Fonfria E, Mattei C, Hill K, et al. (2006) TRPM2 is elevated in the tMCAO stroke model, transcriptionally regulated, and functionally expressed in C13 microglia. J Recept Signal Transduct Res 26:179–198. doi: 10.1080/10799890600637522

Fontaine V, Mohand-Said S, Hanoteau N, et al. (2002) Neurodegenerative and neuroprotective effects of tumor Necrosis factor (TNF) in retinal ischemia: opposite roles of TNF receptor 1 and TNF receptor 2. J Neurosci 22:RC216. doi: 20026253

Frenkel D, Huang Z, Maron R, et al. (2003) Nasal vaccination with myelin oligodendrocyte glycoprotein reduces stroke size by inducing IL-10-producing CD4+ T cells. J Immunol 171:6549–6555.

Fumagalli S, Coles JA, Ejlerskov P, et al. (2011) In vivo real-time multiphoton imaging of T lymphocytes in the mouse brain after experimental stroke. Stroke 42:1429–1436. doi: 10.1161/STROKEAHA.110.603704

Furlan AJ, Eyding D, Albers GW, et al. (2006) Dose Escalation of Desmoteplase for Acute Ischemic Stroke (DEDAS): evidence of safety and efficacy 3 to 9 hours after stroke onset. Stroke 37:1227–1231. doi: 10.1161/01.STR.0000217403.66996.6d

Galea I, Bechmann I, Perry VH (2007) What is immune privilege (not)? Trends Immunol 28:12–18. doi: 10.1016/j.it.2006.11.004

Galea I, Palin K, Newman TA, et al. (2005) Mannose receptor expression specifically reveals perivascular macrophages in normal, injured, and diseased mouse brain. Glia 49:375–384. doi: 10.1002/glia.20124

Garcia JH, Liu KF, Relton JK (1995) Interleukin-1 receptor antagonist decreases the number of necrotic neurons in rats with middle cerebral artery occlusion. Am J Pathol 147:1477–1486.

Garcia JH, Liu KF, Yoshida Y, et al. (1994) Influx of leukocytes and platelets in an evolving brain infarct (Wistar rat). Am J Pathol 144:188–199.

Ge S, Song L, Serwanski DR, et al. (2008) Transcellular transport of CCL2 across brain microvascular endothelial cells. J Neurochem 104:1219–1232. doi: 10.1111/j.1471-4159.2007.05056.x

Gea-Sorlí S, Guillamat R, Serrano-Mollar A, Closa D (2011) Activation of lung macrophage subpopulations in experimental acute pancreatitis. J Pathol 223:417–424. doi: 10.1002/path.2814

Gebel JM, Broderick JP (2000) Intracerebral hemorrhage. Neurol Clin 18:419–438.

Gee JM, Kalil A, Thullbery M, Becker KJ (2008) Induction of immunologic tolerance to myelin basic protein prevents central nervous system autoimmunity and improves outcome after stroke. Stroke 39:1575–1582. doi: 10.1161/STROKEAHA.107.501486

Geissmann F, Jung S, Littman DR (2003) Blood monocytes consist of two principal subsets with distinct migratory properties. Immunity 19:71–82.

Geissmann F, Manz MG, Jung S, et al. (2010) Development of monocytes, macrophages, and dendritic cells. Science 327:656–661. doi: 10.1126/science.1178331

Gelderblom M, Leypoldt F, Steinbach K, et al. (2009) Temporal and spatial dynamics of cerebral immune cell accumulation in stroke. Stroke 40:1849–1857. doi: 10.1161/STROKEAHA.108.534503

Genovese T, Mazzon E, Crisafulli C, et al. (2008) TNF-alpha blockage in a mouse model of SCI: evidence for improved outcome. Shock 29:32–41. doi: 10.1097/shk.0b013e318059053a

Gensel JC, Schonberg DL, Alexander JK, et al. (2010) Semi-automated Sholl analysis for quantifying changes in growth and differentiation of neurons and glia. J Neurosci Methods 190:71–79. doi: 10.1016/j.jneumeth.2010.04.026

Gerzeli S, Tarricone R, Zolo P, et al. (2005) The economic burden of stroke in Italy. The EcLIPSE Study: Economic Longitudinal Incidence-based Project for Stroke Evaluation. Neurol Sci 26:72–80. doi: 10.1007/s10072-005-0439-0

Gesuete R, Storini C, Fantin A, et al. (2009) Recombinant C1 inhibitor in brain ischemic injury. Ann Neurol 66:332–342. doi: 10.1002/ana.21740

Giffard RG, Monyer H, Christine CW, Choi DW (1990) Acidosis reduces NMDA receptor activation, glutamate neurotoxicity, and oxygen-glucose deprivation neuronal injury in cortical cultures. Brain Res 506:339–342.

Gill AS, Binder DK (2007) Wilder Penfield, Pío del Río-Hortega, and the discovery of oligodendroglia. Neurosurgery 60:940–948; discussion 940–948. doi: 10.1227/01.NEU.0000255448.97730.34

Girard S, Brough D, Lopez-Castejon G, et al. (2013) Microglia and macrophages differentially modulate cell death after brain injury caused by oxygen-glucose deprivation in organotypic brain slices. Glia. doi: 10.1002/glia.22478

Goerdt S, Orfanos CE (1999) Other functions, other genes: alternative activation of antigen-presenting cells. Immunity 10:137–142.

Gong C, Qin Z, Betz AL, et al. (1998) Cellular localization of tumor necrosis factor alpha following focal cerebral ischemia in mice. Brain Res 801:1–8.

Gong S, Zheng C, Doughty ML, et al. (2003) A gene expression atlas of the central nervous system based on bacterial artificial chromosomes. Nature 425:917–925. doi: 10.1038/nature02033

Gonzalez B, Leroux P, Lamacz M, et al. (1992) Somatostatin receptors are expressed by immature cerebellar granule cells: evidence for a direct inhibitory effect of somatostatin on neuroblast activity. Proc Natl Acad Sci USA 89:9627–9631.

Gordon GRJ, Choi HB, Rungta RL, et al. (2008) Brain metabolism dictates the polarity of astrocyte control over arterioles. Nature 456:745–749. doi: 10.1038/nature07525

Gordon S (2003) Alternative activation of macrophages. Nat Rev Immunol 3:23–35. doi: 10.1038/nri978

Graeber MB (2010) Changing face of microglia. Science 330:783–788. doi: 10.1126/science.1190929

Gratchev A, Guillot P, Hakiy N, et al. (2001) Alternatively activated macrophages differentially express fibronectin and its splice variants and the extracellular matrix protein betaIG-H3. Scand J Immunol 53:386–392.

Grinberg YY, Milton JG, Kraig RP (2011) Spreading depression sends microglia on Lévy flights. PLoS ONE 6:e19294. doi: 10.1371/journal.pone.0019294

Hacke W, Albers G, Al-Rawi Y, et al. (2005) The Desmoteplase in Acute Ischemic Stroke Trial (DIAS): a phase II MRI-based 9-hour window acute stroke thrombolysis trial with intravenous desmoteplase. Stroke 36:66–73. doi: 10.1161/01.STR.0000149938.08731.2c

Hacke W, Furlan AJ, Al-Rawi Y, et al. (2009) Intravenous desmoteplase in patients with acute ischaemic stroke selected by MRI perfusion-diffusion weighted imaging or perfusion CT (DIAS-2): a prospective, randomised, double-blind, placebo-controlled study. Lancet Neurol 8:141–150. doi: 10.1016/S1474-4422(08)70267-9

Hacke W, Kaste M, Bluhmki E, et al. (2008) Thrombolysis with alteplase 3 to 4.5 hours after acute ischemic stroke. N Engl J Med 359:1317–1329. doi: 10.1056/NEJMoa0804656

Haley EC Jr, Thompson JLP, Grotta JC, et al. (2010) Phase IIB/III trial of tenecteplase in acute ischemic stroke: results of a prematurely terminated randomized clinical trial. Stroke 41:707–711. doi: 10.1161/STROKEAHA.109.572040

Hallenbeck J, Del Zoppo G, Jacobs T, et al. (2006) Immunomodulation strategies for preventing vascular disease of the brain and heart: workshop summary. Stroke 37:3035–3042. doi: 10.1161/01.STR.0000248836.82538.ee

Hamilton NB, Attwell D, Hall CN (2010) Pericyte-mediated regulation of capillary diameter: a component of neurovascular coupling in health and disease. Front Neuroenergetics. doi: 10.3389/fnene.2010.00005

Hanisch U-K (2002) Microglia as a source and target of cytokines. Glia 40:140–155. doi: 10.1002/glia.10161

Hanisch U-K, Kettenmann H (2007) Microglia: active sensor and versatile effector cells in the normal and pathologic brain. Nat Neurosci 10:1387–1394. doi: 10.1038/nn1997

Hardingham GE (2006) Pro-survival signalling from the NMDA receptor. Biochem Soc Trans 34:936–938. doi: 10.1042/BST0340936

Hardingham GE, Bading H (2010) Synaptic versus extrasynaptic NMDA receptor signalling: implications for neurodegenerative disorders. Nat Rev Neurosci 11:682–696. doi: 10.1038/nrn2911

Häusler KG, Prinz M, Nolte C, et al. (2002) Interferon-gamma differentially modulates the release of cytokines and chemokines in lipopolysaccharide- and pneumococcal cell wall-stimulated mouse microglia and macrophages. Eur J Neurosci 16:2113–2122.

Hawkins BT, Davis TP (2005) The blood-brain barrier/neurovascular unit in health and disease. Pharmacol Rev 57:173–185. doi: 10.1124/pr.57.2.4

Haynes SE, Hollopeter G, Yang G, et al. (2006) The P2Y12 receptor regulates microglial activation by extracellular nucleotides. Nat Neurosci 9:1512–1519. doi: 10.1038/nn1805

Helmchen F, Denk W (2005) Deep tissue two-photon microscopy. Nat Methods 2:932–940. doi: 10.1038/nmeth818

Helmchen F, Kleinfeld D (2008) Chapter 10. In vivo measurements of blood flow and glial cell function with two-photon laser-scanning microscopy. Meth Enzymol 444:231–254. doi: 10.1016/S0076-6879(08)02810-3

Hengartner MO (2000) The biochemistry of apoptosis. Nature 407:770–776. doi: 10.1038/35037710

Hesse M, Modolell M, La Flamme AC, et al. (2001) Differential regulation of nitric oxide synthase-2 and arginase-1 by type 1/type 2 cytokines in vivo: granulomatous pathology is shaped by the pattern of L-arginine metabolism. J Immunol 167:6533–6544.

Hoffman JR (2003) Tissue plasminogen activator (tPA) for acute ischaemic stroke: why so much has been made of so little. Med J Aust 179:333–334.

Hoffman JR, Schriger DL (2009) A graphic reanalysis of the NINDS Trial. Ann Emerg Med 54:329–336, 336.e1–35. doi: 10.1016/j.annemergmed.2009.03.019

Hossmann KA (1994) Viability thresholds and the penumbra of focal ischemia. Ann Neurol 36:557–565. doi: 10.1002/ana.410360404

Huang DR, Wang J, Kivisakk P, et al. (2001) Absence of monocyte chemoattractant protein 1 in mice leads to decreased local macrophage recruitment and antigen-specific T helper cell type 1 immune response in experimental autoimmune encephalomyelitis. J Exp Med 193:713–726.

Huang J, Upadhyay UM, Tamargo RJ (2006) Inflammation in stroke and focal cerebral ischemia. Surg Neurol 66:232–245. doi: 10.1016/j.surneu.2005.12.028

Hundhausen C, Misztela D, Berkhout TA, et al. (2003) The disintegrin-like metalloproteinase ADAM10 is involved in constitutive cleavage of CX3CL1 (fractalkine) and regulates CX3CL1-mediated cell-cell adhesion. Blood 102:1186–1195. doi: 10.1182/blood-2002-12-3775

Hurn PD, Subramanian S, Parker SM, et al. (2007) T- and B-cell-deficient mice with experimental stroke have reduced lesion size and inflammation. J Cereb Blood Flow Metab 27:1798–1805. doi: 10.1038/sj.jcbfm.9600482

Hussain ST, Attilo A, Bigotte L, et al. (1985) Cytofluorescence localization of propidium iodide injected intravenously into the nervous system of the mouse. Acta Neuropathol 66:62–67.

Iadecola C, Anrather J (2011) The immunology of stroke: from mechanisms to translation. Nat Med 17:796–808. doi: 10.1038/nm.2399

Imai T, Hieshima K, Haskell C, et al. (1997) Identification and molecular characterization of fractalkine receptor CX3CR1, which mediates both leukocyte migration and adhesion. Cell 91:521–530.

Immke DC, McCleskey EW (2001) Lactate enhances the acid-sensing Na+ channel on ischemia-sensing neurons. Nat Neurosci 4:869–870. doi: 10.1038/nn0901-869

IMS Study Investigators (2007) The Interventional Management of Stroke (IMS) II Study. Stroke 38:2127–2135. doi: 10.1161/STROKEAHA.107.483131

IMS Study Investigators (2006) Hemorrhage in the Interventional Management of Stroke study. Stroke 37:847–851. doi: 10.1161/01.STR.0000202586.69525.ae

IMS Study Investigators (2004) Combined intravenous and intra-arterial recanalization for acute ischemic stroke: the Interventional Management of Stroke Study. Stroke 35:904–911. doi: 10.1161/01.STR.0000121641.77121.98

Ingersoll MA, Platt AM, Potteaux S, Randolph GJ (2011) Monocyte trafficking in acute and chronic inflammation. Trends Immunol 32:470–477. doi: 10.1016/j.it.2011.05.001

Jander S, Kraemer M, Schroeter M, et al. (1995) Lymphocytic infiltration and expression of intercellular adhesion molecule-1 in photochemically induced ischemia of the rat cortex. J Cereb Blood Flow Metab 15:42–51. doi: 10.1038/jcbfm.1995.5

Jayadev S, Nesser NK, Hopkins S, et al. (2011) Transcription factor p53 influences microglial activation phenotype. Glia 59:1402–1413. doi: 10.1002/glia.21178

Jin R, Yang G, Li G (2010) Inflammatory mechanisms in ischemic stroke: role of inflammatory cells. J Leukoc Biol 87:779–789. doi: 10.1189/jlb.1109766

Katzan IL, Furlan AJ, Lloyd LE, et al. (2000) Use of tissue-type plasminogen activator for acute ischemic stroke: the Cleveland area experience. JAMA 283:1151–1158.

Kaufmann AM, Firlik AD, Fukui MB, et al. (1999) Ischemic core and penumbra in human stroke. Stroke 30:93–99.

Kaur J, Zhao Z, Klein GM, et al. (2004) The neurotoxicity of tissue plasminogen activator? J Cereb Blood Flow Metab 24:945–963. doi: 10.1097/01.WCB.0000137868.50767.E8

Kawakami N, Flügel A (2010) Knocking at the brain's door: intravital two-photon imaging of autoreactive T cell interactions with CNS structures. Semin Immunopathol 32:275–287. doi: 10.1007/s00281-010-0216-x

Kerr JF, Wyllie AH, Currie AR (1972) Apoptosis: a basic biological phenomenon with wide-ranging implications in tissue kinetics. Br J Cancer 26:239–257.

Kettenmann H (2007) Neuroscience: the brain's garbage men. Nature 446:987–989. doi: 10.1038/nature05713

Khatri P, Hill MD, Palesch YY, et al. (2008) Methodology of the Interventional Management of Stroke III Trial. Int J Stroke 3:130–137. doi: 10.1111/j.1747-4949.2008.00151.x

Kigerl KA, Gensel JC, Ankeny DP, et al. (2009) Identification of two distinct macrophage subsets with divergent effects causing either neurotoxicity or regeneration in the injured mouse spinal cord. J Neurosci 29:13435–13444. doi: 10.1523/JNEUROSCI.3257-09.2009

Kim JV, Jiang N, Tadokoro CE, et al. (2010) Two-photon laser scanning microscopy imaging of intact spinal cord and cerebral cortex reveals requirement for CXCR6 and neuroinflammation in immune cell infiltration of cortical injury sites. J Immunol Methods 352:89–100. doi: 10.1016/j.jim.2009.09.007

Kim JV, Kang SS, Dustin ML, McGavern DB (2009) Myelomonocytic cell recruitment causes fatal CNS vascular injury during acute viral meningitis. Nature 457:191–195. doi: 10.1038/nature07591

Kim SU, De Vellis J (2005) Microglia in health and disease. J Neurosci Res 81:302–313. doi: 10.1002/jnr.20562

Kivisäkk P, Imitola J, Rasmussen S, et al. (2009) Localizing central nervous system immune surveillance: meningeal antigen-presenting cells activate T cells during experimental autoimmune encephalomyelitis. Ann Neurol 65:457–469. doi: 10.1002/ana.21379

Kleindorfer D, Kissela B, Schneider A, et al. (2004) Eligibility for recombinant tissue plasminogen activator in acute ischemic stroke: a population-based study. Stroke 35:e27–29. doi: 10.1161/01.STR.0000109767.11426.17

Kleindorfer D, Lindsell CJ, Brass L, et al. (2008) National US estimates of recombinant tissue plasminogen activator use: ICD-9 codes substantially underestimate. Stroke 39:924–928. doi: 10.1161/STROKEAHA.107.490375

Kleinschnitz C, Schwab N, Kraft P, et al. (2010) Early detrimental T-cell effects in experimental cerebral ischemia are neither related to adaptive immunity nor thrombus formation. Blood 115:3835–3842. doi: 10.1182/blood-2009-10-249078

Koch S, Katsnelson M, Dong C, Perez-Pinzon M (2011) Remote ischemic limb preconditioning after subarachnoid hemorrhage: a phase Ib study of safety and feasibility. Stroke 42:1387–1391. doi: 10.1161/STROKEAHA.110.605840

Kuwabara Y, Yokoyama A, Yang L, et al. (2003) Two populations of microglial cells isolated from rat primary mixed glial cultures. J Neurosci Res 73:22–30. doi: 10.1002/jnr.10637

Kwan J, Hand P, Sandercock P (2004) A systematic review of barriers to delivery of thrombolysis for acute stroke. Age Ageing 33:116–121. doi: 10.1093/ageing/afh064

Ladeby R, Wirenfeldt M, Garcia-Ovejero D, et al. (2005) Microglial cell population dynamics in the injured adult central nervous system. Brain Res Brain Res Rev 48:196–206. doi: 10.1016/j.brainresrev.2004.12.009

Lai AY, Todd KG (2008) Differential regulation of trophic and proinflammatory microglial effectors is dependent on severity of neuronal injury. Glia 56:259–270. doi: 10.1002/glia.20610

Lalancette-Hébert M, Gowing G, Simard A, et al. (2007) Selective ablation of proliferating microglial cells exacerbates ischemic injury in the brain. J Neurosci 27:2596–2605. doi: 10.1523/JNEUROSCI.5360-06.2007

Lambertsen KL, Clausen BH, Babcock AA, et al. (2009) Microglia protect neurons against ischemia by synthesis of tumor necrosis factor. J Neurosci 29:1319–1330. doi: 10.1523/JNEUROSCI.5505-08.2009

Lampl Y, Boaz M, Gilad R, et al. (2007) Minocycline treatment in acute stroke: an open-label, evaluator-blinded study. Neurology 69:1404–1410. doi: 10.1212/01.wnl.0000277487.04281.db

Lauro C, Catalano M, Trettel F, et al. (2006) The chemokine CX3CL1 reduces migration and increases adhesion of neurons with mechanisms dependent on the beta1 integrin subunit. J Immunol 177:7599–7606.

Leal J, Luengo-Fernández R, Gray A, et al. (2006) Economic burden of cardiovascular diseases in the enlarged European Union. Eur Heart J 27:1610–1619. doi: 10.1093/eurheartj/ehi733

Lecoq J, Parpaleix A, Roussakis E, et al. (2011) Simultaneous two-photon imaging of oxygen and blood flow in deep cerebral vessels. Nat Med 17:893–898. doi: 10.1038/nm.2394

Lecoq J, Tiret P, Najac M, et al. (2009) Odor-evoked oxygen consumption by action potential and synaptic transmission in the olfactory bulb. J Neurosci 29:1424–1433. doi: 10.1523/JNEUROSCI.4817-08.2009

Lees KR, Bluhmki E, Von Kummer R, et al. (2010) Time to treatment with intravenous alteplase and outcome in stroke: an updated pooled analysis of ECASS, ATLANTIS, NINDS, and EPITHET trials. Lancet 375:1695–1703. doi: 10.1016/S0140-6736(10)60491-6

Lefer AM, Ma XL, Weyrich AS, Scalia R (1993) Mechanism of the cardioprotective effect of transforming growth factor beta 1 in feline myocardial ischemia and reperfusion. Proc Natl Acad Sci USA 90:1018–1022.

Lendvai B, Stern EA, Chen B, Svoboda K (2000) Experience-dependent plasticity of dendritic spines in the developing rat barrel cortex in vivo. Nature 404:876–881. doi: 10.1038/35009107

Li P, Murphy TH (2008) Two-photon imaging during prolonged middle cerebral artery occlusion in mice reveals recovery of dendritic structure after reperfusion. J Neurosci 28:11970–11979. doi: 10.1523/JNEUROSCI.3724-08.2008

Liang KJ, Lee JE, Wang YD, et al. (2009) Regulation of dynamic behavior of retinal microglia by CX3CR1 signaling. Invest Ophthalmol Vis Sci 50:4444–4451. doi: 10.1167/iovs.08-3357

Liberatore GT, Samson A, Bladin C, et al. (2003) Vampire bat salivary plasminogen activator (desmoteplase): a unique fibrinolytic enzyme that does not promote neurodegeneration. Stroke 34:537–543.

Liesz A, Suri-Payer E, Veltkamp C, et al. (2009) Regulatory T cells are key cerebroprotective immunomodulators in acute experimental stroke. Nat Med 15:192–199. doi: 10.1038/nm.1927

Linehan JD, Kolios G, Valatas V, et al. (2005) Immunomodulatory cytokines suppress epithelial nitric oxide production in inflammatory bowel disease by acting on mononuclear cells. Free Radic Biol Med 39:1560–1569. doi: 10.1016/j.freeradbiomed.2005.07.019

Liu B, Liao M, Mielke JG, et al. (2006) Ischemic insults direct glutamate receptor subunit 2-lacking AMPA receptors to synaptic sites. J Neurosci 26:5309–5319. doi: 10.1523/JNEUROSCI.0567-06.2006

Lloyd-Jones D, Adams RJ, Brown TM, et al. (2010) Heart disease and stroke statistics--2010 update: a report from the American Heart Association. Circulation 121:e46–e215. doi: 10.1161/CIRCULATIONAHA.109.192667

Lo EH (2008a) Experimental models, neurovascular mechanisms and translational issues in stroke research. Br J Pharmacol 153 Suppl 1:S396–405. doi: 10.1038/sj.bjp.0707626

Lo EH (2008b) A new penumbra: transitioning from injury into repair after stroke. Nat Med 14:497–500. doi: 10.1038/nm1735

Lo EH, Dalkara T, Moskowitz MA (2003) Mechanisms, challenges and opportunities in stroke. Nat Rev Neurosci 4:399–415. doi: 10.1038/nrn1106

Longhi L, Gesuete R, Perego C, et al. (2011) Long-lasting protection in brain trauma by endotoxin preconditioning. J Cereb Blood Flow Metab 31:1919–1929. doi: 10.1038/jcbfm.2011.42

Lossinsky AS, Shivers RR (2004) Structural pathways for macromolecular and cellular transport across the blood-brain barrier during inflammatory conditions. Review. Histol Histopathol 19:535–564.

Lu Y-Z, Lin C-H, Cheng F-C, Hsueh C-M (2005) Molecular mechanisms responsible for microglia-derived protection of Sprague-Dawley rat brain cells during in vitro ischemia. Neurosci Lett 373:159–164. doi: 10.1016/j.neulet.2004.10.004

MacEwan DJ (2002) TNF ligands and receptors--a matter of life and death. Br J Pharmacol 135:855–875. doi: 10.1038/sj.bjp.0704549

Machado LS, Kozak A, Ergul A, et al. (2006) Delayed minocycline inhibits ischemia-activated matrix metalloproteinases 2 and 9 after experimental stroke. BMC Neurosci 7:56. doi: 10.1186/1471-2202-7-56

Machado LS, Sazonova IY, Kozak A, et al. (2009) Minocycline and tissue-type plasminogen activator for stroke: assessment of interaction potential. Stroke 40:3028–3033. doi: 10.1161/STROKEAHA.109.556852

MacVicar BA, Thompson RJ (2010) Non-junction functions of pannexin-1 channels. Trends Neurosci 33:93–102. doi: 10.1016/j.tins.2009.11.007

Magnus T, Chan A, Grauer O, et al. (2001) Microglial phagocytosis of apoptotic inflammatory T cells leads to down-regulation of microglial immune activation. J Immunol 167:5004–5010.

Magnus T, Wiendl H, Kleinschnitz C (2012) Immune mechanisms of stroke. Curr Opin Neurol 25:334–340. doi: 10.1097/WCO.0b013e328352ede6

Mantovani A, Sica A, Sozzani S, et al. (2004) The chemokine system in diverse forms of macrophage activation and polarization. Trends Immunol 25:677–686. doi: 10.1016/j.it.2004.09.015

Mantovani A, Sozzani S, Locati M, et al. (2002) Macrophage polarization: tumor-associated macrophages as a paradigm for polarized M2 mononuclear phagocytes. Trends Immunol 23:549–555.

Marcon J, Gagliardi B, Balosso S, et al. (2009) Age-dependent vascular changes induced by status epilepticus in rat forebrain: implications for epileptogenesis. Neurobiol Dis 34:121–132.

Martinez FO, Gordon S, Locati M, Mantovani A (2006) Transcriptional profiling of the human monocyte-to-macrophage differentiation and polarization: new molecules and patterns of gene expression. J Immunol 177:7303–7311.

Martinez FO, Sica A, Mantovani A, Locati M (2008) Macrophage activation and polarization. Front Biosci 13:453–461.

Masuda T, Croom D, Hida H, Kirov SA (2011) Capillary blood flow around microglial somata determines dynamics of microglial processes in ischemic conditions. Glia 59:1744–1753. doi: 10.1002/glia.21220

Mathiisen TM, Lehre KP, Danbolt NC, Ottersen OP (2010) The perivascular astroglial sheath provides a complete covering of the brain microvessels: an electron microscopic 3D reconstruction. Glia 58:1094–1103. doi: 10.1002/glia.20990

McColl BW, Rothwell NJ, Allan SM (2008) Systemic inflammation alters the kinetics of cerebrovascular tight junction disruption after experimental stroke in mice. J Neurosci 28:9451–9462. doi: 10.1523/JNEUROSCI.2674-08.2008

Metea MR, Newman EA (2006) Glial cells dilate and constrict blood vessels: a mechanism of neurovascular coupling. J Neurosci 26:2862–2870. doi: 10.1523/JNEUROSCI.4048-05.2006

Michelucci A, Heurtaux T, Grandbarbe L, et al. (2009) Characterization of the microglial phenotype under specific pro-inflammatory and anti-inflammatory conditions:

Effects of oligomeric and fibrillar amyloid-beta. J Neuroimmunol 210:3–12. doi: 10.1016/j.jneuroim.2009.02.003

Miller MJ, Wei SH, Parker I, Cahalan MD (2002) Two-photon imaging of lymphocyte motility and antigen response in intact lymph node. Science 296:1869–1873. doi: 10.1126/science.1070051

Minami M, Satoh M (2003) Chemokines and their receptors in the brain: pathophysiological roles in ischemic brain injury. Life Sci 74:321–327.

Miyawaki A (2005) Innovations in the imaging of brain functions using fluorescent proteins. Neuron 48:189–199. doi: 10.1016/j.neuron.2005.10.003

Molina CA, Barreto AD, Tsivgoulis G, et al. (2009) Transcranial ultrasound in clinical sonothrombolysis (TUCSON) trial. Ann Neurol 66:28–38. doi: 10.1002/ana.21723

Morita Y, Fukuuchi Y, Koto A, et al. (1997) Rapid changes in pial arterial diameter and cerebral blood flow caused by ipsilateral carotid artery occlusion in rats. Keio J Med 46:120–127.

Moskowitz MA, Lo EH, Iadecola C (2010) The science of stroke: mechanisms in search of treatments. Neuron 67:181–198. doi: 10.1016/j.neuron.2010.07.002

Mostany R, Portera-Cailliau C (2008) A craniotomy surgery procedure for chronic brain imaging. J Vis Exp. doi: 10.3791/680

Mrass P, Weninger W (2006) Immune cell migration as a means to control immune privilege: lessons from the CNS and tumors. Immunol Rev 213:195–212. doi: 10.1111/j.1600-065X.2006.00433.x

Mulligan SJ, MacVicar BA (2004) Calcium transients in astrocyte endfeet cause cerebrovascular constrictions. Nature 431:195–199. doi: 10.1038/nature02827

Murata Y, Rosell A, Scannevin RH, et al. (2008) Extension of the thrombolytic time window with minocycline in experimental stroke. Stroke 39:3372–3377. doi: 10.1161/STROKEAHA.108.514026

Murphy TH, Li P, Betts K, Liu R (2008) Two-photon imaging of stroke onset in vivo reveals that NMDA-receptor independent ischemic depolarization is the major cause of rapid reversible damage to dendrites and spines. J Neurosci 28:1756–1772. doi: 10.1523/JNEUROSCI.5128-07.2008

Murray KN, Buggey HF, Denes A, Allan SM (2013) Systemic immune activation shapes stroke outcome. Mol Cell Neurosci 53:14–25. doi: 10.1016/j.mcn.2012.09.004

Nadeau JO, Shi S, Fang J, et al. (2005) TPA use for stroke in the Registry of the Canadian Stroke Network. Can J Neurol Sci 32:433–439.

Nagaraja TN, Karki K, Ewing JR, et al. (2008) Identification of variations in blood-brain barrier opening after cerebral ischemia by dual contrast-enhanced magnetic resonance imaging and T 1sat measurements. Stroke 39:427–432. doi: 10.1161/STROKEAHA.107.496059

Nahrendorf M, Swirski FK, Aikawa E, et al. (2007) The healing myocardium sequentially mobilizes two monocyte subsets with divergent and complementary functions. J Exp Med 204:3037–3047. doi: 10.1084/jem.20070885

Nakajima K, Yamamoto S, Kohsaka S, Kurihara T (2008) Neuronal stimulation leading to upregulation of glutamate transporter-1 (GLT-1) in rat microglia in vitro. Neurosci Lett 436:331–334. doi: 10.1016/j.neulet.2008.03.058

Nakase H, Kempski OS, Heimann A, et al. (1997) Microcirculation after cerebral venous occlusions as assessed by laser Doppler scanning. J Neurosurg 87:307–314. doi: 10.3171/jns.1997.87.2.0307

Namura S, Zhu J, Fink K, et al. (1998) Activation and cleavage of caspase-3 in apoptosis induced by experimental cerebral ischemia. J Neurosci 18:3659–3668.

Nawashiro H, Brenner M, Fukui S, et al. (2000) High susceptibility to cerebral ischemia in GFAP-null mice. J Cereb Blood Flow Metab 20:1040–1044. doi: 10.1097/00004647-200007000-00003

Ndubuizu O, LaManna JC (2007) Brain tissue oxygen concentration measurements. Antioxid Redox Signal 9:1207–1219. doi: 10.1089/ars.2007.1634

Neumann J, Gunzer M, Gutzeit HO, et al. (2006) Microglia provide neuroprotection after ischemia. FASEB J 20:714–716. doi: 10.1096/fj.05-4882fje

Nimmagadda A, Park H-P, Prado R, Ginsberg MD (2008) Albumin therapy improves local vascular dynamics in a rat model of primary microvascular thrombosis: a two-photon laser-scanning microscopy study. Stroke 39:198–204. doi: 10.1161/STROKEAHA.107.495598

Ning K, Pei L, Liao M, et al. (2004) Dual neuroprotective signaling mediated by downregulating two distinct phosphatase activities of PTEN. J Neurosci 24:4052–4060. doi: 10.1523/JNEUROSCI.5449-03.2004

Nishimura N, Schaffer CB, Friedman B, et al. (2007) Penetrating arterioles are a bottleneck in the perfusion of neocortex. Proc Natl Acad Sci USA 104:365–370. doi: 10.1073/pnas.0609551104

O'Collins VE, Macleod MR, Donnan GA, et al. (2006) 1,026 experimental treatments in acute stroke. Ann Neurol 59:467–477. doi: 10.1002/ana.20741

Obrenovitch TP (1995) The ischaemic penumbra: twenty years on. Cerebrovasc Brain Metab Rev 7:297–323.

Odoardi F, Kawakami N, Klinkert WEF, et al. (2007) Blood-borne soluble protein antigen intensifies T cell activation in autoimmune CNS lesions and exacerbates clinical disease. Proc Natl Acad Sci USA 104:18625–18630. doi: 10.1073/pnas.0705033104

Oheim M, Beaurepaire E, Chaigneau E, et al. (2001) Two-photon microscopy in brain tissue: parameters influencing the imaging depth. J Neurosci Methods 111:29–37.

Ohsawa K, Kohsaka S (2011) Dynamic motility of microglia: Purinergic modulation of microglial movement in the normal and pathological brain. Glia 59:1793–1799. doi: 10.1002/glia.21238

Ohtaki H, Ylostalo JH, Foraker JE, et al. (2008) Stem/progenitor cells from bone marrow decrease neuronal death in global ischemia by modulation of inflammatory/immune responses. Proc Natl Acad Sci USA 105:14638–14643. doi: 10.1073/pnas.0803670105

Olney JW, Sharpe LG (1969) Brain lesions in an infant rhesus monkey treated with monsodium glutamate. Science 166:386–388.

Orr AG, Orr AL, Li X-J, et al. (2009) Adenosine A(2A) receptor mediates microglial process retraction. Nat Neurosci 12:872–878. doi: 10.1038/nn.2341

Orsini F, Villa P, Parrella S, et al. (2012) Targeting Mannose Binding Lectin Confers Long Lasting Protection with a Surprisingly Wide Therapeutic Window in Cerebral Ischemia. Circulation. doi: 10.1161/CIRCULATIONAHA.112.103051

Ortolano F, Colombo A, Zanier ER, et al. (2009a) c-Jun N-terminal kinase pathway activation in human and experimental cerebral contusion. J Neuropathol Exp Neurol 68:964–971. doi: 10.1097/NEN.0b013e3181b20670

Ortolano F, Maffia P, Dever G, et al. (2010) Advances in imaging of new targets for pharmacological intervention in stroke: real-time tracking of T-cells in the ischaemic brain. Br J Pharmacol 159:808–811. doi: 10.1111/j.1476-5381.2009.00527.x

Ortolano F, Maffia P, Dever G, et al. (2009b) Imaging T-cell movement in the brain during experimental cerebral malaria. Parasite Immunol 31:147–150. doi: 10.1111/j.1365-3024.2008.01090.x

Owens T, Bechmann I, Engelhardt B (2008) Perivascular spaces and the two steps to neuroinflammation. J Neuropathol Exp Neurol 67:1113–1121. doi: 10.1097/NEN.0b013e31818f9ca8

Pabon MM, Bachstetter AD, Hudson CE, et al. (2011) CX3CL1 reduces neurotoxicity and microglial activation in a rat model of Parkinson's disease. J Neuroinflammation 8:9. doi: 10.1186/1742-2094-8-9

Park H-P, Nimmagadda A, DeFazio RA, et al. (2008) Albumin therapy augments the effect of thrombolysis on local vascular dynamics in a rat model of arteriolar thrombosis: a two-photon laser-scanning microscopy study. Stroke 39:1556–1562. doi: 10.1161/STROKEAHA.107.502195

Parsons MW, Miteff F, Bateman GA, et al. (2009) Acute ischemic stroke: imaging-guided tenecteplase treatment in an extended time window. Neurology 72:915–921. doi: 10.1212/01.wnl.0000344168.05315.9d

Peng X, Carhuapoma JR, Bhardwaj A, et al. (2002) Suppression of cortical functional hyperemia to vibrissal stimulation in the rat by epoxygenase inhibitors. Am J Physiol Heart Circ Physiol 283:H2029–2037. doi: 10.1152/ajpheart.01130.2000

Peng X, Zhang C, Alkayed NJ, et al. (2004) Dependency of cortical functional hyperemia to forepaw stimulation on epoxygenase and nitric oxide synthase activities in rats. J Cereb Blood Flow Metab 24:509–517. doi: 10.1097/00004647-200405000-00004

Penninger JM, Irie-Sasaki J, Sasaki T, Oliveira-dos-Santos AJ (2001) CD45: new jobs for an old acquaintance. Nat Immunol 2:389–396. doi: 10.1038/87687

Peppiatt CM, Howarth C, Mobbs P, Attwell D (2006) Bidirectional control of CNS capillary diameter by pericytes. Nature 443:700–704. doi: 10.1038/nature05193

Perego C, Fumagalli S, De Simoni M-G (2011) Temporal pattern of expression and colocalization of microglia/macrophage phenotype markers following brain ischemic injury in mice. J Neuroinflammation 8:174. doi: 10.1186/1742-2094-8-174

Pinard E, Nallet H, MacKenzie ET, et al. (2002) Penumbral microcirculatory changes associated with peri-infarct depolarizations in the rat. Stroke 33:606–612.

Ponomarev ED, Maresz K, Tan Y, Dittel BN (2007) CNS-derived interleukin-4 is essential for the regulation of autoimmune inflammation and induces a state of alternative activation in microglial cells. J Neurosci 27:10714–10721. doi: 10.1523/JNEUROSCI.1922-07.2007

Porcheray F, Viaud S, Rimaniol A-C, et al. (2005) Macrophage activation switching: an asset for the resolution of inflammation. Clin Exp Immunol 142:481–489. doi: 10.1111/j.1365-2249.2005.02934.x

Porta C, Riboldi E, Totaro MG, et al. (2011) Macrophages in cancer and infectious diseases: the "good" and the "bad". Immunotherapy 3:1185–1202. doi: 10.2217/imt.11.116

Porta C, Rimoldi M, Raes G, et al. (2009) Tolerance and M2 (alternative) macrophage polarization are related processes orchestrated by p50 nuclear factor kappaB. Proc Natl Acad Sci USA 106:14978–14983. doi: 10.1073/pnas.0809784106

Pradillo JM, Denes A, Greenhalgh AD, et al. (2012) Delayed administration of interleukin-1 receptor antagonist reduces ischemic brain damage and inflammation in comorbid rats. Journal of Cerebral Blood Flow and Metabolism: Official Journal of the International Society of Cerebral Blood Flow and Metabolism. doi: 10.1038/jcbfm.2012.101

Prinz M, Priller J (2010) Tickets to the brain: role of CCR2 and CX3CR1 in myeloid cell entry in the CNS. J Neuroimmunol 224:80–84. doi: 10.1016/j.jneuroim.2010.05.015

Puro DG (2007) Physiology and pathobiology of the pericyte-containing retinal microvasculature: new developments. Microcirculation 14:1–10. doi: 10.1080/10739680601072099

Quintana A, Giralt M, Rojas S, et al. (2005) Differential role of tumor necrosis factor receptors in mouse brain inflammatory responses in cryolesion brain injury. J Neurosci Res 82:701–716. doi: 10.1002/jnr.20680

Qureshi AI, Mendelow AD, Hanley DF (2009) Intracerebral haemorrhage. Lancet 373:1632–1644. doi: 10.1016/S0140-6736(09)60371-8

Raes G, Van den Bergh R, De Baetselier P, et al. (2005) Arginase-1 and Ym1 are markers for murine, but not human, alternatively activated myeloid cells. J Immunol 174:6561; author reply 6561–6562.

Raes G, Noël W, Beschin A, et al. (2002) FIZZ1 and Ym as tools to discriminate between differentially activated macrophages. Dev Immunol 9:151–159.

Raichle ME, Mintun MA (2006) Brain work and brain imaging. Annu Rev Neurosci 29:449–476. doi: 10.1146/annurev.neuro.29.051605.112819

Raine CS, Cannella B, Duijvestijn AM, Cross AH (1990) Homing to central nervous system vasculature by antigen-specific lymphocytes. II. Lymphocyte/endothelial cell adhesion during the initial stages of autoimmune demyelination. Lab Invest 63:476–489.

Ramprasad MP, Terpstra V, Kondratenko N, et al. (1996) Cell surface expression of mouse macrosialin and human CD68 and their role as macrophage receptors for oxidized low density lipoprotein. Proc Natl Acad Sci USA 93:14833–14838.

Ransohoff RM (2011) Microglia and monocytes: 'tis plain the twain meet in the brain. Nat Neurosci 14:1098–1100. doi: 10.1038/nn.2917

Ransohoff RM, Cardona AE (2010) The myeloid cells of the central nervous system parenchyma. Nature 468:253–262. doi: 10.1038/nature09615

Ransohoff RM, Prinz M (2013) Editors' preface: Microglia--A new era dawns. Glia 61:1–2. doi: 10.1002/glia.22439

Read SJ, Hirano T, Abbott DF, et al. (1998) Identifying hypoxic tissue after acute ischemic stroke using PET and 18F-fluoromisonidazole. Neurology 51:1617–1621.

Reddrop C, Moldrich RX, Beart PM, et al. (2005) Vampire bat salivary plasminogen activator (desmoteplase) inhibits tissue-type plasminogen activator-induced potentiation of excitotoxic injury. Stroke 36:1241–1246. doi: 10.1161/01.STR.0000166050.84056.48

Reed-Geaghan EG, Reed QW, Cramer PE, Landreth GE (2010) Deletion of CD14 attenuates Alzheimer's disease pathology by influencing the brain's inflammatory milieu. J Neurosci 30:15369–15373. doi: 10.1523/JNEUROSCI.2637-10.2010

Reeves MJ, Arora S, Broderick JP, et al. (2005) Acute stroke care in the US: results from 4 pilot prototypes of the Paul Coverdell National Acute Stroke Registry. Stroke 36:1232–1240. doi: 10.1161/01.STR.0000165902.18021.5b

Relton JK, Martin D, Thompson RC, Russell DA (1996) Peripheral administration of Interleukin-1 Receptor antagonist inhibits brain damage after focal cerebral ischemia in the rat. Exp Neurol 138:206–213. doi: 10.1006/exnr.1996.0059

Rhoney DH, McAllen K, Liu-DeRyke X (2010) Current and future treatment considerations in the management of aneurysmal subarachnoid hemorrhage. J Pharm Pract 23:408–424. doi: 10.1177/0897190010372334

Richard Green A, Odergren T, Ashwood T (2003) Animal models of stroke: do they have value for discovering neuroprotective agents? Trends Pharmacol Sci 24:402–408. doi: 10.1016/S0165-6147(03)00192-5

Rogers JT, Morganti JM, Bachstetter AD, et al. (2011) CX3CR1 deficiency leads to impairment of hippocampal cognitive function and synaptic plasticity. J Neurosci 31:16241–16250. doi: 10.1523/JNEUROSCI.3667-11.2011

Rosamond W, Flegal K, Friday G, et al. (2007) Heart disease and stroke statistics--2007 update: a report from the American Heart Association Statistics Committee and Stroke Statistics Subcommittee. Circulation 115:e69–171. doi: 10.1161/CIRCULATIONAHA.106.179918

Rosidi NL, Zhou J, Pattanaik S, et al. (2011) Cortical microhemorrhages cause local inflammation but do not trigger widespread dendrite degeneration. PLoS ONE 6:e26612. doi: 10.1371/journal.pone.0026612

Rush CM, Millington OR, Hutchison S, et al. (2009) Characterization of CD4+ T-cell-dendritic cell interactions during secondary antigen exposure in tolerance and priming. Immunology 128:463–471. doi: 10.1111/j.1365-2567.2009.03124.x

Sacco RL, Chong JY, Prabhakaran S, Elkind MSV (2007) Experimental treatments for acute ischaemic stroke. Lancet 369:331–341. doi: 10.1016/S0140-6736(07)60155-X

Sacco S, Stracci F, Cerone D, et al. (2011) Epidemiology of stroke in Italy. Int J Stroke 6:219–227. doi: 10.1111/j.1747-4949.2011.00594.x

Saederup N, Chan L, Lira SA, Charo IF (2008) Fractalkine deficiency markedly reduces macrophage accumulation and atherosclerotic lesion formation in CCR2-/- mice: evidence for independent chemokine functions in atherogenesis. Circulation 117:1642–1648. doi: 10.1161/CIRCULATIONAHA.107.743872

Saenger AK, Christenson RH (2010) Stroke biomarkers: progress and challenges for diagnosis, prognosis, differentiation, and treatment. Clin Chem 56:21–33. doi: 10.1373/clinchem.2009.133801

Sandercock P, Wardlaw JM, Lindley RI, et al. (2012) The benefits and harms of intravenous thrombolysis with recombinant tissue plasminogen activator within 6 h of acute ischaemic stroke (the third international stroke trial [IST-3]): a randomised controlled trial. Lancet 379:2352–2363. doi: 10.1016/S0140-6736(12)60768-5

Schaffer CB, Friedman B, Nishimura N, et al. (2006) Two-photon imaging of cortical surface microvessels reveals a robust redistribution in blood flow after vascular occlusion. PLoS Biol 4:e22. doi: 10.1371/journal.pbio.0040022

Schilling M, Besselmann M, Müller M, et al. (2005) Predominant phagocytic activity of resident microglia over hematogenous macrophages following transient focal cerebral ischemia: an investigation using green fluorescent protein transgenic bone marrow chimeric mice. Exp Neurol 196:290–297. doi: 10.1016/j.expneurol.2005.08.004

Schroeter M, Jander S, Witte OW, Stoll G (1994) Local immune responses in the rat cerebral cortex after middle cerebral artery occlusion. J Neuroimmunol 55:195–203.

Scotton CJ, Martinez FO, Smelt MJ, et al. (2005) Transcriptional profiling reveals complex regulation of the monocyte IL-1 beta system by IL-13. J Immunol 174:834–845.

Sedgwick JD, Schwender S, Imrich H, et al. (1991) Isolation and direct characterization of resident microglial cells from the normal and inflamed central nervous system. Proc Natl Acad Sci USA 88:7438–7442.

Shepro D, Morel NM (1993) Pericyte physiology. FASEB J 7:1031–1038.

Shichita T, Sugiyama Y, Ooboshi H, et al. (2009) Pivotal role of cerebral interleukin-17-producing gammadeltaT cells in the delayed phase of ischemic brain injury. Nat Med 15:946–950. doi: 10.1038/nm.1999

Shih AY, Driscoll JD, Drew PJ, et al. (2012) Two-photon microscopy as a tool to study blood flow and neurovascular coupling in the rodent brain. Journal of Cerebral Blood Flow and Metabolism: Official Journal of the International Society of Cerebral Blood Flow and Metabolism. doi: 10.1038/jcbfm.2011.196

Shih AY, Friedman B, Drew PJ, et al. (2009) Active dilation of penetrating arterioles restores red blood cell flux to penumbral neocortex after focal stroke. J Cereb Blood Flow Metab 29:738–751. doi: 10.1038/jcbfm.2008.166

Shin J-W, Lee JK, Lee JE, et al. (2011) Combined effects of hematopoietic progenitor cell mobilization from bone marrow by granulocyte colony stimulating factor and AMD3100 and chemotaxis into the brain using stromal cell-derived factor-1α in an Alzheimer's disease mouse model. Stem Cells 29:1075–1089. doi: 10.1002/stem.659

Sica A, Mantovani A (2012) Macrophage plasticity and polarization: in vivo veritas. J Clin Invest 122:787–795. doi: 10.1172/JCI59643

Sierra A, Encinas JM, Deudero JJP, et al. (2010) Microglia shape adult hippocampal neurogenesis through apoptosis-coupled phagocytosis. Cell Stem Cell 7:483–495. doi: 10.1016/j.stem.2010.08.014

Sigler A, Murphy TH (2010) In vivo 2-photon imaging of fine structure in the rodent brain: before, during, and after stroke. Stroke 41:S117–123. doi: 10.1161/STROKEAHA.110.594648

Simard AR, Soulet D, Gowing G, et al. (2006) Bone marrow-derived microglia play a critical role in restricting senile plaque formation in Alzheimer's disease. Neuron 49:489–502. doi: 10.1016/j.neuron.2006.01.022

De Simoni MG, Storini C, Barba M, et al. (2003) Neuroprotection by complement (C1) inhibitor in mouse transient brain ischemia. J Cereb Blood Flow Metab 23:232–239.

Smith CJ, Emsley HC, Udeh CT, et al. (2012) Interleukin-1 receptor antagonist reverses stroke-associated peripheral immune suppression. Cytokine 58:384–389. doi: 10.1016/j.cyto.2012.02.016

Smorodchenko A, Wuerfel J, Pohl EE, et al. (2007) CNS-irrelevant T-cells enter the brain, cause blood-brain barrier disruption but no glial pathology. Eur J Neurosci 26:1387–1398. doi: 10.1111/j.1460-9568.2007.05792.x

Soeller C, Cannell MB (1999) Two-photon microscopy: imaging in scattering samples and three-dimensionally resolved flash photolysis. Microsc Res Tech 47:182–195. doi: 10.1002/(SICI)1097-0029(19991101)47:3<182::AID-JEMT4>3.0.CO;2-4

Solovjov DA, Pluskota E, Plow EF (2005) Distinct roles for the alpha and beta subunits in the functions of integrin alphaMbeta2. J Biol Chem 280:1336–1345. doi: 10.1074/jbc.M406968200

Soltys Z, Orzylowska-Sliwinska O, Zaremba M, et al. (2005) Quantitative morphological study of microglial cells in the ischemic rat brain using principal component analysis. J Neurosci Methods 146:50–60. doi: 10.1016/j.jneumeth.2005.01.009

Soriano SG, Amaravadi LS, Wang YF, et al. (2002) Mice deficient in fractalkine are less susceptible to cerebral ischemia-reperfusion injury. J Neuroimmunol 125:59–65.

Sriram K, Matheson JM, Benkovic SA, et al. (2006) Deficiency of TNF receptors suppresses microglial activation and alters the susceptibility of brain regions to MPTP-induced neurotoxicity: role of TNF-alpha. FASEB J 20:670–682. doi: 10.1096/fj.05-5106com

Stefanovic B, Hutchinson E, Yakovleva V, et al. (2008) Functional reactivity of cerebral capillaries. J Cereb Blood Flow Metab 28:961–972. doi: 10.1038/sj.jcbfm.9600590

Stein M, Keshav S, Harris N, Gordon S (1992) Interleukin 4 potently enhances murine macrophage mannose receptor activity: a marker of alternative immunologic macrophage activation. J Exp Med 176:287–292.

Stein VM, Baumgärtner W, Schröder S, et al. (2007) Differential expression of CD45 on canine microglial cells. J Vet Med A Physiol Pathol Clin Med 54:314–320. doi: 10.1111/j.1439-0442.2007.00926.x

Stevens SL, Bao J, Hollis J, et al. (2002) The use of flow cytometry to evaluate temporal changes in inflammatory cells following focal cerebral ischemia in mice. Brain Res 932:110–119.

Stoll G, Jander S (1999) The role of microglia and macrophages in the pathophysiology of the CNS. Prog Neurobiol 58:233–247.

Stoll G, Jander S, Schroeter M (1998) Inflammation and glial responses in ischemic brain lesions. Prog Neurobiol 56:149–171.

Stoll G, Kleinschnitz C, Nieswandt B (2008) Molecular mechanisms of thrombus formation in ischemic stroke: novel insights and targets for treatment. Blood 112:3555–3562. doi: 10.1182/blood-2008-04-144758

Storini C, Bergamaschini L, Gesuete R, et al. (2006) Selective inhibition of plasma kallikrein protects brain from reperfusion injury. J Pharmacol Exp Ther 318:849–854. doi: 10.1124/jpet.106.105064

Strbian D, Durukan A, Pitkonen M, et al. (2008) The blood-brain barrier is continuously open for several weeks following transient focal cerebral ischemia. Neuroscience 153:175–181. doi: 10.1016/j.neuroscience.2008.02.012

Strong AJ, Smith SE, Whittington DJ, et al. (2000) Factors influencing the frequency of fluorescence transients as markers of peri-infarct depolarizations in focal cerebral ischemia. Stroke 31:214–222.

Sunderkötter C, Nikolic T, Dillon MJ, et al. (2004) Subpopulations of mouse blood monocytes differ in maturation stage and inflammatory response. J Immunol 172:4410–4417.

Svoboda K, Block SM (1994) Biological applications of optical forces. Annu Rev Biophys Biomol Struct 23:247–285. doi: 10.1146/annurev.bb.23.060194.001335

Svoboda K, Yasuda R (2006) Principles of two-photon excitation microscopy and its applications to neuroscience. Neuron 50:823–839. doi: 10.1016/j.neuron.2006.05.019

Swanson RA, Morton MT, Tsao-Wu G, et al. (1990) A semiautomated method for measuring brain infarct volume. J Cereb Blood Flow Metab 10:290–293. doi: 10.1038/jcbfm.1990.47

Takano T, Han X, Deane R, et al. (2007) Two-photon imaging of astrocytic Ca2+ signaling and the microvasculature in experimental mice models of Alzheimer's disease. Ann N Y Acad Sci 1097:40–50. doi: 10.1196/annals.1379.004

Tanswell P, Modi N, Combs D, Danays T (2002) Pharmacokinetics and pharmacodynamics of tenecteplase in fibrinolytic therapy of acute myocardial infarction. Clin Pharmacokinet 41:1229–1245.

Taoufik E, Petit E, Divoux D, et al. (2008) TNF receptor I sensitizes neurons to erythropoietin- and VEGF-mediated neuroprotection after ischemic and excitotoxic injury. Proc Natl Acad Sci USA 105:6185–6190. doi: 10.1073/pnas.0801447105

Taoufik E, Valable S, Müller GJ, et al. (2007) FLIP(L) protects neurons against in vivo ischemia and in vitro glucose deprivation-induced cell death. J Neurosci 27:6633–6646. doi: 10.1523/JNEUROSCI.1091-07.2007

Tasdemiroglu E, Macfarlane R, Wei EP, et al. (1992) Pial vessel caliber and cerebral blood flow become dissociated during ischemia-reperfusion in cats. Am J Physiol 263:H533–536.

Terao S, Yilmaz G, Stokes KY, et al. (2008) Inflammatory and injury responses to ischemic stroke in obese mice. Stroke 39:943–950. doi: 10.1161/STROKEAHA.107.494542

Tétrault S, Chever O, Sik A, Amzica F (2008) Opening of the blood-brain barrier during isoflurane anaesthesia. Eur J Neurosci 28:1330–1341. doi: 10.1111/j.1460-9568.2008.06443.x

Thompson RJ, Zhou N, MacVicar BA (2006) Ischemia opens neuronal gap junction hemichannels. Science 312:924–927. doi: 10.1126/science.1126241

Thored P, Heldmann U, Gomes-Leal W, et al. (2009) Long-term accumulation of microglia with proneurogenic phenotype concomitant with persistent neurogenesis in adult subventricular zone after stroke. Glia 57:835–849. doi: 10.1002/glia.20810

Tremblay M-È, Stevens B, Sierra A, et al. (2011) The role of microglia in the healthy brain. J Neurosci 31:16064–16069. doi: 10.1523/JNEUROSCI.4158-11.2011

Tsai PS, Kaufhold JP, Blinder P, et al. (2009) Correlations of neuronal and microvascular densities in murine cortex revealed by direct counting and colocalization of nuclei and vessels. J Neurosci 29:14553–14570. doi: 10.1523/JNEUROSCI.3287-09.2009

Tsien RY (1998) The green fluorescent protein. Annu Rev Biochem 67:509–544. doi: 10.1146/annurev.biochem.67.1.509

Tu W, Xu X, Peng L, et al. (2010) DAPK1 interaction with NMDA receptor NR2B subunits mediates brain damage in stroke. Cell 140:222–234. doi: 10.1016/j.cell.2009.12.055

Tymianski M (2011) Emerging mechanisms of disrupted cellular signaling in brain ischemia. Nat Neurosci 14:1369–1373. doi: 10.1038/nn.2951

Unal Cevik I, Dalkara T (2003) Intravenously administered propidium iodide labels necrotic cells in the intact mouse brain after injury. Cell Death Differ 10:928–929. doi: 10.1038/sj.cdd.4401250

Valledor AF, Ricote M (2004) Nuclear receptor signaling in macrophages. Biochem Pharmacol 67:201–212.

VANDER EECKEN HM, ADAMS RD (1953) The anatomy and functional significance of the meningeal arterial anastomoses of the human brain. J Neuropathol Exp Neurol 12:132–157.

Venkatachalam K, Montell C (2007) TRP channels. Annu Rev Biochem 76:387–417. doi: 10.1146/annurev.biochem.75.103004.142819

Villalta SA, Nguyen HX, Deng B, et al. (2009) Shifts in macrophage phenotypes and macrophage competition for arginine metabolism affect the severity of muscle pathology in muscular dystrophy. Hum Mol Genet 18:482–496. doi: 10.1093/hmg/ddn376

Vinet J, Weering HRJ van, Heinrich A, et al. (2012) Neuroprotective function for ramified microglia in hippocampal excitotoxicity. J Neuroinflammation 9:27. doi: 10.1186/1742-2094-9-27

Wahlgren N, Ahmed N, Eriksson N, et al. (2008) Multivariable analysis of outcome predictors and adjustment of main outcome results to baseline data profile in randomized controlled trials: Safe Implementation of Thrombolysis in Stroke-MOnitoring STudy (SITS-MOST). Stroke 39:3316–3322. doi: 10.1161/STROKEAHA.107.510768

Wajant H, Pfizenmaier K, Scheurich P (2003) Tumor necrosis factor signaling. Cell Death Differ 10:45–65. doi: 10.1038/sj.cdd.4401189

Wake H, Moorhouse AJ, Jinno S, et al. (2009) Resting microglia directly monitor the functional state of synapses in vivo and determine the fate of ischemic terminals. J Neurosci 29:3974–3980. doi: 10.1523/JNEUROSCI.4363-08.2009

Wang X, Yue TL, Young PR, et al. (1995) Expression of interleukin-6, c-fos, and zif268 mRNAs in rat ischemic cortex. J Cereb Blood Flow Metab 15:166–171. doi: 10.1038/jcbfm.1995.18

Wardlaw JM, Murray V, Berge E, Del Zoppo GJ (2009) Thrombolysis for acute ischaemic stroke. Cochrane Database Syst Rev CD000213. doi: 10.1002/14651858.CD000213.pub2

Watson BD, Prado R, Veloso A, et al. (2002) Cerebral blood flow restoration and reperfusion injury after ultraviolet laser-facilitated middle cerebral artery recanalization in rat thrombotic stroke. Stroke 33:428–434.

Wei L, Craven K, Erinjeri J, et al. (1998) Local cerebral blood flow during the first hour following acute ligation of multiple arterioles in rat whisker barrel cortex. Neurobiol Dis 5:142–150. doi: 10.1006/nbdi.1998.0199

Wei L, Rovainen CM, Woolsey TA (1995) Ministrokes in rat barrel cortex. Stroke 26:1459–1462.

Wiessner C, Gehrmann J, Lindholm D, et al. (1993) Expression of transforming growth factor-beta 1 and interleukin-1 beta mRNA in rat brain following transient forebrain ischemia. Acta Neuropathol 86:439–446.

Wilson EH, Harris TH, Mrass P, et al. (2009) Behavior of parasite-specific effector CD8+ T cells in the brain and visualization of a kinesis-associated system of reticular fibers. Immunity 30:300–311. doi: 10.1016/j.immuni.2008.12.013

Wilson EH, Weninger W, Hunter CA (2010) Trafficking of immune cells in the central nervous system. J Clin Invest 120:1368–1379. doi: 10.1172/JCI41911

Wolburg H, Wolburg-Buchholz K, Engelhardt B (2005) Diapedesis of mononuclear cells across cerebral venules during experimental autoimmune encephalomyelitis leaves tight junctions intact. Acta Neuropathol 109:181–190. doi: 10.1007/s00401-004-0928-x

Wong GKC, Wong R, Mok V, et al. (2010) Natural history and medical treatment of cognitive dysfunction after spontaneous subarachnoid haemorrhage: review of current literature with respect to aneurysm treatment. J Neurol Sci 299:5–8. doi: 10.1016/j.jns.2010.08.059

Worthmann H, Tryc AB, Goldbecker A, et al. (2010) The temporal profile of inflammatory markers and mediators in blood after acute ischemic stroke differs depending on stroke outcome. Cerebrovasc Dis 30:85–92. doi: 10.1159/000314624

Xu H, Chen M, Mayer EJ, et al. (2007a) Turnover of resident retinal microglia in the normal adult mouse. Glia 55:1189–1198. doi: 10.1002/glia.20535

Xu H-T, Pan F, Yang G, Gan W-B (2007b) Choice of cranial window type for in vivo imaging affects dendritic spine turnover in the cortex. Nat Neurosci 10:549–551. doi: 10.1038/nn1883

Yamasaki Y, Matsuo Y, Zagorski J, et al. (1997) New therapeutic possibility of blocking cytokine-induced neutrophil chemoattractant on transient ischemic brain damage in rats. Brain Res 759:103–111.

Yang G, Pan F, Parkhurst CN, et al. (2010) Thinned-skull cranial window technique for long-term imaging of the cortex in live mice. Nat Protoc 5:201–208. doi: 10.1038/nprot.2009.222

Yaroslavsky AN, Schulze PC, Yaroslavsky IV, et al. (2002) Optical properties of selected native and coagulated human brain tissues in vitro in the visible and near infrared spectral range. Phys Med Biol 47:2059–2073.

Yen MR, Saier MH Jr (2007) Gap junctional proteins of animals: the innexin/pannexin superfamily. Prog Biophys Mol Biol 94:5–14. doi: 10.1016/j.pbiomolbio.2007.03.006

Yenari MA, Kauppinen TM, Swanson RA (2010) Microglial activation in stroke: therapeutic targets. Neurotherapeutics 7:378–391. doi: 10.1016/j.nurt.2010.07.005

Yermolaieva O, Leonard AS, Schnizler MK, et al. (2004) Extracellular acidosis increases neuronal cell calcium by activating acid-sensing ion channel 1a. Proc Natl Acad Sci USA 101:6752–6757. doi: 10.1073/pnas.0308636100

Yilmaz G, Arumugam TV, Stokes KY, Granger DN (2006) Role of T lymphocytes and interferon-gamma in ischemic stroke. Circulation 113:2105–2112. doi: 10.1161/CIRCULATIONAHA.105.593046

Zanier ER, Montinaro M, Vigano M, et al. (2011) Human umbilical cord blood mesenchymal stem cells protect mice brain after trauma. Crit Care Med 39:2501–2510. doi: 10.1097/CCM.0b013e31822629ba

Zaremba J, Skrobanski P, Losy J (2001) Tumour necrosis factor-alpha is increased in the cerebrospinal fluid and serum of ischaemic stroke patients and correlates with the volume of evolving brain infarct. Biomed Pharmacother 55:258–263.

Zhang S, Boyd J, Delaney K, Murphy TH (2005) Rapid reversible changes in dendritic spine structure in vivo gated by the degree of ischemia. J Neurosci 25:5333–5338. doi: 10.1523/JNEUROSCI.1085-05.2005

Zhang S, Murphy TH (2007) Imaging the impact of cortical microcirculation on synaptic structure and sensory-evoked hemodynamic responses in vivo. PLoS Biol 5:e119. doi: 10.1371/journal.pbio.0050119

Zhang S-J, Zou M, Lu L, et al. (2009) Nuclear calcium signaling controls expression of a large gene pool: identification of a gene program for acquired neuroprotection induced by synaptic activity. PLoS Genet 5:e1000604. doi: 10.1371/journal.pgen.1000604

Zhang ZG, Zhang L, Jiang Q, et al. (2000) VEGF enhances angiogenesis and promotes blood-brain barrier leakage in the ischemic brain. J Clin Invest 106:829–838. doi: 10.1172/JCI9369

Zhao W, Belayev L, Ginsberg MD (1997) Transient middle cerebral artery occlusion by intraluminal suture: II. Neurological deficits, and pixel-based correlation of histopathology with local blood flow and glucose utilization. J Cereb Blood Flow Metab 17:1281–1290. doi: 10.1097/00004647-199712000-00003

Ziegler-Heitbrock L (2007) The CD14+ CD16+ blood monocytes: their role in infection and inflammation. J Leukoc Biol 81:584–592. doi: 10.1189/jlb.0806510

Zinselmeyer BH, Dempster J, Gurney AM, et al. (2005) In situ characterization of CD4+ T cell behavior in mucosal and systemic lymphoid tissues during the induction of oral priming and tolerance. J Exp Med 201:1815–1823. doi: 10.1084/jem.20050203

Zlokovic BV (2005) Neurovascular mechanisms of Alzheimer's neurodegeneration. Trends Neurosci 28:202–208. doi: 10.1016/j.tins.2005.02.001

Zonta M, Angulo MC, Gobbo S, et al. (2003) Neuron-to-astrocyte signaling is central to the dynamic control of brain microcirculation. Nat Neurosci 6:43–50. doi: 10.1038/nn980

Del Zoppo G, Ginis I, Hallenbeck JM, et al. (2000) Inflammation and stroke: putative role for cytokines, adhesion molecules and iNOS in brain response to ischemia. Brain Pathol 10:95–112.

Del Zoppo GJ (2004) Lessons from stroke trials using anti-inflammatory approaches that have failed. Ernst Schering Res Found Workshop 155–184.

Del Zoppo GJ (1997) Microvascular responses to cerebral ischemia/inflammation. Ann N Y Acad Sci 823:132–147.

Del Zoppo GJ (2009) Inflammation and the neurovascular unit in the setting of focal cerebral ischemia. Neuroscience 158:972–982. doi: 10.1016/j.neuroscience.2008.08.028

Del Zoppo GJ, Mabuchi T (2003) Cerebral microvessel responses to focal ischemia. J Cereb Blood Flow Metab 23:879–894. doi: 10.1097/01.WCB.0000078322.96027.78

Zujovic V, Benavides J, Vigé X, et al. (2000) Fractalkine modulates TNF-alpha secretion and neurotoxicity induced by microglial activation. Glia 29:305–315.